LBL--19482

DE85 012610

NON-COLLECTIVE HIGH-SPIN STATES IN ^{148}Dy

by

Eugene Liviu Dines

April 1985

Nuclear Science Division
Lawrence Berkeley Laboratory
University of California
Berkeley, California 94720

and

Physics Department
University of California at Davis
Davis, California 95616

DISCLAIMER

This report was prepared as an account of work sponsored by an agency of the United States Government. Neither the United States Government nor any agency thereof, nor any of their employees, makes any warranty, express or implied, or assumes any legal liability or responsibility for the accuracy, completeness, or usefulness of any information, apparatus, product, or process disclosed, or represents that its use would not infringe privately owned rights. Reference herein to any specific commercial product, process, or service by trade name, trademark, manufacturer, or otherwise does not necessarily constitute or imply its endorsement, recommendation, or favoring by the United States Government or any agency thereof. The views and opinions of authors expressed herein do not necessarily state or reflect those of the United States Government or any agency thereof.

This work was supported by the Director, Office of Energy Research, Division of Nuclear Physics of the Office of High Energy and Nuclear Physics of the U.S. Department of Energy under Contract DE-AC03-76SF00098.

DISTRIBUTION OF THIS DOCUMENT IS UNLIMITED

To my parents, Leonard and Ileana,

my grand-father, Alexander,

and my uncle, Maurice,

and to the memory of my

grand-mother, Otilia

Non-Collective High-Spin States in ^{148}Dy

by

Eugene Liviu Dines

Abstract

General physical concepts regarding nuclear high-spin states are given. The high-spin states in ^{148}Dy(Z = 66, N = 82) were produced via the reaction ^{112}Cd(Pb-backed)(^{40}Ar,4n) at E_{lab}= 175 , at the 88-inch Cyclotron at Lawrence Berkeley Laboratory.

The data were collected with an array of 12 Compton-suppressed pure Ge detectors, and sorted in the E_γX E_γ, 2D-coincidence matrix format for prompt and delayed gates placed on the RF - Ge TAC(which can give the time distribution of a given coincident γ-ray relative to of formation of the compound nucleus). A Ge - Ge TAC was also recorded, thus giving one distributions of time intervals elapsed between detections of any given two coincident γ-rays. The data were also sorted in the RF - Ge TAC X E_γ, Ge - Ge TAC X E_γ, (0°, 90°), (0°, 0°) and (90°, 90°) formats, where the last three gave information about the angular correlations. The format (0°, 90°), for example, refers to coincidences between a given γ-ray detected in the backward direction and another detected at 90°, with respect ot the beam axis, respectively.

Methods for placing gates on various transitions above and below the 480 nsec isomer at 10^+(known from previous work), as well as for calculating transition intensities and their associated errors are given. Calculations of angular correlations for multiple γ-ray cascades, assuming non-zero-width distributions in m-states for some given spin state, were done and compared to experimental values. Analysis of RF - Ge and Ge - Ge TAC spectra for transitions above the 480 nsec isomer implied lifetimes of $\lesssim$ 5 nsec(except for the 327.2 keV transition). Using such analysis, some 19 new γ-ray transitions were discovered above the isomer, thereby extending the ^{148}Dy level scheme up to spin I = 31$\hbar$. Assignments of spins and parities for the new levels are made based on information obtained from angular correlations and the lifetime limits. Previous work on the 11 transitions below the 480 nsec isomer is confirmed.

Below the isomer, the even-spin and -parity levels(up to 10^+) have been interpreted as excited states of the $\pi h^2_{11/2}$ configuration(with the ^{146}Gd core unexcited), while the 3^-, 5^- and 7^- states have been interpreted as: the $(\pi f^2_{11/2})_0$ X 3^-(3^- refers to the core octupole), $(\pi h_{11/2} s_{1/2})5^-$ and $(\pi h_{11/2} d_{3/2})7^-$ configurations, respectively. Above the 480 nsec isomer, the 11^-, 12^- and 13^- levels at E*= 3980, 4476 and 4851 keV, respectively, have been discussed with relation to levels of the two-particle-core-octupole coupling $(\pi h^2_{11/2})_{I'}$ X 3^-, where I' = 10

for the 12^- and 13^-, and $I' = 8$ and 10 for the 11^-. Theoretical values for energies of the 11^-(after interaction matrix diagonalization in the 2D basis made by $I' = 8$ and 10) and the 13^- levels are obtained using second-order perturbation theory, and found to be in reasonable agreement with the experimental values. The rest of the experimental levels above the 480 nsec isomer are interpreted as deformed-independent-particle-model states.

Table of Contents

Chapter 1 : High-Spin States in Nuclei: Generalities.....1

Chapter 2 : Experimental Procedure.....16

Section 2.1 : Gamma-Ray Doppler Broadening and Shift.....16

Section 2.2 : The Detectors Used in the Data Acquisition.....18

Section 2.3 : The Quality of the Data Acquired with the Pure-Ge Array.....25

Section 2.4 : Experimental Set-up.....31

Chapter 3 : The Analysis.....34

Section 3.1 : The Sorting of the Data.....34

Section 3.2 : The RF - Ge Time Distribution of the Coincident Gamma-Rays.....41

Section 3.3 : Method for Analyzing Discrete Coincidence Spectra.....42

Section 3.4 : Ge Relative Efficiency.....48

Section 3.5 : Method for Obtaining Transition Intensities and their Uncertainties.....54

Chapter 4 : The Level Scheme of ^{148}Dy.....63

Section 4.1 : The Transitions Above the 480 nsec Isomer.....63

Section 4.2 : Deduction of the Relative Intensities of Branchings and Transition Cross-Overs.....95

Section 4.3 : The Transitions Below the 480 nsec Isomer.....101

Chapter 5 : Multipolarity(and Parity)Information from Angular Correlation and the RF - Ge and Ge - Ge TAC's, Respectively.....107

Section 5.1 : The Angular Correlation Measurements.....109

Section 5.2 : Life-Time Information from the RF - Ge and Ge - Ge TAC'.....150

Chapter 6 : Two-Particle-Octupole Exchange Coupling and the Deformed Independent Particle Model as Applied to the Discrete Levels of ^{148}Dy.....179

Section 6.1 : The $\pi h^2_{11/2}$ Spectrum and the Negative Parity States Below the 480 nsec Isomer.....182

Section 6.2 : Two-Particle-Octupole Exchange.....184

Section 6.3 : The Use of the Deformed Independent Particle Model(DIPM) for the Levels Not Explained in the Previous Section.....204

Appendix.....213

References.....228

Figure Captions.....232

Chapter 1.....232

Chapter 2.....233

Chapter 3.....235

Chapter 4.....238

Chapter 5.....239

Chapter 6.....241

Appendix 242

Acknowledgements.....243

This report was done with support from the Department of Energy. Any conclusions or opinions expressed in this report represent solely those of the author(s) and not necessarily those of The Regents of the University of California, the Lawrence Berkeley Laboratory or the Department of Energy.

Reference to a company or product name does not imply approval or recommendation of the product by the University of California or the U.S. Department of Energy to the exclusion of others that may be suitable.

Chapter 1

High-Spin States in Nuclei: Generalities

Recent developments in experimental techniques have made possible the study of nuclear properties at very high angular momenta, around 40-50ħ, nearing the value that a nucleus with mass around 160 can sustain against an 8 MeV fission barrier. The use of heavy-ion beams, such as ^{40}Ar, at lab energies in excess of 4-5 MeV/incident nucleon, has brought angular momenta of 50-60ħ into the compound systems formed with masses around 160. The equation below enables one to calculate such a maximum value of the angular momentum imparted to the compound nuclear system:

$$l_{max} = 0.22(R_1 + R_2)[\mu(E_{CM} - V_{CB})]^{1/2}, \qquad (1.0.1)$$

where R_1 and R_2 are the projectile and target radii, respectively, V_{CB} is the Coulomb barrier energy given by $1.4Z_{proj}Z_{tgt}/(R_1+R_2+d)$ (d being the difuseness parameter, usually taken around 1.2 fm)in MeV, E_{CM} and μ are the center-of-mass energy and the reduced mass of the projectile-target system, respectively. The expression above can be easily obtained from $\sigma = \pi(R_1 + R_2)^2(1 - V_{CB}/E_{CM}) = \pi\lambda_{CM}^2 * l_{max}(l_{max} + 1)$, the classical expression for the cross section for such heavy-ion collisions, where the heavy-ion wavelengths, λ_{CM}

are much smaller than the dimensions of the collision systems.

Fig. 1.1 shows the dependence of the maximum angular momentum of such a compound nuclear system on its mass, A, for possibilities of de-excitation. In order to live more than 10^{-21} sec, any nuclear system must have a non-vanishing barrier against fission, and the solid curve in the figure represents the dependence of the maximum angular momentum (when the fission barrier vanishes) that a "cold" nucleus can hold vs its mass, along the β-stability line(Cohen et al, 1974). The curve descends for higher A because of increasing Coulomb repulsion and for lower A because of lower surface energies and higher rotational frequencies required by lower moments of inertia. Heavy-ion reactions also bring in considerable amounts of excitation energy(around 40-50 MeV) which greatly increases the chance for fission, and the subsequent loss of the angular momentum to the relative motion of the outgoing fragments. At such excitation energies, only particle evaporation can prevent fission. The time scale(Diamond and Stephens, 1980) for particle evaporation(for normal binding energies) is about 10^{-18}- 10^{-17} sec, which necessitates a fission barrier of around 8 MeV(approximately the neutron binding

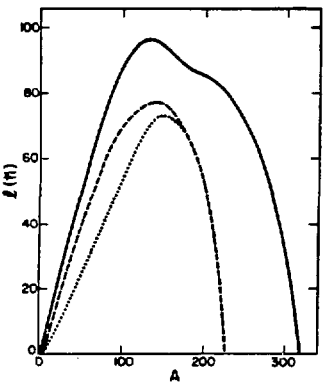

Fig. 1.1

energy) in order for fission to slow down to such times. The dashed line in Fig. 1.1 corresponds to an 8-MeV fission barrier, below which particle emission(mostly neutrons) dominates. In the time interval 10^{-21}- 10^{-17} sec, or between the solid and the dashed curves in Fig. 1.1, only the fission of the compound nucleus can be studied, which gives little information about this region. When the particle evaporation is slowed down by the decreasing level density(which goes like $\exp(\sqrt{E - E_{yr}})$, where the yrast energy E_{yr} is defined on the next page; Diamond and Stephens, 1980)sufficiently, the γ-ray de-excitation takes over the process of nuclear decay into the ground state. This happens at around 10^{-15} sec which is the halflife of the fastest typical E1(~ 1 MeV)γ-ray transition(see Fig. 5.2.15). Also, this starts to happen when the excitation energy is below the neutron binding energy. Thus, between the dashed and the dotted lines in Fig. 1.1, one can study the nuclear states via particle evaporation, which is more sensitive to nuclear structure than fission, but less so than the study of the γ-ray decay, which corresponds to the region below the dotted line. Estimates have been made about the maximum angular momentum surviving particle evaporation, based on γ-ray and α-particle emission probabilities(see Diamond and Stephens, 1980), represented by the dotted line in Fig. 1.1 .

The rest of this chapter will attempt to give a flavor of the studies of the γ-ray decay of high-spin states(thus restricted to the region below that dotted line) in general, while the following chapters will present, in detail, the γ-ray decay of the high-spin states of ^{148}Dy. Looking at Fig. 1.1, one can easily see why

nuclear systems with masses around 140-150 have been picked in the beginning of such studies, since spins up to ~ 70ħ could tentatively be reached.

Fig. 1.2 shows the decay modes of the reaction indicated(whose 4n product is the object of investigation of the subsequent chapters) in the (E^*, I) space. At the lab energy of 175 MeV, the ^{152}Dy compound nucleus is formed with an excitation energy of about 75 MeV($E^* = E_{CM} - Q$) and with a maximum angular momentum brought in by the reaction of about 56ħ(according to (1.0.1)). Actually, compound nuclei initially formed in the reaction considered have a rounded triangular distribution in spin, thus concentrating the formed nuclei at spins around 50-60ħ, while from Fig. 1.1, one can see that for such a compound nucleus, fission(for a barrier of ~ 8 MeV) will start beyond spins of about 70ħ. At spins lower than 70ħ and $E^* = 75$ MeV, the nucleus can de-excite by emitting nucleons which carry relatively small amounts of angular momentum, about 1-2ħ per. When the nucleus has de-excited down to within one neutron binding energy(~ 8 MeV) of the yrast line, it has no option but to lose its remaining excitation energy and angular momentum by γ-ray decay. The yrast line is defined to be the locus of all points in the (E^*, I) space which have the lowest excitation energy E^* for a given total spin I. From Fig. 1.2, it can be easily seen that higher spins(associated with higher excitation energies)correspond to fewer neutrons emitted and also longer γ-ray cascades, since $L \leqslant 2$. The γ-ray paths of de-excitation the nucleus follows after no more neutrons can be emitted(i.e. below the entry line in Fig. 1.3), contain two main types of transitions

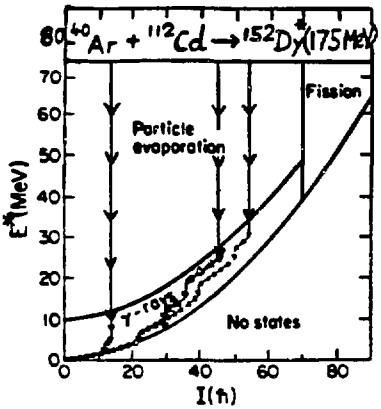

Fig. 1.2

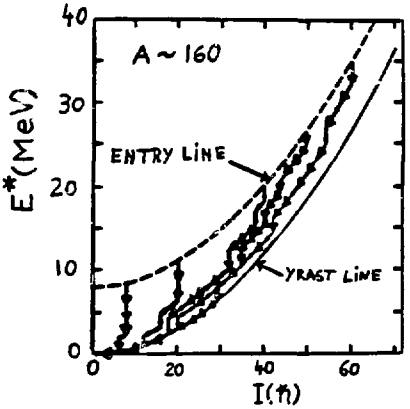

Fig. 1.3

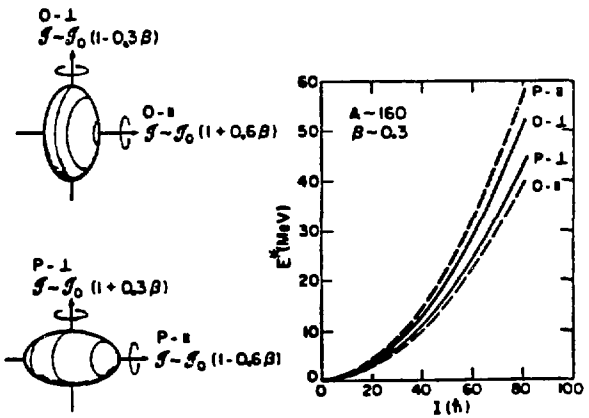

Fig. 1.4

(see Fig. 1.3): "yrast-like", i.e. those parallel, or nearly so, to the yrast line, which carry angular momentum but little excitation energy, and "statistical"(which depend on average matrix elements and level densities; see Diamond and Stephens, 1980), which run nearly perpendicular to the spin axis, and thus carry relatively little amounts of angular momenta, but considerable amounts of excitation energy, thus rapidly "cooling" the nucleus towards the yrast line. Until the nucleus reaches a region near the yrast line, it has virtually infinitely many paths of de-excitation at its disposal, with the result that no single transition has enough intensity to stand out in the spectrum. This is the "continuum" region, and recent developments of the method of the "frequency(or transition energy) slicing" of the continuum has given hope that one might get a quantitative idea as to what the probability is that the nucleus will pick one path or another to decay. However, when the nucleus reaches the yrast line, or regions near by, enough population will collect into only a few possible pathways, so that the transitions belonging to those pathways can be resolved as discrete lines. For the case presently under investigation, this seems to happen at spins around 31ħ, this being as far up as the level scheme of ^{148}Dy could be extended, although for other, more rotational, nuclei, with masses around 160, such as ^{158}Er, for example, discrete transitions were observed from spins around 40ħ, employing high-resolution γ-ray spectroscopy techniques(such as described in chapters 2 and 3).

Nuclei carry angular momentum in two basic ways: by the collective motion of the whole nucleus, or by single-particle

alignment. Fig. 1.5 illustrates the collective rotation(quantum mechanics prevents a nucleus from rotating collectively except with respect to an axis perpendicular to its symmetry axis!) of ^{158}Er, interrupted by a pronounced "backbend" and two progressively weaker "upbends", which otherwise follows rather well the expression for thelevel energies of a rigid rotor:

$$E^* = (\hbar^2/2\mathcal{J})I(I+1) \; ; \; E_\gamma = (\hbar^2/2\mathcal{J})(4I-2) \qquad (1.0.2)$$

for I = 0, 2, 4, . . . , and where $\mathcal{J}$ is the moment of inertia, which is also defined as $\mathcal{J} = I(dE^*/dI)^{-1} = I/\omega$, where ω is the rotational frequency of the whole nucleus with respect to an axis perpendicular to its symmetry axis(see Fig. 1.5). The two canonical variables I and ω are related to each other via $\omega = (dE^*/dI)$, and since one can always define $E_{rot} = (1/2)\mathcal{J}\hbar\omega^2$ and $\hbar\sqrt{I(I+1)} = \mathcal{J}\hbar\omega$, one can obtain the following connection to the γ-ray transition energy, E_γ, which is an experimental quantity:

$$\hbar\omega = 2\sqrt{I(I+1)}\,[dE_{rot}(I)/d(I(I+1))] = \qquad (1.0.3)$$

$$= 2\sqrt{I(I+1)}\,(dE_{rot}(I)/dI)[dI/d(I(I+1))] =$$

$$= 2\sqrt{I(I+1)}(2I+1)^{-1}[dE_{rot}(I)/dI] \simeq [dE_{rot}(I)/dI]$$

(for I > 1)

$$\hbar\omega \simeq [(E_{rot}(I+1) - E_{rot}(I-1)]/[(I+1) - (I-1)] \simeq E_\gamma/2$$

The expression above, relating the angular frequency of rotation of the nucleus as a collective ensemble to the energy of the γ-ray emitted, applies for the γ-ray decay of good rotors, which most of the quadrupole-deformed nuclei are, and for which the γ-ray de-excitation in the (E^*, I) space proceeds via $\Delta I = 2$ steps. Steps of different ΔI also give an ω linearly proportional to E_γ, except that instead of 1/2 in front of it as for the $\Delta I = 2$ case, one has 1 for the case of $\Delta I = 1$, for example. Gamma-ray decays via ΔI greater than 2(i.e. γ-ray multipolarities greater than 2) are quite unlikely, although one stretched E3 γ-ray has been tentatively reported in the present work on ^{148}Dy(see chapter 5). Using an extreme example to illustrate this point, one can see that when a photon is emitted, its momentum is $p = E/c$(if recoil is neglected), and the maximum angular momentum that it can carry is $|\vec{L}| = |\vec{R} \times \vec{p}| = RE_\gamma/\hbar c = RE_\gamma/197$ MeV*fm. This says that a 1 MeV γ-ray can carry one unit of orbital angular momentum at $R \approx 200$ fm away from the center of the nucleus! If this 1 MeV γ-ray is emitted in the course of the de-excitation of a collectively rotating nucleus(thus, most likely being a stretched E2) then, at the moment of emission, the required rotational frequency is $\hbar\omega$ = 500 keV, which translates into about 10^{21} revolutions per second. Interestingly enough, Earth has spun about 10^{21} revolutions around its axis since its creation !

For a classical rotor, the moment of inertia(see (1.0.2)) depends on nuclear macroscopic quantities like shape and flow pattern, expected to be rigid at very high spins, and such a rigid ellipsoid has moments of inertia given by(Diamond and Stephens, 1980)

$$\mathcal{I}_z = (1/5)M(r_x^2 + r_y^2) = (1/2)(a_x^2 + a_y^2)\mathcal{I}_o \qquad (1.0.4)$$

where the axes x,y,z can be cyclically permutated, and the semi-axes $r_{x,y,z}$ are related to the mean radius R by $r_{x,y,z} = a_{x,y,z}R$, and $\mathcal{I}_o$ is the rigid-sphere moment of inertia given by $(2\mathcal{I}_o/\hbar^2) = 0.01913R_s^2A$ MeV^{-1}, where the nuclear radius $R_s = 1.28A^{1/3} - 0.76 + 0.8A^{-1/3}$(fm). The coefficients $a_{x,y,z}$ are expressed in terms of the shape parameters β and γ as follows:

$$a_x = \exp[(\beta/1.6)\cos(\gamma - 2\pi/3)]; \qquad (1.0.5)$$
$$a_y = \exp[(\beta/1.6)\cos(\gamma + 2\pi/3)];$$
$$a_z = \exp[(\beta/1.6)\cos\gamma]$$

The moment of inertia in (1.0.4) is actually an "effective" value, due to the coupling of the single particles to the rotation axis, for the states of very high spins. For an oblate shape, spinning around its symmetry axis, z, one can easily see how (1.0.4-5) with $\gamma = 60°$, give for $\mathcal{I}_z$, to its lowest order expansion,

$$\mathcal{I}_z = (1/2)[\exp(\beta/1.6) + \exp(\beta/1.6)]\mathcal{I}_o = \qquad (1.0.6)$$
$$= \exp(\beta/1.6)\mathcal{I}_o = (1 + 0.6\beta)\mathcal{I}_o ,$$

for small values of the deformation parameter β. Similar lowest order expansions in $\mathcal{I}_z$ for other three basic classical rotating shapes are depicted in Fig. 1.4, with the triaxial shapes between those limits.

The deviations of expansions such as (1.0.6) from exact expressions start at $\beta \approx 0.3$(as we will see in chapter 6, $|\beta| \approx 0.18$ for ^{148}Dy, "effectively" averaged over its yrast states), and, just like the liquid-drop shapes of minimum energy as a function of spin(Diamond and Stephens, 1980), give oblate shapes(of moderate deformation) through most of the spin range, becoming prolate when $\beta \approx 0.8$(just before fission). From Fig. 1.4, one can see that the lowest energy trajectory(thus highest moment of inertia) corresponds to an oblate rigid shape spinning around its symmetry axis. Earth is a living example of the application of the solid-line O-II curve in the figure above! Real rotating nuclei, however, are not oblate due to shell effects, extensively discussed in the references above.

In general, nuclei are not rigid, and thus, nucleons can move throughout the nuclear volume with pairing interactions between one another, which can reduce the moments of inertia by factors of 2-3 from the rigid-sphere values, at low spins. As the spin increases, the pairing is considerably reduced by the Coriolis force, thus enabling the moment of inertia to increase with spin or $\hbar\omega \approx E_\gamma/2$. However, the Coriolis force(proportional to the j of the nucleon) will act most strongly on the high-j nucleons, so that the gradually increasing slope of a plot of the moment of inertia vs $\hbar\omega$(e.g. Fig. 1.5, for the case of ^{158}Er) is occasionally interrupted by more or less sharp increases, where it is energetically more favorable for the nucleus to break a pair of high-j nucleons and align them more or less completely(Stephens and Simon, 1972) along the rotational axis. The aligned high-j orbitals above are also known as "intruder" orbi-

tals(Diamond and Stephens, 1980), brought down by the spin-orbit interaction(e.g. the proton $h_{11/2}$ orbitals into the N = 4 shell, which play an important role in ^{148}Dy; see chapter 6). At this point the first band and the band containing the aligned nucleons(also with a larger moment of inertia)cross, resulting in the latter band becoming the yrast line above the crossing $\hbar\omega$. This also results in the nucleus slowing down in its rotation with respect to an axis perpendicular to its symmetry axis, because of the sudden gain in the aligned spin i.

Fig. 1.5 depicts the moment of inertia, total spin I and the aligned spin i, all plotted vs $\hbar\omega$, for the case of ^{158}Er.

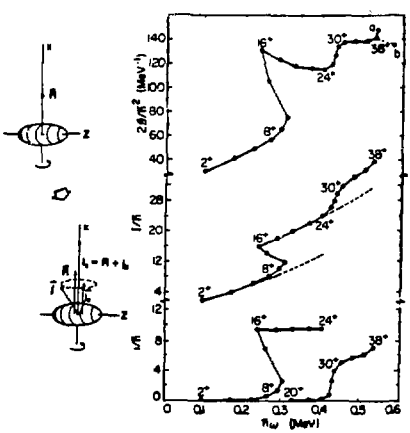

Fig. 1.5

It is an $i_{13/2}$ pair of neutrons that is responsible for the sudden decrease of $\hbar\omega$(or E_γ) with total spin I(or aligned spin i)(phenomenon known as "backbend"(see Johnson et al, 1971))occuring at $\hbar\omega \approx 0.25$ MeV, while a pair of $h_{11/2}$ protons seems to cause the "upbend" at $\hbar\omega \approx 0.43$ MeV, where, by then, one has four particles aligned along the rotational axis. At still higher spin, of about 38ħ, it seems that ^{158}Er may start a third yrast irregularity (at $\hbar\omega \approx 0.50$ MeV), whereby a pair of $h_{9/2}$ neutrons may be aligned.

Details about the observation of these three potential yrast irregularities in ^{158}Er are found in a May 1982 Physical Review Letters publication(see Burde et al, 1982).

Thus, certain nuclei such as ^{158}Er,(with 68 protons and 90 neutrons, far from the double-closed spherical shells at the "semi--magical" Z = 64 and the "magical" N = 82) can start out as prolate shapes rotating with respect to axes perpendicular to their symmetry axes, their smooth collective rotations being occasionally interrupted by backbends and/or upbends whereby pairs of high-j nucleons align their angular momenta along the rotation axis. On the average, this behaviour cooresponds to the solid-lined trajectories on the E^* vs I plot in Fig. 1.4 . True collective rotations with strongly enhanced E2 transition rates(about two orders of magnitude faster than the single-particle transitions) and spins which, on the average, increase smoothly with $\hbar\omega$.

At the other extreme of nuclear behaviour, one has the dashed-line trajectories in Fig. 1.4, which represent the average location of states with single-particle character, thus spaced irregularly in E^* and I . In this case, the nuclear states are non-collective, and the angular momentum is carried by high-j nucleons with large projections of their angular momenta on the symmetry axis of the nucleus. Bohr and Mottelson(1975) considered nucleon angular momentum alignment along the symmetry axis as an "effective" nuclear rotation around that axis. This concept hereby completes the making of the four basic E^* vs I trajectories sketched in Fig. 1.4, meaningfully applicable to nuclei. Such an irregular yrast line thus

leads to weak, if any, collective transitions. One can have isomers, or "yrast traps", in this spin region(as high as 30ħ)(Bohr and Mottelson, 1974),as a result of the fact that statistical transitions(usually dipoles)compete better against the yrast-like ones, such that more population is cooled down at relatively high spins. The collective E2 transitions are enhanced by about 100-200 times over the single-particle unit and thus characterized by short average lifetimes. For nuclei such as ^{148}Dy, collective E2 transitions are considerably hindered with respect to single-particle transitions de-exciting from irregularly spaced yrast states in the high-spin region. In addition, to a smaller but nevertheless important degree, the irregularity of the yrast states introduces the possible existence of low-energy dipole γ's de-exciting from high spins, which can be 2-3 orders of magnitude slower than the collective E2's.(Transition rates are proportional to E_γ^{2L+1}.) Conversely, the presence of high-spin isomers can be taken as an indication of non-collective rotation.

The ^{148}Dy nucleus(magic number of 82 neutrons and 2 protons higher than the semi-magical number of 64) shows irregular level spacing and the existence of isomeric states, characteristic of non-collective behaviour. Theoretical calculations(Dæssing et al, 1977 and Cerkaski et al, 1977) have indicated this region of isotopes as especially prone to exhibit yrast traps, based on the oblate-coupling scheme. On the other hand, some isomeric states can be explained by the shell model only (Horn et al, 1977).

In the case of a nearly spherical nucleus, such as ^{148}Dy,

alignment of individual high-j nucleons along the rotation axis seems to be, as we will see in chapter 6, just about the only way this nucleus can carry angular momentum. Fig. 1.6 below illustrates this mode, which is irregular in level spacing, and characterized by various types of electromagnetic transitions(E1, M1, E2, E3; stretched and non-stretched). A few transitions in ^{148}Dy, however, are probably collective(see section 6.2), thus introducing(to the degree of tentativeness of the discussion in section 6.2) interplay between collective and single-particle motions.

Fig. 1.6

The most recent previous work on ^{148}Dy(Julin et al, 1982) extended and confirmed previous work (Haas et al, 1981) on the level scheme, up to spins of 22-23ħ, with electromagnetic properties of transitions deduced up to I=18ħ. The reaction used was (^{16}O,4n) on ^{136}Ce, from which γ-γ coincidence analysis was done, while angular distribution information was obtained from the reaction (α,8n) on ^{152}Gd. Conversion-electron analysis gave unambiguous L_π assignments to the 6263.2 kev 17^- level, while below the 480 nsec isomer at the 2919.1 kev 10^+ level, extensive previous work (Haas et al, 1981 and Ward et al, 1983) established a strong sequence of five transitions of energies E_γ= 86.9, 94.1, 389.8, 660.8, and 1687.5 kev, together with six other weaker, and more or less parallel, lines with energies

E_γ= 101.2, 304.3, 382.7, 739.2, 749.4 and 1677.3 keV (the above 11 energies were deduced from the present work). Those works also gave unambiguous electromagnetic multipolarity character to the 11 transitions below the isomer: all being stretched E2's except for the 94.1, 382.7 and 739.2 kev γ's(these being strecthed E1's) and the 1687.5 kev γ-ray which has been identified as an E3.

In my trying to extend the decay scheme and determine the electromagnetic properties of the transitions involved, a variety of experimental techniques were used: prompt and delayed γ-γ coincidences, γ-γ angular correlations and γ-γ-TAC(time-to-amplitude converter) spectra.

Chapter 2

Experimental Procedure

The high-spin states in ^{148}Dy have been produced in the reaction ^{112}Cd (^{40}Ar,4n) at lab energies of 175 and 185 MeV, using the 88-inch Cyclotron facility at L.B.L. . The ^{112}Cd target was 1 mg/cm^2(0.0012 mm) thick and Pb-backed. The ^{40}Ar beam(the ions were in the 8^+ charge state) had an R.F. of about 14 MHz(in the third harmonic, i.e. three times the particle frequency of about 4.7 MHz), with a 70 nsec separation between beam bursts, whose average length was about a few nanoseconds.

2.1 Gamma-Ray Doppler Broadening and Shift

Due to the finite thickness of the target, the beam loses energy going through it. Consequently, the recoiling ^{148}Dy are formed with about 6.2 and 6.0 MeV(for the 175 and 185 MeV lab energies, respectively)less center-of-mass (C.M.) energy at the side of the target touching the Pb than at the side where the ^{40}Ar beam enters the target.(Through the 1 mg/cm^2 of ^{112}Cd, the ^{40}Ar ions lose about 8.4 and 8.2 MeV at incident lab energies of 175 and 185 MeV, res-

pectively.

The ^{148}Dy nuclei formed near the Pb backing, recoil with about 43.8 and 46.5 MeV, respectively, into the Pb, traveling a range of 6.9 and 7.1 mg/cm^2(0.0061 and 0.0063 mm, respectively), respectively before stopping(see Northcliffe and Schilling 1970). The stopping time, T, for such objects, can be calculated from the range, R, as follows:

$$T = R/\langle v\rangle = R/Cv = (R/cC)(mc^2/2E)^{1/2} \qquad (2.1.1)$$
$$= [R/C(3.0\times10^8\ m/s)](931\ MeV/a.m.u./2)^{1/2}(m_A/E)^{1/2}$$

where m_A is the traveling particle mass(in a.m.u.), E is the kinetic energy, in lab(in MeV), and the constant C is usually taken about 0.5 since the recoiling ^{148}Dy slow down with constant dv/dt . The stopping time then becomes the simple expression

$$T = 1.4 \times 10^{-7} R(m_A/E)^{1/2}, \qquad (2.1.2)$$

which gives us 1.4×10^{-12} and 1.6×10^{-12} sec, respectively for the two beam energies used in the lab.

At the other extreme, for the ^{148}Dy nuclei formed right where the ^{40}Ar beam enters the target, the ^{148}Dy nuclei start to recoil with about 46.1 and 48.7 MeV, respectively, and by the time they enter the Pb backing, they have lost about 16.0 and 16.6 MeV, respectively, which means they will stop after traveling about 5.2 and 6.1 mg/cm^2 (0.0046 and 0.0054, respectively)in Pb, respectively. This translates

into about 1.3×10^{-12} and 1.6×10^{-12} sec, respectively. (Naturally, the thickness of the Pb backing was more than ample to accomodate the ranges of the recoiling ^{148}Dy calculated above.)

The actual experimental case is an average of the two extreme cases discussed above. It is therefore deduced that the recoiling ^{148}Dy nuclei stop in about one-and-a-half picosecond. Experimentally, no broadening of any γ-lines was found implying lifetimes of the order of nsec(also see section 5.2). The same implication can be made from the absence of any Doppler shift($\Delta E_\gamma = E_\gamma^0(v_{rec}/c)\cos\theta_p$; v_{rec} is the recoil velocity of ^{148}Dy and Fig. 2.2.1(c) defines θ_p)of the high-energy γ-ray lines, the majority of which seem to de-excite from low spins, as we will see.(The time it takes the ^{148}Dy nucleus to de-excite down the whole main cascade(Fig. 4.1.1) is of the order of nanoseconds.)

2.2 The Detectors Used in the Data Acquisition

The approximately 70×10^6 events, recorded event-by-event on eight 6250 B.P.I. magnetic tapes with the ModComp Classic Computer, were taken with the Diamond/Stephens High Resolution Ge Array(Diamond, 1984). This consisted, at the time of the experiment, of 12 Compton-suppressed intrinsic Ge detectors(see Fig. 2.2.1(a))extending from about 77° to 154° with respect to the beam axis(see Fig. 2.2.1(c)). Each Ge detector was Compton-suppressed by a bismuth-ger-

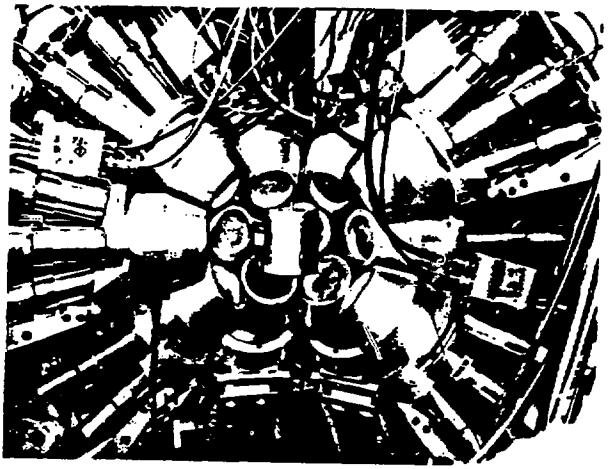

(a)

Fig. 2.2.1

(b)

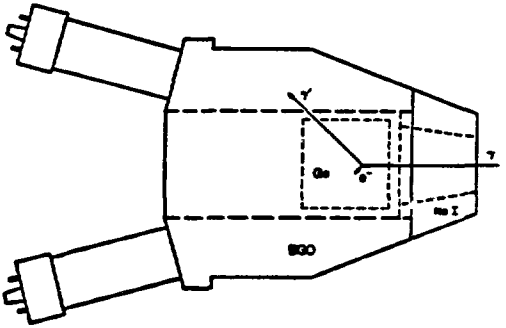

Fig. 2.2.1(c)

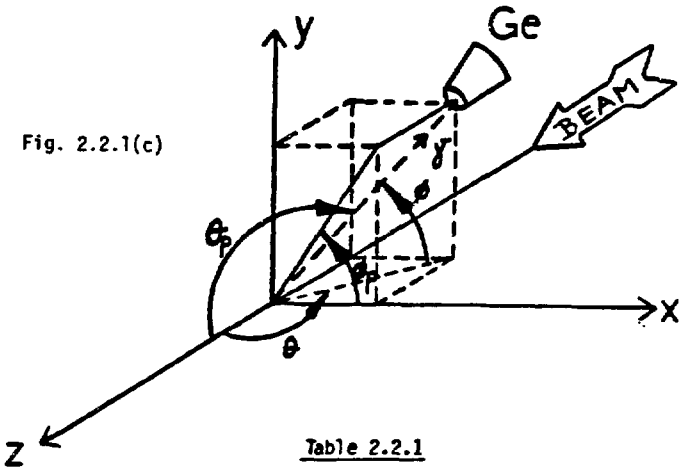

Table 2.2.1

The Ge detector angles.

Ge no.	Record'g Seq.	Angles θ	φ	θp	φp
1	1	180.0°	34.5°	145.5°	90.0°
2	4	205.7°	0.0°	154.3°	180.0°
3	3	180.0°	325.5°	145.5°	270.0°
4	7	154.3°	0.0°	154.3°	0.0°
5	5	231.4°	325.5°	120.9°	221.3°
6	6	257.1°	0.0°	102.9°	180.0°
7	2	231.4°	34.5°	120.9°	138.7°
8	8	128.6°	325.5°	120.9°	318.7°
9	9	128.6°	34.5°	120.9°	41.3°
10	10	102.9°	0.0°	102.9°	0.0°
11	12	77.1°	325.5°	79.4°	324.8°
12	11	77.1°	34.5°	79.4°	35.2°

manate($Bi_4Ge_3O_{12}$, or BGO, for short)shield, through which it viewed the target. A diagram of such a Compton-suppressed Ge is showed in Fig. 2.2.1(b), which shows two of the six phototubes belonging to its BGO shield, as well as a simple diagram of the Compton scattering taking place in the Ge . Table 2.2.1 gives the positions of the 12 Ge's in terms of the angle θ and azimuthal angle ϕ, as well as the polar angles θ_p and ϕ_p. Also given in this table is the sequence in which the firing Ge's were recorded on tape for each event.

When completed, the High Resolution Array will consist of a nearly 4π ball of 40 BGO sectors surrounding 20 Compton-suppressed(as described above) intrinsic Ge detectors aranged in three rings. In Fig. 2.2.1(a) we can see the three rings, one in the median plane, one in the plane above it and the third in the plane below, each plane with only four detectors at the time. One can also see some of the phototubes of the BGO shields. This inner castle of BGO sectors will act as a 4π sum spectrometer with an energy resolution and efficiency almost as good as for the larger NaI balls. Since it has a smaller number of detectors than larger NaI balls, the present BGO ball will have worse multiplicity resolution. The high density of BGO(7.13 g/cm^3) by comparison to NaI, enables one to achieve such a compact arrangement as the present set-up.(See Diamond, 1984 for details.)

Germanium detectors offer a unique combination of energy resolution and efficiency for γ-ray discrete spectroscopic studies. It takes about 2.96 eV to create a charge carrier(a electron-hole pair) at 77°K.(Ge detectors must be cooled(usually at 77°K with liquid nitrogen) in order to minimize the thermal noise current whose amplitude depends

on the absolute temperature T like $T^{3/2}\exp(-E_g/2kT)$; E_g is the band-gap energy:0.75 and 0.67 eV at 0° and 300°K, respectively(Knoll, 1979).) This means that, e.g. a 60 keV γ-ray will create about 20,000 such electron-hole pairs, or carriers. In a Tl-activated NaI crystal only about 8 keV of the γ-ray will be converted by the scintillator (usually with an efficiency of about 13 percent) into visible light with a 4 eV average photon energy, thus producing only about 2,000 scintillation photons per pulse. Allowing for some light loss at crystal surface and crystal-phototube interface, only about 1,500 such photons will reach the photocathode. Assuming a reasonable 20 percent average quantum efficiency of the photocathode over the entire scintillation spectrum, only 300 photoelectrons will be produced. This is the minimum number in the signal chain since subsequent photomultiplier stages will multiply this number. It is this minimum number of photoelectrons which determines the resolution of such a NaI(Tl) detector, namely $R \approx 2.35/(300)^{1/2} \approx 14$ percent, for the 60 keV γ-ray detected. Sources other than statistical can worsen the resolution of a NaI(Tl)(e.g. non-uniformity in light collection, non-linearity of the NaI(Tl) scintillation response, etc; see Knoll, 1979). High quality NaI(Tl) scintillators(coupled to modern P.M.T.) can offer energy resolutions of 6-7 percent at 0.662 MeV(^{137}Cs). Some of the NaI(Tl) counters routinely used in "continuum" experiments at L.B.L. have been known to offer resolutions of around 9 percent at 1.17 MeV (^{60}Co).

When one deals with Ge detectors, the pulse amplitude will fluctuate due to the inherent statistical variation in the number of

electron-hole pairs(aside from other sources, such as incomplete charge collection or electronics following the Ge, for whose treatment the reader is referred to Knoll(1979)). Assuming Poisson statistics, the standard deviation in the number of such charge carriers will be the square root of the mean number produced. However, the Poisson model holds if all events along the track of the ionizing particle were independent, and thus predicts that the variance in the total number of electron-hole pairs is equal to the total number of such pairs produced, i.e. E_γ/ϵ . In order to adjust for departures from such an ideal process, one should use an adjustment factor, called the Fano factor, F, (Knoll, 1979), relating the observed variance to the Poisson-predicted variance(i.e. F = (observed statistical variance)/(E_γ/ϵ)). Thus, the energy resolution for a Ge detector will actually be $R = 2.35F/(E_\gamma/\epsilon_{\ carrier})^{1/2}$). An improvement factor of around 50 is found in resolution of a Ge detector over NaI(Tl) for the E_γ used in the example above, using an F = 0.12 at 77°K (Knoll, 1979). The pure(intrinsic n-type) Ge detectors used in this experiment were able to achieve resolutions of better than 0.20 percent at the ^{60}Co energies, which translates into an average resolution of about 2 keV at 1 MeV.

Such high-resolution in-beam γ-ray spectroscopy can be spoiled by the Doppler broadening of the peaks. Approximately, such width is given by the following expression :

$$(\Delta E_\gamma^0/E_\gamma^0) = (v/c) \sin\theta \sin\phi \quad , \qquad (2.2.1)$$

where v is the velocity of the emitting nucleus, θ is the angle between the recoil velocity and the γ-ray emission, and ϕ is the opening angle of the γ-ray detector. In the worst case, one has $\theta = 90^\circ$ and $\phi \sim 20^\circ$, and with a projectile like ^{40}Ar at about 180 MeV lab energy, one has $v/c \sim 2.5$ percent, which gives $\Delta E_\gamma^0/E_\gamma^0 \sim$ 1 percent, or $\Delta E_\gamma^0 \sim 10$ keV at 1 MeV, which is about five times the Ge resolution mentioned above. Fortunately, this serious problem is avoided if the γ-rays are emitted after the time that it takes the recoiling nucleus to stop in the Pb foil backing the target. As we saw earlier that time is of the order of 1 psec, and the ^{148}Dy nucleus and other nuclei near closed shells have been known for some time to have de-excitation times much longer than 1 psec.(Their non-collectivity implies enhanced single-particle nature of their excited states, thus transition rates slower by factors of 100-200 over collective transitions(proceeding with lifetimes of ~ 1psec); see chapter 1.). For $^{144,146,148,150}Gd$, $^{148,150,152,154}Dy$ and $^{152,154,156,158}Er$, i.e. nuclei just above the $Z = 64$, $N = 82$ double closed shell, it is expected that essentially all discrete γ-rays are emitted after the respective recoiling product nucleus stops in Pb. Thus, the experimental resolution is around 2 keV at 1 MeV .

For γ-ray spectroscopy, germanium is superior to silicon. Its Z number(32 vs 14,respectively) offers better photoelectric absorbtion (which varies like Z^{4-5}/E_γ^3). Also, Ge offers a slightly lower energy per electron-hole pair(2.96 vs 3.76 eV, respectively, at 77°K).

2.3 The Quality of the Data Acquired with the Pure-Ge Array

The germanium detectors thus offer a rather unique combination of energy resolution and efficiency which is quite an asset for γ-ray spectroscopic studies. Since they are almost never very large, there is a high probability that a Compton-scattered γ-ray will escape from the detector, so that only a fraction of the incident γ-ray energy will actually be deposited in the detector. One gets a poor peak(full energy)-to-total area ratio(P/T), which is about 0.20 for a 1.33 MeV γ-ray for a germanium detector of about 2" diameter by 2" thick and about "20 percent"(the 20 percent is relative to the peak efficiency of a 3" X 3" NaI(Tl) detector for 1.33 MeV γ-rays)(see Fig. 2.3.1).

Table 2.3.1(a) shows that for a γ-γ coincidence spectrum only 4 percent of the events are full energy - full energy(P^2), and thus interesting to analyze, being obscured by the other 96 percent "garbage" events which waste the storage space. For γ-γ-γ, or triple coincidences, the situation is a lot sadder: 99.992 percent of the events are "garbage", obscuring 0.8 percent of the events which are interesting(P^3); still worse, for the quadruples, only 0.16 percent of the events are useful(P^4), while the "garbage" accounts for more than 99.998 percent of the total events. In this experiment, we will not, however, be interested in coincidences higher than doubles, because of statistics problems, as transpires from Table 2.3.1(b),

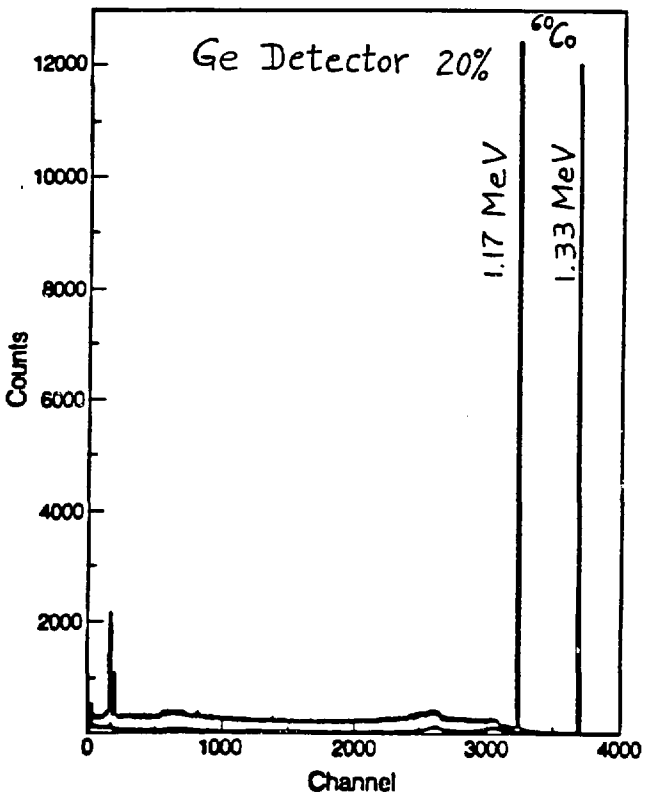
Ge Detector 20%
60Co
1.17 MeV
1.33 MeV
12000
10000
8000
6000
4000
2000
Counts
0
1000
2000
3000
4000
Channel

Fig. 2.3.1

Table 2.3.1

Ge Detector 20 percent(of 3" X 3" NaI at 1.33 MeV)

(a)

	Ge	Ge^2	Ge^3	Ge^4
PEAK/TOTAL	0.2	0.04	0.008	0.0016
COMPTON-SUPPRESSED PEAK/TOTAL	0.5	0.25	0.13	0.06
IMPROVEMENT	2.5	6	16	39

(b)

10^5 Triggers/sec Counts/sec

Days to collect 50 X 10^6 events

$M_\gamma = 20$	Ge^2	Ge^3	Ge^4
5 Detectors	870	25	0.35
12 cm	0.7	23	4.5 yrs
12 Detectors	4700	450	29
12 cm	0.12	1.3	20
21 Detectors	11000	2200	280
12 cm	0.05	0.25	2.1

discussed shortly below. In order to increase the proportion of useful(full energy coincidences) events over the remaining unnecessary events (which account for peak - Compton, Compton - peak and Compton - Compton coincidences) a scintillation material(BGO elements in our set-up) was used to surround the Ge detector, so that the γ-rays scattered out of the Ge detector can be detected in the scintillator and used in anti-coincidence modules to veto the partial-energy pulse left in the Ge detector. While this solution is only partial, Table 2.3.1(a) shows how dramatic the (P/T)'s improve: from a P/T of 0.50 for a single event to a $(P/T)^2$ of 0.25 for a double, to a $(P/T)^3$ of 0.13 and a $(P/T)^4$ of 0.06 for triples and quadruples, respectively. These numbers translate into improvement factors(over the non-Compton-suppressed case) of 2.5, 6, 16 and a whopping 39 for singles, doubles, triples and quadruples, respectively. Impressingly enough, the double-coincidence spectra(of particular interest in the present work)contain, with Compton-suppression on, about 25 percent more useful events(i.e. P^2)than the non-Compton-suppresed single spectra have(i.e. P).

As far as the rates of coincidence events are concerned, they are affected principally by two factors: distance between source and detectors and number of detectors. One usually selects the minimum desirable distance at the point where summing effects, or pile-up(simultaneous arrival of two coincident γ-rays in the same detector) are in excess of the maximum tolerable value of about 10 percent. For average γ-ray multiplicities of about 20, this gives an upper limit of about 0.5 percent for the efficiency and

a lower limit of about 13 cm for the distance to source, for a 20 percent Ge detector. Going farther away than this will mean a sizeable loss in statistics for doubles, since they fall off as the fourth power of the average distance between detector and source. The small size of the BGO shields making up the anti-Compton suppressors allowed the 12 Ge detectors used in the run to fit around the source at a distance of about 13 cm. Approximately, the rates for doubles go up as the square of the number of detectors, for triples as the cube and so on, and the Table 2.3.1(b) shows that with only 12 detectors we had doubles coming in at only about 42 percent the rate one would have with all 20 Ge's . The calculations are based on production of about 10^5 compound nuclei(or "triggers")per second, and with an average γ-ray multiplicity of about 20. The numbers below the rates (in parantheses)represent the days it would take to collect about 50 X 10^6 events, which would fit on about five 6250 B.P.I. magnetic tapes. It would take less than half the time with the completed ball to take the same number of doubles as it did with the 12 Ge's, and less than a fifth of the time for triples! In calculating all the rates shown in Table 2.3.1(b), use was made of the following approximate expression for the probability, $P_{M,N,p}$, of detecting p-fold coincidences with N detectors, assuming an average γ-ray multiplicity of M :

$$P_{M,N,p} = \binom{M}{p}\binom{N}{p}p!\Omega^p[1 - (N - p/2)\Omega]^{M-p} \qquad (2.3.1)$$

where Ω is the total efficiency(above 300 keV) of a Ge detector used,

and which was taken to be about 2×10^{-3} .(See Diamond and Stephens, 1984.)

The impressing numbers for the rates for high-order coincidences(doubles, triples, etc) displayed in Table 2.3.1(b) are important because of the effective resolution problem. For a single detector, one defines the energy resolution as the inverse of the number of resolvable points below a certain peak. For example, (Stephens, 1984), a 2 keV resolution at 1 MeV(the case for our Ge detectors)gives one about $1/500 = 2 \times 10^{-3}$ for such energy resolution, in such a one-dimensional case. For a two-dimensional matrix one has $(500)^2$ resolvable points, giving an effective resolution of 4×10^{-6} , while for triple coincidences this value becomes 8×10^{-9} . This analysis says, essentially, that two γ-rays of identical energy, while being unresolved in one dimensional analysis, will have very different coincident relationships, and thus, they will be easily resolved in two-dimensional analysis.

In general, the higher the order of coincidences analyzed(i.e., the higher the dimensionality of the coincidence matrix), the higher the number of γ-rays of identical energy which can be easily resolved. To illustrate with an example, if one has N unbranched rotational bands, each with about 20 γ-rays spread over about 1 MeV, one has about $N(20)^2$ doubles(D). Since there are $(500)^2$ resolvable doubles(D_r) in the sub-matrix 1 MeV X 1 MeV, one has

$$D/D_r = N/(25)^2 \sim N \times 1.6 \times 10^{-3} \qquad (2.3.2)$$

For the one-dimensional(singles) case the value above becomes N X X 4 X 10^{-2}, which tells us that, for only 2 bands, a little less than 10 percent of the resolvable points are used-up, while for the two-dimensional case (doubles) it would take about 60 such bands to use-up about 10 percent of the corresponding matrix.(Similar calculations give about 2,000 bands for triples !.)

2.4 Experimental Set-Up

A diagram of the electronics set-up is shown in Fig. A.1(in the appendix). As we can see from it, each event written on tape consisted of at least 5 parameters: at least 2 Ge's, one RF - Ge TAC, one Ge - Ge TAC and a Ge Tag Word. The events were of variable length, since parameters with zero-channel values were skipped by hardware("zero-skip mode").

Two TAC's were used in this experiment in the hope of providing life-time information. The RF - Ge TAC gave the time between the arrival of the beam burst relative to the phase of the cyclotron RF(which is also the time the compound nucleus ^{152}Dy is formed)and the time when the second Ge fired(i.e. the later of the coincident pair of γ-rays). As far as the time scale dealt with in the present work(nanoseconds) is concerned, the time of formation of the compound nucleus is the same as the time when the γ-ray decay starts, since the nucleus exhausts all excitation options down to the γ-ray entry

line(see chapter 1) in about 10^{-15} seconds. Between this time and compound nucleus formation only fission and particle emission dominate. A Ge majority box(a "Multiplicity Logic Unit"), set to fire only when at least 2 inputs(2 Ge's) were present, provided the start of the RF - Ge TAC, while the RF(present all the time) provided the stop. The same Ge majority box provided the start for the Ge - Ge TAC, whose stop was supplied by the output of the Ge "OR" unit(which provided an output if any one Ge fired). Thus, the Ge - Ge TAC essentially gave the distribution of times elapsed between the 2 γ-rays in the coincident pair.(If more than 2 γ-rays were detected, the Ge - Ge TAC only gave the distribution of elapsed time between the first 2 γ-rays, since the "OR" unit fired when the first γ-ray was detected while the majority box fired when the second γ-ray was detected.)

The Ge Tag Word put out a bit which represented the label of the second (or later) Ge detector. A unit pulse was thus created in a channel number equal to 2 raised to the power equal to the total number of Ge's(i.e. 12) minus the Ge label in question. This Tag Word, when associated with the Ge - Ge TAC can give potential information about the ordering of the 2 coincident γ-rays in question. However, this is true only when the time between such 2 γ-rays is more than the resolution of the Ge - Ge TAC, which is about 5 nsec(FWHM), as we will see in chapter 5.

No such delays among coincident γ-rays were found in ^{148}Dy above the 480 nsec 10^+ isomer(with the possible exception of the 327.2 keV transition; see section 5.2). This indicates that all the transitions above that isomer are prompt with respect to one

another(within about 7 nsec, according to the analysis in section 5.2). The same holds true for the transitions below that isomer, with the exception of the 86.9 keV transition relative in time to the other 10 transitions which are obtained after the 86 nsec(Haas et al, 1981, Julin et al, 1982(p.78) and Ward et al, 1983) 8^+ level decays. However, as we will see in section 5.2, poor statistics(in the present run)prevents one from obtaining a believable value for the lifetime of that level.

Chapter 3

The Analysis

The $^{40}Ar + ^{112}Cd$ reaction(Q = -55.5 MeV) at 175 and 185 MeV lab energy made $^{*152}Dy$ compound nuclei with excitation energies of ~ 73.5 and ~ 80.8 MeV, respectively. For the two bombarding energies, the maximum angular momentum brought into the compound system(see chapter 1) is ~ 56 and 70ħ, respectively. The 4 neutrons remove a negligible amount of angular momentum (~ 3-4ħ), and thus, states with very high spins(~ 52-53 and ~ 66-67ħ, respectively) are populated in the residual ^{148}Dy. The 4 neutrons each carry, however, about 12 MeV of binding plus kinetic energy, thus leaving the high-spin states in ^{148}Dy with about 25.5 or 32.8 MeV of excitation, respectively.

3.1 The Sorting of the Data

The data were sorted in the format of 3 two-dimensional E_γ vs E_γ coincidence spectra(each 2048 X 2048 (channels)^2), one for each of the 3 RF - Ge TAC slices(gates), as shown in Fig. 5.2.2 . The energy calibration being 1.199 keV/channel(zero intercept)(as

deduced from ^{152}Eu calibration; see the appendix), each one of the 3 E_γ vs. E_γ spectra spanned nearly 2455 X 2455 (keV)^2 of the two-dimensional space of γ-γ coincidences. Fig. 3.1.1 shows a "bird's eye" view of such a two-dimensional Ge X Ge spectrum.

In addition, a two-dimensional spectrum of RF - Ge TAC vs E_γ was constructed, wherein there were incremented points of coordinates (E_γ,RF - Ge TAC channel), where E_γ refers to the at least 2 coincident Ge's present in each event. The size of this spectrum was 2048 X 512 (channels)^2. A later sorting was done whereby a two-dimensional spectrum of Ge - Ge TAC vs E_γ(see Fig. 5.2.11 for a full projection on the TAC axis) was constructed for all the γ's in coincidence with the 1061.1 keV transition(the one right above the 480 nsec isomer), and also in coincidence with the RF - Ge TAC slice 1(the prompt peak). A similar spectrum was constructed for the 660.8 keV transition(below the 480 nsec isomer) and in coincidence with the RF - Ge TAC slice 3(the "late" gate). The size of each of these 2 two-dimensional spectra was also 2048 X 512 (channels)^2, and they were built in order to ascertain the promptness of the transitions with respect to 1061.1 and 660.8 keV transitions, respectively(and separately). The analysis of such two-dimensional spectra involving the RF - Ge and the Ge - Ge TAC's is done in section 5.2 .

This type of analysis was done for each of the two sets of data: the 175 MeV set, with about 47 million events, and the 185 MeV set, with about 23 million events(see Table 3.1.1 for the 175 MeV data). However, as it can be seen from the Table 3.1.1(b), the extra 10 MeV of lab energy(even though it enhanced the high-spin states in the 4n

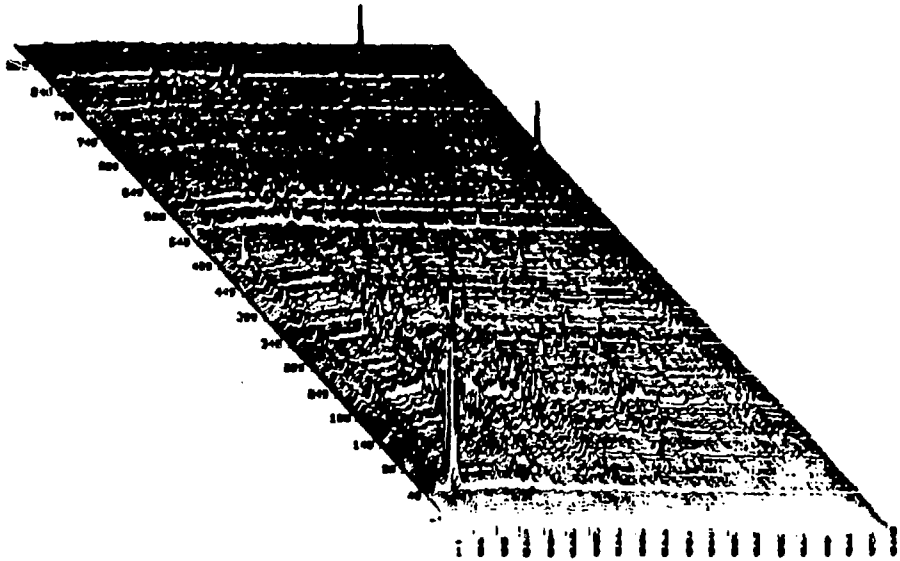

Fig. 3.1.1

Table 3.1.1

(a) The 175 MeV $^{40}Ar + ^{112}Cd$ Run with 12 Ge's

Sorting of coincidences with all detectors.

Events Record'd	RF-Ge TAC Gate 1	RF-Ge TAC Gate 2	RF-Ge TAC Gate 3	Sum of Gates 1-3	Correc-ted*	Lost Ev's
47298500	3,300,225	5,941,351	3,326,994	42,275,570	46,356,549	-2%/o

Total RF - Ge TAC counts: 44,389,349; Total Ge - Ge TAC counts: 44,200,000

Discrepancy: ~ 0.4 percent

* During the first tape, Ge no.9 drifted all throughout, and it was neglected during sorting: 12X11/11X10 = 1.20, i.e. ~ 20 percent of the 9836000 events on that tape were discarded. The RF - Ge TAC gates were adjacent, and did not cover the entire RF-Ge TAC spectrum(leaving 2,113,778 events out, i.e. not sorted in any format).

(b) P/B ratios of the first five transitions in the main band above the isomer, measured for the 175 and 185 MeV sets of data(in the full projection spectra). Energy resolution was the same for sets of data. P/B refers to heights.

E_γ(keV)		1061.1	462.7	495.8	1045.5	279.0*
P/B	175 MeV	2.05(1)	1.48(2)	1.58(2)	1.82(2)	1.58(3)
	185 MeV	1.50(7)	1.01(6)	1.11(6)	1.42(7)	1.25(7)

* Values of P/B in that column include contributions from impurities(^{146}Gd and ^{148}Tb).

Table 3.1.1 (cont'd)

(c) Sorting of coincidences for angular correlations. Comparison of statistics to all detectors case(in terms of numbers of coincident Ge pairs for given formats).

Above isomer(in coincidence with RF - Ge TAC gate 1)

Sorting Formats	No. counts	Ratio to all detectors case	Prediction*
0°- 90°	7,382,296	0.22	0.24
0°- 0°	2,991,091	0.09	0.09
90°- 90°	2,893,624	0.09	0.09

Below isomer(in coincidence with RF - Ge TAC gate 3)

	No. counts	Ratio to all detectors case	Prediction*
0°- 90°	1,042,071	0.31	0.24
0°- 0°	469,424	0.14	0.09
90°- 90°	382,333	0.11	0.09

* For the 0°- 90° case: (4X4)/(12!/2!10!)=0.24

For the 0°- 0° and 90°- 90° cases: (4!/2!2!)/(12!/2!10!)=0.09

(12!/2!10!) represents the no. of different pairs out of 12 Ge's, for example.

channel vs. the 3n one(chapter 1))brought considerably more quasi-continuum. It seems the extra temperature lifted the top of the γ-ray cascade to points in the (E^*, I) space(see chapter 1) from where considerably more numerous paths of γ-ray de-excitation are available.This is evidenced by the considerably poorer peak-to--background ratio(P/B) for the 185 MeV set of data than for the 175 MeV one. Such being the case, further analysis of the 185 MeV data was abandoned, and all efforts were concentrated in analyzing the 47 million events of the 175 MeV data, due to its much better quality(i.e., P/B) and statistics.

The possibility of sorting the triple(Ge^3) events, while attractive because of the cleanliness of the ensuing spectrum, was not deemed feasible due to poor statistics(see Table 2.3.1(b), which shows the triples were only about 10 percent of the doubles !). The ~ 5 million "triple" events would have given us statistical fluctuations more than 3 times worse than for the doubles.

The sorting was done with the "EVA5" version(Belshe, 1984) of the EVAL Program(Holm, 1979), which also enabled the user to closely monitor the incrementing of counts in each of the 12 single Ge spectra, for the purpose of making all 12 detectors have the same peaks as closely aligned as possible. The degree of such peak alignment in all 12 detectors was better than 25 percent of the FWHM of peaks at ~ 1 MeV.

The data were also sorted in angular correlation format(see Table 3.1.1(c)) : 4 detectors at $\theta \approx 180^\circ$ and 4 detectors at $\theta \approx 0^\circ$(see Table 2.2.1), with respect to the beam axis, respectively,

were chosen, and the former were incremented along the x-dimension while the latter along the y-dimension of a two-dimensional 2455 X 2455 $(keV)^2$ spectrum. In addition to this 0°- 90° format, the data were also sorted in the 0°- 0° and 90°- 90° formats, each in a 2455 X 2455 $(keV)^2$ matrix, whereby there were incremented coincidences between any 2 Ge's in the backward direction, and coincidences between any 2 Ge's at 90°, respectively. These last two matrices were constructed because, as we will see in section 5.2, they provide results more sensitive to multipolarity for cases when the two coincident γ-rays carry the same angular momentum, while the 0°- 90° format provides results more sensitive to multipolarity for cases when the 2 γ's carry different angular momenta.

The angular correlations results(in all the above 3 formats) were found to be more or less isotropic for the transitions below the 480 nsec isomer(see section 5.1). This was mainly caused by the paramagnetic relaxation effects(hyperfine fields created in the target material during the reaction) which tend to destroy the orientation of the nuclear spins populated in the reaction. Therefore, as far as the 11 transitions below the 480 nsec isomer were concerned, we had to use the (I,π) assignments made in previous works on ^{148}Dy, involving linear polarization and conversion electron measurements(Haas et al, 1981 and Julin et al, 1982(p.78)).

3.2 The RF - Ge Time Distribution of the Coincident Gamma-Rays

The present work seems to agree with the (I,π) assignments of the 1061.1, 495.8, 1045.5, 462.7, 279.0, 763.4 and 1170.5 keV transitions above the 480 nsec isomer, within experimental error. The 11 transitions below that isomer were oberved with a much better P/B when the gate on the RF - Ge TAC was the one marked 3 in Fig. 5.2.2, while just the opposite is true for the approximately 34 transitions(including the 19 new ones observed in this work) above the 480 nsec isomer, which clearly have the best P/B for the RF - Ge TAC gate 1(the "prompt" gate). The gate 3 corresponds to coincident transitions taking place much later after the compound nucleus formation than the "prompt" transitions in gate 1. The time scale in Fig. 5.2.2 increases right to left(just like all TAC figures). As the figure indicates, the prompt peak has a FWHM of about 9 nsec(while the width of gate 1, actually used in sorting, is about 11 nsec), and is symmetric, within about 1 nsec, with respect to the line marking the centroid. In order to show this, the base of the "prompt" peak was chosen to be the second horizontal line from the bottom of Fig. 5.2.2, and this is probably the best line one can choose such as the regions L and R are nearly the same, area- and shape-wise. One can see that L still includes mostly prompt transitions, just like R, however, lowering the second horizontal line below where it was chosen, makes rapid inclusion of "tail", or late, transitions, very

much different than the ones in R .

All of the transitions above the 480 nsec isomer are time-distributed within an interval of about 7 nsec, after quadratically subtracting the jitter of the beam pulse relative to the RF(~ 6-7 nsec(Diamond, private communication)) from the experimental value of 9 nsec. Since the nuclear γ-decay and cyclotron-RF jitter are independent phenomena, the respective widths they introduce in the time distribution of the transitions detected can roughly be added quadratically. Since the the RF - Ge TAC spectrum for the 1061.1 keV transition(placed at the bottom of the "prompt" cascade, just above the 480 nsec isomer, in the present work) seems to have the narrowest(FWHM ~ 7.5 nsec;see Fig. 5.2.3) and most symmetrical prompt peak(with very little, if any, tail), it was chosen as the "prompt reference", i.e. with respect to which the RF - Ge TAC spectra for all the other transitions above the 480 nsec isomer will be analyzed (see section 5.2).

3.3 Method for Analyzing Discrete Coincidence Spectra

In order to establish the γ-ray decay scheme of ^{148}Dy, prompt γ-γ coincidences were analyzed. Cuts(gates) were placed on the x-dimension of the symmetrized 2455 X 2455 (keV)^2 two-dimensional matrix(in coincidence with the given RF - Ge TAC gate), on γ-ray peaks(foreground), as well as on backgrounds(quasi-continuum) on both

sides of the respective γ peaks(see Fig. 3.3.1, for example). Fig. 3.3.2 shows the spectrum obtained from projecting(or collapsing) all the rows, from 20 to 2000(i.e. from 24 to ~ 2400 keV) in the prompt coincidence two-dimensional $E_\gamma X E_\gamma$ matrix, onto the x-axis of that matrix. Various impurities are indicated in the figure caption, as well as the reaction channels to which they belong, together with their relative proportions. One can also see that the transitions below the 480 nsec 10^+ state isomer are markedly suppressed in their intensities, relative to the transitions above that isomer. Comparisons of intensity ratios of a representative transition below the isomer to one such transition above the isomer, to ratios of pertinent RF - Ge TAC gates areas, are depicted in Table 3.3.1 . The spectra in coincidence with background gates were averaged, and normalized to the number of channels used in the gate on the γ-ray peak, and then subtracted, channel-by-channel, from the spectrum in coincidence with the γ-ray peak of interest.(See Fig. 3.3.1 for placing such gates.)

The spectrum depicted in Fig. 3.3.3 was obtained in the same way as Fig. 3.3.2, only it represents the full projection of the two-dimensional coincidence matrix in coincidence with the RF - Ge TAC gate 3(the delayed gate), showing the transitions above the 480 nsec isomer appropriately reduced in P/B(and intensity). If one follows the P/B of the 1061.1 keV transition from Fig. 3.3.2 to 3.3.3 ,by way of the similar spectrum in coincidence with RF - Ge TAC gate 2(not shown here), one notices the reduction in the P/B numbers: 8.05(1)/1.13(2)/0.75(3), respectively.

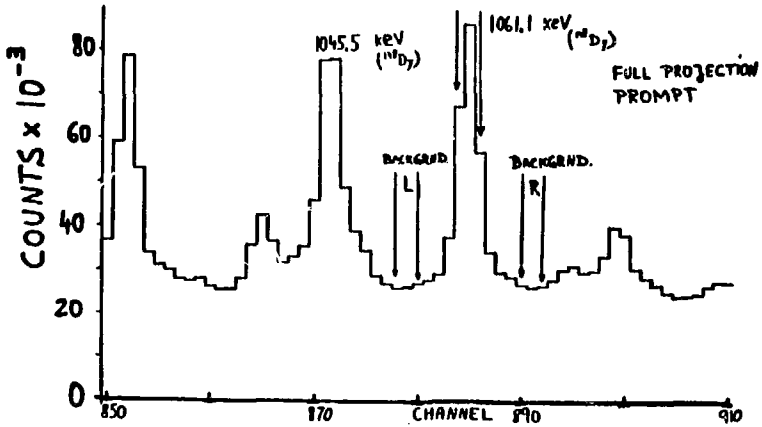
COUNTS x 10^-3
80
60
40
20
0
850
870
CHANNEL
890
910
1045.5 keV
(160Dy)
1061.1 keV
(160Dy)
FULL PROJECTION
PROMPT
BACKGRND.
L
BACKGRND.
R

Fig. 3.3.1

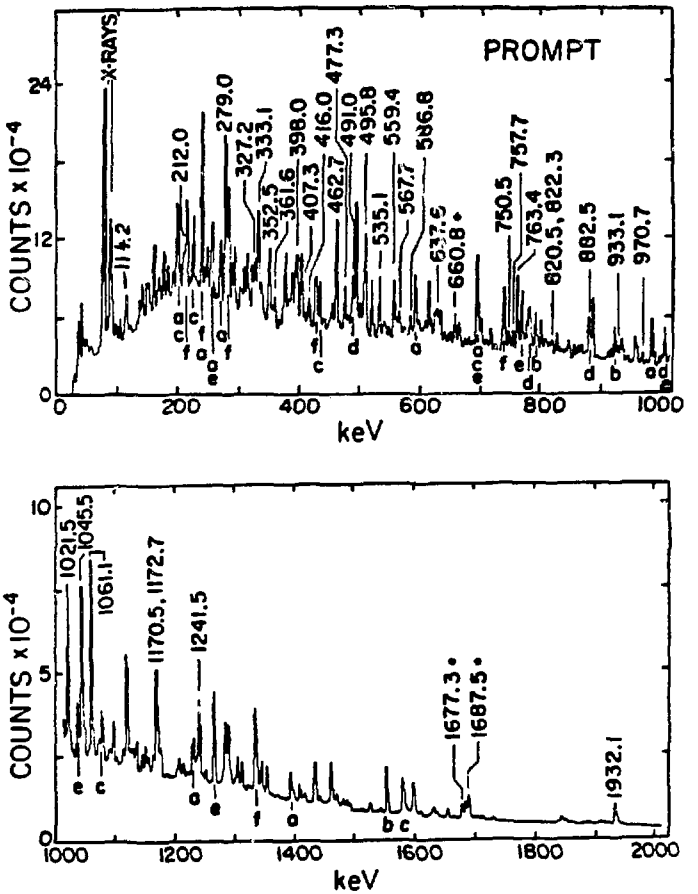
PROMPT
X-RAYS
COUNTS x 10⁻⁴
keV
114.2
212.0
279.0
327.2
333.1
352.5
361.6
398.0
407.3
416.0
462.7
477.3
491.0
495.8
535.1
559.4
567.7
586.8
637.5
660.8*
750.5
757.7
763.4
820.5, 822.3
882.5
933.1
970.7
1021.5
1045.5
1061.1
1170.5, 1172.7
1241.5
1677.3*
1687.5*
1932.1

Fig. 3.3.2

Table 3.3.1

Comparisons of ratios of intensities of transitions(above and below the isomer;see below) to ratios of areas of "prompt" to "delayed" RF-Ge TAC gates.

	Intensity of the transitions (keV) 1687.5	1061.1	Ratio of intensities of the transitions 1061.1 keV to 1687.5 keV transition	Ratio of areas of RF-Ge TAC Slices 3/1 Un-nor/nor*	Ratio of RF-Ge TAC slice 1 FWHM/Width to isomer life-time
(a) — Gate on the 660.8 keV transition(< isomer)					
	35690 ±195	1400 ±150	3.93×10^{-2} $\pm .42 \times 10^{-2}$	$10\times10^{-2}/6\times10^{-2}$	$2.08/2.92\times10^{-2}$
(b) — Sum of gates on 1061.1, 462.7, 495.8, 1045.5 and 279.0 keV transitions (>isomer)					
	096.9 ±70	5927.5 ±86	15.1×10^{-2} $\pm 1.2 \times 10^{-2}$	$10\times10^{-2}/6\times10^{-2}$	$2.08/2.92\times10^{-2}$

* normalized(or not) to same no. of channels as in RF-Ge TAC slice 1.

"<" and ">" refer to transitions below and above the isomer, respectively.

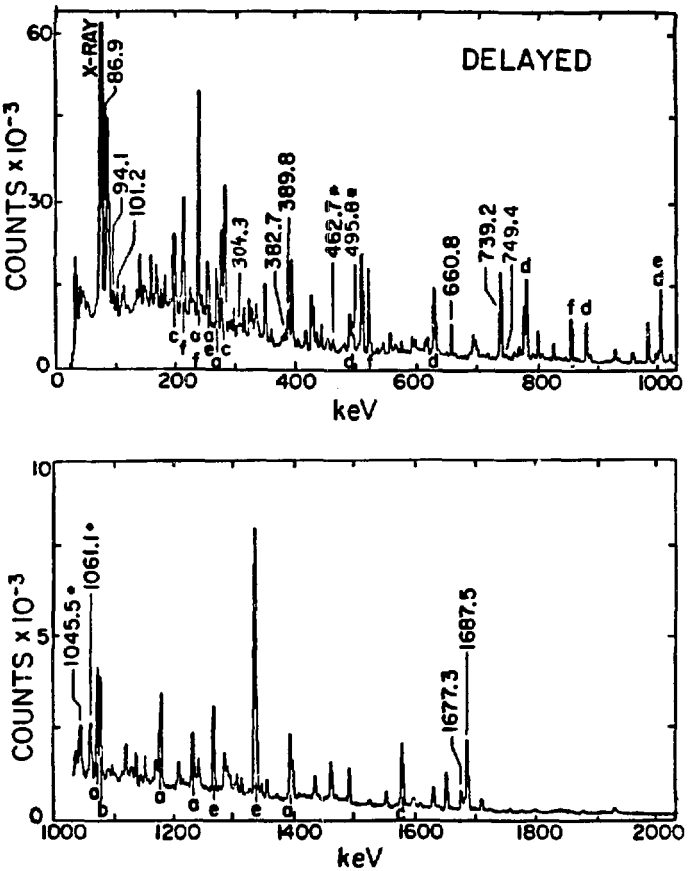
DELAYED
X-RAY
86.9
94.1
101.2
304.3
382.7
389.8
462.7*
495.8*
660.8
739.2
749.4
COUNTS x 10⁻³
keV
1045.5*
1061.1*
1677.3
1687.5

Fig. 3.3.3

The technique of analyzing spectra in coincidence with discrete transitions is rather simple. The spectrum in coincidence with a given γ line(after proper background subtraction, as discussed above) should not return that given γ line, but all the others in coincidence with it; the lines below it in the level scheme(allowing for possible branching, $W(\Omega)$, and electron conversion) should appear with equal intensities(also the intensity of the transition gated on), while the γ's above such transition in the level scheme(again, allowing for possible branching) should appear with their own, rather smoothly decreasing intensities. This is so, because in order to de-excite from the state from which the transition gated on comes, the nucleus can only follow the band(if there are such bands) to which the transition above belongs, or bands which branch out below that transition. Data for gates placed on transitions de-exciting from higher-spin levels show that the continuum is more intense at higher spins.

3.4 Ge Relative Efficiency

In order to obtain transition intensities, one needs the γ-ray intensity and the corresponding electron conversion coefficients. The total absolute efficiency of the Ge's as a function of E_γ was needed to obtain the γ-ray intensities. This total absolute efficiency is $\epsilon_{abs} = \epsilon_{int} * (\Omega/4\pi)$ (Ω being the solid angle subten-

ded by the detector), where ϵ_{int} is the total intrinsic efficiency, which is defined as ϵ_{int} = (no. of pulses recorded)/(no. of γ's incident on the detector). Therefore, ϵ_{abs} = (no. of pulses recorded in peak)/(no. of γ's emitted from the Pb-backed target during the reaction). Both ratios above are on an event-by-event basis. We speak of "total" efficiency, such as for the two above, since they are meant to include effects due to the absorbers(made of Sn and Ag backed by Cu(to absorb the Sn and Ag X-rays)) which covered the entrance window of each Ge in order to remove low energy back-scattering.

Following the run, a ^{152}Eu source(E_γ = 122, 245, 344, 444, 689, 779, 868, 963, 1086, 1112 and 1408 keV; see Lederer et al, 1978)replaced the ^{112}Cd target, and double coincidences in the form of histograms were recorded on tape. Subsequent analysis of the ^{152}Eu γ-ray intensities done for 4 Ge's, randomly chosen, gave a total relative efficiency(all we need is to compare γ-ray intensities to each other(after being corrected for conversion)) curve of the shape $\epsilon_{rel} \sim E_\gamma^{-0.791}$, for E_γ > 245 keV. Below 245 keV, the 122 keV point from the ^{152}Eu run together with the ^{133}Ba data (taken with similar Ge's) give an efficiency which varies $\sim E_\gamma^2$ between 80 - 120 keV, and $\sim (E_\gamma)^{1/2}$, between 120 - 160 keV(Fig. 3.4.1).(The 80, 82 and 162 keV points from ^{133}Ba, together with the 122 keV point from ^{152}Eu, were used to find the shape of the efficiency below 160 keV, where it curves downwardly, due to the absorbers placed on the front of the Ge's.) The ^{133}Ba data(Lederer et al, 1978) was taken from a different run involving the same kind of Ge's and was normalized such that the line obtained from a least

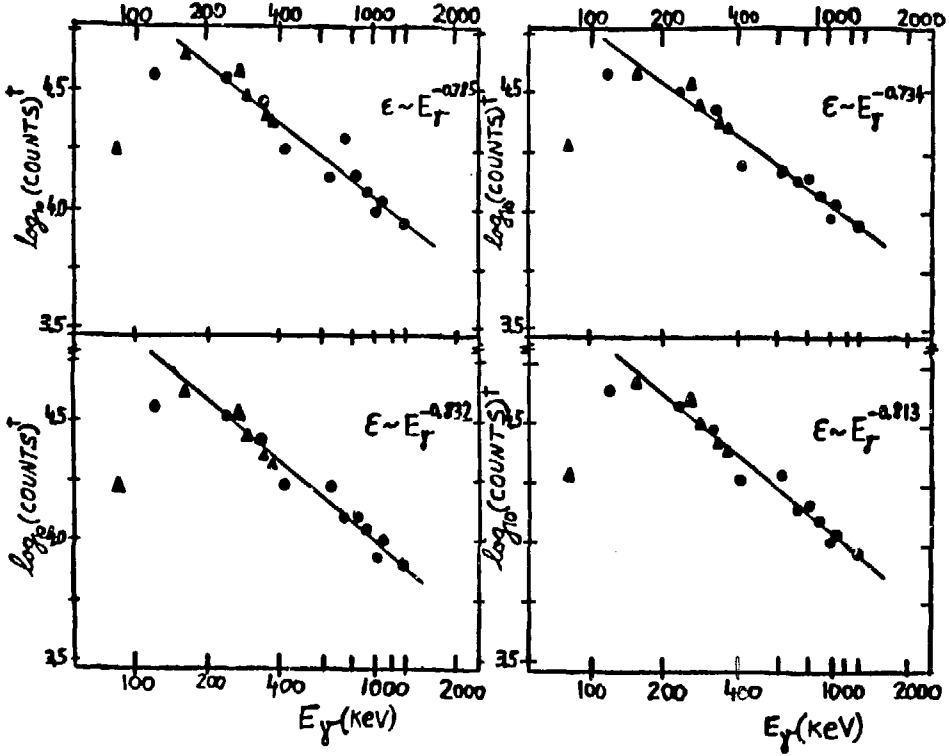
$\varepsilon \sim E_\gamma^{-0.715}$
$\varepsilon \sim E_\gamma^{-0.734}$
$\varepsilon \sim E_\gamma^{-0.832}$
$\varepsilon \sim E_\gamma^{-0.813}$
$\log_{10}(\text{COUNTS})^{\dagger}$
E_γ(KeV)
100
200
400
1000
2000
4.5
4.0
3.5

Fig. 3.4.1

squares fit to the 276, 303, 356 and 384 keV points coincidded with the line $E_\gamma^{-0.791}$ obtained from ^{152}Eu.

Inspection of the ^{152}Eu data revealed that absorbtion started to set in at about 160 keV. The ^{152}Eu data, taken in the same run with the ^{133}Ba data, showed the 122 keV point to lie in the same relation to the other points(see Fig. 3.4.1(a)) as it does for the ^{148}Dy run(Fig. 3.4.1). The arrows departing from the numbers 1, 5, 6 and 10 in Fig. 3.4.1(a), indicate where the 122 keV point lies with respect to the other points from ^{152}Eu, for Ge's 1, 5, 6 and 10, respectively. The ^{152}Eu E_γ's above 245 keV, taken with this latter run gave an exponent of -0.793, remarkably close to the average exponent obtained from Fig. 3.4.1(even though different Ge's were involved in different completion stages of the BGO Ball).

The four log-log plots of the relative efficiency vs E_γ (see Fig.3.4.1), show that, on the average, the 122 keV point lies within the scatter of the other points with respect to the best line drawn. Therefore, one could take $\epsilon_{rel} \sim E_\gamma^{-0.791}$ for $E_\gamma > 122$ keV, without making a large error. However, in the light of the discussion above, a compromise was reached to have the efficiency decrease like $E_\gamma^{-0.791}$ from 160 keV on. The exponent 0.791 is the average of the values indicated on the four plots in Fig.3.4.1(error in 0.791 is about 0.025), and Fig. 3.4.2 shows the shape of the average relative efficiency curve thus found and used in the present work. It was not necessary to do this relative efficiency analysis for all 12 Ge's: in the event that they were not similar, one could only use an average value of the relative efficiency closest to only two detec-

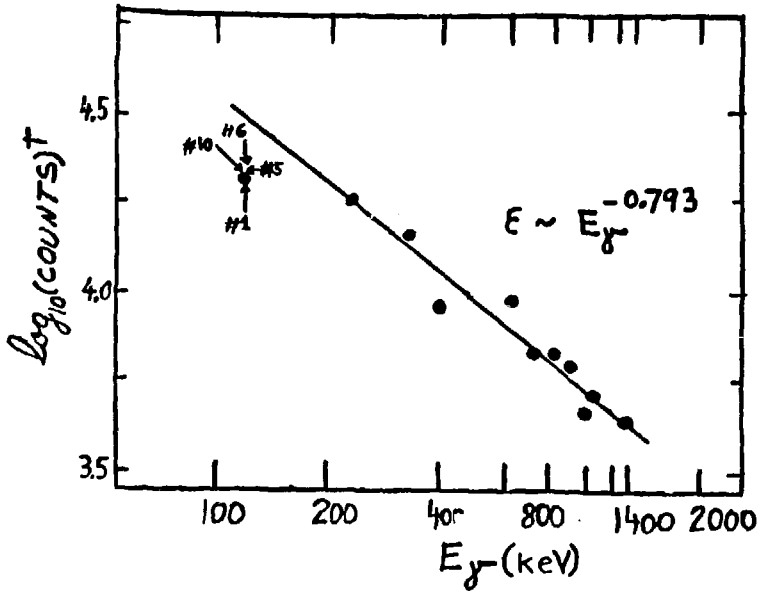
4.5
4.0
3.5
$\log_{10}(\text{COUNTS})^{T}$
#10
#6
#5
#1
$\varepsilon \sim E_{\gamma}^{-0.793}$
100
200
400
800
1400
2000
E_{γ} (keV)

Fig. 3.4.1(a)

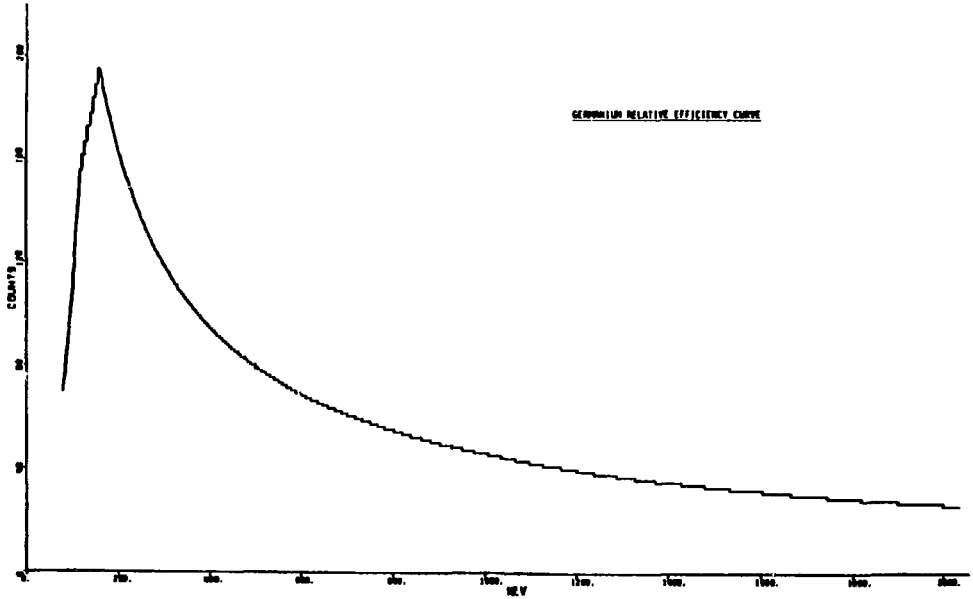

Fig. 3.4.2

tors(e.g. no. 1 and no. 10) anyway, since all possible pairs of Ge's were incremented in one and the same two-dimensional $E_\gamma X E_\gamma$-coincidence matrix.

3.5 Method for Obtaining Transition Intensities and Their Uncertainties

The integration of the γ-ray peaks is done with the help of the "FIT" routine of the spectrum analysis program "SUSIE"(see Appendix), or by direct summation of counts in the peak + background underneath and then proper subtraction of background counts. The latter method was employed whenever statistics made gaussian-fitting of the peaks (involving setting the background around the peak) noticeably inaccurate(especially in angular correlation work). The errors in such peak areas(i.e. γ-ray intensities) are calculated according to the following expression:

$$\sigma = (A_\gamma + 2N\sigma_{phys}^2)^{1/2}, \qquad (3.5.1)$$

where A_γ is the net area under the γ-ray peak in question(i.e. above the background), obtained with "SUSIE", N is the number of channels in the peak and σ_{phys} is the jitter that the quasi--continuum and the background statistics under the peak itself introduce in the number of counts) of each of the N channels

in the peak.

As we can see from Figs 3.3.1 and 3.5.1, if one goes roughly 3 times the FWHM of the peak, to the left and to the right away from the peak, one has the spectrum fluctuating greater than the statistics of any channel in those ranges(see below). In the example taken, looking at the spectrum in coincidence with the 1061.1 keV transition, after subtraction of the average of the spectra in coincidence with the two background gates shown, analysis indicates that the r.m.s.(root-mean-square) deviations of the number of counts in the channels in the L and R regions, are $\sigma_L = 53.5$ and $\sigma_R = 60.0$, respectively. These numbers were obtained according to:

$$\sigma^2 = (1/N)\sum_i [(\text{counts})_i - \langle\text{counts}\rangle_N]^2, \qquad (3.5.2)$$

where $(\text{counts})_i$ is the number of counts in channel i, and <counts> is the average of the number of counts over the N channels taken at the right and left of the peak(see Fig. 3.5.1). These numbers are about 3 times the statistics in the average typical channel, which is of the order of $\sim (400)^{1/2} = 20$.(The value of 400 is obtained by adding about 85(the average number of counts in the same channel regions in the background spectra) to about 315, which is the number of counts in a typical channel in regions R and L in the spectrum in coincidence with the foreground. This operation is necessary, since Fig. 3.5.1 represents the result of subraction of background spectra from the foreground spectrum.) While σ_L and σ_R are about the order of the statistics in such average typical channel for the

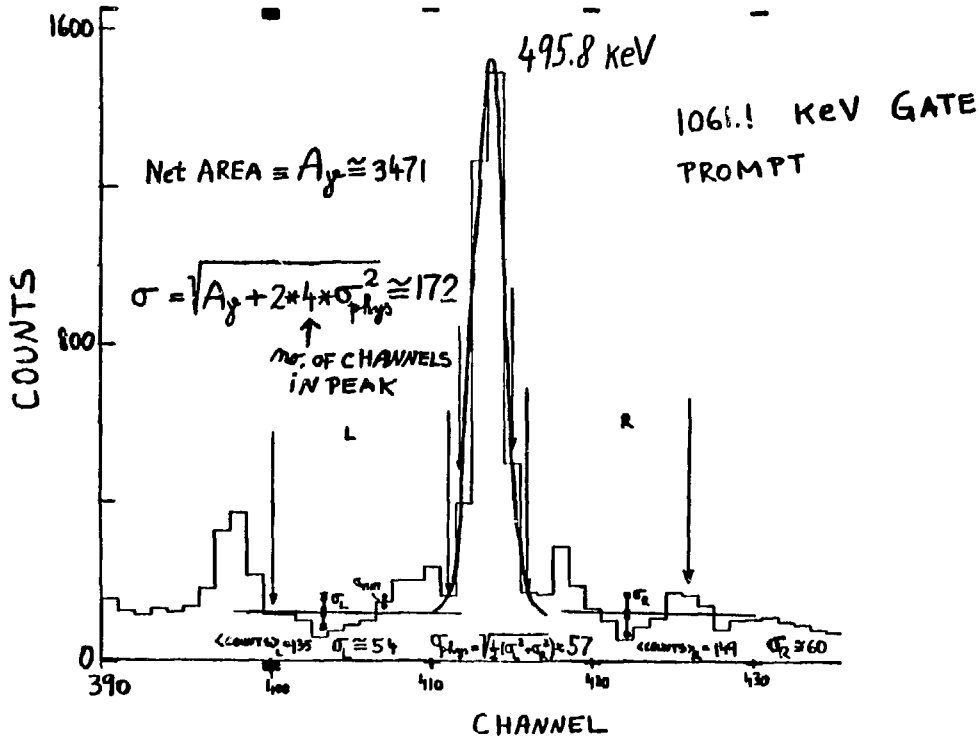
1600
800
0
COUNTS
390
400
410
420
430
CHANNEL
495.8 keV
1061.1 keV GATE
PROMPT
Net AREA ≡ $A_\gamma \cong 3471$
$\sigma = \sqrt{A_\gamma + 2*4*\sigma_{phys}^2} \cong 172$
no. OF CHANNELS IN PEAK
L
R
$\sigma_L \cong 54$
$\sigma_{phys} = \sqrt{\frac{1}{2}(\sigma_L^2 + \sigma_R^2)} \cong 57$
$\sigma_R \cong 60$

Fig. 3.5.1

spectra in coincidence with the background gates, they become at least 4 times those statistics when one adds the average of the two background spectra to the net(background-subtracted) spectrum. In conclusion, the calculation of σ_{phys} according to (3.5.2) takes into account the statistics of the background as well as the presence of any quasi-continuum fluctuations. The result is calculated per channel(see (3.5.2)), and, therefore, it is necessary to multiply σ^2_{phys} by the number of channels in the peak, in (3.5.1). The additional factor of 2 comes from the fact that (3.5.1) represents the error in the net area of the γ-ray peak, which is the result of the subtraction of the background(with its statistics and quasi-continuum fluctuations) from the sum of the net area and the same background.

It can be easily seen that (3.5.1) is physically meaningful in the following extreme cases: When the quasi-continuum fluctuations are zero, (3.5.2) will only give us the σ due to the statistics, i.e. (3.5.2) will essentially give us the background per channel under the peak(B/channel). Thus, (3.5.1) becomes the familiar $(A_\gamma + 2B)^{1/2}$, which is the pure statistics error. This might be the case for a very good rotational nucleus, with de-excitation paths standing out pronouncedly even at spins around 30-40$\hbar$. In the extreme case of perfect statistics(running forever!) and quasi-continuum fluctuations under the peak, the fluctuations in the background under the peak due to statistics will be negligibly smaller than those due to the quasi-continuum. In this case, (3.5.2) will only represent r.m.s. fluctuations per channel due to the quasi-continuum peaklets under the γ-ray

peak, and (3.5.1) simply represents the addition in quadrature of errors given by two independent processes: the statistics(represented by A_γ) and the quasi-continuum(whose shape at any given spin is independent of how long one runs!)(given by $2N\sigma^2_{phys}$).

This sort of analysis, involving quasi-continuum around the peak in question, might raise questions of objectivity. One might argue that different people might choose the L and R regions differently, larger, for instance, to include peaklets with higher P/B's than chosen here, or go farther away from the peak in question finding regions where it is possible to have a much weaker quasi-continuum. In the light of the dicussion in section 3.3, however, it is the opinion of the author that calculation of σ_{phys} as described above is realistic: a non-collective nucleus, such as ^{148}Dy, is expected to exhibit more quasi-continuum, since it lacks a well defined de-excitation path(which is characteristic of more rotational nuclei), over a wide spin range.

As far as choosing regions such as R and L, one can reasonably allow peaklets(or quasi-continuum fluctuations) of the order of σ_L and σ_R, respectively. Looking at Fig. 3.5.1, one should realize that this is a reasonably objective procedure. The net area of the 495.8 keV peak becomes, after subtraction of the net peak areas in the background-gated spectra from the net peak area in the spectrum in coincidence with the foreground, 3640 ± 166, which is in excellent agrrement with 3470 ± 172, as obtained from the result of subtracting the two spectra in coincidence with the background on the right and left of the peak. The errors above were arrived at as

follows:

<u>For ± 172</u> : In the spectrum in coincidence with the 1061.1 keV γ line, minus the average background spectrum, σ_{phys}, for the 495.8 keV peak, is ≈ 57.0(from averaging σ_L and σ_R), which gives, after insertion into (3.5.1) together with A_γ(see Fig. 3.5.1), a value of about 172 .

<u>For ± 166</u> : The same analysis gives σ's of ≈ 51 and 42 for the errors in the net area of the 495.8 keV peak in the L and R background-gated spectra, respectively, which average(upon averaging the two background spectra) quadratically to a σ ≈ $47([(51^2+42^2)/2]^{1/2})$. From the spectrum in coincidence with the 1061.1 keV foreground peak(i.e. including the background underneath) it was found σ_{phys} ≈ 52.0, which gives (using A_γ≈ 3640 in (3.5.1), and quadratically adding the background conribution of 47 found above to the result) σ ≈ 166 . The excellent agreement of the two uncertainties above shows that one only needs to calculate σ in the net gated spectrum(left after subtraction of the necessary background-gated spectra), which does reflect the background subtraction in its statistics and quasi-continuum.

In order to find the relative intensities of transitions, corrections must be made for electron conversion. If w_{obs} is the probability(or the intensity with which) the transition $\Delta E_{if} = E_i - E_f$ is observed, and $w_\gamma^{EM(L)}$ is the probability(or the intensity with which) it proceeds by γ-ray emission of parity and multipolarity EM(L), respectively, then one defines the electron

conversion coefficient as

$$\alpha_L(\Delta E_{if};\ EM) = w^L_{conv}/w^{EM(L)}_{\gamma}\ . \qquad (3.5.3)$$

The coefficient defined above represents the number of converted electrons per γ-ray emitted during the $E_i \rightarrow E_f$ nuclear transition. The following simple expressions can be obtained by manipulating (3.5.3) above:

$$w^{rel}_{obs} = w^{rel}_{obs}(\Delta E_{if};EM(L)) = \qquad (3.5.4)(a)$$

$$= [1 + \alpha_L(\Delta E_{if};EM)]w^{rel}_{\gamma}(\Delta E_{if};EM(L))$$

$$w^{rel}_{\gamma} = w^{rel}_{obs}(\Delta E_{if};EM(L))/[1 + \alpha_L(\Delta E_{if};EM)] \qquad (b)$$

The script "rel" indicates the intensity of some transition relative to the intensity of some reference transition, usually at the bottom of the level scheme. In the present case, the reference transition will be the 1061.1 keV one, which has been placed, in this work, as well as previous ones(Haas et al, 1981, Julin et al, 1982 (p.78) and Ward et al, 1983), at the bottom of the main "prompt" band.

If one now corrects for the γ-ray efficiency of the Ge detector, $\epsilon_{\gamma}(E_{\gamma})$, then the following expression for w^{rel}_{obs} is obtained:

$$w^{rel}_{obs}(\Delta E_{if};EM(L)) = [1 + \alpha_L(\Delta E_{if};EM)] * \qquad (3.5.5)$$

$$* \; w_{\gamma}^{rel}(E_{\gamma};EM(L))/\varepsilon_{\gamma}(E_{\gamma}),$$

where $E_{\gamma} = E_i - E_f$, if the transition proceeds entirely via γ-ray emission. The theory of electron conversion is well known, and it will not be dealt with further in this work, except for depicting the dependence of α_T(the total conversion coefficient) on ΔE_{if} and transition multipolarity and parity(Fig. 3.5.2).

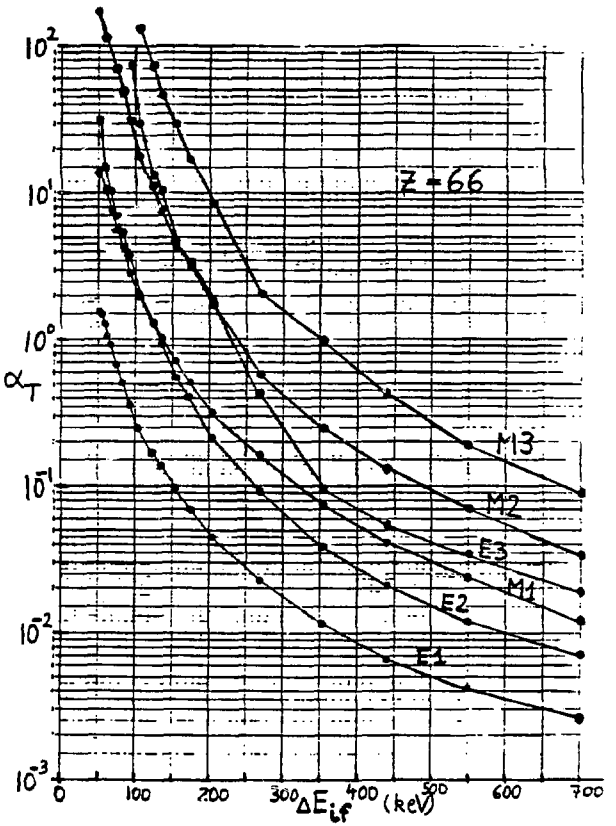
Z = 66
M3
M2
E3
M1
E2
E1
α_T
10^2
10^1
10^0
10^{-1}
10^{-2}
10^{-3}
0
100
200
300
400
500
600
700
ΔE_{if} (keV)

Fig. 3.5.2

Chapter 4

The Level Scheme of ^{148}Dy

In Fig. 4.1.1, is shown the level scheme of ^{148}Dy, above and below the 480 nsec 10^+ isomer, including some 19 new transitions(all above the isomer) observed in the present work. The transitions represented by broken arrows have been found to be questionable in their existence and/or respective position in the level scheme, nonetheless, likely to be there. The respective degree of such likeliness is discussed in what follows, on grounds of transition intensities and their associated uncertainties.

4.1 The Transitions Above the 480 nsec Isomer

The 1061.1 keV transition, used in the examples in the preceding section, illustrate the manner in which gates on various transitions and their respective backgrounds were made. Fig. 3.3.2 shows the presence of numerous discrete γ lines belonging to various impurities (^{149}Dy, $^{145,146,148}Gd$, $^{147,148}Tb$), in addition to the γ lines belonging to ^{148}Dy. Setting a gate on the 1061.1 keV transition(and subtracting the spectra in coincidence with the backgrounds around

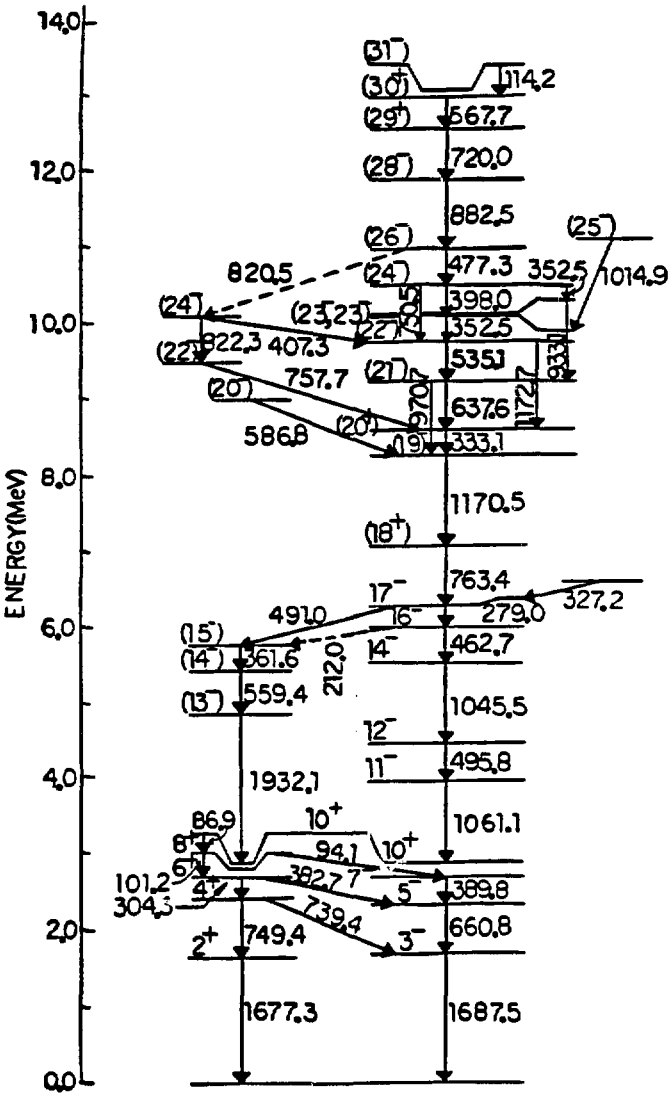
ENERGY(MeV)
14.0
12.0
10.0
8.0
6.0
4.0
2.0
0.0
(31⁻)
(30⁺)
114.2
(29⁺)
567.7
(28⁻)
720.0
882.5
(26⁻)
(25⁻)
820.5
(24⁻)
477.3
352.5
1014.9
(24⁻)
(23⁻,23⁺)
398.0
(22⁻)
822.3
407.3
352.5
(22⁻)
757.7
(21⁻)
535.1
933.1
(20⁻)
970.1
1172.7
637.6
(20⁺)
586.8
(19⁻)
333.1
1170.5
(18⁺)
763.4
17⁻
327.2
491.0
16⁻
279.0
(15⁻)
(14⁻)
361.6
212.0
14⁻
462.7
(13⁻)
559.4
1045.5
12⁻
11⁻
495.8
1932.1
86.9
10⁺
1061.1
8⁺
94.1
10⁺
6⁺
101.2
382.7
7⁻
4⁺
5⁻
389.8
304.3
739.4
2⁺
749.4
3⁻
660.8
1677.3
1687.5

Fig. 4.1.1

the peak, as discussed in the preceding chapter) returns all of the newly observed γ lines above the isomer, as well as the eleven γ's below the isomer, appropriately reduced in intensity. This is shown in Fig. 4.1.2, which shows the prompt 1061.1 keV transition gate. In order to establish the position of the 1061.1 keV transition just above the isomer, i.e. at the bottom of the "prompt" cascade, a gate was set on the 660.8 keV γ line (in coincidence with the late RF - Ge TAC gate 3), below the isomer.

The spectrum in coincidence with this gate is shown in Fig. 4.3.1, where we see the 7 transitions, 1061.1, 495.8, 1045.5, 462.7, 279.0, 763.4 and 1170.5 keV(all appropriately reduced in intensity, compared to the γ's below the isomer), with intensities shown in Table 4.1.1(a). The relative proportion of the 1932.1 keV transition(later shown to belong to the lower side-band to the left of the main-band in Fig. 4.1.1) to the 1061.1 keV one is also given. At the bottom of the table, is also shown the relative proportion of the 1677.3 and 1687.5 keV transitions, below the isomer, obtained from the sum of prompt gates on the 1061.1, 495.8, 1045.5, 462.7, 279.0 and 763.4 keV γ lines, above the isomer.

Table 4.1.1(b) shows the relative intensities(with respect to the 1061.1 keV transition) of the same transitions above the isomer treated in (a), as obtained from the sum of the prompt 660.8 and 1687.5 keV gates. The intensity values seem(within the experimental uncertainties) to position the 1061.1 and 495.8 keV transitions at the bottom of the main cascade above the isomer. Since all the transitions above the isomer have been found prompt with respect to one

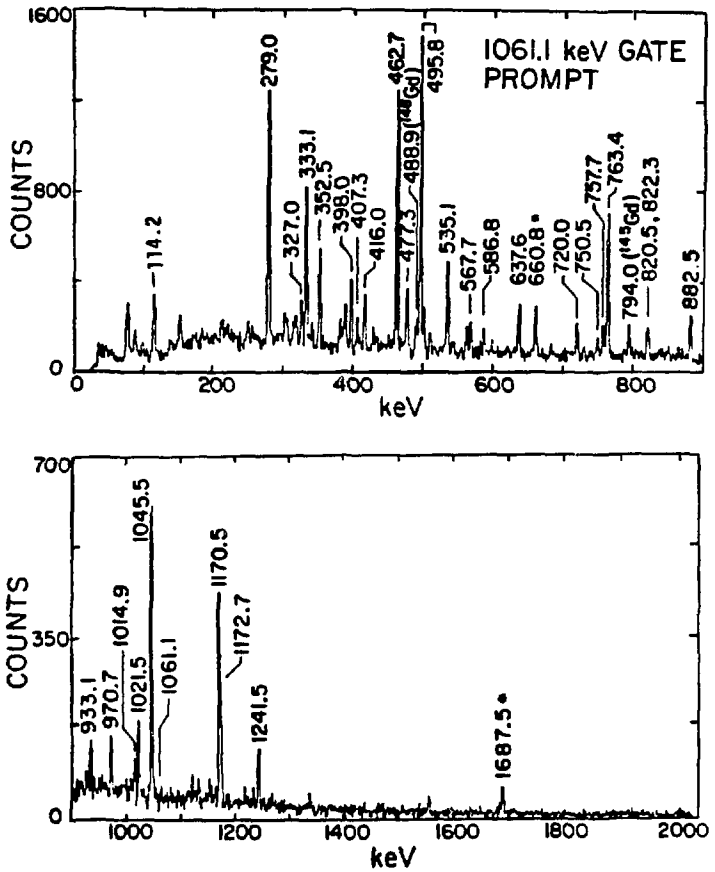
1061.1 keV GATE
PROMPT
COUNTS
keV
1600
800
0
200
400
600
1000
1200
1400
1600
1800
2000
700
350
114.2
279.0
327.0
333.1
352.5
398.0
407.3
416.0
462.7
488.9(148Gd)
495.8
535.1
567.7
586.8
637.6
660.8*
720.0
750.5
757.7
763.4
794.0(145Gd)
820.5, 822.3
882.5
933.1
970.7
1014.9
1021.5
1045.5
1061.1
1170.5
1172.7
1241.5
1687.5*

Fig. 4.1.2

Table 4.1.1

(a)Relative intensities of the 1061.1, 462.7, 495.8, 1045.5, 279.0, 763.4, 1932.1^{S}, 559.4^{S} and 361.6^{S}(^{S} meaning side band) transitions above the isomer, from the delayed gate on the 660.8 keV transition below the isomer. Relative intensities of the 1677.3 and 1687.5 keV transitions below the isomer(marked with with $^{<}$) from the sum of prompt gates on the 1061.1, 462.7, 495.8, 1045.5 and 279.0 keV transitions above the isomer.

Level Scheme Order	E_γ	No. of counts	I_γ^{rel}
1	1061.1	1400 ± 130	1.00
2	462.7	1330 ± 118	0.95 ± 0.12
3	495.8	1250 ± 120	0.90 ± 0.12
4	1045.5	1240 ± 108	0.90 ± 0.11
5	279.0	1040 ± 105	0.75 ± 0.10
6	763.4	1170 ± 120	0.84 ± 0.12
7	1170.5*	1130 ± 170	0.81 ± 0.14
	1932.1^{S}	1000 ± 95	0.72 ± 0.10
	559.4^{S}	690 ± 70	0.49 ± 0.07
	361.6^{S}	400 ± 40	0.31 ± 0.05
	1687.5$^{<}$	897 ± 62	1.00$^{<}$

$1677.3^{<}$	239 ± 13	$0.27 \pm 0.02^{<}$

(b)Relative intensities of the 1061.1, 495.8, 1045.5, 462.7, 279.0, 763.4 and 1170.5 keV transitions(listed below in the order adopted in the present work(see text)) and 1932.1^{S}, 559.4^{S} and 361.6^{S} keV transitions(^{S} having the same meaning as in (a)) as obtained from the sum of the prompt 660.8 and 1687.5 keV transitions(located below the isomer). As in (a), the proper corrections for Ge relative efficiency and electron conversion were made, while the uncertainties were obtained in the manner discussed in section 3.5 .

Level Scheme Order	E_γ	No. of counts	I_γ
1	1061.1	9363 ± 870	1.00
2	495.8	7473 ± 750	0.80 ± 0.11
3	1045.5	6985 ± 608	0.75 ± 0.09
4	462.7	5532 ± 491	0.59 ± 0.08
5	279.0	6795 ± 680	0.73 ± 0.10
6	763.4	7658 ± 785	0.82 ± 0.11
7	1170.5^{*}	5894 ± 886	0.63 ± 0.12
	1932.1^{S}	2640 ± 265	0.28 ± 0.04
	559.4^{S}	2388 ± 240	0.25 ± 0.03
	361.6^{S}	1590 ± 160	0.17 ± 0.03

*Its intensity represents about 0.77 of the fat peak including the 1170.5 and 1172.7 keV transitions(see text).

another within about 7 nsec(see section 5.2), Tables 4.1.1(a) and (b) should give the same sequence for the seven transitions in the main cascade above the isomer. This is the case here, even though Table 4.1.1(a) gives a slightly different order: given the size of the experimental uncertainties in Tables 4.1.1(a) and (b)(especially in (a)), it is considered that the agreement is good enough.(The size of the uncertainties in Table 4.1.1(a) makes the order of the 462.7, 495.8 and 1045.5 keV transitions unclear.) The spectrum(not shown) in prompt coincidence with the 660.8 and 1687.5 keV transitions below the isomer shows much better P/B ratios and statistics for the seven transitions above the isomer than the corresponding delayed gates, thus indicating that there may exist another 660.8 and/or 1687.5 keV transition(s) in prompt coincidence with a given number of the seven transitions above the isomer in ^{148}Dy, or perhaps in impurities created by this reaction. This hypothesis was not pursued any further, and the information contained in Table 4.1.1(b) should be taken with a large grain of salt.(However, see the paragraph below.)

The sequence of the first seven transitions given in Table 4.1.1(b) agrees with the sequence above the 495.8 keV transition obtained from the prompt 1061.1 keV gate(see Table 4.1.2). It is also in agreement with Julin et al(1982(p.78)). In addition, the relative intensities of the 1932.1, 559.4 and 361.6 keV transitions from Table 4.1.1(a) are in large discrepancy with the values from (b). The relative intensities of the three transitions above from Table 4.1.1(b) agree very well with the values obtained from the prompt 1932.1 keV gate(see Table 4.1.3(a)). However, since both Table

4.1.1(a) and (b) give the same general sequence of the seven transitions above the isomer, except for the position of the 462.7 keV transition, it was decided to average the relative intensity values from (a) and (b) for the 495.8 keV transition(they are within experimental uncertainty anyway!). This average is listed in Table 4.1.2, which also lists the relative intensities of all transitions above the isomer(with respect to the 1061.1 keV transition), as obtained from the prompt 1061.1 keV gate(except as noted). The intensities of the transitions in the prompt 1061.1 keV gate were first obtained relative to the 495.8 keV transition, and subsequently normalized to the intensity of the 1061.1 keV transition, with the help of Table 4.1.1 .

The prompt 1061.1 keV gate(Fig. 4.1.2) shows three transitions at 416.0, 1021.5 and 1241.5 keV, which have also been found in the prompt 462.7 keV gate(not shown). No other gates in ^{148}Dy seem to return the 416.0, 1021.5 and 1241.4 keV transitions. While all this might point to placing the 1061.1 and 462.7 kev transitions at the bottom of the prompt main cascade, it was decided this kind of evidence was not good enough: only two of all the more or less established ^{148}Dy transitions are involved plus other explanations(e.g. impurities, or the possible presence of a cascade parallel to the main one in ^{148}Dy) are possible. In addition, the energies of the peaks associated with the 1061.1 and 462.7 keV transitions as returned in the 416.0, 1021.5 and 1241.5 keV prompt gates were both off by about 1 keV. The issue was not deemed worth pursuing any further.

In the manner described above, gates were placed on all transi-

Table 4.1.2

Intensities(relative to the 1061.1 keV transition), spin and parity assignments(see chapter 5)(parantheses indicate tentativeness) of all observed transitions in ^{148}Dy(above the 480 nsec isomer). Only coincidences with RF - Ge TAC gate 1(prompt) were considered.

I_i^π →	I_f^π	E_{level} (keV)	E_γ	I_γ^{rel}	E	M	λ
11^- →	10^+	3980.2	1061.1(4)	1.00	E		1
12^- →	11^-	4476.0	495.8(3)	0.85(11)*		M	1
14^- →	12^-	5521.5	1045.5(4)	0.64(5)	E		2
16^- →	14^-	5984.2	462.7(2)	0.60(5)	E		2
17^- →	16^-	6263.2	279.0(2)	0.41(5)		M	1
(18^+)→	17^-	7026.6	763.4(2)	0.49(6)	(E)		1
(19^-)→	(18^+)	8197.1	1170.5(5)	0.46(9)	E		1
(20^-)→	(19^-)	8530.2	333.1(1)	0.34(4)		(M)	1
(21^-)→	(20^-)	9167.8	637.6(2)	0.14(2)	(E)		2^n
(21^-)→	(19^-)	9167.8	970.7(3)	0.09(2)	(E)		2
(22^-)→	(21^-)	9702.9	535.1(2)	0.20(3)	(E)		2^n
(22^-)→	(20^-)	9702.9	1172.7(5)	0.14(3)	(E)		2
(23^-)→	(22^-)	10055.4	352.5(3)	0.10(2)		(M)	1
(23^-)→	(21^-)	10100.9	933.1(4)	0.09(2)	(E)		2
(24^-)→	$(23^-)'$	10453.4	352.5(3)'	0.08(3)		(M)	1
(24^-)→	(23^-)	10453.4	398.0(2)	0.12(2)	(E)		2^n
(24^-)→	(22^-)	10453.4	750.5(4)	0.05(2)	(E)		2

$(26^-) \rightarrow (24^-)$	10930.7	477.3(2)	0.15(3)	(E)	2
$(28^-) \rightarrow (26^-)$	11813.2	882.5(5)	0.13(3)	(E)	2
$(29^+) \rightarrow (28^-)$	12533.2	720.0(3)	0.11(3)	(E)	1
$(30^+) \rightarrow (29^+)$	13100.9	567.7(3)	0.06(2)	(E)	2^n
$(31^-) \rightarrow (30^+)$	13215.1	114.2(3)	0.05(2)**	(E)	1
$(22^-)^{us} \rightarrow (20^-)$	9287.9	757.7(3)	0.07(2)	(E)	2
$(24^-)^{us} \rightarrow (22^-)^{us}$	10110.2	822.3(5)	0.10(2)	(E)	2
$(24^-)^{us} \rightarrow (22^-)$	10110.2	407.3(2)	0.05(2)	(E)	2
$(26^-) \rightarrow (24^-)^{us}$	10930.7	820.5(5)	0.09(3)	(E)	2
$(13^-)^{11s} \rightarrow (10^+)$	4851.2	1932.1(5)	0.28(3)*	(E)	3
$(14^-)^{11s} \rightarrow (13^-)^{11s}$	5410.6	559.4(3)	0.25(3)*	(E)	2^n
$(15^-)^{11s} \rightarrow (14^-)^{11s}$	5772.2	361.6(2)	0.17(2)*	(M)	1
$16^- \rightarrow (15^-)^{11s}$	6263.2	212.0(3)	0.03(1)	(M)	1
$17^- \rightarrow (15^-)^{11s}$	6263.2	491.0(3)	0.10(2)	(E)	2

Individual Side Transitions

(***) $\rightarrow 17^-$	6590.4	327.2(2)	0.10(2)**	***	
$(20^-) \rightarrow (19^-)$	8783.9	586.8(3)	0.06(2)	(E)	2^n
$(25^-) \rightarrow (23^-)$	11070.3	1014.9(5)	0.06(2)	(E)	2

* Obtained from the sum of the 660.8 and 1687.5 keV prompt

gates(below the 480 nsec isomer). In the case of the 361.6 keV transition, its intensity relative to the 559.4 keV was found to be very nearly the same in the 1932.1 keV prompt gate as in the sum of the two prompt gates above. In the case of the 495.8 keV transition, the number tabulated is the average of the corresponding numbers listed in Table 4.1.1(a) and (b)(see text).

** It does not take into account the possible existence of a lifetime(however, see chapter 5).

*** A multipolarity value could not be derived from angular correlation measurements(see section 5.1).

us Refers to the upper side band(see Fig. 4.1.1).

lls Refers to the left lower side band(see Fig. 4.1.1).

' after a spin or transition energy indicates there is another level of same respective spin, or another transition of same transition energy, respectively.

$\underline{\lambda}$ denotes the angular mometum carried by the transition in question.

n denotes non-stretched transitions.

All relative intensities above have been properly corrected for Ge relative efficiency as well as for electron conversion(based on the multipolarities and electromagnetic character deduced in chapter 5).

tions shown in Fig. 4.1.1, and all corresponding relative intensities and their uncertainties worked out appropriately. The relative intensity of the 279.0 keV transition is lower than the one for the 764.3 keV transition, but one has to add the relative intensity of the 491.0 keV transition to the relative intensity of the 279.0 keV transition, in order to compare relative intensities properly(based on the level scheme). Also, the pectrum in coincidence with the 1170.5 keV transition(Fig. 4.1.3) shows that the sum of intensities of the 491.0 and 279.0 keV transitions adds(within experimental error) to the intensity of the 763.4 keV transition. This can also be seen from the spectrum in coincidence with the 720.0 keV transition (Fig. 4.1.5).

Five cross-over transitions have been found(1172.7, 970.7, a second 352.5, 933.1 and 750.5 keV; see Fig. 4.1.1), and, from Table 4.1.3(a), one can see the 637.6 and 535.1 keV transitions(which the 1172.7 keV transition crosses) are greatly reduced in intensity, what little is measured being due to the fact that placing a gate on the 1172.7 keV transition will inevitably include some fraction of the 1170.5 keV transition. Fig. 4.1.4 shows the spectrum in coincidence with the 1172.7 keV transition, which markedly contrasts with Fig. 4.1.3, which shows the strong presence of the 637.6 and 535.1 keV transitions, with same relative intensity(within statistics) as they are observed in the gate on the 1061.1 keV transition. In similar manner, the position of the other four cross-over transitions was established.

The level scheme in Fig. 4.1.1 presents a few transitions placed

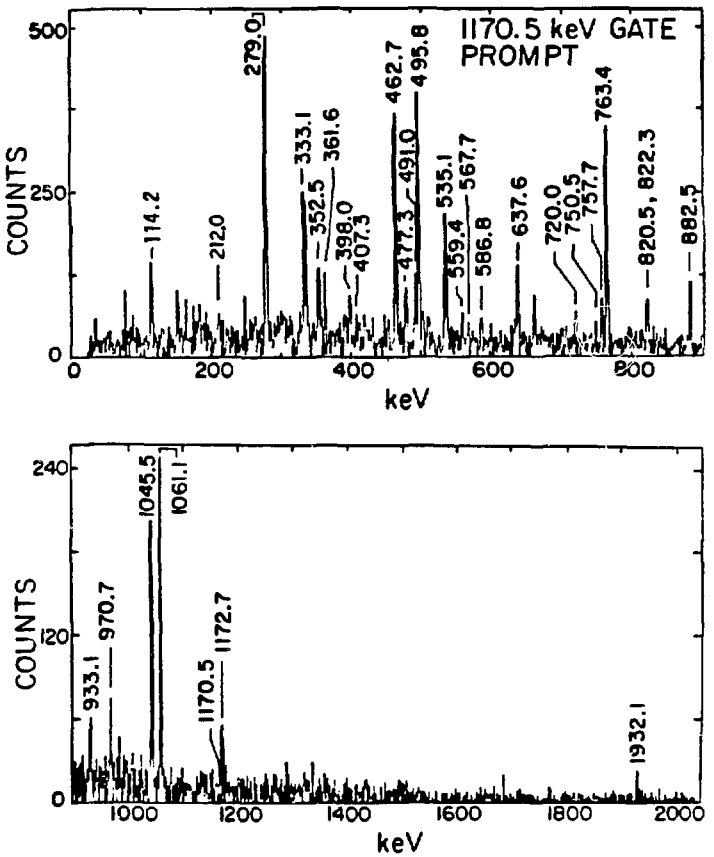
1170.5 keV GATE
PROMPT
COUNTS
keV
114.2
212.0
279.0
333.1
352.5
361.6
398.0
407.3
462.7
477.3
491.0
495.8
535.1
559.4
567.7
586.8
637.6
720.0
750.5
757.7
763.4
820.5, 822.3
882.5
933.1
970.7
1045.5
1061.1
1170.5
1172.7
1932.1

Fig. 4.1.3

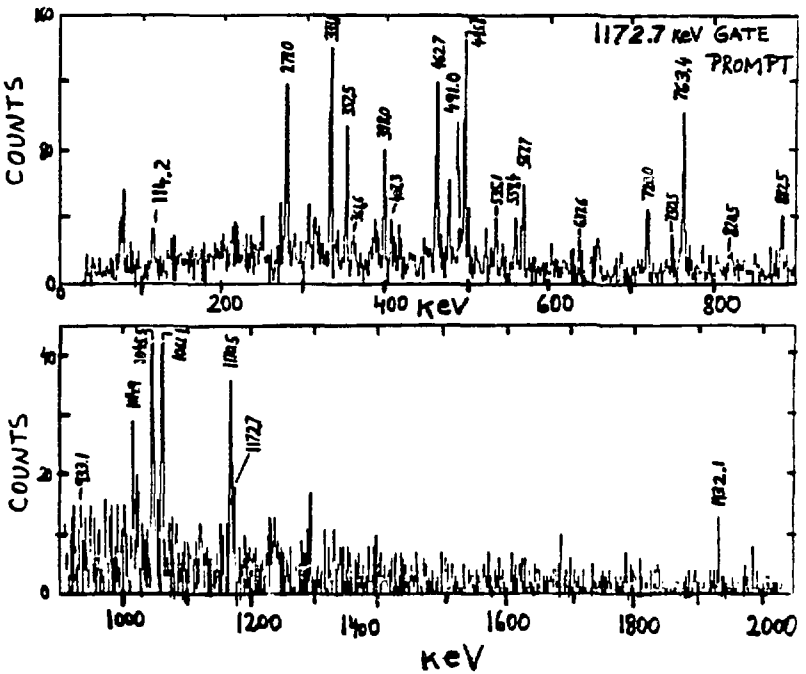
1172.7 keV GATE
PROMPT
COUNTS
keV
200
400
600
800
1000
1200
1400
1600
1800
2000
1172.7

Fig. 4.1.4

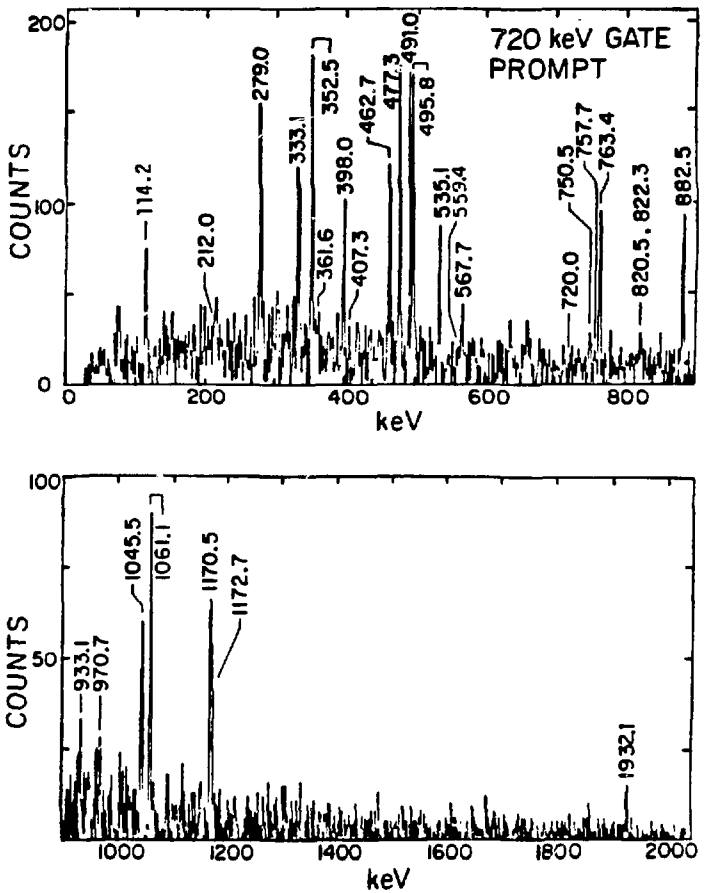
720 keV GATE
PROMPT
COUNTS
keV
114.2
212.0
279.0
333.1
352.5
361.6
398.0
407.3
462.7
477.3
491.0
495.8
535.1
553.4
567.7
720.0
750.5
757.7
763.4
820.5, 822.3
882.5
933.1
970.7
1045.5
1061.1
1170.5
1172.7
1932.1

Fig. 4.1.5

with a high degree of tentativeness(marked by broken arrows): A 212.0 keV transition has been observed and tentatively positioned from the 16^- level of the main band to the 15^- of the right lower side band(see Fig. 4.1.1). The same degree tentativeness seems to be present in the case of the 820.5 keV transition, of the upper side band, also displayed by a broken arrow(see Fig. 4.1.1). Its intensity, added to the intensity of the 477.3 keV transition is considerably higher than the intensity of the 882.5 keV transition(see Table 4.1.2). Such rather large discrepancy(not found below $I = 24\ \hbar$, as it can be readily established from inspecting Table 4.1.2)is due to the quasi-continuum. This behaviour is probably typical for non-collective nuclei, such as ^{148}Dy.

Fig. 4.1.6 shows the spectrum in coincidence with the prompt 491.0 keV transition, belonging to the left side-band(see Fig. 4.1.1). A few points must be clarified before this transition is placed on the level scheme of ^{148}Dy. The spectrum shows the presence of transitions very close in energy to the 495.8, 1045.5 and 1061.1 keV transitions in ^{148}Dy: actually, they belong to ^{148}Gd, where there exists a 488.9 keV transition(Lunardi et al, 1984). The 491.0 keV transition seems to occur also in ^{149}Dy(Julin et al, 1982(p.76)), confirmed by the present work: gating on the prompt 491.0 keV transition returned numerous transitions previously placed in the ^{149}Dy and vice-versa. In addition, a 334.6 keV transition has been found(in the present work)in ^{149}Dy in coincidence with the 491.0 keV transition(Gating on the prompt 334.6 keV transition also returned a lot of previously established ^{149}Dy and vice-versa.).

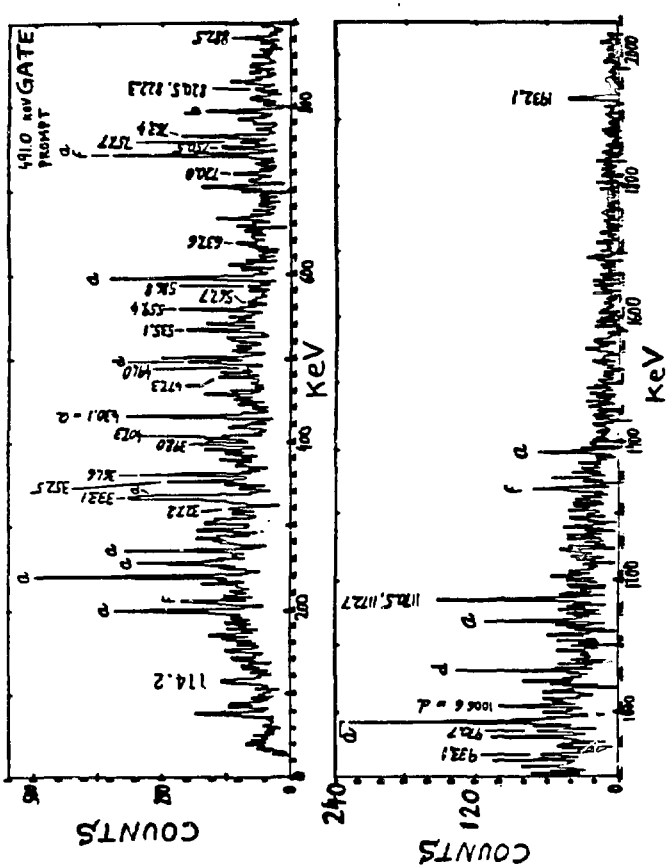
COUNTS
KeV
GATE
PROMPT
114.2
1932.1
1125.1127
1006.6 = d
923.1
972.7
1125.1123
1527
1740
4326
5127
5129
5325
3331
3240
4013
4801 = a
4723
4910
535.1
559.4
5127
5148
3331
3325
3240
4013
4801 = a
4723
4910
535.1
559.4
5127
5148
4326
1740
1527
1125.1123
1125

Fig. 4.1.6

The prompt 491.0 keV transition gate enabled us to measure the intensity of the 430.2 keV transition in ^{149}Dy(see Julin et al, 1982(p.76)) and its relative proportion to the 334.6 keV transition. Since the 430.2 and 491.0 keV transitions in ^{149}Dy are nearly equally intense(this being established from gating on the prompt 984.8 keV transition in ^{149}Dy) and are prompt with respect to the 5eam(established from RF - Ge TAC analysis), it was possible to deduce how much of the 334.6 keV transition is present relative to the 333.1 keV transition in ^{148}Dy, and thus perform the proper correction to the area under the slighly fat peak at around 333.1 keV thus produced. There is also a 334.8 keV transition in ^{148}Gd (Lunardi et al, 1984), also in coincidence with the 488.9 keV transition mentioned above. However, there is a 17.5 nsec isomer separating them, and the 334.8 keV transition is about a fifth of the intensity of the 1006.6 keV transition in that nucleus. Inspecting the spectrum in Fig. 4.1.6, leads one to believe that this additional correction is too small to worry about. Such analysis, ultimately has placed the 491.0 keV transition, together with the 361.6, 559.4 and 1932.1 keV transitions, in the side band on the left of the main band.

Gating on the prompt 882.5 keV transition in ^{148}Dy returns numerous transitions in ^{148}Gd with greater intensity than the transitions in ^{148}Dy. The ^{148}Gd nucleus has 882.2 and 883.5 keV transitions(the latter with a lifetime of 17.5 nsec; see Lunardi et al, 1984). The existence of a 882.5 keV transition in ^{148}Dy has been established from prompt gating on a variety of ^{148}Dy transitions not present(as far as it is known so far)in impurities, such as the

763.4 keV transition. The placement of the 882.5 keV transition on the level scheme was, however, quite solid(within experimental error) based on relative intensity analysis from gates placed on transitions at the bottom of the level scheme(e.g. the 1061.1 keV transition) as well as from the spectrum in coincidence with the 882.5 keV transition itself. Placing a gate on the delayed 882.5 keV transition(i.e. RF - Ge TAC gate 3 in Fig. 5.2.10) shows the clean presence of only the 394.7, 631.7 and 784.3 keV transitions, which together with the 883.5 keV transition, occur below the 17.5 nsec isomer in ^{148}Gd(see Lunardi et al, 1984).

Table 4.1.2 gives the intensities of all transitions above the 480 nsec isomer, relative to the intensity of the 1061.1 keV transition, sitting at the bottom of the main prompt band. Multipolarity and parity assignments are given(tentativeness indicated by parantheses), and they are discussed in chapter 5. Calculation of errors in relative intensities was done in the manner described in section 3.5, where an example was given involving the gate on the 1061.1 keV transition. Intensities of the cross-over 352.5(different from the 352.5 keV transition in the main cascade) and 1172.7 keV transitions were first obtained(from gates above them) relative to well established transitions in the main cascade(from gates above them) and subsequently normalized to the 1061.1 kev transition. The same procedure was used for the 491.0 and 820.5 and 822.3 keV transitions, obtained first relative to the 279.0 and 398.0 keV transitions(from gates above them), respectively, and then normalized to the 1061.1 kev transition(section 4.2).

A quantitative analysis of how the transitions above the 480 nsec isomer are stacked in the level scheme, can be done with the help of bar plots, such as those displayed in Figs. 4.1.7-8. The bar plot corresponding to the gate on the 763.4 keV transition, for example, depicts intensities(equal to the height of corresponding bars) of transitions in coincidence with that transition. Branching of transitions as well as cross-overs were properly represented by stacking of corresponding bars on top of one another. Appropriate error bars are displayed to the right of corresponding bars. The smooth drop in the height of bars and/or their appropriate stacking, as one proceeds to ascend(in spin or level energy) the main prompt band is readily noticeable. Both Fig. 4.1.7 and 4.1.8 show that the transitions below the corresponding gates(accounting for branching and cross-overs) have the same intensity(within experimental errors), or bar height. The height of the bars in Figs. 4.3.7-8 are normalized such that the height of the 495.8 keV transition bar equals the number of counts(i.e. the area under the 495.8 keV peak) as it appears in the given raw gated spectrum(not corrected for Ge efficiency or electron conversion).

More quantitative support for the reported level scheme in Fig. 4.1.1 is given in Table 4.1.3(a), where the columns contain intensities of all transitions above the 480 nsec isomer, measured from the spectrum in coincidence with several selected transitions, whose energies appear at the top of columns. The numbers in the columns are normalized in exactly the same way as heights of the bars in Figs. 4.3.7-8 discussed above. As in the case of the bar

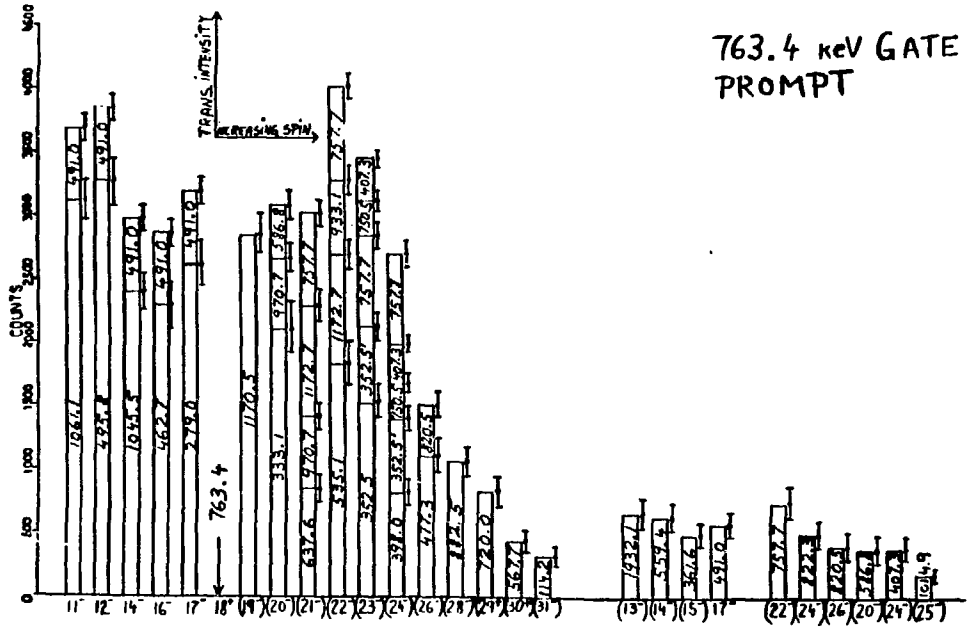
763.4 keV GATE
PROMPT
COUNTS
TRANS. INTENSITY
INCREASING SPIN
763.4

Fig. 4.1.7

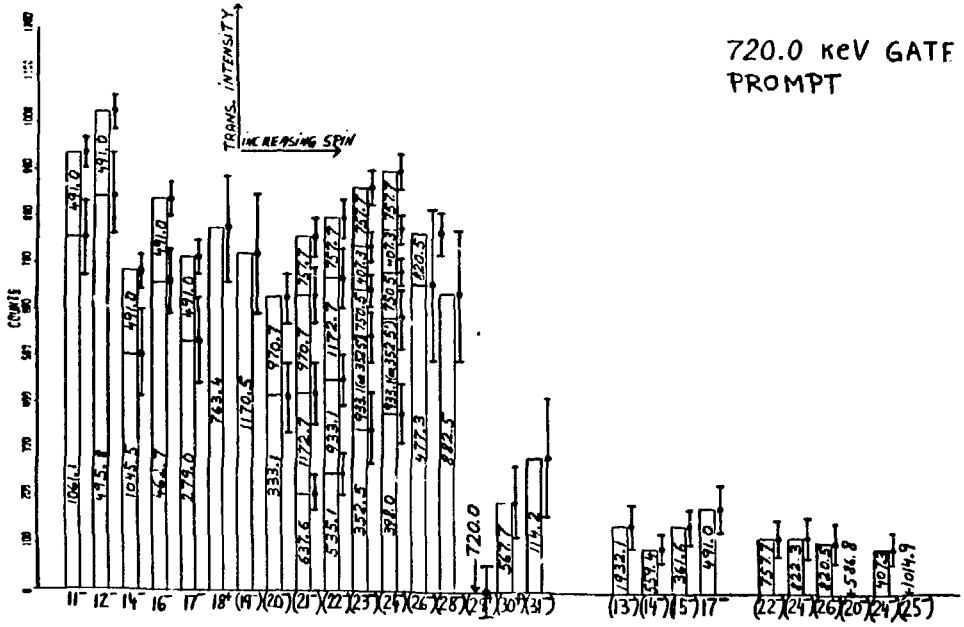
720.0 keV GATE
PROMPT
TRANS. INTENSITY
INCREASING SPIN
COUNTS
720.0

Fig. 4.1.8

plots, appropriate corrections for Ge efficiency and electron conversion(according to (3.5.5)) have been made(i.e. down a column). In addition, the above corrections have also been made along the row(i.e. the gating energies), so that the resulting coincidence table should be symmetric(where applicable, since it is not square) with respect to the diagonal. The entries along the diagonal are all equal to zero(within experimental uncertainty)since there are no two coincident transitions of the same energy(the two 352.5 keV transitions are not in coincidence!), and, naturally, no transition can be in coincidence with itself. The resulting Table 4.1.3(a) has entries of the form $(E_{\gamma 1}, E_{\gamma 2})$, for which it is expected that $(E_{\gamma 1}, E_{\gamma 2}) = (E_{\gamma 2}, E_{\gamma 1})$, and this equality holds true for most of the entries(within experimental error). The few instances for which the discrepancies run about 30 percent(apparently outside the experimental errors), can probably be blamed on the respective transitions found in impurities, or the existence of weak transitions of nearly the same energy in other parts of the level scheme of ^{148}Dy, which could not be identified in the present work due to lack of better statistics.

Table 4.1.3(b) illustrates the symmetry discussed above for a square coincident matrix made of a subset of Table 4.1.3(a) plus a few more transitions. The entries are raw intensities, i.e. areas under the γ-ray peaks appearing in coincidence with a given gate(the heads of the columns). One can see the entries symmetric with respect to the diagonal are equal within about 10-15 percent(the order of the experimental error), except for a cases with up to about 30 percent

Table 4.1.3

(a)Intensities of all transitions above the 480 nsec isomer, as deduced from spectra(corrected for Ge efficiency and electron conversion (based on the findings in section 5.1)down the column and along the row of gate energies)in coincidence with some eleven selected transition above the isomer. A column contains intensities(with the appropriate experimental errors * in parantheses below) of all transitions in coincidence with the corresponding transition, whose energy appears at the head of the column. The numbers at the heads of columns and rows refer to transition energies in keV, as averaged over all the gated spectra where the transition in question appears as well as over all possible sets of channels on which the gate on the respective transition can be placed(investigated from the full projection spectrum in Fig. 3.3.2).

	279.0	333.1	361.6	398.0	491.0	535.1
114.2	253	210	58	42	36	135
	(75)	(75)	(16)	(14)	(12)	(45)
279.0	0	1705	0	662	0	1126
	(95)	(172)	(80)	(125)	(130)	(185)
333.1	1431	0	297	538	565	739
	(160)	(150)	(60)	(80)	(120)	(87)
327.2	173	0	85	0	64	0

	(65)	(60)	(45)	(45)	(22)	(25)
352.5†	800	566	158	662	246.1	278
	(120)	(150)	(55)	(90)	(54)	(75)
361.6	0	263	0	157	414	178
	(70)	(50)	(50)	(65)	(65)	(55)
398.0	464	502	162	0	207	818
	(80)	(110)	(65)	(50)	(70)	(200)
407.3	434	156	23	0	127	635
	(131)	(40)	(15)	(20)	(45)	(180)
462.7	3214	1306	0	491	0	1151
	(285)	(120)	(130)	(75)	(80)	(180)
477.3	537	412	125	606	178	500
	(110)	(85)	(45)	(100)	(70)	(180)
491.0	0	562	365	192	0	272
	(130)	(120)	(60)	(85)	(90)	(90)
495.8	4190	1973	0	826	330	1825
	(380)	(200)	(100)	(95)	(160)	(350)
535.1	1093	622	221	750	263	0

	(120)	(140)	(68)	(130)	(85)	(87)
559.0	0.0	402	870	152	346	330
	(130)	(72)	(105)	(70)	(86)	(97)
567.7	450	249	120	84	70	269
	(140)	(80)	(48)	(55)	(35)	(86)
586.8	224	0	61	0	0	119
	(85)	(80)	(30)	(45)	(40)	(75)
637.6	600	995	225	330	276	698
	(150)	(175)	(115)	(90)	(61)	(175)
720.0	528	392	117	258	221	307
	(180)	(127)	(60)	(82)	(71)	(107)
750.5	221	203	76	0	100.1	186
	(85)	(67)	(35)	(80)	(45)	(87)
757.7	335	669	111	0	106	0
	(90)	(180)	(55)	(52)	(40)	(45)
763.4	2535	2037	481	755	571	1814
	(320)	(185)	(85)	(120)	(144)	(310)
820.5	560	431	227	122	154	220

822.3	(177)	(140)	(72)	(91)	(65)	(67)
882.5	726	494	198	576	260	387
	(248)	(166)	(85)	(95)	(83)	(135)
933.1	263	211	153	0	121	0
	(85)	(75)	(65)	(60)	(52)	(35)
970.7	411	29	166	180	101	543
	(130)	(80)	(75)	(72)	(50)	(135)
1014.9	328	104	52	133	100	169
	(120)	(65)	(45)	(90)	(45)	(45)
1045.5	3140	1546	0	475	115	1592
	(345)	(145)	(75)	(85)	(81)	(286)
1061.1	3521	1827	0	777	426	1535
	(325)	(182)	(73)	(124)	(145)	(275)
1170.5	2883	1798	479	794	707	1774
	(415)	(235)	(82)	(150)	(252)	(324)
1172.7	910	568	151	251	223	0
	(143)	(155)	(46)	(96)	(66)	(50)
1932.1	0	413	795	207	408	362

	(90)	(165)	(123)	(72)	(163)	(106)

	757.5	882.5	970.7	1172.7	1932.1
114.2	28	135	45	75	86
	(13)	(73)	(20)	(36)	(30)
279.0	367	576	460	457	0
	(125)	(110)	(135)	(58)	(21)
333.1	700	562	0	424	627
	(250)	(105)	(53)	(123)	(175)
327.2	0	0	0	0	191
	(178)	(34)	(36)	(18)	(71)
352.5†	0	462	409	216	352
	(176)	(115)	(108)	(63)	(98)
361.6	111	182	150	83	812
	(50)	(44)	(52)	(37)	(223)
398.0	0	386	213	261	287
	(58)	(74)	(83)	(76)	(82)

407.3	0	96	131	125	375
	(63)	(34)	(52)	(43)	(110)
462.7	438	493	494	469	0
	(152)	(128)	(141)	(137)	(49)
477.3	0	379	190	216	275
	(31)	(96)	(75)	(71)	(95)
491.0	93	212	118	75	425
	(43)	(81)	(51)	(32)	(121)
495.8	596	806	627	554	0
	(181)	(205)	(185)	(151)	(55)
535.1	0	463	572	154**	419
	(46)	(162)	(198)	(107)	(151)
559.0	182	139	84	141	1254
	(63)	(36)	(31)	(49)	(362)
567.7	51	145	80	139	103
	(25)	(46)	(27)	(64)	(53)
586.8	0	36	0	0	92
	(21)	(37)	(28)	(39)	(51)

637.6	0	308	0	122**	378
	(41)	(94)	(32)	(91)	(110)
720.0	118	603	229	283	179
	(42)	(209)	(115)	(103)	(49)
750.5	68	47	87	149	88
	(50)	(36)	(57)	(55)	(58)
757.7	0	191	0	145	182
	(49)	(63)	(24)	(102)	(71)
763.4	675	1103	606	604	858
	(145)	(325)	(267)	(198)	(295)
820.5+‡‡	578	172	79	93	336
822.3	(213)	(48)	(52)	(54)	(78)
882.5	210	0	167	347	369
	(100)	(31)	(61)	(112)	(121)
933.1	0	47	197	38	132
	(35)	(26)	(83)	(37)	(61)
970.7	0	239	0	51	255
	(31)	(86)	(51)	(36)	(83)

1014.9	0	40	0	59	88
	(30)	(36)	(21)	(37)	(37)
1045.5	588	630	448	535	0
	(210)	(183)	(128)	(176)	(40)
1061.1	544	957	584	616	0
	(172)	(273)	(186)	(211)	(45)
1170.5	409	1112	588	473	645
	(165)	(292)	(197)	(161)	(221)
1172.7	0	313	0	0	148
	(36)	(98)	(54)	(84)	(55)
1932.1	201	164	135	71	0
	(87)	(66)	(57)	(34)	(23)

* Same method in the examples in section 3.5 was used.

† Includes both 352.5 keV transitions except for the 398.0, 535.1 and 1172.7 keV columns, in which it refers only to the 352.5 keV transition in the main band(see Fig. 4.1.1).

†† Includes both the 820.5 and 822.3 keV transitions, except for the 535.1, 970.7 and 1172.7 keV columns in which it refers only to the 820.5 keV transition(see Fig. 4.1.1).

** Gate on the 1172.7 keV transition includes some of 1170.5 keV transition.

A separate row was used for the 1170.5 and 1172.7 keV transitions, respectively, since they have the larger energy separation than the other two such cases(the two 352.5 keV and 820.5 and 822.3 keV transitions, respectively) and better statistics.

(b)Square array composed of a subset of the coincidence matrix in (a) plus columns for the 1061.1, 495.8, 763.4 and 720.0 keV transitions(last two columns being represented in Figs. 4.1.7-8), illustrating the symmetry of the entries with respect to the diagonal (indicated by the straight line drawn) along which the entries are zero(within experimental uncertainty;see Table 4.1.3(a)). The entries are raw numbers, uncorrected for Ge efficiency or electron conversion. The numbers at the heads of the rows and columns are transition energies(in keV) rounded-off to the nearest integer.

$E_\gamma \rightarrow$

↓	279	333	362	398	491	496	535	720	758	763	971	1061
279		3200	574	1076		6025	1450	541	359	2537	370	2294
333	2680		521	875	779	2873	951	409	685	1913		1728
362		462		240	535		215	134	102	411	113	
398	754	817	247		248	988	916	227		641	149	552
491		775	472	230		385	258	134	67	409	70	176
496	5733	2700		982	332		1716	625	426	2325	368	3471
535	1407	802	267	848	249	1792		185		1195	316	757
720	536	400	112	228	166	672	215		63	438	100	329
758	328	655	102		76	438		63		374		217
763	2465	1982	439	638	409	2593	1213	408	343		253	1428
971	330	23	125	126	60	374	300	89		246		200
1061	2640	1370		506	235	3417	791	307	213	1210	188	

deviation, blamed on the possibilities dicussed in the last paragraph.

Before leaving this section, it was deemed necessary to explain a few inconsistencies about the placement of the 327.2 and 1014.9 keV transitions: The 327.2 keV prompt gate(not shown) returns the 763.4 and 1170.5 keV transitions with about a third of the intensity of the 279.0, 462.7, 1045.5, 495.8 and 1061.1 keV transitions(see Fig. 4.1.1) and thus, it is possible that a second 327.2 keV transition exists feding into the 1170.5 keV transition. However, it was felt that the available evidence was not good enough to actually place such a transition on the level scheme(impurity reaction channels might also provide the necessary explanation, although the issue was not pursued any further). The 1014.9 keV prompt gate(not shown either) seems to show a sizeable amount of the 882.5 keV transition, but none of the other transitions in the main cascade above the 23^- level(see Fig. 4.1.1), or in the upper side-band. The "impurity button" is pushed again at this point, as no other explanation was found.

4.2 Deduction of the Relative Intensities of Branchings and Transition Cross-Overs

Before I discuss the level scheme below the 480 nsec isomer, I would like to comment on the pros and cons of considering one gate or summing a few, when deducing relative intensities for transitions above the gate(s) in question, or for branching or cross-overs: The

prompt 1061.1 keV gate alone was used in deducing the relative intensities of all the other transitions above the 480 nsec(except for the 495.8 keV transition and the transitions belonging to the lower left band(see Fig. 4.1.1);see Table 4.1.2), since, sitting at the bottom of the main prompt cascade, it is in coincidence not only with all other transitions above it(except for the four transitions in the left lower side band) but also with all the quasi-continuum which decays into each and every of those transitions. The relative transition intensities thus obtained(those depicted in Table 4.1.2) represent the probability the nucleus decays via the discrete transition in question rather than through whatever quasi-continuum exists at the corresponding level energy. Summing gates as we go up the level scheme, in order to deduce relative intensities will restrict the observation of the proper quasi-continuum, and thus, the numbers obtained for those relative intensities would not truly represent how the discrete path stands out over the quasi-continuum. The same would be true for placing gates above transitions in question: the transitions below appear with the intensity of the gate, not with their own, as was discussed in section 3.3 .

However, in order to find branching ratios of transitions de-exciting the same level, and which are so close in energy(such as the 1172.7 keV, close enough to the 1170.5 keV transition) that they appear as one fat peak in gates which return them together use must be made of gates placed on transitions above the level in question. As an example, gating on transitions below the 1170.5 keV peak would only return both it and the 1172.7 keV transition in one fat peak,

thus rendering their relative intensity impossible to determine. However, placing gates on transitons above both of them, will feed the 763.4 and 1170.5 keV transitions(according to Fig. 4.1.1) with equal intensity, one determining the intensity of the 1172.7 keV transition simply by subtracting the intensity of 763.4 keV peak from the fat peak containing both the 1170.5 and 1172.7 keV transitions.

In determining the branching ratio of the 279.0 and 491.0 keV transitions(branching out of the 17^- level), only the sum of the spectra gated on the prompt 763.4 and 1170.5 keV transitions was used, and not the sum of other gates above them, since the level scheme has a certain degree of tentativeness above the 1170.5 keV transition. A branching ratio of 4.27(.87) : 1 was found for the 279.0 keV transition, relative to the 491.0 keV one. The same gates (763.4 and 1170.5 keV) were used to determine a branching ratio of 12.3(4.21) : 1 for the 279.0 keV transition relative to the 212.0 keV one.

In the case of finding the intensity of the 1172.7 keV transition relative to the 535.1 or 637.6 keV ones(which it crosses), it was deemed necessary to sum the prompt spectra gated on the 352.5, 398.0, 477.3 and 720.0 keV transitions(above the 535.1, 637.7 and 1172.7 keV transitions), because of statistics reasons. The intensities of the four transitions roughly add up to the intensity of the 1170.5 keV transition(within experimental error; see Table 4.1.2). A branching ratio of 1.54(.30) : 1 was found for the 535.1 keV transition relative to the 1172.7 keV one.

In order to find the branching ratio of the cross-over 352.5 keV

transition(different from the 352.5 keV transition in the main branch!) relative to the 398.0 keV transition, for example, the prompt 720.0 keV gate was used: this gate fed the 352.5 and 933.1 keV transitions(the cross-overs) with equal intensity, and thus, the intensity of the latter relative to the 398.0 keV transition was the same as that of the 352.5 keV transition to the 398.0 keV one. The ratio found is 1.38(.51) : 1 for the 398.0 keV transition relative to the cross-over 352.5 keV one.

The use of the same technique as in the case of the two cross-overs above, and of the 720.0 keV gate, gave branching ratios of 2.44(.66) : 1 and 2.23(.50) : 1 for the 398.0 keV transition relative to the 820.5 keV and 822.3 keV transitions, respectively. The 398.0 keV transition was taken as reference here, and not the 477.3 keV transition, as it might seem more proper, because the latter was found more intense than the former in the prompt 720.0 keV gate than in the promtp 1061.1 keV gate. This is not understood presently, except for the possibility of the existence of another transition of energy nearly, or exactly, 477.3 keV, which somehow is in coincidence with the 720.0 keV transition, but not with the 1061.1 keV one.(The amount of 398.0 keV transition relative to other transitions present in the prompt 720.0 keV gate was found to be about the same as for in the prompt 1061.1 keV gate.) All branching ratios above have been derived from the information depicted in Table 4.2.1, and translated into intensities relative to the 1061.1 keV transition in Table 4.1.2.

One can see from Table 4.1.2 how the population flow is nicely

Table 4.2.1

Intensities of various transitions(branch-outs and cross-overs) (corrected for Ge efficiency and electron conversion(according to results of chapter 5))with their experimental errors, obtained from the gates indicated below. The sign "+" indicates summing of gates in the gate column, and the presence of two transitions in the peak whose intensity is entered in the intensity column.

Gate(keV)	E_γ(keV)	Intensity(no. of counts)
763.4 +	279.0	6402 ± 630
1170.5	491.0	1501 ± 270
	212.0	520 ± 175
352.5 +	763.4	4832 ± 475
398.0 +	535.1	2377 ± 275
477.3 +	1170.5 + 1172.7	6379 ± 650
720.0		
720.0	398.0	263 ± 52
	933.1	191 ± 60
720.0	757.7	118 ± 33
	820.5 + 822.3	226 ± 112

conserved at the levels to or from which branching and/or cross-over transitions collect or de-excite, respectively. At the 19^- level in the main branch, for example: the relative intensities of the 333.1, 970.7 and 586.8 keV transitions add up to .49 ± .05, which is in excellent agreement with the relative intensity of the 1170.5 keV transition, of 0.46 ± 0.09 . In the light of the discussion in section 3.3, one can see similar cases of such population conservation as the one above(from inspection of Table 4.1.2 and Fig. 4.1.1). The rather large discrepancy between the incoming and outgoing "discrete" population flows at the level $I = 26^-$ is due to the quasi-continuum.

One would like to use, in the analysis above, methods involving as few assumptions about the level scheme to be established as possible, thus keeping as far as possible from the dangers of circular logic. A case in point is the use of the sum of the 352.5, 398.0, 477.3 and 720.0 keV gates in order to derive the intensities of the 1172.7 keV cross-over transition. The use of four such gates involves a lot more assumptions about the level scheme in that region than the use of one such gate. However, the statistics involved was deemed enough of a reason to warrant the use of the gate sum above. Thus a certain amount of quality in the analysis of the data was sacrificed for a certain needed gain in statistics. Inspection of the spectrum in coincidence with the prompt 720.0 keV transition and Fig. 4.1.8, makes one realize that ~4 times the number of counts(and thus halving the statistical fluctuations in the spectrum) would make life much easier in deducing the intensity of the 1172.7 keV transition relative to either the 535.1 or 637.6 keV transitions, for example.

Thus, one could use only one gate on only one transition, instead of four, significantly reducing the number of assumptions about the level scheme.

4.3 The Transitions Below the 480 nsec Isomer

As far as the level scheme below the 480 nsec isomer is concerned, the Table 4.3.1 gives the necessary quantitative tools for setting up the level scheme. Fig. 4.3.1 shows the spectrum in delayed coincidence with a transition below that isomer, namely the 660.8 keV transition. Table 4.3.2 displays the intensities of all the transitions below the isomer, relative to the 1687.5 keV transition. The previous work(Haas et al, 1981 and Julin at al,1982(p.78)) on the level scheme below the 480 nsec isomer is confirmed in the present work, except that the 749.4 keV transition is found to have be about three times more intense than previously reported(Julin et al, 1982(p.78)).

Table 4.3.1

Intensities of all the 11 transitions below the 480 nsec isomer, as deduced from spectra(corrected for Ge efficiency and internal electron conversion down the column but not along the row of gate energies) in coincidence with all the 11 transitions. A column contains intensities (and the appropriate experimental errors* in parantheses below)of all transitions in coincidence with the corresponding transition, whose energy appears at the head of the column. The numbers at the heads of columns and rows refer to transition energies in keV.

	86.9	94.1	101.2	304.3	382.7	389.8
86.9	0.0	109.8	235.3	6.1	26.7	49.3
	(30)	(37)	(15)	(2)	(2)	(5)
94.1	100.0	0.0	0.0	0.0	0.0	28.5
	(30)	(40)	(15)	(3)	(2)	(3)
101.2	175.0	0.0	0.0	4.7	27.7	0.0
	(40)	(40)	(15)	(1)	(3)	(4)
304.3	205.0	0.0	58.8	0.0	0.0	0.0
	(40)	(40)	(15)	(3)	(3)	(4)
382.7	101.0	0.0	191.2	0.0	0.0	0.0
	(30)	(40)	(31)	(3)	(3)	(4)

389.8	125.0	67.8	0.0	0.0	0.0	0.0
	(25)	(30)	(25)	(3)	(3)	(4)
660.8	205.0	70.7	323.5	0.0	60.5	154.5
	(30)	(20)	(30)	(3)	(6)	(16)
739.2	90.0	0.0	0.0	14.6	0.0	0.0
	(26)	(25)	(30)	(3)	(4)	(5)
749.4	210.0	0.0	73.5	10.6	0.0	0.0
	(52)	(25)	(25)	(2)	(4)	(5)
1677.3	260.0	6.6	57.4	13.1	9.3	32.2
	(55)	(3)	(16)	(3)	(2)	(4)
1687.5	325.0	70.3	125.1	13.8	50.6	132.0
	(71)	(19)	(21)	(3)	(6)	(14)

	660.8	739.2	749.4	1677.3	1687.5
86.9	95.5	12.9	4.4	21.7	115.4
	(10)	(3)	(2)	(5)	(29)
94.1	69.7	0.0	0.0	3.6	56.4
	(8)	(4)	(2)	(2)	(20)

101.2	48.5	6.5	4.1	6.5	19.2
	(6)	(2)	(2)	(2)	(8)
304.2	0.0	19.8	12.6	28.3	33.3
	(6)	(3)	(4)	(4)	(9)
382.7	96.9	0.0	0.0	12.9	87.2
	(11)	(4)	(2)	(2)	(23)
389.8	248.5	0.0	0.0	26.9	183.3
	(27)	(4)	(2)	(3)	(48)
660.8	0.0	0.0	0.0	39.5	226.2
	(7)	(4)	(2)	(4)	(45)
739.2	0.0	0.0	0.0	0.0	32.1
	(7)	(4)	(2)	(4)	(12)
749.4	0.0	0.0	0.0	19.6	0.0
	(7)	(4)	(2)	(3)	(12)
1677.3	64.4	0.0	17.2	0.0	0.0
	(7)	(5)	(3)	(5)	(13)
1687.5	351.5	16.9	0.0	0.0	0.0
	(39)	(3)	(3)	(4)	(13)

* Same method used in the examples in section 3.5 was used.

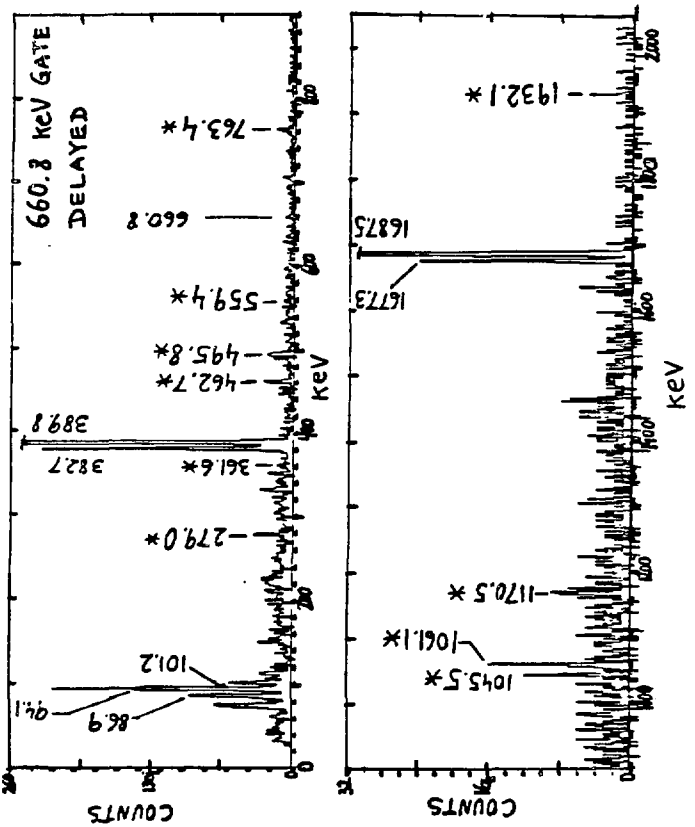
660.8 KeV GATE
DELAYED
COUNTS
KeV
44.1
86.9
101.2
279.0*
361.6*
382.7
389.8
462.7*
495.8*
559.4*
660.8
763.4*
1045.5*
1061.1*
1170.5*
1677.3
1687.5
1932.1*

Fig. 4.3.1

Table 4.3.2

Intensities(relative to the 1687.5 keV transition), spin and parity assignments for all observed transitions in ^{148}Dy, below the 480 nsec isomer. Only coincidences with the RF - Ge TAC gate 3(late) were considered(except as noted).

$I_i^\pi \rightarrow I_f^\pi$	E_{level}(keV)	E_γ(keV)	I_γ^{rel}	E	M	λ^*
$2^+ \rightarrow 0^+$	1677.3	1677.3(5)	0.27(2)**	E		2
$3^- \rightarrow 0^+$	1687.5	1687.5(5)	1.00	E		3
$5^- \rightarrow 3^-$	2348.3	660.8(3)	0.90(4)	E		2
$4^+ \rightarrow 2^+$	2426.7	749.4(3)	0.18(2)	E		2
$4^+ \rightarrow 3^-$	2426.7	739.2(3)	0.03(1)	E		1
$6^+ \rightarrow 4^+$	2731.0	304.3(2)	0.20(2)	E		2
$6^+ \rightarrow 5^-$	2731.0	382.7(2)	0.08(1)	E		1
$7^- \rightarrow 5^-$	2738.1	389.8(2)	0.58(5)	E		2
$8^+ \rightarrow 6^+$	2832.2	101.2(3)	0.16(2)	E		2
$8^+ \rightarrow 7^-$	2832.2	94.1(3)	0.30(2)	E		1
$10^+ \rightarrow 8^+$	2919.1	86.9(3)	0.60(6)	E		2

* Taken from Haas et al, 1981 and Ward et al, 1983, and verified(where statistics allowed) via angular correlation measurements in the present work(see section 5.1).

** Obtained from the sum of prompt gates on the 1061.1, 462.7, 495.8, 1045.5 and 279.0 keV transitions above the isomer.

Chapter 5

Multipolarity(and Parity)Information from Angular Correlations and the RF - Ge and Ge - Ge TAC's, Respectively.

The information derivable from angular correlations depends on the type of radiation observed(i.e. whether it's α, β, γ or e^-), and whether the experiment yielded the direction, polarization or the energy of the respective radiation, as well as the extra-nuclear fields acting on the nucleus in question. Gamma-gamma directional correlation(i.e. the observation of the directions of the two coincident γ-rays involved) yields the spins of the nuclear levels, but not their parities. If one also observed the polarization of the γ-rays(in addition to their directional correlation), or if one observed the directional correlations between conversion electrons(e^-), one could deduce the parities in question.

The figure below depicts the simplest example of an angular correlation experiment. The two γ-rays, γ_1 and γ_2, are emitted rapidly one after each other. One then asks for the probability

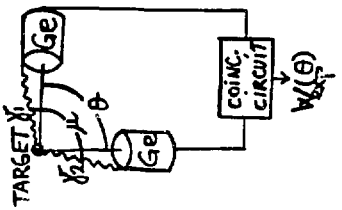

Fig. 5.0.0

$W(\theta)d\Omega$ that γ_2 is emitted into the solid angle $d\Omega$ at an angle θ with respect to $\vec{k}_1$, the direction of emission of γ_1. Experimentally one records the number of coincidences between γ_1 and γ_2 as a function of the angle θ between the detectors in question. Actually the numbers so obtained are the averages of the true correlation function $W(\mu)$ over the angles μ distributed around θ. This is so because of the finite acceptance angle of any given detector used. For the present case, $(\mu - \theta)/\theta$ is around 10 percent, and thus one probably does not make a large error if one neglects such correction in obtaining $W_{exp}(\theta)$. The comparison of $W_{exp}(\theta)$ with theory finally will provide tentative information as to the multipolarities the transitions observed in ^{148}Dy carry, as well as whether they are stretched or not.

The RF - Ge and Ge - Ge TAC's provide information about the meanlife of the transitions in question, and about their promptness with respect to each other. This information will give tentative assignments to the parities carried by the transitions in question. This together with the information given by the angular correlation will tentatively assign spin and parity values to the experimental levels observed in ^{148}Dy.

5.1 The Angular Correlation Measurements

The very simple case of a cascade of two γ-rays(Fig. 5.1.1) poses the question of finding the directional correlation function $W(\vec{k}_1,\vec{k}_2)$, where $W(\vec{k}_1,\vec{k}_2)d\Omega_1 d\Omega_2$ is defined as the probability that a nucleus, decaying through the cascade $I_i \rightarrow I \rightarrow I_f$ emits the two radiations R_1 and R_2 in the directions $\vec{k}_1$ and $\vec{k}_2$ into the solid angles $d\Omega_1$ and $d\Omega_2$. This case is the basis for generalizing to the most general case of a large number of γ-rays in the cascade, where a beam direction or the observation of some γ-ray in a fixed direction selects an ensemble of nuclei with a non-isotropic distribution of spin orientations. The succeding coincident radiations then show a definite angular correlations with respect to the direction of the emission of the first(i.e. the γ-ray on which one gates).

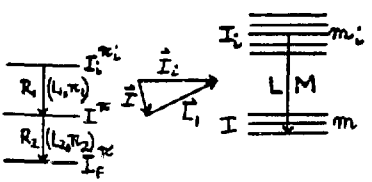

Fig. 5.1.1

The details about deriving expressions for $W(\vec{k}_1,\vec{k}_2)$ are described clearly in the literature(Frauenfelder et al,1965), where use was made of first order perturbation theory and the corresponding density matrices: The nucleus in question decays from the initial level i with spin I_i, described by the density matrix ρ_i, to the intermediate level with spin I by emitting the radiation R_1

observed in the direction $\vec{k}_1$. First order perturbation theory yields the density matrix $\rho(\vec{k}_1)$, through which the intermediate state is thus fully described, the argument $\vec{k}_1$ indicating the density matrix depends on the direction the radiation R_1 was observed. The second step in the cascade leads to the density matrix of the final state, $\rho_f(\vec{k}_1,\vec{k}_2)$, which is the result of the preceding transition.

The advantage of incorporating the density matrix and first order perturbation theory becomes apparent when one has to deal with external fields which tend to split the degenerate states of the intermediate nuclear level, thus causing a perturbation on the angular correlation. It also becomes apparent when one has to take into account that the initial level has a certain distribution of m-states which tends to widen as one progresses down the cascade. In the present case, calculations of the angular correlations were done assuming a gaussian distribution in the m-states with HWHM(half-width-at-half-maximum) taking values of 0, 4, 6, and infinity, the latter being the case for the transitions below the 480 nsec isomer. The long life of the 10^+ level is ample for the paramagnetic fields created around the target to deorient the nuclear spins induced by the reaction, such that every m-state becomes equally probable.

The unperturbed angular correlation for the case of only two rapidly succeding coincident γ-rays is given by the complicated expression below(see Frauenfelder et al(1965) for its derivation):

$$W(\vec{k}_1,\vec{k}_2) = (-1)^{2I-I_i-I_f} \sum\sum\sum (-1)^{K-L_1-L_2} \begin{Bmatrix} I & I & K \\ L_1 & L_1 & I_i \end{Bmatrix} * \tag{5.1.1}$$

$$* \begin{Bmatrix} I & I & K \\ L_2 & L_2 & I_f \end{Bmatrix} |\langle I \| L_1 \pi_1 \| I_i \rangle|^2 |\langle I_f \| L_2 \pi_2 \| I \rangle|^2 C^{\dagger}_{K\tau_1}(L_1) C^{\dagger}_{K\tau_2}(L_2) D^K_{\tau_2\tau_1}(\vec{K}_2 \to \vec{K}_1)$$

where c_k is the Racah radiation coefficient, which is an eigenfunction of the operaror $L_z = \frac{\hbar}{i}\frac{\partial}{\partial\gamma}$ with eigenvalue τ. γ is the angle denoting a rotation with respect to the direction of propagation of the radiation in question. In the present analysis, polarization of the observed radiations is not considered(since no such sorting of the data was made due to statistics considerations), but only the directions of the two radiations in question, R_1 and R_2. In this case, τ becomes zero since $W(\vec{k}_1,\vec{k}_2)$ must be independent of the Euler angle γ. The representations D^k become then Legendre polynomials and (5.1.1) simplifies into:

$$W(\vec{k}_1,\vec{k}_2) = W(\theta) = \sum_{K=\text{even}} A_{kk} P_k(\cos\theta), \tag{5.1.2}$$

where θ is the angle between $\vec{k}_1$ and $\vec{k}_2$, and the coefficients A_{kk} break up into two factors, each depending on only one transition in the cascade:

$$A_{kk} = A_k(L_1 I_i I) A_k(L_2 I_f I) \tag{5.1.3}$$

$$A_k(L_1 I_i I) = \sum (-1)^{L_1} C^{\dagger}_{K0}(L_1) \begin{Bmatrix} I & I & K \\ L_1 & L_1 & I_i \end{Bmatrix} |\langle I \| L_1 \pi_1 \| I_i \rangle|^2$$

and similarly for $A_k(L_2 I_f I)$. In the expressions above $\langle \| \| \rangle$ are the usual reduced matrix elements, and the 6-j symbols above must

satisfy the triangle rule $0 < k < \mathrm{Min}(2I, 2L_1, 2L_2)$, otherwise they vanish.

All the treatment above was done for the case of pure multipole radiation(i.e. no mixing). The most general case of many γ-rays emitted in coincidence down a cascade can be treated in the same format, only more complicated sums involving 6-j and 9-j coefficients are involved, which goes beyond the scope of the present dissertation. It is easy to calculate angular correlations between coincident γ-rays which do not necessarily follow each other, as long as the transitions in between are stretched(i.e. $L = |I_i - I_f|$), in which case it is as if they are not there at all. In the case when the intermediate transitions are non-stretched(i.e. $L > |I_i - I_f|$), angular correlation calculations are considerably more complicated.

Experimentally, the data were sorted in the $0^\circ - 90^\circ$, $0^\circ - 0^\circ$ and $90^\circ - 90^\circ$ formats(see chapter 2 and the appendix) whereby coincidences were considered between detectors in the backward direction and those around 90°, as well as between detectors in the backward direction and between detectors at 90°, respectively. Table 2.2.1 gives the positions of the detectors in question(1,2,3 and 4 in the backward direction, and 6,10,11 and 12 clustered around 90° with respect to the beam direction), as well as the corresponding polar angles. Gates were then placed on various transitions(appearing with a good counting rate in the deacy scheme) detected in the backward direction, and at 90° while the intensities of various coincident transitions detected at 90°, in the backward direction(and vice versa) were measured.

For the transitions below the 480 nsec isomer, where previous

work(Haas et al, 1981 and Julin et al, 1982(p.78))has given rather unambiguous assignments for the multipolarities(and parities) of those eleven transitions, the present data were compared to calculations done with an infinite HWHM of the m-states distribution for a state with spin equal to 10(Draper, 1984, private communication). The format of comparison was (0°, 90°), (90°, 0°), (0°, 0°), (90°, 90°), normalized so the (90°, 0°) column was unity. Table 5.1.1 shows the experimental values obtained(and their uncertainties), while Table 5.1.2 shows ratios of the deviations of the experimental values from theory to the magnitude of the experimental uncertainty. The last column displays the Figure-of-Merit(F.O.M.) of the experimental table, (i.e. Table 5.1.1)which is the square root of the sum of the squares of the percent deviations in the three columns(calculated row by row). Since the uncertainties include the statistical part as well as the part due to the quasi-continuum peaklets (see chapter 3), which have a random nature, the F.O.M.'s should average to unity. Indeed, the average of the numbers in the F.O.M. column comes to about 0.93, not far from unity.

The previously assigned values for the multipolarities below the 480 nsec isomer thus seem to be agree(within experimental error) in the present work, which provides a good test of the data for angular correlations to be used above the isomer, where there exist a lot more unknowns. Table 5.1.5 shows the theoretical calculations (Draper, 1984, private communication)(treated in the same way as the data), and Table 5.1.3 shows the experimental values for the angular correlations for all the transitions observed above the isomer, while

Table 5.1.1

Angular correlations measurements(for all transitions below the 480 nsec isomer) in the (0°, 90°), (90°, 0°), (0°, 0°) and (90°, 90°) formats, normalized such that the (90°, 0°) column is unity(and therefore omitted).

Transition		Gate		(0°, 90°)	(0°, 0°)	(90°, 90°) *
E_γ	λ	E_γ	λ			
1687.5	3	660.8	2	1.09 ± .35	1.15 ± .50	1.12 ± .50
389.8	2	660.8	2	1.16 ± .26	1.19 ± .40	1.27 ± .45
94.1	1	660.8	2	1.23 ± .43	1.03 ± .46	1.14 ± .51
382.7	1	660.8	2	1.21 ± .30	1.14 ± .51	1.36 ± .61
101.2	2	660.8	2	.83 ± .29	.89 ± .40	.67 ± .29
86.9	2	660.8	2	.95 ± .47	1.02 ± .48	.95 ± .43
1677.3	2	660.8	2	.95 ± .45	.96 ± .44	1.10 ± .51
739.2	1	1687.5	3	3.50 ± 2.21	3.33 ± 2.07	1.33 ± 1.26
660.8	2	1687.5	3	.97 ± .28	1.14 ± .39	1.27 ± .46
389.8	2	1687.5	3	1.01 ± .32	1.04 ± .47	1.30 ± .60
382.7	1	1687.5	3	.85 ± .26	1.37 ± .57	1.25 ± .56
304.3	2	1687.5	3	2.01 ± 1.03	1.07 ± .52	1.33 ± .70
101.2	2	1687.5	3	**	**	**
94.1	1	1687.5	3	1.29 ± .68	1.90 ± 1.01	1.71 ± .92
86.9	2	1687.5	3	1.33 ± .74	1.99 ± 1.06	1.33 ± .72

* Averaged over the azimuthal angle values, $\phi = 0°$ and 90° .

** Poor statistics prevented obtaining a value.

Table 5.1.2

Deviations of angular correlations results for all transitions below the 480 nsec isomer(see Table 5.1.1) from theoretical values(see text and Table 5.1.5). The deviations below, Δ_{th}, are ratios of the magnitudes of differences between experimental and theoretical values to the magnitude of the absolute error in the values given in Table 5.1.1 . The last column below displays the figure-of-merit(FOM) of experimental data(see text).

Transition		Gate		(0°, 90°)	(0°, 0°)	(90°, 90°)	FOM
E_γ	λ	E_γ	λ	Δ_{th}	Δ_{th}	Δ_{th}^*	
1687.5	3	660.8	2	0.26	0.28	0.06	0.39
389.8	2	660.8	2	0.58	0.06	0.42	0.72
94.1	1	660.8	2	0.53	0.23	0.37	0.69
382.7	1	660.8	2	0.70	0.47	0.68	1.08
101.2	2	660.8	2	0.59	0.69	1.43	1.69
86.9	2	660.8	2	0.11	0.31	0.31	0.45
1677.3	2	660.8	2	0.11	0.47	0.04	0.48
739.2	1	1687.5	3	1.13	1.21	0.33	1.69
660.8	2	1687.5	3	0.11	0.39	0.27	0.49
389.8	2	1687.5	3	0.03	0.54	0.26	0.60
382.7	1	1687.5	3	0.58	0.96	0.60	1.27
304.3	2	1687.5	3	0.98	0.43	0.26	1.10
101.2	2	1687.5	3	**	**	**	**
94.1	1	1687.5	3	0.42	1.06	0.86	1.43
86.9	2	1687.5	3	0.45	0.66	0.25	0.84

* Deviations with respect to averages of theoretical values over the azimuthal angle values, $\phi = 0°$ and $90°$.

** Poor statistics prevented obtaining values(see Table 5.1.1).

Table 5.1.4 displays the comparison to theory, done just like for the transitions below the isomer(except that the F.O.M. for the three formats, (0° and 90°), (0°, 0°) and (90°, 90°), is the square root of the average of the squares of the percent deviations from experiment). Table 5.1.4(c) summarizes the final choices for the transition multipolarities, indicating in parantheses the F.O.M.'s for the four HWHM's(0, 4, 6 and infinity). For almost all transition-gate combinations, one can see that F.O.M.'s and the corresponding HWHM are resonable(the latter being close to zero for gate and/or transition close to the top of the level scheme, and increasing to values of 4 or 6 towards the bottom of the level scheme).

Table 5.1.4(c) lists the F.O.M.'s for the 1061.1, 495.8, 1045.5, 462.7, 279.0 and 1932.1 keV transitions for multipolarities smaller by one unit than the ones tentatively chosen. This has been done in effort to explore other ways to match the spins up to I = 17⁻(see Fig. 4.1.1) than making the 1932.1 keV transition a stretched E3. Overall, the F.O.M.'s marginally seem to favor an E3 for the 1932.1 keV transition, one not being able, however, to eliminate the possibility of a stretched E2. Similarly, listed are the F.O.M.'s for the 361.6 and 559.4 keV transitions, such that they are assigned multipolarities greater by one unit than the ones tentatively chosen. While it appears that the 361.6 keV transition can safely be chosen to have a stretched multipolarity of 1, it seems it is quite possible to make the 559.4 keV transition a stretched E2(although only marginally). Finally, the same discussion applies to the 1932.1 keV transition. The 491.0 keV transition had already been tentatively found to

Table 5.1.3

(a) Angular correlations measurements (for all transitions above the 480 nsec isomer) in the (90°, 0°), (0°, 90°), (0°, 0°) and (90°, 90°) formats, where the two angles inside each paranthesis represent the angles for the transition ("XN") and its corresponding gate, respectively (see text). The numbers in each of the four columns below, are the actual areas under the γ-ray peaks, (normalized to the same number of Ge pairs firing coincidently; see text), together with their uncertainties (in the "+-" columns) (obtained by the prescription described in section 3.5). The areas tabulated below need no and have not been corrected for Ge efficiency or electron conversion. The presence of "99" indicates that it was not possible to obtain a value for the respective entry, due to poor statistics.

ROW	GATE	XN	(90°,0°)	+-	(0°,90°)	+-	(0°,0°)	+-	(90°,90°)	+-
1	333.1	114.2	89	18	102	18	69	20	123	21
2	333.1	279.8	436	44	313	31	219	23	608	61
3	333.1	352.4*	123	17	131	18	65	18	227	23
4	333.1	361.7	81	16	60	15	20	16	85	19
5	333.1	398.1	95	16	133	17	101	19	113	19
6	333.1	406.9	43	14	60	15	51	17	67	18
7	333.1	462.5	153	18	285	29	203	22	237	24
8	333.1	477.5	45	14	79	15	108	19	55	17
9	333.1	491.1	72	15	130	17	117	19	99	18
10	333.1	496.1	255	26	293	29	205	22	444	44
11	333.1	535.0	89	15	112	16	120	19	128	19
12	333.1	559.3	39	14	63	14	53	16	81	17
13	333.1	567.8	36	13	32	13	13	14	59	17
14	333.1	637.8	107	16	237	24	155	20	105	18
15	333.1	720.5	47	13	44	13	43	15	49	15
16	333.1	750.5	26	12	32	12	43	15	41	15
17	333.1	758.0	96	15	90	16	22	14	148	19
18	333.1	763.9	215	22	266	26	213	21	372	37
19	333.1	822.2*	43	13	87	14	49	16	53	15
20	333.1	883.0	43	12	93	14	53	16	44	14
21	333.1	933.2	21	11	47	12	31	13	41	14
22	333.1	971.1	17	11	14	11	3	12	19	13
23	333.1	1014.9		99		99		99		99
24	333.1	1045.9	114	14	166	17	141	18	160	18
25	333.1	1061.4	170	17	124	16	160	19	190	19
26	333.1	1171.2*	153	16	230	23	166	18	233	23
27	333.1	1032.1	6	7	22	8	20	9	30	10
28	763.4	114.2	115	15	92	15	59	16	101	17
29	763.4	278.9	361	36	281	28	262	25	677	58

ROW	GATE	XN	(90°,0°)	+-	(0°,90°)	+-	(0°,0°)	+-	(90°,90°)	+-
30	763.4	327.2			NOT IN THE		GATE			
31	763.4	333.2	296	30	243	24	229	23	361	36
32	763.4	352.5*	169	17	101	14	113	17	221	22
33	763.4	361.4	62	12	69	13	65	14	103	16
34	763.4	398.2	80	12	100	14	103	16	61	14
35	763.4	407.1	49	12	32	11	13	12	111	17
36	763.4	462.7	225	23	306	31	251	25	299	30
37	763.4	477.4	70	13	83	13		99		99
38	763.4	491.0	44	11	81	13	80	15	69	14
39	763.4	496.0	306	31	312	31	291	29	441	44
40	763.4	535.3	94	13	212	21	135	17	167	18
41	763.4	559.3	26	10	100	13	40	13	83	15
42	763.4	567.8	60	12	33	11	40	13	64	14
43	763.4	586.9	29	10	52	11	16	11	29	12
44	763.4	637.9	65	11	100	13	60	13	97	15
45	763.4	720.2	55	11	60	11	44	12	73	14
46	763.4	750.2	27	10	33	10	40	12	44	12
47	763.4	757.6	63	11	70	12	33	12	77	14
48	763.4	821.7*	40	10	88	12	51	12	87	14
49	763.4	882.6	40	10	134	14	85	14	64	13
50	763.4	933.3	55	11	55	11	45	12	41	11
51	763.4	970.6	16	8	30	10	36	11	60	12
52	763.4	1015.0	7	8	20	9	19	10	27	10
53	763.4	1045.7	126	13	184	18	164	17	192	19
54	763.4	1061.3	135	14	208	21	112	15	232	23
55	763.4	1170.0*	191	19	194	19	163	17	267	27
56	763.4	1932.3	15	6	22	7	15	7	23	8
57	1061.1	114.2	63	10	80	11	39	10	34	10
58	1061.1	279.0	305	39	245	25	251	25	469	47
59	1061.1	327.3	53	9	16	7	41	10	69	12
60	1061.1	333.0	203	20	223	22	189	19	239	24
61	1061.1	352.6*	103	12	92	11	85	13	191	19
62	1061.1	399.0	81	11	83	11	80	13	80	12
63	1061.1	407.2	23	7	22	7	45	10	32	9
64	1061.1	416.2?	42	9	66	10	43	10	137	15
65	1061.1	462.6	331	33	332	33	316	32	379	38
66	1061.1	477.2	69	10	113	12	72	12	124	14
67	1061.1	496.0	382	38	353	35	388	39	447	45
68	1061.1	535.1	101	11	112	12	120	14	125	14
69	1061.1	567.8	28	7	33	8	13	7	51	10
70	1061.1	586.9	16	7	21	7	12	7	27	8
71	1061.1	637.5	47	9	60	9	85	12	53	10
72	1061.1	720.1	60	9	23	7	40	10	101	13
73	1061.1	750.4	23	7	45	8	35	9	24	8
74	1061.1	757.6	52	9	44	8	37	9	45	10
75	1061.1	763.5	223	22	158	16	156	16	272	27
76	1061.1	821.3*	37	8	81	10	85	12	49	10
77	1061.1	882.6	31	7	60	9	53	10	57	10
78	1061.1	933.2	10	5	21	6	40	9	32	8
79	1061.1	970.9	25	7	23	6	60	10	34	8
80	1061.1	1015.0	16	6	26	7	19	7	11	6
81	1061.1	1021.7?	10	5	76	10	40	9	41	9
82	1061.1	1045.5	186	19	234	23	159	16	177	18
83	1061.1	1171.0*	141	14	145	15	142	15	229	23
84	1061.1	1241.7?	40	8	66	9	13	6	51	9

(b) Angular correlation values (i.e. the areas and their uncertainties) from (a) normalized to the (90°, 0°) column (i.e. all entries in the (90°, 0°) column are unity, and omitted). Entries with "99.999" or ".99" denote poor statistics.

ROW	GATE	XN	(0°,90°)	+-	(0°,0°)	+-	(90°,90°)	+-
1	333.1	114.2	1.146	.31	.775	.27	1.382	.37
2	333.1	279.0	.718	.10	.502	.07	1.394	.20
3	333.1	352.4*	1.065	.21	.531	.16	1.843	.32
4	333.1	361.7	.741	.24	.247	.20	1.053	.31
5	333.1	399.1	1.400	.30	1.067	.27	1.193	.29
6	333.1	406.9	1.163	.52	1.178	.56	1.550	.66
7	333.1	462.5	1.863	.28	1.325	.21	1.551	.24
8	333.1	477.5	1.756	.65	2.400	.86	1.215	.53
9	333.1	491.1	1.806	.44	1.630	.43	1.370	.38
10	333.1	496.1	1.149	.16	.805	.12	1.741	.25
11	333.1	535.0	1.258	.28	1.348	.32	1.438	.33
12	333.1	559.3	1.359	.59	1.350	.63	2.085	.85
13	333.1	567.8	.889	.50	.370	.43	1.926	.86
14	333.1	637.8	2.215	.39	1.445	.28	.984	.22
15	333.1	720.5	.936	.38	.922	.41	1.050	.44
16	333.1	750.5	1.231	.75	1.641	.95	1.590	.93
17	333.1	758.0	.938	.21	.229	.15	1.542	.31
18	333.1	763.9	1.191	.17	.992	.14	1.730	.24
19	333.1	822.2*	2.023	.67	1.147	.48	1.240	.50
20	333.1	883.0	2.163	.70	1.240	.49	1.023	.44
21	333.1	933.2	2.238	1.32	1.460	1.00	1.968	1.23
22	333.1	971.1	.849	.85	.162	.71	1.131	1.06
23	333.1	1014.9	99.999	.99	99.999	.99	99.999	.99
24	333.1	1045.9	1.456	.23	1.240	.22	1.404	.24
25	333.1	1061.4	.729	.11	.989	.15	1.118	.16
26	333.1	1171.2*	1.503	.21	1.020	.16	1.525	.22
27	333.1	1932.1	3.667	4.38	3.333	4.09	5.000	5.93
28	763.4	114.2	.800	.17	.513	.15	.878	.19
29	763.4	278.9	.778	.11	.598	.10	1.599	.23
30	763.4	327.2	----		NOT IN THE GATE —			
31	763.4	333.2	.821	.12	.775	.11	1.221	.17
32	763.4	352.5*	.598	.10	.671	.12	1.310	.19
33	763.4	361.4	1.327	.40	1.051	.37	1.974	.56
34	763.4	398.2	1.667	.42	1.711	.45	.844	.29
35	763.4	407.1	.653	.28	.272	.25	2.259	.65
36	763.4	462.7	1.360	.19	1.114	.16	1.327	.19
37	763.4	477.4	1.186	.28	99.999	.99	99.999	.99
38	763.4	491.0	1.862	.57	2.023	.64	1.594	.53
39	763.4	496.0	1.020	.14	.950	.13	1.442	.20
40	763.4	535.3	2.255	.39	1.433	.27	1.773	.32
41	763.4	559.3	3.845	1.62	1.538	.79	3.179	1.39
42	763.4	567.8	.550	.21	.667	.25	1.067	.31
43	763.4	586.9	1.776	.75	.552	.44	.989	.55
44	763.4	637.9	1.818	.45	1.091	.33	1.770	.46

ROW	GATE	XN	$(0^o,90^o)$	+-	$(0^o,0^o)$	+-	$(90^o,90^o)$	+-
45	763.4	720.2	1.055	.30	.800	.28	1.333	.37
46	763.4	750.2	1.222	.58	1.778	.79	1.630	.74
47	763.4	757.6	1.111	.27	.529	.21	1.228	.31
48	763.4	821.7*	2.200	.64	1.267	.45	2.167	.66
49	763.4	882.6	3.350	.91	2.133	.64	1.600	.51
50	763.4	933.3	1.009	.28	.832	.27	.758	.26
51	763.4	970.6	2.452	1.47	2.323	1.45	3.871	2.26
52	763.4	1015.0	2.857	3.40	2.762	3.38	3.810	4.48
53	763.4	1045.7	1.460	.21	1.302	.19	1.524	.22
54	763.4	1061.3	1.541	.22	.930	.14	1.719	.24
55	763.4	1170.8*	1.016	.14	.852	.12	1.396	.20
56	763.4	1932.3	1.483	.78	1.057	.66	1.563	.85
57	1061.1	114.2	1.270	.27	.619	.19	.540	.12
58	1061.1	279.0	.636	.09	.651	.09	1.219	.17
59	1061.1	327.3	.283	.14	.780	.23	1.308	.32
60	1061.1	333.0	1.099	.16	.933	.13	1.176	.17
61	1061.1	352.6*	.888	.15	.828	.15	1.851	.28
62	1061.1	398.0	1.025	.19	1.086	.21	.988	.20
63	1061.1	407.2	.957	.44	1.971	.77	1.391	.60
64	1061.1	416.2?	1.560	.40	1.016	.32	3.270	.76
65	1061.1	462.6	1.003	.14	.955	.14	1.144	.16
66	1061.1	477.2	1.638	.29	1.043	.23	1.797	.33
67	1061.1	496.0	.924	.13	1.016	.14	1.169	.17
68	1061.1	535.1	1.109	.17	1.188	.19	1.241	.20
69	1061.1	567.8	1.179	.42	.476	.29	1.810	.60
70	1061.1	586.9	1.313	.69	.750	.55	1.667	.86
71	1061.1	637.5	1.266	.30	1.016	.42	1.135	.30
72	1061.1	720.1	.383	.13	.800	.20	1.689	.34
73	1061.1	750.4	1.957	.68	1.507	.59	1.043	.46
74	1061.1	757.6	.846	.21	.718	.21	.949	.25
75	1061.1	763.5	.709	.10	.700	.10	1.220	.17
76	1061.1	821.3*	2.189	.53	2.414	.60	1.333	.38
77	1061.1	882.6	1.935	.53	1.720	.51	1.849	.54
78	1061.1	933.2	2.100	1.31	4.000	2.35	3.200	1.93
79	1061.1	970.9	.920	.36	2.400	.76	1.360	.49
80	1061.1	1015.0	1.625	.73	1.167	.61	.667	.46
81	1061.1	1021.7?	7.600	4.14	4.800	2.71	4.067	2.33
82	1061.1	1045.5	1.258	.18	.853	.12	.953	.13
83	1061.1	1171.0*	1.028	.15	1.007	.14	1.626	.23
84	1061.1	1241.7?	1.375	.29	.278	.14	1.056	.26

For (a):

* Represents two transitions, as follows: two 352.5 keV transitions(the one de-exciting from 24^- being 28% of the total area); the 822.3 keV transition is 45% of the total area(820.5 + 822.3 keV); the 1172.7 keV transition is 24% of the total area(1170.5 + 1172.7 keV). (See Table 4.1.2 .)

? Means the respective entries were not used in any angu-

lar correlation comparison with theory, because those three transitions could not be placed on the level scheme due to lack of positive evidence(see chapter 4).

For (b):

* The entry can determine the same multipolarity for the two transitions involved(see (a)).

? Same interpretation as in (a).

For (a) and (b):

The entries under "GATE" and "XN" are in keV.

The γ-ray energy under "GATE" is the value obtained from all-detector coincidence work(see chapter 4) and thus more exact than the values under "XN", which are the averages of the γ-ray energies as obtained from the four angular correlation formats(with a lot poorer statistics than for all-detector format).

Table 5.1.4

(a)Deviations of experiment from theory divided by experimental uncertainties for the (0°, 90°), (0°, 0°) and (90°, 90°) formats(referred to below as cells). The first four digits refer to the transition angular momenta(see Table 5.1.5). The last column of each group(for a given HWHM) is the F.O.M.(see text). The "ROW" refers to Table 5.1.5 row numbers.

ROW. GATE. TRANSITION (KEV)= 67 1061.1 496. IN EACH GROUP, NORM'D TO (90°,0°) OR (0°,90°), ARE ITS MATE,(0°,0°),(L90°,90°) AS .8 OF 90°,90° & .2 OF 0°,0°(90°,90°).
#1 ROW OF 20 PAIRS IS NORM'D TO (L1,L2)=(90°,0°). #2 TO (0°,90°).
GROUPS L TO R ARE GAUSSIAN HW=0,4,6,INF, RESP. LAST COL IS ROWB. 9.8 MEANS ERROR > 3.5 SIGMAS IN AT LEAST 1 OF 3 CELLS. LISTED IS (DAT-THEOR)/UNCERT.

11	00	-0.6	+2.7	-3.0	2.4	-0.6	+1.9	-1.5	1.5	-0.6	+1.1	-0.6	0.8	-0.6	-0.4	+0.7	0.6	1
11	00	-0.6	+2.7	-3.0	2.4	-0.6	+1.9	-1.6	1.5	-0.6	+1.1	-0.6	0.8	-0.6	-0.4	+0.7	0.6	2
12	00	+4.3	+2.7	+3.9	9.8	+3.3	+2.1	+3.2	2.9	+2.1	+1.6	+2.7	2.2	-0.6	+0.8	+1.5	1.1	3
12	00	-9.9	-4.7	-1.6	9.8	-8.3	-3.0	-0.6	9.8	-4.8	-1.4	+0.3	9.8	-0.6	+0.8	+1.5	1.1	4
13	00	+5.1	+2.0	+4.9	9.8	+4.3	+2.1	+4.4	9.8	+3.0	+1.8	+3.7	9.8	-0.6	+1.3	+1.9	1.4	5
13	00	-9.9	-9.9	-1.4	9.8	-9.9	-6.4	-0.2	9.8	-7.3	-2.8	+0.7	9.8	-0.6	+1.3	+1.9	1.4	6
22	00	-0.6	-4.7	+2.4	9.8	-0.6	-3.3	+2.3	2.3	-0.6	-2.3	+1.7	1.7	-0.6	-1.1	+0.2	0.7	7
22	00	-0.6	-4.7	+2.4	9.8	-0.6	-3.3	+2.3	2.3	-0.6	-2.3	+1.7	1.7	-0.6	-1.1	+0.2	0.7	8
23	00	+1.7	-4.8	+3.8	9.8	+1.4	-3.4	+3.3	2.8	+0.7	-2.7	+2.3	2.1	-0.6	-1.9	-0.4	1.2	9
23	00	-3.9	-9.9	+2.4	9.8	-3.2	-7.0	+2.0	9.8	-2.2	-4.7	+1.3	9.8	-0.6	-1.9	-0.4	1.2	10
33	00	+0.6	-9.9	+3.4	9.8	-0.6	-7.3	+2.8	9.8	-0.6	-5.7	+1.6	9.8	-0.6	-3.8	-1.7	9.8	11
33	00	-0.6	-9.9	+3.4	9.8	-0.6	-7.3	+2.8	9.8	-0.6	-5.7	+1.6	9.8	-0.6	-3.8	-1.7	9.8	12
11	05	+4.7	+2.8	+4.3	9.8	+3.6	+2.1	+3.6	9.8	+2.4	+1.7	+3.8	2.4	+0.6	+1.0	+1.6	1.1	13
11	05	-9.9	-6.5	-1.7	9.8	-9.9	-4.0	-0.6	9.8	-5.5	-1.8	+0.4	9.8	-0.6	+1.0	+1.6	1.1	14
11	55	-0.7	-6.9	+3.1	9.8	-0.7	-4.8	+2.4	9.8	-0.6	-3.7	+1.5	9.8	-0.6	-2.2	-0.6	1.4	15
11	55	-0.4	-6.6	+3.1	9.8	-0.5	-4.6	+2.5	9.8	-0.5	-3.6	+1.6	9.8	-0.6	-2.2	-0.6	1.4	16
12	01	+3.1	+2.9	+1.7	2.6	+1.7	+2.1	+1.0	1.6	+0.8	+1.5	+0.8	1.1	-0.6	-0.8	+0.9	0.6	17
12	01	-7.5	-0.9	-3.2	9.8	-3.7	+0.0	-1.5	9.8	-2.2	+0.3	-0.5	1.3	-0.6	-0.8	+0.9	0.6	18
12	06	-9.9	-2.5	-9.9	9.8	-3.3	+1.7	-4.4	9.8	-1.5	+0.7	-1.5	1.3	-0.6	-0.5	+0.6	0.6	19
12	06	+6.5	+6.3	-2.5	9.8	+1.4	+3.1	-1.4	2.1	+0.2	+1.4	-0.5	0.9	-0.6	-0.5	+0.6	0.6	20
12	50	-2.0	-6.9	+2.4	9.8	-1.3	-4.5	+2.8	9.8	-1.0	-3.3	+1.4	2.1	-0.6	-1.8	-0.3	1.1	21
12	50	+0.6	-4.6	+3.1	9.8	+0.1	-3.4	+2.5	2.4	-0.2	-2.7	+1.7	1.9	-0.6	-1.8	-0.3	1.1	22
12	51	-6.4	-6.9	+2.5	9.8	-5.9	-5.0	+1.4	9.8	-4.2	-3.0	+1.1	9.8	-0.5	+0.5	+1.3	0.9	23
12	51	-2.7	-6.9	+4.5	9.8	+2.6	-0.0	+3.7	9.8	+1.9	+0.2	+3.0	2.1	-0.6	+0.5	+1.3	0.9	24
12	56	-9.9	-7.0	-9.9	9.8	-9.9	-2.0	-2.4	9.8	-5.6	-0.2	+0.3	9.8	-0.6	+1.5	+2.0	1.4	25
12	56	+5.7	+6.5	+4.0	9.8	+4.2	+3.7	+3.5	9.8	+2.4	+2.7	+3.0	2.7	-0.6	+1.5	+2.0	1.4	26
22	01	-4.3	-5.0	+2.8	9.8	-4.8	-3.3	+1.6	9.8	-3.1	-2.1	+1.2	2.3	-0.6	+0.4	+1.2	0.8	27
22	01	+1.9	-1.1	+4.2	9.8	+1.0	-0.1	+3.3	2.2	+1.3	+0.2	+2.7	1.7	-0.6	+0.4	+1.2	0.8	28
22	11	-1.0	-1.4	+0.5	1.0	-0.4	+0.2	+0.2	0.3	-0.3	+0.3	+0.1	0.3	-0.6	-0.6	+0.5	0.6	29
22	11	-0.2	-0.9	+0.8	0.7	-0.8	+0.0	-0.8	0.5	-0.9	+0.0	-0.1	0.5	-0.6	-0.6	+0.5	0.6	30
22	06	-9.9	-1.8	-9.9	9.8	-9.9	-2.6	-3.2	9.8	-5.3	-1.0	-0.3	9.8	-0.6	+0.8	+1.5	1.0	31
22	06	+6.3	+6.1	+3.2	9.8	+4.0	+3.2	+3.0	9.8	+2.3	+2.1	+2.5	2.3	-0.6	+0.8	+1.5	1.0	32
22	16	-9.9	+3.0	-9.9	9.8	-7.7	-0.7	-3.0	9.8	-3.7	-0.2	-0.9	9.8	-0.6	+0.1	+1.0	0.7	33
22	16	+5.7	+6.3	+2.8	9.8	+3.1	+3.0	+1.9	2.7	+1.6	+1.9	+1.4	1.7	-0.6	+0.1	+1.0	0.7	34
22	66	+6.6	+7.0	-9.9	9.8	+0.4	+1.0	-5.2	9.8	-0.2	-0.7	-2.5	1.5	-0.6	-2.1	-0.5	1.3	35
22	66	-9.9	+6.6	-9.9	9.8	-1.7	+0.1	-7.0	9.8	-1.0	-1.0	-3.0	1.9	-0.6	-2.1	-0.5	1.3	36
13	01	+4.7	+2.9	+4.5	9.8	+2.7	+2.1	+2.6	2.5	+1.6	+1.5	+2.0	1.7	-0.6	+0.5	+1.2	0.9	37
13	01	-9.9	-6.4	+1.4	9.8	-6.4	-1.0	-0.9	9.8	-3.6	-0.7	+0.0	9.8	-0.6	+0.5	+1.3	0.9	38
13	50	+0.7	-6.9	+3.6	9.8	+0.7	-4.9	+2.9	9.8	+0.3	-4.2	+1.7	9.8	-0.6	-2.4	-1.4	2.1	39
13	50	-2.2	-9.8	+2.8	9.8	-2.1	-7.3	+2.0	9.8	-1.6	-5.7	+1.0	9.8	-0.6	-3.4	-1.4	2.1	40
13	51	-1.1	-6.9	+3.0	9.8	-2.9	-4.7	+1.6	9.8	-2.1	-3.0	+1.2	2.2	-0.6	-0.7	+0.4	0.6	41
13	51	-0.1	-5.9	+3.3	9.8	+1.2	-1.9	+2.9	2.1	+0.7	-1.3	+2.2	1.5	-0.6	-0.7	+0.4	0.6	42
23	01	+0.4	-5.2	+2.8	9.8	-1.5	-3.3	+2.0	2.4	-1.4	-2.2	+1.4	1.7	-0.6	-0.6	+0.6	0.6	43
23	01	-1.7	-6.9	+2.3	9.8	+0.3	-2.1	+2.5	1.9	+0.2	-1.3	+2.0	1.4	-0.6	-0.6	+0.6	0.6	44
23	10	+2.4	-1.1	+5.2	9.8	+3.2	+0.2	+4.5	9.8	+2.4	+0.8	+3.0	9.8	-0.6	+1.5	+2.0	1.5	45
23	10	-0.8	-9.8	+2.7	9.8	-7.9	-6.3	-2.0	9.8	-5.4	-3.2	+1.0	9.8	-0.6	+1.5	+2.0	1.5	46
23	11	+2.1	-1.6	+4.5	9.8	+1.1	+0.2	+3.0	1.8	+0.7	+0.4	+2.4	1.5	-0.6	+0.7	+1.4	1.0	47
23	11	+4.0	-6.4	+3.2	9.8	-2.7	-1.7	+1.9	2.1	-2.1	-0.9	+1.5	1.6	-0.6	+0.7	+1.4	1.0	48
23	60	+7.0	-6.9	+4.9	9.8	+4.6	+4.0	+4.3	9.8	+2.0	+3.1	+3.7	9.8	-0.6	+2.2	+2.5	1.9	49
23	60	-9.9	-9.8	-9.9	9.8	-9.9	-2.5	-1.6	9.8	-6.7	+0.8	+1.0	9.8	-0.6	+2.2	+2.5	1.9	50
23	61	+7.0	-6.9	+1.7	9.8	+3.2	+3.9	+1.4	9.8	+1.5	+2.4	+1.3	1.8	-0.6	+0.4	+1.2	0.8	51
23	61	-9.9	-5.0	-9.9	9.8	-0.0	+0.7	-4.2	9.8	-3.4	+0.6	-0.9	2.1	-0.6	+0.4	+1.2	0.8	52
33	01	-1.7	-9.6	+3.5	9.8	-4.2	-7.0	+1.9	9.8	-3.0	-4.5	+1.3	9.8	-0.6	-1.1	+0.2	0.7	53
33	01	+0.4	-7.5	+4.0	9.8	+1.9	-2.5	+3.6	9.8	+1.2	-1.0	+2.7	2.0	-0.6	-1.1	+0.2	0.7	54
33	11	-3.5	-9.9	+0.8	9.8	-0.8	-1.3	+2.2	1.5	-0.6	-0.6	+1.8	1.1	-0.6	+0.2	+1.1	0.7	55
33	11	+1.5	-6.9	+2.5	9.8	-0.4	-1.1	+2.3	1.5	-0.5	-0.6	+1.8	1.1	-0.6	+0.2	+1.1	0.7	56

ROW, GATE, TRANSITION (KEV)= 34 767.4 38E.2 . IN EACH GROUP, NORM'D TO (90°,0°) OF (0°,90°), ARE ITS MATE.(0°,0°),(90°,90°) AS .8 OF 90°90°0° & .2 OF 90°090°0°).
#1 ROW OF 28 PAIRS IS NORM'D TO (L1,L2)=(90°,0°). #2 TO (0°,90°).
GROUPS L TO R ARE GAUSSIAN HW=0,4,6,INF, RESP. LAST COL IS ROWS. 9.0 MEANS ERROR > 3.5 SIGMAS IN AT LEAST 1 OF 3 CELLS. LISTED IS (DAT-THEOR)/UNCERT.

11	00	+1.6+2.4-2.9	2.4	+1.6+2.2-2.0	1.9	+1.6+1.9-1.5	1.7	+1.6+1.4-0.7	1.3	1
11	00	+1.6+2.4-2.9	2.4	+1.6+2.2-2.0	1.9	+1.6+1.9-1.5	1.7	+1.6+1.4-0.7	1.3	2
12	00	+3.1+2.4+1.1	2.4	+2.8+2.2+0.7	2.1	+2.4+2.1+0.4	1.9	+1.6+1.8-0.3	1.4	3
12	00	-2.5+0.0-2.0	1.9	-0.8+0.6-1.5	1.0	+0.3+1.1-0.9	0.9	+1.6+1.0-0.3	1.4	4
13	00	+3.4+2.4+1.7	2.6	+3.1+2.2+1.4	2.4	+2.7+2.1+1.0	2.1	+1.6+2.0-0.1	1.5	5
13	00	-5.4+1.6-1.9	9.0	-2.5-0.5-1.3	1.7	-0.5+0.6-0.7	0.6	+1.6+2.0-0.1	1.5	6
22	00	+1.6+0.0+0.2	0.9	+1.6+0.5+0.2	1.0	+1.6+0.8-0.2	1.0	+1.6+1.2-1.0	1.3	7
22	00	+1.6+0.0+0.2	0.9	+1.6+0.5+0.2	1.0	+1.6+0.8-0.2	1.0	+1.6+1.2-1.0	1.3	8
23	00	+2.3+0.0+1.0	1.5	+2.2+0.5+0.8	1.4	+2.0+0.7+0.2	1.2	+1.6+0.9-1.3	1.3	9
23	00	+0.6-1.6+0.2	1.0	+0.0-0.7+0.0	0.6	+1.1+0.0-0.4	0.7	+1.6+0.9-1.3	1.3	10
33	00	+1.6-1.7+0.8	1.4	+1.6-0.0+0.5	1.1	+1.6-0.3-0.2	0.9	+1.6+0.3-2.1	1.5	11
33	00	+1.6-1.7+0.8	1.4	+1.6-0.0+0.5	1.1	+1.6-0.3-0.2	0.9	+1.6+0.3-2.1	1.5	12
11	05	+3.2+2.5+1.3	2.5	+2.9+2.2+0.9	2.2	+2.5+2.1+0.6	1.9	+1.6+1.9-0.2	1.4	13
11	05	-3.6-0.5-2.1	9.0	-1.3+0.3-1.5	1.1	+0.1+1.0-0.9	0.8	+1.6+1.9-0.7	1.4	14
11	55	+1.6-0.6+0.6	1.0	+1.6+0.0+0.2	0.9	+1.6+0.4-0.3	0.9	+1.6+0.9-1.4	1.3	15
11	55	+1.6-0.6+0.7	1.1	+1.6+0.1+0.3	1.0	+1.6+0.4-0.2	1.0	+1.6+0.9-1.4	1.3	16
12	01	+2.7+2.5-0.2	2.1	+2.3+2.2-0.5	1.9	+2.0+2.0-0.7	1.7	+1.6+1.5-0.6	1.3	17
12	01	-0.6+1.3-3.0	1.9	+0.6+1.6-2.0	1.5	+1.1+1.6-1.4	1.4	+1.6+1.5-0.6	1.3	18
12	06	-9.9+0.7-9.9	9.0	+0.0-2.1-3.6	9.0	+1.3+1.8-1.9	1.7	+1.6+1.4-0.8	1.3	19
12	06	+3.0+3.6-2.5	9.0	+2.2+2.6-1.9	2.2	+1.9+2.0-1.4	1.8	+1.6+1.4-0.6	1.3	20
12	50	+1.1-0.7+0.2	0.8	+1.4+0.1+0.0	0.8	+1.5+0.5-0.3	0.9	+1.6+1.0-1.3	1.3	21
12	50	+2.0+0.1+0.6	1.2	+1.8+0.5+0.3	1.1	+1.7+0.7-0.2	1.1	+1.6+1.0-1.3	1.3	22
12	51	-0.2-0.6+0.3	0.4	-0.1-0.0-0.3	0.2	+0.5+0.6-0.5	0.5	+1.6+1.7-0.4	1.4	23
12	51	+2.6+1.3+1.4	1.9	+2.6+1.6+1.0	1.8	+2.4+1.6+0.6	1.7	+1.6+1.7-0.4	1.4	24
12	56	-9.9-0.7-9.9	9.0	-2.4+0.9-2.5	2.0	+0.0+1.5-1.0	1.0	+1.6+2.0-0.0	1.5	25
12	56	+3.9+3.6+1.2	9.0	+3.1+2.7+0.9	2.4	+2.6+2.4+0.6	2.1	+1.6+2.0-0.0	1.5	26
22	01	+0.4-0.1+0.4	0.4	+0.5+0.5-0.2	0.4	+0.8+0.9-0.4	0.7	+1.6+1.7-0.4	1.4	27
22	01	+2.4+1.2+1.3	1.7	+2.3+1.5+0.8	1.7	+2.2+1.6+0.4	1.6	+1.6+1.7-0.4	1.4	28
22	11	+1.5+1.1-0.9	1.2	+1.7+1.6-1.0	1.5	+1.7+1.6-1.0	1.5	+1.6+1.4-0.8	1.3	29
22	11	+1.7+1.3-0.7	1.3	+1.5+1.6-1.1	1.4	+1.5+1.6-1.2	1.4	+1.6+1.4-0.8	1.3	30
22	06	-9.9+1.0-9.9	9.0	-2.0+0.7-2.9	2.1	+0.1+1.2-1.3	1.0	+1.6+1.8-0.3	1.4	31
22	06	+3.7+3.5+0.7	9.0	+3.0+2.6+0.8	2.3	+2.5+2.2+0.3	1.9	+1.6+1.8-0.3	1.4	32
22	16	-9.2+2.5-9.9	9.0	-0.6+1.3-2.8	1.8	+0.6+1.5-1.6	1.3	+1.6+1.6-0.6	1.3	33
22	16	+3.6+3.6+0.5	9.0	+2.8+2.5-0.0	2.2	+2.3+2.2-0.3	1.8	+1.6+1.6-0.6	1.3	34
22	66	+3.9+3.0-9.9	9.0	+1.9+1.9-4.1	9.0	+1.7+1.3-2.6	1.9	+1.6+2.9-1.4	1.3	35
22	66	-9.9+3.7-9.9	9.0	+1.3+1.6-5.1	9.0	+1.5+1.2-2.0	2.0	+1.6+0.9-1.4	1.3	36
13	01	+2.3+2.5+1.4	2.5	+2.6+2.2+0.3	2.0	+2.3+2.0+0.0	1.8	+1.6+1.7-0.4	1.4	37
13	01	-3.8-0.5-1.9	9.0	-0.2+1.0-1.6	1.1	+0.7+1.3-1.1	1.1	+1.6+1.7-0.4	1.4	38
13	50	+2.0-0.6+0.9	1.3	+2.0-0.0+0.5	1.2	+1.9+0.2-0.1	1.1	+1.6+0.5-1.9	1.5	39
13	50	+1.1-1.6+0.5	1.1	+1.1-0.8+0.0	0.8	+1.3-0.3-0.5	0.8	+1.6+0.5-1.9	1.5	40
13	51	+1.4-0.6+0.6	1.0	+0.9+0.1-0.2	0.5	+1.1+0.6-0.5	0.8	+1.6+1.3-0.9	1.3	41
13	51	+1.8-0.3+0.7	1.1	+2.2+0.9+0.5	1.4	+2.0+1.1+0.1	1.3	+1.6+1.3-0.9	1.3	42
23	01	+1.9-0.1+0.5	1.1	+1.3+0.5+0.0	0.8	+1.3+0.9-0.3	0.9	+1.6+1.4-0.6	1.3	43
23	01	+1.3-0.7+0.2	0.8	+1.9+0.9+0.3	1.2	+1.8+1.1+0.0	1.2	+1.6+1.4-0.6	1.3	44
23	10	+2.8+1.2+1.7	2.0	+2.8+1.6+1.4	2.0	+2.5+1.8+1.1	1.5	+1.6+2.0-0.0	1.5	45
23	10	-1.0-1.6+0.4	1.1	-0.7-0.5+0.0	0.5	+0.1+0.5-0.1	0.3	+1.6+2.0-0.0	1.5	46
23	11	+2.5+1.0+1.5	1.8	+2.1+1.6+0.6	1.6	+2.0+1.7+0.3	1.5	+1.6+1.8-0.3	1.4	47
23	11	+0.3-0.5+0.7	0.5	+0.9+1.0-0.0	0.8	+1.1+1.3-0.3	1.0	+1.6+1.8-0.3	1.4	48
23	60	+4.0+3.8+1.6	9.0	+3.2+2.8+1.3	2.6	+2.7+2.6+1.0	2.2	+1.6+2.3+0.3	1.6	49
23	60	-9.9-1.6-9.9	9.0	-3.4+0.8-2.0	2.3	-0.3+1.6-0.5	1.0	+1.6+2.3+0.3	1.6	50
23	61	+4.0+3.8-0.2	9.0	+2.0+2.8-0.3	2.3	+2.2+2.3-0.4	1.9	+1.6+1.7-0.4	1.4	51
23	61	-9.9-0.3-9.9	9.0	-0.7+1.8-3.5	2.3	+0.7+1.8-1.6	1.4	+1.6+1.7-0.4	1.4	52
33	01	+1.2-1.5+0.9	1.3	+0.5-0.7-0.0	0.5	+0.9+0.1-0.4	0.5	+1.6+1.2-1.0	1.3	53
33	01	+1.9-0.9+1.2	1.4	+2.4+0.7+0.9	1.5	+2.2+1.0+0.4	1.4	+1.6+1.2-1.0	1.3	54
33	11	+0.7-2.4-0.7	1.5	+1.5+1.1+0.1	1.1	+1.6+1.4-0.1	1.2	+1.6+1.6-0.5	1.3	55
33	11	+2.3-0.7+0.3	1.4	+1.7+1.2+0.2	1.2	+1.6+1.4-0.1	1.2	+1.6+1.6-0.5	1.3	56

ROW, GATE, TRANSITION (KEV)= 18 333.1 763.9 . IN EACH GROUP, NORM'D TO (90°,0°, OR (0°,90°, ARE ITS MATE,(0°,0°),(90°,90° AS .8 OF 90°90° & .2 OF 90°0°,0°).
#1 ROW OF 28 PAIRS IS NORM'D TO (L1,L2)=(90°,0°; #2 TO (0°,90°).
GROUPS L TO R ARE GAUSSIAN HW=0,4,6,INF, RESP. LAST COL IS ROW#. 9.8 MEANS
ERROR > 3.5 SIGMAS IN AT LEAST 1 OF 3 CELLS. LISTED IS (DAT-THEOR./UNCERT.)

11	00	+1.1+2.6+0.2	1.6	+1.1+1.0+1.2	1.4	+1.1+0.9-1.9	1.4	+1.1-0.6+2.7	1.7	1
11	00	+1.1+2.6+0.2	1.6	+1.1+1.0+1.2	1.4	+1.1+0.9+1.9	1.4	+1.1-0.6+2.7	1.7	2
12	00	+4.9+2.6+4.9	9.8	+4.1+1.9+4.5	9.8	+3.2+1.4+4.1	9.8	+1.1+0.7+3.3	2.1	3
12	00	-9.0-5.0+1.2	9.8	-4.9-3.3+1.9	9.0	-2.1-1.6+2.5	2.1	+1.1+0.7+3.3	2.1	4
13	00	+5.6+2.7+5.6	9.8	+4.9+2.0+5.3	9.8	+3.9+1.7+4.8	9.8	+1.1+1.2+3.6	9.6	5
13	00	-9.9-9.9+1.3	9.8	-9.1-6.7+2.1	9.8	-4.0-3.1+2.8	9.8	+1.1+1.2+3.6	9.8	6
22	00	+1.1-5.0+3.9	9.0	+1.1-3.5+3.8	9.8	+1.1-2.6+3.4	2.6	+1.1-1.2+2.4	1.7	7
22	00	+1.1-5.0+3.9	9.0	+1.1-3.5+3.8	9.8	+1.1-2.6+3.4	2.6	+1.1-1.2+2.4	1.7	8
23	00	+2.9-5.1+4.0	9.8	+2.7-3.6+4.5	9.8	+2.1-3.0+3.9	9.8	+1.1-2.1+2.0	1.8	9
23	00	-1.4-9.5+3.9	9.8	-0.9-7.3+3.6	9.8	-0.1-5.0+3.2	9.8	+1.1-2.1+2.0	1.8	10
33	00	+1.1-9.9+4.6	9.0	+1.1-7.6+4.2	9.8	+1.1-6.0+3.4	9.8	+1.1-4.0+1.2	9.8	11
33	00	+1.1-9.9+4.6	9.8	+1.1-7.6+4.2	9.8	+1.1-6.0+3.4	9.8	+1.1-4.0+1.2	9.0	12
11	05	+5.2+2.7+5.2	9.8	+4.4+2.0+4.7	9.8	+3.4+1.5+4.3	9.8	+1.1+0.8+3.4	2.1	13
11	05	-9.9-6.9+1.1	9.8	-6.1-4.2+1.9	9.0	-2.7-2.0+2.5	2.4	+1.1+0.8+3.4	2.1	14
11	55	+1.0-7.2+4.4	9.8	+1.1-5.0+3.9	9.8	+1.1-3.9+3.3	9.8	+1.1-2.4+1.9	1.9	15
11	55	+1.2-6.9+4.4	9.8	+1.2-4.9+4.0	9.8	+1.2-3.9+3.3	9.8	+1.1-2.4+1.9	1.9	16
12	01	+4.0+2.8+2.4	9.8	+2.9+2.0+3.0	2.6	+2.2+1.3+2.8	2.2	+1.1-0.2+2.9	1.8	17
12	01	-4.3-1.1+0.1	9.8	-1.3-0.1+1.3	1.1	-0.1+0.1+1.9	1.1	+1.1-0.2+2.9	1.8	18
12	06	-9.9-2.7-9.9	9.8	-0.9+1.6-0.7	1.1	+0.4+0.6+1.3	0.9	+1.1-0.7+2.7	1.7	19
12	06	+6.6+6.3+0.6	9.8	+2.7+3.0+1.3	2.4	+1.0+1.3+1.9	1.7	+1.1-0.7+2.7	1.7	20
12	50	+0.0-7.2+3.9	9.8	+0.5-4.7+3.7	9.8	+0.8-3.5+3.2	9.8	+1.1-2.0+2.1	1.8	21
12	50	+2.1-4.9+4.4	9.8	+1.7-3.7+4.0	9.8	+1.4-3.0+3.4	2.7	+1.1-2.0+2.1	1.8	22
12	51	-3.4-7.2+4.0	9.8	-3.0-5.2+3.3	9.8	-1.7-3.3+3.1	2.8	+1.1+0.3+3.2	1.9	23
12	51	+3.7-1.0+5.3	9.8	+3.6-0.2+4.8	9.8	+3.1+0.1+4.4	9.8	+1.1+0.3+3.2	1.9	24
12	56	-9.9-7.3-9.9	9.8	-8.5-2.2+0.7	9.8	-2.8-0.4+2.5	2.2	+1.1+1.3+3.6	9.8	25
12	56	+6.8+6.4+5.0	9.8	+4.8+3.6+4.7	9.8	+3.5+2.6+4.3	9.8	+1.1+1.3+3.6	9.8	26
22	01	-1.8-5.3+4.2	9.8	-1.5-3.6+3.4	9.0	-0.8-2.3+3.1	2.3	+1.1+0.2+3.1	1.9	27
22	01	+3.1-1.3+5.1	9.8	+3.0-0.3+4.5	9.8	+2.6+0.1+4.1	9.8	+1.1+0.2+3.1	1.9	28
22	11	+0.8-1.6+2.6	1.8	+1.3+0.1+2.4	1.6	+1.3+0.1+2.4	1.6	+1.1-0.8+2.6	1.7	29
22	11	+1.5-1.1+2.8	2.0	+1.0-0.1+2.3	1.4	+0.9-0.1+2.2	1.4	+1.1-0.8+2.6	1.7	30
22	06	-9.9-2.0-9.9	9.8	-7.8-2.8+0.2	9.8	-2.5-1.2+2.1	2.0	+1.1+0.7+3.3	2.1	31
22	06	+6.4+6.1+4.5	9.8	+4.7+3.1+4.3	9.8	+3.4+2.0+4.0	9.8	+1.1+0.7+3.3	2.1	32
22	16	-9.9+2.9-8.8	9.8	-4.4-0.9+0.3	9.9	-1.3-0.4+1.7	1.3	+1.1-0.1+3.0	1.8	33
22	16	+6.0+6.3+4.2	9.8	+4.0+2.9+3.6	9.8	+2.9+1.8+3.3	2.7	+1.1-0.1+3.0	1.9	34
22	66	+6.7+7.0-9.9	9.8	+1.9+0.9-1.2	1.4	+1.4-0.8+0.6	1.0	+1.1-2.3+1.9	1.9	35
22	66	-9.9+6.6-9.9	9.8	+0.3-0.1-2.4	1.4	+0.8-1.2+0.2	0.9	+1.1-2.3+1.9	1.9	36
13	01	+5.2+2.8+5.3	9.8	+3.7+1.9+4.0	9.8	+2.0+1.4+3.7	9.8	+1.1+0.3+3.2	1.9	37
13	01	-9.9-6.7+1.3	9.8	-3.4-2.0+1.7	2.5	-1.2-0.9+2.3	1.6	+1.1+0.3+3.2	1.9	38
13	50	+2.2-7.2+4.7	9.8	+2.1-5.2+4.2	9.8	+1.8-4.5+3.5	9.8	+1.1-3.6+1.3	9.8	39
13	50	-8.1-9.9+4.2	9.8	-8.1-7.7+3.7	9.8	+0.3-6.0+3.0	9.8	+1.1-3.6+1.3	9.8	40
13	51	+0.7-7.2+4.3	9.8	-0.7-4.9+3.4	9.8	-0.1-3.2+3.1	2.6	+1.1-0.9+2.6	1.7	41
13	51	+1.5-6.2+4.5	9.8	+2.5-2.1+4.2	9.8	+2.1-1.5+3.7	9.8	+1.1-0.9+2.6	1.7	42
23	01	+1.9-5.5+4.2	9.8	+0.4-3.5+3.6	9.8	+0.5-2.4+3.3	2.4	+1.1-0.7+2.7	1.7	43
23	01	+0.3-7.3+3.8	9.8	+1.0-2.4+4.0	9.8	+1.7-1.5+3.6	9.8	+1.1-0.7+2.7	1.7	44
23	10	+4.2-1.2+5.7	9.8	+4.0+0.1+5.3	9.8	+3.4+0.6+4.9	9.8	+1.1+1.3+3.6	9.8	45
23	10	-5.3-9.9+4.1	9.8	-4.6-5.6+3.6	9.8	-2.6-3.4+3.5	3.2	+1.1+1.3+3.6	9.8	46
23	11	+3.2-1.8+5.4	9.8	+2.4+0.8+4.3	9.8	+2.1+0.3+3.9	9.8	+1.1+0.5+3.3	2.0	47
23	11	-2.1-6.7+4.4	9.8	-0.5-1.9+3.6	9.8	-0.1-1.1+3.3	2.0	+1.1+0.5+3.3	2.0	48
23	60	+7.0+6.9+5.6	9.8	+5.2+3.9+5.2	9.8	+3.8+3.1+4.8	9.8	+1.1+2.1+4.0	9.8	49
23	60	-9.9-9.9-9.9	9.8	-9.9-2.7+1.2	9.8	-3.6-0.1+3.0	9.8	+1.1+2.1+4.0	9.8	50
23	61	+7.0+6.9+3.4	9.8	+4.1+3.8+3.2	9.8	+2.7+2.2+3.2	2.7	+1.1+0.3+3.1	1.9	51
23	61	-9.9-6.1-9.9	9.8	-4.7+0.6-0.5	9.8	-1.1+0.5+1.7	1.2	+1.1+0.3+3.1	1.9	52
33	01	+0.3-9.9+4.7	9.8	-1.7-7.4+3.6	9.8	-0.7-4.8+3.2	9.8	+1.1-1.3+2.4	1.7	53
33	01	+1.9-7.9+5.0	9.0	+3.0-2.0+4.7	9.8	+2.5-2.0+4.1	9.8	+1.1-1.3+2.4	1.7	54
33	11	+1.1-9.9+2.0	9.8	+1.0-1.5+3.0	9.8	+1.0-0.8+3.5	2.2	+1.1+0.0+3.0	1.9	55
33	11	+2.0-7.3+4.0	9.0	+1.3-1.3+3.0	9.8	+1.2-0.7+3.5	9.8	+1.1+0.0+3.0	1.9	56

(b)Summaries of arrays such as in (a), given below for all transitions above the isomer, in coincidence with the 333.1, 763.4 and 1061.1 keV prompt gates. Listed are the best multipolarities involved (the first four digits), the row no. and HWHM group no.(in paran-theses) followed by the F.O.M.'s of increasing order. Underlined are the final choices made on life-time and other considerations(see text).

SUMMARY OF ABOVE LISTS OF BEST FITS, (ALL ANGLES)////(0.90/1)

[illegible]

333.1 275 1206(20,2).6/1201(17,1)2/2216(34,2)2/1100(1,1)2.1/1100(2,1)2.1/2206(32,3)2.6////2216(34,3).1/1201(17,2).1/1206(20,2).2/2201(20,2).3/1251(24,3).4/1200(3,3).7/2206(32,3)1/1105(13,3)1.1/1256(26,3)1.1/1250(22,1)1.2/2266(35,2)1.5/2211(30,1)2.2/2211(29,3)2.4/1155(16,1)2.6/1100(1,1)2.0/1100(2,1)2.0/2200(7,1)2.0/2200(0,1)2.0/1155(15,3)2.9/

333.1 352.4 1100(1,1).5/1100(2,1).5/1206(19,2)1.2/1206(20,2)1.2/2266(35,2)1.4/1201(17,3)1.9/2266(36,2)1.9/1201(18,3)1.9/2211(29,3)2/2216(34,3)2.1/2211(30,3)2.1/2216(33,3)2.3/2206(32,3)2.4/2201(20,3)2.7/1256(25,3)2.8////2211(29,1)0/1250(21,3).1/2266(36,3).1/2211(30,3).1/1155(15,1).2/1206(19,3).3/1100(1,1).3/1100(2,1).3/2200(7,1).3/2200(0,1).3/1155(16,3).4/2266(35,3).6/1250(22,3).6/1201(18,3).7/1206(20,3).8/1201(17,3)1.2/2201(27,3)1.3/2201(28,3)1.5/2216(33,3)1.7/2216(34,3)1.7/1251(24,3)1.9/1251(23,3)2/1200(3,3)2/2206(32,3)2.2/1105(13,3)2.2/1256(26,3)2.2/1200(4,3)2.3/2206(31,3)2.6/1105(14,3)2.8/1256(25,3)2.9/

333.1 361.4 1206(20,2)1.1/2216(34,2)1.1/1201(17,1)1.2/1256(26,3)1.3/2206(32,2)1.4/1200(3,2)1.7/1100(1,2)1.7/1100(2,2)1.7/1105(13,3)1.7/1206(19,3)2.2/2266(35,2)2.6////1206(20,2)0/2201(20,3)0/2216(34,3).1/1201(17,2).1/1251(24,3).3/1200(3,3).4/1250(22,1).4/2206(32,3).5/1105(13,3).5/2266(35,2).6/1256(26,3).6/2211(30,1).9/2211(29,3).9/1155(16,1)1/1100(1,1)1.1/1100(2,1)1.1/2200(7,1)1.1/2200(0,1)1.1/1155(15,3)1.1/2266(36,3)1.3/1250(21,3)1.3/1206(19,3)1.6/1201(18,3)2/2201(27,3)2.5/2216(33,3)2.8/

333.1 396.1 2216(33,3).2/1201(18,3).4/2206(31,3).5/1200(4,3).5/1256(25,3).5/1105(14,3).7/2201(27,3).7/2211(30,3).7/2211(29,1).8/1206(19,3).8/1100(1,3).9/1100(2,3).9/1251(23,3).9/1206(20,3)1.1/2200(7,3)1.2/2200(0,3)1.2/2266(35,3)1.2/2266(36,3)1.2/1250(21,3)1.2/1201(17,3)1.3/1250(22,3)1.3/1155(15,3)1.4/1155(16,3)1.4/2201(20,3)1.6/2216(34,3)1.6/1251(24,3)1.8/1200(3,3)1.8/2206(32,3)1.9/1105(13,3)1.9/1256(26,3)2.1////2216(33,3)0/1201(18,2)0/1206(19,2).2/2201(27,2).2/1251(23,3).3/1200(4,3).5/1250(21,1).7/2206(31,3).7/1105(14,3).8/1256(25,3).8/2266(36,2).8/2211(29,1)1.1/2211(30,3)1.2/1155(15,1)1.3/1100(1,1)1.3/1100(2,1)1.3/2200(7,1)1.3/2200(0,1)1.3/1155(16,3)1.4/2266(35,3)1.6/1250(22,3)1.5/1206(20,3)1.7/1201(17,3)1.9/2201(20,3)2.2/2216(34,3)2.3/1251(24,3)2.4/1200(3,3)2.5/2206(32,3)2.6/1105(13,3)2.6/1256(26,3)2.6/

333.1 406.3 2216(36,3).2/2266(35,3).2/1206(19,3).3/1201(18,3).3/2216(33,3).4/2211(30,3).4/2211(29,1).4/1100(1,3).4/1100(2,3).4/1206(20,3).5/2201(27,3).6/1200(4,3).6/2206(31,3).6/1250(21,3).6/2200(7,3).6/2200(0,3).6/1250(22,3).7/1105(14,3).7/1251(23,3).7/1256(25,3).7/1155(15,3).7/1155(16,3).7/1201(17,3).7/2216(34,3).8/2201(20,3).8/1251(24,3)1/1200(3,3)1/2206(32,3)1/1105(13,3)1.1/1256(26,3)1.1////2266(36,2)0/1250(21,1).1/1256(19,3).1/1201(18,3).1/2211(29,1).2/2211(30,3).2/1155(15,1).3/1100(1,1).3/1100(2,1).3/2200(7,1).3/2200(0,1).3/2201(27,3).3/1155(16,3).3/2266(35,3).4/1250(22,3).4/2216(33,3).5/1206(20,3).5/1251(23,3).6/1201(17,3).7/1200(4,3).7/2201(20,3).8/2206(31,3).9/2216(34,3).9/1105(14,3).9/1251(24,3).9/1256(25,3).9/1200(3,3)1/2206(32,3)1/1105(13,3)1.1/1256(26,3)1.1/

7 333.1 472.3 1201(18,1).6/2216(33,2).6/1200(4,2).8/2206(31,3)1.1/1105(14,3)1.2
/1256(26,3)1.4/1251(23,3)1.6/2266(36,3)1.7/2201(27,3)1.8/1206(19,3).9/2266(35,3
).9/2211(29,1)2/2211(30,3)2.1/1200(21,3)2.3/1100(1,3)2.3/1100(2,3)2.3/2200(7,3)
2.4/2200(8,3)2.4/1155(16,3)2.4/1155(16,3)2.4/1250(22,3)2.6/1206(20,3)2.5////1201
(18,1).2/2216(33,2).2/1251(23,1).6/1200(4,2).5/1255(25,3).7/1105(14,3).8/2206(31
,3).8/2201(27,1)1.3/1206(19,2)1.8/1250(21,1)2.4/2266(36,2)2.5/2211(29,1)2.8/2211
(30,3)2.9/1155(15,1)3/

8 333.1 477.6 1251(23,2).6/1200(4,2).7/1105(14,2).7/2201(27,1).7/1250(21,1).7/2
206(31,3).8/1256(26,3).9/1155(15,1).9/2200(7,1).9/2200(8,1).9/1155(16,3).9/2216(
33,3)1/1201(18,1)1/2211(29,1)1/1250(22,3)1/2211(30,1)1.1/2266(36,3)1.1/1206(19,3
)1.2/2266(35,3)1.2/1100(1,3)1.2/1100(2,3)1.2/1206(20,3)1.3/1201(17,3)1.4/2201(20
,3)1.4/1251(24,3)1.6/2216(34,3)1.6/1200(3,3)1.6/2266(32,3)1.6/1105(13,3).6/1256
(26,3)1.7////1251(23,1)8/1256(25,3).2/1105(14,3).2/2206(31,3).2/1201(18,1).2/221
6(33,2).3/1200(4,3).3/2201(27,1).4/1205(19,2).8/1250(21,1).9/2266(36,2).9/2211(2
9,1)1.1/2211(30,3)1.1/1155(15,1)1.1/1100(1,1)1.2/1100(2,1)1.2/2200(7,1)1.2/2200(
8,1)1.2/1155(16,3)1.2/2266(35,3)1.2/1250(22,3)1.2/1206(20,3)1.3/1201(17,3)1.4/22
01(20,3)1.5/2216(34,3)1.6/1251(24,3)1.7/1200(3,3)1.7/2206(32,3)1.7/1105(13,3)1.8
/1256(26,3)1.8/

9 333.1 491.1 1200(4,2).4/1105(14,2).6/1251(23,2).7/2206(31,3).7/1201(18,1).8/2
216(33,2).8/2201(27,2).9/1256(25,3).9/1250(21,3)1.2/2211(29,1)1.2/1155(15,3)1.2/
2266(36,3)1.2/1155(16,3)1.3/1206(19,3)1.3/2211(30,3)1.3/2200(7,3)1.3/2200(8,3)1.
3/2266(35,3)1.4/1250(22,3)1.4/1100(1,3)1.5/1100(2,3)1.5/1206(20,3)1.6/1201(17,3)
1.8/2201(20,3)1.9/2216(34,3)2/1251(24,3)2/1200(3,3)2.1/2206(32,3)2.2/1105(13,3)2
.2/1256(26,3)2.3////1251(23,1).1/1201(18,1).2/2216(33,2).3/1256(25,3).3/1105(14,
3).4/2206(31,3).4/1200(4,2).5/2201(27,1).7/1206(19,2)1/1250(21,1)1.4/2266(36,2)1
.5/2211(29,1)1.7/2211(30,3)1.7/1155(15,1)1.8/1100(1,1)1.8/1100(2,1)1.8/2200(7,1)
1.8/2200(8,1)1.8/1155(16,3)1.8/2266(35,3)1.9/1250(22,3)1.9/1206(20,3)2.1/1201(17
,3)2.2/2201(20,3)2.4/2216(34,3)2.5/1251(24,3)2.6/1200(3,3)2.6/2206(32,3)2.7/1105
(13,3)2.7/1256(26,3)2.7/

10 333.1 496.1 1206(19,2).8/1100(1,2)1/1100(2,2)1/2266(35,2)1.2/1201(18,3)1.4/1
206(20,3)1.5/2266(36,2)1.7/2211(30,3)1.7/2211(29,3)1.8/2216(33,3)1.8/1201(17,3)2
/2216(34,3)2.5/1256(25,3)2.6/2206(31,3)2.7////2266(36,2)8/1206(19,3).2/1250(21,1
).3/1201(18,3).4/2211(29,1).6/2211(30,3).7/1155(15,1).8/1100(1,1).9/1100(2,1).9/
2200(7,1).9/2200(8,1).9/1155(16,3)1/2201(27,3)1.1/2266(35,3)1.2/1250(22,3)1.2/12
06(20,3)1.6/2216(33,3)1.6/1201(17,3)2/1251(23,3)2/1200(4,3)2.4/2201(20,3)2.4/221
6(34,3)2.7/2206(31,3)2.8/1251(24,3)2.9/

11 333.1 535 2216(33,3).7/2266(36,3).7/1201(18,2).7/2211(29,1).8/2266(35,3).8/1
200(4,3).8/2201(27,3).8/1206(19,3).8/2211(30,3).9/2206(31,3).9/1251(23,3).9/1105
(14,3)1/1250(21,3)1/1100(1,3)1.1/1100(2,3)1.1/2200(7,3)1.1/2200(8,3)1.1/1155(15,
3)1.1/1155(16,3)1.1/1256(25,3)1.1/1250(22,3)1.1/1206(20,3)1.3/1201(17,3)1.5/2201
(20,3)1.8/2216(36,3)1.8/1251(24,3)1.9/1200(3,3)2/2206(32,3)2.1/1105(13,3)2.2/125
6(26,3)2.3////1201(18,3).2/1250(21,1).2/2201(27,3).3/1206(19,2).3/2266(36,2).4/2
216(35,3).5/2211(29,1).7/1251(23,3).8/2211(30,3).8/1155(15,1).8/1100(1,1).9/1100
(2,1).9/2200(7,1).9/2200(8,1).9/1155(16,3).9/1200(4,3)1/2266(35,3)1.1/1250(22,3)
1.1/2206(31,3)1.2/1206(20,3)1.3/1105(14,3)1.3/1256(25,3)1.4/1201(17,3)1.5/2201(2
0,3)1.8/2216(34,3)1.9/1251(24,3)2.1/1200(3,3)2.2/2206(32,3)2.3/1105(13,3)2.3/125
6(26,3)2.3/

12 333.1 555.3 2266(36,2).4/1206(19,2).5/1201(18,2).6/2266(36,3).6/2216(33,3).6
/2206(31,3).7/1200(4,3).7/1105(14,3).7/2211(29,1).7/2211(30,3).8/2201(27,3).8/12
51(23,3).8/1256(25,3).8/1100(1,3).8/1100(2,3).8/1250(21,3).8/1206(20,3).9/1155(1
6,3).9/2200(7,3).9/2200(8,3).9/1155(16,3).9/1250(22,3).9/1201(17,3)1/2201(20,3)1
.1/2216(34,3)1.1/1251(24,3)1.2/1200(3,3)1.3/2206(32,3)1.3/1105(13,3)1.3/1256(26,
3)1.4////1206(19,2)8/2201(27,3)8/2216(33,3).1/1201(18,2).1/1251(23,3).2/1250(21,
1).3/1200(4,3).3/2266(36,2).4/2206(31,3).4/1105(14,3).5/1256(25,3).5/2211(29,1).
5/2211(30,3).5/1155(15,1).5/1100(1,1).6/1100(2,1).6/2200(7,1).6/2200(8,1).6/1155
(16,3).6/2266(35,3).7/1250(22,3).7/1206(20,3).8/1201(17,3).9/2201(20,3)1/2216(34
,3)1.1/1251(24,3)1.1/1200(3,3)1.2/2206(32,3)1.2/1105(13,3)1.3/1256(26,3)1.3/

13 333.1 567.8 1100(1,1).4/1100(2,1).4/1206(20,2).5/2266(35,2).7/1206(19,2).8/1
201(17,2).8/2216(34,3).9/2266(36,2).9/2206(32,3)1/1256(26,3)1/2211(29,3)1/1201(1
8,3)1/2211(30,3)1/1200(3,3)1/1106(13,3)1.1/2201(20,3)1.2/2216(33,3)1.2/1251(24,3
)1.2/1256(25,3)1.6/2206(31,3)1.4/1200(4,3)1.5/2200(7,3)1.5/2200(8,3)1.5/2201(27,
3)1.5/1250(22,3)1.5/1105(14,3)1.5/1250(21,3)1.7/1155(16,3)1.7/1251(23,3)1.7/1155
(15,3)1.7////1206(20,3)0/2266(36,2)0/1250(22,2)0/2211(30,2)1.1/1201(17,3).1/2211(
29,3).2/1155(16,1).2/1100(1,1).2/1100(2,1).2/2200(7,1).2/2200(8,1).2/1155(15,3).
2/2201(20,3).3/2266(36,3).3/1250(21,3).3/2216(34,3).4/1206(19,3).4/1206(19,3).5/
1200(3,3).5/2206(32,3).5/1105(13,3).5/1256(25,3).6/1201(18,3).7/2201(27,3).9/221
6(33,3)1.1/1251(23,3)1.2/1200(4,3)1.3/2206(31,3)1.5/1105(14,3)1.5/1256(25,3)1.6/

14 333.1 637.8 1105(14,2).8/1200(4,2).8/1251(23,2)1/2201(27,2)1.2/1256(25,3)1.2
/2266(31,3)1.2/2216(33,3)1.7/1250(21,3)1.7/2211(29,1)1.8/1155(15,3)1.8/2200(7,3)
1.8/2200(8,3)1.8/1155(16,3)1.8/1201(18,2)1.9/1250(22,3)1.9/2211(30,1)2/1206(19,3
)2.3/1100(1,3)2.3/1100(2,3)2.3/1206(20,3)2.5/2266(35,3)2.5/2266(36,3)2.6////1105
(14,2)0/1200(4,2).5/2206(31,2).7/2216(33,2).7/1201(18,1).8/1256(25,2)1.1/1251(23
,1)1.2/2201(27,1)1.9/1206(19,2)2.2/1250(21,1)2.6/2266(36,2)2.7/2211(29,1)3/

15 333.1 720.9 2211(29,3).2/1201(17,3).2/2211(30,2).3/1100(1,3).3/1100(2,3).3/1
206(20,3).3/2216(34,3).5/1201(18,3).5/2201(20,3).5/1206(19,3).6/1200(3,3).6/2200
(7,3).6/2200(8,3).6/1251(24,3).6/2206(32,3).7/1250(22,3).7/1105(13,3).7/2266(35,
3).8/1256(26,3).8/2216(33,3).8/2201(27,3).8/1250(21,3).8/1155(16,3).8/1155(15,3)
.9/2266(36,3).9/1200(4,3)1/2206(31,3)1.1/1256(25,3)1.1/1251(23,3)1.1/1105(14,3)1
.2////2211(30,1)0/1250(22,3)0/2266(35,3)0/2211(29,3).1/1206(20,3).1/1155(16,1).1
/1100(1,1).2/1100(2,1).2/2200(7,1).2/2200(8,1).2/1155(15,3).2/1201(17,3).3/2266(
36,3).3/1250(21,3).3/2201(20,3).5/1206(19,3).5/2216(34,3).6/1251(24,3).7/1201(18
,3).7/1200(3,3).8/2206(32,3).8/1105(13,3).9/1256(26,3).9/2201(27,3)1/2216(33,3)1
.2/1251(23,3)1.4/1200(4,3)1.5/2206(31,3)1.8/1105(14,3)1.8/1256(25,3)1.9/

16 333.1 750.5 2266(36,3).3/2266(35,3).4/1201(18,2).4/2216(33,3).4/2211(29,1).4
/1250(21,3).4/1251(23,3).4/2201(27,3).4/1155(15,3).6/1200(4,3).5/1155(16,3).5/12
06(19,3).5/2206(31,3).5/2211(30,3).5/1105(14,3).5/2200(7,3).5/2200(8,3).5/1250(2
2,3).5/1100(1,3).5/1100(2,3).5/1256(25,3).6/1206(20,3).6/1201(17,3).7/2201(20,3)
.8/2216(34,3).8/1251(24,3).8/1200(3,3).9/2206(32,3).9/1105(13,3).9/1256(26,3)1/
//1201(18,3)0/1250(21,1).1/2266(36,2).1/2201(27,3).1/1206(19,3).1/2211(29,1).2/2
216(33,3).2/2211(30,3).3/1155(15,1).3/1100(1,1).3/1100(2,1).3/2200(7,1).3/2200(6
,1).3/1155(16,3).3/1251(23,3).3/2266(35,3).4/1250(22,3).4/1206(20,3).4/1206(20,3)
.5/2206(31,3).5/1201(17,3).5/1105(14,3).5/1256(25,3).6/2201(27,3).6/2216(34,3).7
/1251(24,3).7/1200(3,3).8/2206(32,3).8/1105(13,3).8/1256(26,3).8/

17 333.1 758 1206(20,2)1.5/1100(1,1)1.6/1100(2,1)1.6/2216(34,2)2.2/1201(17,1)2.
2/1256(26,3)2.4/2206(32,2)2.5/1200(3,2)2.8/1105(13,2)////2211(30,1)0/1250(22,3)
.1/2266(35,3).1/2211(29,3).1/1155(16,1).2/1206(20,3).2/1100(1,1).3/1100(2,1).3/2
200(7,1).3/2200(8,1).3/1155(15,3).3/2266(36,3).5/1201(17,3).5/1250(21,3).6/1206(
19,3).9/2201(20,3).9/2216(34,3)1.1/1251(24,3)1.2/1201(18,3)1.3/1200(3,3)1.4/2206
(32,3)1.5/1105(13,3)1.6/1256(26,3)1.6/2201(27,3)1.9/2216(33,3)2.3/1251(23,3)2.6/
1200(4,3)2.9/

18 333.1 763.9 1206(19,3).9/2266(36,3).9/2266(35,3)1/1201(18,2)1.1/2216(33,3)1.
3/1100(1,3)1.4/1100(2,3)1.4/2211(30,3)1.4/2211(29,2)1.6/1206(20,3)1.7/2206(31,3)
2/1200(4,3)2.1/1256(25,3)2.2/1201(17,3)2.2/2201(27,3)2.3/1105(14,3)2.4/2200(7,3)
2.6/2200(8,3)2.6/2216(34,3)2.7/1250(22,3)2.7/1251(23,3)2.8////1250(21,1)0/1201(1
8,3).1/2266(36,2).3/1206(19,3).4/2211(29,1).8/2201(27,3).8/2211(30,3).9/1155(15,
1)1/1100(1,1)1.1/1100(2,1)1.1/2200(7,1)1.1/2200(8,1)1.1/1155(16,3)1.2/2216(33,3)
1.3/2266(35,3)1.4/1250(22,3)1.5/1251(23,3)1.7/1206(20,3)1.8/1200(4,3)2.1/1201(17
,3)2.2/2206(31,3)2.5/2201(20,3)2.6/1105(14,3)2.7/1256(25,3)2.8/2216(34,3)2.9/

19 333.1 822.2 2206(31,3).4/1200(4,2).4/1256(25,3).4/1105(14,3).4/2216(33,2).5/
1201(18,1).5/1251(23,3).7/2201(27,3).7/1206(19,3).8/2211(29,1).8/2211(30,3).9/11
00(1,3).9/1100(2,3).9/2266(36,3)1/1250(21,3)1/2200(7,3)1/2200(8,3)1/2266(35,3)1/
1206(20,3)1/1250(22,3)1.1/1155(16,3)1.1/1155(16,3)1.1/1201(17,3)1.1/2201(20,3)1.
3/2216(34,3)1.3/1251(24,3)1.3/1200(3,3)1.4/2206(32,3)1.4/1105(13,3)1.4/1256(25,3

)1.6////1200(4,2)0/2216(33,2).1/1201(10,1).2/1106(14,2).3/1251(23,1).6/1256(25,3
).6/2206(31,3).6/2201(27,1).0/1206(19,2)1/1250(21,1)1.2/2266(36,2)1.3/2211(29,1)
1.6/2211(30,3)1.5/1155(15,1)1.5/1100(1,1)1.5/1100(2,1)1.5/2200(7,1)1.5/2200(6,1)
1.5/1155(16,3)1.5/2266(35,3)1.5/1250(22,3)1.6/1206(20,3)1.7/1201(17,3)1.0/2201(2
0,3)1.9/2216(34,3)1.0/1251(24,3)2/1200(3,3)2/2206(32,3)2.1/1105(13,3)2.1/1256(26
,3)2.1/

20 333.1 [illegible] 1200(4,2).4/1105(14,3).4/1256(25,3).5/2206(31,3).5/1251(23,3).6/22
01(27,2).7/2216(33,3).0/1201(10,2).9/2211(29,1).9/1250(21,3)1/2200(7,3)1/2200(6,
3)1/2211(30,3)1/1155(15,3)1/1250(22,3)1/1155(16,3)1/1206(19,3)1.1/1100(1,3)1.1/1
100(2,3)1.1/1206(20,3)1.2/1201(17,3)1.2/2266(36,3)1.3/2266(35,3)1.3/2201(26,3)1.
3/2216(34,3)1.3/1251(24,3)1.3/1200(3,3)1.4/2206(32,3)1.5/1105(13,3)1.5/1256(26,3
)1.5////1105(14,2)1.1/1200(4,2)1.2/2216(33,2).3/1201(10,1).6/2206(31,2).5/1251(23,
1).6/1256(25,2).7/2201(27,1)1/1206(19,2)1.2/1250(21,1)1.4/2266(36,2)1.5/2211(29,
1)1.6/2211(30,3)1.6/1155(15,1)1.6/1100(1,1)1.7/1100(2,1)1.7/2200(7,1)1.7/2200(6,
1)1.7/1155(16,3)1.7/2266(35,3)1.7/1250(22,3)1.7/1206(20,3)1.0/1201(17,3)1.9/2201
(26,3)2/2216(34,3)2.1/1251(24,3)2.1/1200(3,3)2.2/2206(32,3)2.2/1105(13,3)2.2/1256
(26,3)2.2/

21 333.1 [illegible] 2206(31,2).2/1201(10,1).3/1256(25,2).3/2216(33,2).3/1105(14,2).3
/1200(4,2).3/1206(19,2).6/1251(23,2).6/2266(36,3).6/2201(27,2).6/2266(35,3).6/22
11(29,1).7/2211(30,3).7/1250(21,3).7/1100(1,3).7/1100(2,3).7/1155(16,3).7/1155(1
6,3).7/2200(7,3).7/2200(8,3).7/1250(22,3).0/1206(20,3).0/1201(17,3).0/2201(26,3/
.9/2216(34,3).9/1251(24,3)1/1200(3,3)1/2206(32,3)1/1105(13,3)1/1256(26,3)1.1////
1105(14,2)0/1200(4,2).2/2206(31,2).2/2216(33,2).2/1201(10,1).2/1256(25,2).3/1251
(23,1).4/2201(27,1).6/1206(19,2).7/1250(21,1).8/2266(36,2).6/2211(29,1).9/2211(3
0,3).9/1155(15,1).9/1100(1,1).9/1100(2,1).9/2200(7,1).9/2200(8,1).9/1155(16,3).9
/2266(35,3)1/1250(22,3)1/1206(20,3)1/1201(17,3)1.1/2201(26,3)1.1/2216(34,3)1.2/1
251(24,3)1.2/1200(3,3)1.2/2206(32,3)1.2/1105(13,3)1.2/1256(26,3)1.2/

22 333.1 [illegible] 1206(20,2).4/2216(34,2).4/1201(17,1).4/1256(26,3).5/1100(1,1).5/
1100(2,1).5/2206(32,2).5/1200(3,3).6/1105(13,3).6/1206(19,3).7/2211(29,3).7/2211
(30,2).7/2201(28,3).7/1201(16,3).7/1251(24,3).7/2266(35,2).6/2216(33,3).6/2266(3
6,3).9/1256(25,3).9/2206(31,3)1/2200(7,3)1/2200(8,3)1/1200(4,3)1/2201(27,3)1/1250
(22,3)1/1105(14,3)1/1250(21,3)1.1/1155(16,3)1.1/1251(23,3)1.1/1155(15,3)1.1////
1250(22,1)0/2266(35,2)0/1201(17,3)0/1206(20,3)1/2211(30,1).1/2201(26,3).1/2211(
29,3).1/1155(16,1).2/2216(34,3).2/1100(1,1).2/1100(2,1).2/2200(7,1).2/2200(8,1).
2/1155(15,3).2/1251(24,3).2/1200(3,3).2/2266(36,3).2/1250(21,3).2/2206(32,3).3/1
105(13,3).3/1256(26,3).3/1206(19,3).3/1201(16,3).4/2201(27,3).6/2216(33,3).7/1251
(23,3).7/1200(4,3).0/2206(31,3).9/1105(14,3).9/1256(25,3).9/

23 333.1 1014.3 //// No data available

24 333.1 1015.3 2216(33,3).6/1201(10,2).6/2206(31,3).5/1200(4,3).7/1105(14,3).9
/1256(25,3)1/2201(27,3)1.1/1251(23,3)1.2/1206(19,3)1.2/2266(36,3)1.2/2211(29,1)1
.2/2211(30,3)1.3/2266(35,3)1.4/1100(1,3)1.5/1100(2,3)1.5/1250(21,3)1.6/2200(7,3)
1.7/2200(8,3)1.7/1155(15,3)1.0/1250(22,3)1.0/1155(16,3)1.6/1206(20,3)1.0/1201(17
,3)2.1/2201(28,3)2.5/2216(34,3)2.5/1251(24,3)2.7/1200(3,3)2.6////2201(27,2)0/1251
(23,3).1/1201(10,2).2/2216(33,3).2/1200(4,3).4/1206(18,2).5/2206(31,3).7/1105(1
4,3).8/1256(25,3).0/1250(21,1).1/2266(36,2).3/2211(29,1).7/2211(30,3).6/1155
(15,1).9/1100(1,1).0/1100(2,1).0/2200(7,1).9/2200(8,1).9/1155(16,3)2/2266(3
5,3)2.2/1250(22,3)2.2/1206(20,3)2.4/1201(17,3)2.7/

25 333.1 1061.4 1201(17,3).9/2216(34,3)1.2/1206(20,3)1.2/2211(29,3)1.2/2211(30,
1).3/2201(28,3).4/1100(1,3).5/1100(2,3).6/1251(24,3).7/1200(3,3).7/2206(32
,3).0/1105(13,3).0/2266(35,3)2.1/2200(7,3)2.1/2200(8,3)2.1/1250(22,3)2.2/1256(
26,3)2.2/1206(19,3)2.3/1250(21,3)2.6/2266(36,3)2.7////1206(20,2).2/2216(34,3).2/
2201(28,3).2/1201(17,2).2/1251(24,3).5/1200(3,3).7/2206(32,3)1/1250(22,3)1/1105(
13,3)1/1256(26,3)1.1/2266(35,2)1.3/2211(30,1).0/2211(29,3)2.1/1155(16,1)2.2/1
100(1,1)2.4/1100(2,1)2.4/2200(7,1)2.4/2200(8,1)2.4/1155(15,3)2.5/2266(36,3)2.6/1
250(21,3)2.9/

26 333.1 1171.2 \20(\18,2).4/2216(33,3).6/2206(31,3)/1/1206(18,3)/1.2/1256(25,3)/1
.2/1200(4,3)/1.3/2266(36,3)/1.4/1105(14,3)/1.5/2266(35,3)/1.5/2211(30,3)/1.6/1100(1,3
)/1.6/1100(2,3)/1.6/2211(29,2)/1.8/2201(27,3)/1.9/1206(20,3)/2/1251(23,3)/2.2/1201(17,
3)/2.4/2200(7,3)/2.5/2200(8,3)/2.5/1250(21,3)/2.6/1250(22,3)/2.7/1155(15,3)/2.9/1155(1
6,3)/2.9////2201(27,1)/1.1/1251(23,3)/1.1/1200(4,3)/2/1201(18,2)/1.4/2216(33,3)/1.4/2206(
31,3)/1.5/1105(14,3)/1.6/1256(25,3)/1.7/1206(19,2)/1.7/1250(21,1)/1.6/2266(36,2)/1.7/2211(
29,1)/2.1/2211(30,3)/2.2/1155(15,1)/2.3/1100(1,1)/2.4/1100(2,1)/2.4/2200(7,1)/2.4/2200(
8,1)/2.4/1155(16,3)/2.4/2266(35,3)/2.6/1250(22,3)/2.6/1206(20,3)/2.9/

27 333.1 1132.1 1300(?,0,)/
1105(14,1)/1.0/1200(4,1)/1.4/2206(31,2)/1.5/1256(25,2)/1.6/2216(33,1)/1.5
/1201(18,1)/1.5/1251(23,1)/1.6/2266(36,2)/1.6/2201(27,1)/1.6/1250(21,1)/1.6/1206(19,2)/1.6/1
155(15,1)/1.6/2266(35,3)/1.6/1155(16,1)/1.6/2200(7,1)/1.6/2200(8,1)/1.6/2211(25,1)/1.6/1250(
22,3)/1.6/2211(30,3)/1.6/1100(1,1)/1.6/1100(2,1)/1.6/1206(20,3)/1.6/1201(17,3)/1.6/2201(26,3
)/1.7/2216(34,3)/1.7/1251(24,3)/1.7/1200(3,3)/1.7/2206(32,3)/1.7/1105(13,3)/1.7/1256(26,3)/1.7
////1105(14,1)/1.1/1200(4,1)/2/1256(25,2)/2/2206(31,2)/3/2216(33,2)/4/2201(18,1)/1.4
/1251(23,1)/1.4/2201(27,1)/1.5/1206(19,2)/1.5/1250(21,1)/1.6/2266(36,2)/1.6/2211(29,1)/1.6/2
211(30,3)/1.6/1155(15,1)/1.6/1100(1,1)/1.6/1100(2,1)/1.6/2200(7,1)/1.6/2200(8,1)/1.6/1155(16
,3)/1.6 2216(35,3)/1.6/1250(22,3)/1.6/1206(20,3)/1.6/1201(17,3)/1.6/2201(26,3)/1.7/2216(34,3
)/1.7/1251(24,3)/1.7/1200(3,3)/1.7/2206(32,3)/1.7/1105(13,3)/1.7/1256(26,3)/1.7/
▼1300(?,0,)/

28 333.1 114.2 1201(17,2)/1.9/2216(34,3)/1.9/1256(25,3)/1.2205(32,3)/1.1/1200(7,3)/1.3
1105(13,3)/1.3/1206(20,2)/1.6/2201(28,2)/1.9/1100(1,3)/1.9/1100(2,3)/1.9/1251(23,3)/1.
9/2211(29,3)/2/2211(30,2)/2.2/1206(19,2)/2.5/1201(18,2)/2.5////1201(17,3)/1.1/1252(22,
1)/2.2/2201(29,3)/2.3/1206(20,2)/2.4/2266(35,2)/2.4/2216(34,2)/2.5/1251(24,3)/2.7/2211(30,1)/
.9/1200(3,3)/1.9/2211(29,3)/2206(32,3)/1.1/1155(16,1)/1.1/1105(13,3)/1.1/1256(26,3)/1
.2/1200(4,1)/1.2/1100(1,1)/1.2/2200(7,1)/1.2/2200(8,1)/1.2/1155(16,3)/1.2/2266(36,3)/1
.5/1250(21,3)/1.5/1206(19,3)/1.9/1201(18,3)/2.5/

29 763.4 276.5 1206(20,2)/1.9/1100(1,1)/1.2/1100(2,1)/1.2/1201(17,2)/1.6/2266(35,2)/1
.6/2216(34,3)/1.6/2211(29,3)/2.2/1206(19,3)/2.2/2211(30,2)/2.5////2201(26,3)/2/1206(
20,2)/3/1201(17,3)/1.4/1250(22,1)/1.6/2216(34,3)/1.6/2266(35,2)/1.9/1251(24,3)/1.9/1200(3,
3)/1.2/2206(32,3)/1.4/2211(30,1)/1.5/1105(13,3)/1.5/1256(26,3)/1.6/2211(29,3)/1.7/1155
(16,1)/1.9/1100(1,1)/2/1100(2,1)/2/2200(7,1)/2/2200(8,1)/2/1155(16,3)/2.1/2266(36,3)/2.
5/1250(21,3)/2.5/

30 SKIPPED

31 763.4 335.2 1206(20,3)/1.4/1201(17,3)/1.6/1100(1,3)/1100(2,3)/2216(34,3)/1.1/22
11(29,3)/1.3/2211(30,2)/1.6/1206(19,3)/1.8/2206(32,3)/1.9/1200(3,3)/1.9/2201(26,3)/2/1
105(13,3)/2.1/1201(16,3)/2.2/1256(26,3)/2.2/2266(35,3)/2.3/1251(24,3)/2.3////2201(17,
3)/1250(22,1)/2.2/2266(35,2)/1.4/2201(26,3)/1.6/1206(20,3)/1.6/2216(34,3)/1/2211(30,1)/1.
4/1251(24,3)/1.2/2211(29,3)/1.2/1155(16,1)/1.4/1200(3,3)/1.5/1100(1,1)/1.6/1100(2,1)/1
.5/2200(7,1)/1.5/2200(8,1)/1.5/1155(15,3)/1.6/2206(32,3)/1.7/1105(13,3)/1.8/1256(26,3
)/1.9/2266(36,3)/2/1250(21,3)/2/1206(19,3)/2.6/

32 763.4 352.5 1206(20,2)/1/1201(17,2)/1.2/2216(34,3)/1.4/2206(32,3)/1.7/1200(3,3)/1
.9/1256(26,3)/2/1105(13,3)/2/2201(20,3)/2.5/1251(24,3)/2.5////1256(26,3)/1.1/1251(24,2
)/1/1105(13,3)/1/2206(32,3)/2/1200(3,3)/.8/1201(17,1)/.7/2201(20,1)/.7/2216(34,2)/.8
/1206(20,2)/1.4/1250(22,1)/2.4/2266(35,2)/2.7/

33 763.4 361.5 1206(19,2)/1.4/2266(36,2)/1.5/1201(18,2)/1.8/2266(35,3)/1.7/2216(33,3)/1.7
/1100(1,1)/1.5/1100(2,1)/1.8/2206(31,3)/1.8/2211(30,3)/1.9/1200(4,3)/1/1256(25,3)/1/2211(2
9,2)/1/1206(20,3)/1/1105(14,3)/1.1/2201(27,3)/1.1/1251(23,3)/1.2/1201(17,3)/1.3/2200(7
,3)/1.3/2200(8,3)/1.3/1250(21,3)/1.3/1250(22,3)/1.4/1155(15,3)/1.4/1155(16,3)/1.4/2216
(34,3)/1.5/2201(28,3)/1.5/1251(24,3)/1.6/1200(3,3)/1.7/2206(32,3)/1.7/1105(13,3)/1.7/1

2066(26,3)1.8///2201(27,3)0/1205(19,2).1/2216(33,3).2/1201(16,2).2/1250(21,1).3/
1251(23,3).4/2266(36,2).5/1200(4,3).5/2211(29,1).7/2206(31,3).7/2211(30,3).7/115
5(15,1).8/1105(14,3).8/1100(1,1).8/1100(2,1).8/2200(7,1).8/2200(8,1).6/1256(25,3
).8/1155(16,3).8/2266(35,3).9/1250(22,3).8/1206(20,3).1/1201(17,3).3/2201(29,3
).4/2216(34,3)1.5/1251(24,3)1.6/1200(3,3)1.7/2206(32,3)1.6/1105(13,3)1.6/1256(2
6,3)1.8/

14 763.4 395.2 : 1251(23,2).2/2201(27,1).4/1105(14,3).8/1250(21,1).8/1200(4,3).9/
1155(15,2).9/2200(7,1).8/2200(8,1).8/1155(16,2)1/1256(25,3)1/2206(31,3)1/2250(22
,3)1.1/2211(29,1)1.2/2211(30,1)1.3/2216(33,3)1.3/1201(16,3)1.4/2201(20,3)1.6/110
0(1,3)1.7/1100(2,3)1.7/1201(17,3)1.7/1251(24,3)1.7/2206(19,3)1.7/1206(20,3)1.6/2
216(34,3)1.8/1200(3,3)1.8/1105(13,3)1.8/2266(35,3)1.8/2206(32,3)1.8/2266(36,3)2/
1256(26,3)2.1////1256(25,3)0/1105(14,3).1/1251(23,2).1/2206(31,3).1/1200(4,3).3/
1201(27,1).4/1201(16,1).6/2216(33,3).6/1206(19,2).8/1250(21,1)1.1/2266(36,2)1.3/
2211(29,1)1.6/2211(30,3)1.6/1155(15,1)1.6/1100(1,1)1.6/1100(2,1)1.6/2200(7,1)1.6
/2200(8,1)1.6/1155(16,3)1.6/2266(35,3)1.7/1250(22,3)1.7/1206(20,3)1.9/1201(17,3)
2/2201(28,3)2.2/2216(34,3)2.3/1251(24,3)2.4/1200(3,3)2.4/2206(32,3)2.5/1105(13,3
)2.5/1256(26,3)2.6/

15 763.4 407.1 1206(20,2)1/1100(1,1).2/1100(2,1).2/2266(35,2).5/1201(17,1).
5/2216(34,2).5/1256(26,3).6/2206(32,2).6/1200(3,2).6/1105(13,3).6/1206(19,2
).9/2266(36,2)2/2211(29,3)2/2211(30,2)2.1/2201(28,3)2.1/1251(24,3)2.2/1201(16,3
)2.2/2216(33,3)2.5/2206(31,3)3////1200(3,3)0/2201(28,1).1/1251(24,3).1/2206(32,3
).1/1105(13,3).2/1256(26,3).2/1201(17,2).2/2216(34,3).2/1206(20,2).3/1250(22,1).
7/2266(35,2).8/2211(30,1)1/2211(29,3).1/1155(16,1).2/1100(1,1).2/1100(2,1).2
/2200(7,1).2/2200(8,1).2/1155(15,3).3/2266(36,3).4/1250(21,3).4/1206(19,3).4
.7/1201(18,3)2/2201(27,3)2.4/2216(33,3)2.7/1251(23,3)3/

16 763.4 402.7 2216(33,3).3/1201(18,2).5/2206(31,3).8/1200(4,3).9/1206(15,3).1
/1250(25,3)1.1/2211(30,3)1.1/2211(29,1).2/1105(14,3).2/2201(27,3).3/2266(36,3
).4/1160(1,3).4/1100(2,3).4/2266(35,3).6/1251(23,3).7/1206(20,3).8/2200(7,
3).9.2200(8,3).9/1250(21,3)2/1250(22,3)2.1/1201(17,3)2.2/1155(15,3)2.3/1155(16
,3)2.3/2201(28,3)2.6/2216(34,3)2.7////1206(19,2).1/2201(27,3).1/2216(33,3).3/1201
(18,2).3/1251(23,3).6/1250(21,1).9/1200(4,3)1/2266(36,2).1/2206(31,3).3/1105(
14,3).5/1256(25,3).5/2211(29,1).6/2211(30,3).7/1155(15,1).8/1100(1,1).8/1
100(2,1).8/2200(7,1).9/2200(8,1).9/1155(16,3).8/2266(35,3)2.1/1250(22,3)2.1/1
206(20,3)2.4/1201(17,3)2.6/

17 763.4 477.4 ///1250(21,1)0/1201(19,3).1/2266(36,2).1/1206(19,3).2/2211(29,1)
.5/2201(27,3).5/2211(30,3).5/1155(15,1).6/1100(1,1).7/1100(2,1).7/2200(7,1).7/22
00(8,1).7/1156(16,3).7/2216(33,3).9/2266(35,3).8/1250(22,3).6/1251(23,3)1/1206(2
0,3)1/1200(4,3)1.3/1201(17,3)1.3/2206(31,3)1.5/2201(26,3)1.5/1105(14,3)1.6/1256(
25,3)1.7/2216(34,3)1.7/1251(24,3)1.6/1200(3,3)1.6/2206(32,3)2/1105(13,3)2/1256(2
6,3)2.1/

18 763.4 491 1105(14,2).6/1200(4,2).6/1251(23,2).8/1201(18,1).6/2216(33,2).8/22
06(31,2).9/2201(27,2)1/1256(25,2)1/1250(21,1).1/2266(36,3).1/1155(15,3).2/2211
(29,1).2/1156(16,3).2/2266(35,3).2/1206(19,3).3/2200(7,1).3/2200(8,1).3/2
211(30,3)1.3/1250(22,3)1.3/1100(1,3)1.4/1100(2,3)1.4/1206(20,3)1.5/1201(17,3).6
/2201(28,3)1.7/2216(34,3).8/1251(24,3).8/1200(3,3)1.9/2206(32,3)1.9/1105(13,3)
2/1256(26,3)2////1201(18,1).1/2216(33,2).1/1251(23,1).2/1200(4,2).3/1256(25,3).4
/1105(14,3).4/2206(31,3).4/2201(27,1).7/1206(19,2).8/1250(21,1).1/2266(36,2).3
/2211(29,1).4/2211(30,3).4/1155(15,1).5/1100(1,1).5/1100(2,1).5/2200(7,1).
5/2200(8,1).6/1155(16,3).6/2266(35,3).6/1250(22,3).6/1206(20,3).7/1201(17,3
).8/2201(28,3).9/2216(34,3)2/1251(24,3)2.1/1200(3,3)2.1/2206(32,3)2.2/1105(13,
3)2.2/1256(26,3)2.2/

19 763.4 456 1206(19,3).5/1100(1,3).6/1100(2,3).6/2211(30,3).8/2266(35,3).6/221
1(29,3).9/1206(20,3).9/1201(16,3)1/2266(36,3)1.1/1201(17,3)1.6/2216(33,3)1.7/221
6(34,3)2.1/2200(7,3)2.3/2200(8,3)2.3/2201(27,3)2.4/1250(22,3)2.5/2206(32,3)2.7/
///1156(15,1)0/2211(30,2).1/1100(1,1).1/1100(2,1).1/2200(7,1).1/2200(8,1).1/1155(
16,3).2/2266(36,3).2/1250(21,3).2/2211(29,1).3/2266(35,3).5/1250(22,3).5/1206(19
,3).7/1206(20,3).9/1201(16,3)1.4/1201(17,3)1.4/2201(26,3)1.9/2216(34,3)2.2/2201(
27,3)2.2/1251(24,3)2.4/1200(3,3)2.6/2216(33,3)2.7/2206(32,3)2.8/1105(13,3)2.8/12
06(26,3)2.9/

```
50 763.4 535.3  2206(31,2).4/1256(25,2).8/120(1(16,1).8/2216(33,2).8/1105(14,2)1/
1200(4,2)7/1251(23,3)1.8/2266(36,3)1.8/1206(19,2)1.8/2201(27,2)2/2266(36,3)2.1/2
2(1(29,1)2.2/2221(30,3)2.3/1250(21,3)2.3/1100(1,3)2.4/1100(2,3)2.4/1155(15,3)2.4
/1155(16,3)2.4/2200(7,3)2.5/2200(8,3)2.5/1250(22,3)2.5/1206(20,3)2.6/////1105(14,
2)1/2206(31,2).6/1200(4,2).6/2216(33,2).8/120(1(16,1).9/1256(25,2)1/1251(23,1)1.
3/2201(27,1)2/1206(19,2)2.3/1250(21,1)2.7/2266(36,2)2.6/

51 763.4 555.3  2206(31,2).8/1256(25,2).8/1105(14,1).8/1200(4,1).8/2216(33,1)1/1
20(1(18,1)1/2266(36,2)1.1/1206(19,2)1.2/1251(23,2)1.2/2266(35,2)1.3/2201(27,2)1.3
/2211(29,1)1.3/2211(30,3)1.4/1250(21,3)1.4/1100(1,3)1.4/1100(2,3)1.4/1155(15,3)1
.4/1155(16,3)1.4/2200(7,3)1.4/2200(8,3)1.4/1250(22,3)1.4/1206(20,3)1.4/1201(17,3
)1.5/2201(26,3)1.6/2216(34,3)1.6/1251(24,3)1.6/1200(3,3)1.6/2206(32,3)1.6/1105(1
3,3)1.7/1256(26,3)1.7////1105(14,1).4/1200(4,1).7/1256(25,2).7/2206(31,2).8/2216
(33,1)1/120(1(18,1)1.2/1251(23,1)1.3/2201(27,1)1.5/1206(19,2)1.5/1250(21,1)1.6/22
66(36,2)1.7/2211(29,1)1.7/2211(30,3)1.7/1155(15,1)1.7/1100(1,1)1.8/1100(2,1)1.8/
2200(7,1)1.8/2200(8,1)1.8/1155(16,3)1.8/2266(35,3)1.8/1250(22,3)1.8/1206(20,3)1.
8/1201(17,3)1.9/2201(26,3)1.9/2216(34,3)1.9/1251(24,3)2/1200(3,3)2/2206(32,3)2/1
105(13,3)2/1256(26,3)2/

52 763.4 567.8  1201(17,1)1.4/2216(34,2)1.4/2206(32,3)1.6/1256(26,3)1.7/1200(3,3)1.7/
1105(13,3)1.8/1206(20,2)1.6/1251(24,3)1.1/2201(26,3)1.1/2211(29,3)1.4/1100(1,3)1.4
/1100(2,3)1.4/2211(30,2)1.6/2266(35,3)1.6/1206(19,3)1.8/1201(16,3)2/2200(7,3)2/2
200(8,3)2/1250(22,3)2.1/2266(36,3)2.1/1250(21,3)2.4/1155(15,3)2.4/////1251(24,1)
1/1201(17,1)1.1/2216(34,2)1.2/1200(3,2)1.3/1256(26,3)1.3/1105(13,3)1.3/2206(32,3)1.3/2
201(26,1)1.6/1206(20,2)1.9/1250(22,1)1.4/2266(35,2)1.5/2211(30,1)1.5/2211(29,3)2/1
155(16,1)2.1/1100(1,1)2.2/1100(2,1)2.2/2200(7,1)2.2/2200(8,1)2.2/1155(15,3)2.2/2
266(36,3)2.4/1250(21,3)2.4/1206(19,3)2.7/

53 763.4 586.3  1256(25,3)1.7/1201(16,3)1.8/1100(1,3)1.8/1100(2,3)1.8/2216(33,3)1.8/1
20(1(17,3)1.9/1206(20,3)1.8/1206(19,3)1.8/2206(31,3)1.8/2211(29,3)1.9/2211(30,2)1.9/2211
6(34,3)1.9/1200(4,3)1.9/2206(32,3)1.9/1256(26,3)1/1200(3,3)1/1105(14,3)1/1105(13,3)
1/2201(26,3)1/2201(27,3)1.1/1251(24,3)1.1/2266(35,3)1.2/1251(23,3)1.2/2200(7,3)1
.2/2200(8,3)1.2/2266(36,3)1.2/1250(22,3)1.3/1250(21,3)1.4/1155(16,3)1.4/1155(15,
3)1.4/////1251(23,1)1.0/1256(25,3)1.2/1201(18,1)1.2/1105(14,3)1.2/2216(33,2)1.2/2206(3
1,3)1.2/1200(4,3)1.3/2201(27,1)1.4/1206(19,2)1.6/1250(21,1)1.6/2266(36,2)1.6/2211(29,1
)2211(30,3)1/1155(15,1)1/1100(1,1)1/1100(2,1)1/2200(7,1)1/2200(8,1)1/1155(16,3)1
/2266(35,3)1.1/1250(22,3)1.1/1206(20,3)1.2/1201(17,3)1.3/2201(26,3)1.4/2216(34,
3)1.4/1251(24,3)1.5/1200(3,3)1.5/2206(32,3)1.5/1105(13,3)1.6/1256(26,3)1.6/

54 763.4 637.3  1201(18,1)1.2/2216(33,2)1.2/2206(31,3)1.7/1206(19,2)1.8/1256(25,3)1.8
/1200(4,2)1.9/1105(14,3)1.9/2266(36,3)1/2266(35,3)1/1251(23,3)1/2201(27,3)1/2
211(30,3)1.3/1100(1,3)1.3/1100(2,3)1.3/2211(29,1)1.3/1206(20,3)1.4/1250(21,3)1.
6/2200(7,3)1.6/2200(8,3)1.6/1201(17,3)1.7/1250(22,3)1.7/1155(15,3)1.7/1155(16,3)
1.7/2216(34,3)1.9/2201(26,3)1.9/1251(24,3)2/1200(3,3)2.1/2206(32,3)2.1/1105(13,3
)2.1/1256(26,3)2.2////1251(23,1)1.1/1201(18,1)1.2/2216(33,2)1.2/1256(25,3)1.4/1105(1
4,3)1.4/1200(4,2)1.4/2266(31,3)1.5/2201(27,1)1.7/1206(19,2)1/1250(21,1)1.4/2266(36,2
)1.5/2211(29,1)1.7/2211(30,3)1.7/1155(15,1)1.8/1100(1,1)1.8/1100(2,1)1.8/2200(7,
1)1.8/2200(8,1)1.8/1155(16,3)1.8/2266(35,3)1.9/1250(22,3)1.9/1206(20,3)2.1/1201(
17,3)2.2/2201(26,3)2.4/2216(34,3)2.5/1251(24,3)2.6/1200(3,3)2.6/2206(32,3)2.7/11
05(13,3)2.7/1256(26,3)2.7/

55 763.4 720.3  1100(1,3)2.2/1100(2,3)2/1206(19,3)1.3/1206(20,3)1.3/1201(18,3)1.5/2
211(30,3)1.5/2211(29,3)1.5/1201(17,3)1.6/2266(35,3)1.8/2216(33,3)1.9/2266(36,3)1.8/221
6(34,3)1.9/2201(26,3)1.2/1200(3,3)1.2/2206(32,3)1.2/1256(25,3)1.3/2206(31,3)1.3/2
```

20)<27,3>1.3/125)<24,3>1.3/1200)<4,3>1.3/1105)<13,3>1.3/2200)<7,3>1.3/2200)<6,3>1.3/1256)<26,3>1.4/1250)<22,3>1.6/1105)<14,3>1.6/1250)<21,3>1.6/1155)<16,3>1.7/125)<23,3>1.7/1155)<16,3>1.7////1250)<21,3>0/22)<29,1>0/2266)<36,3>0/22)<30,3>.1/1155)<15,1>.1/1100)<1,1>.2/1100)<2,1>.2/2200)<7,1>.2/2200)<8,1>.2/1155)<15,3>.2/1206)<18,3>.2/2266)<35,3>.3/1250)<22,3>.4/120)<18,3>.5/1206)<20,3>.5/120)<17,3>.8/220)<27,3>.9/220)<20,3>/2216)<34,3>1.2/2216)<33,3>1.2/125)<24,3>1.3/1200)<3,3>1.4/125)<23,3>1.4/2206)<32,3>1.6/1105)<13,3>1.6/1256)<26,3>1.6/1200)<4,3>1.6/2206)<31,3>1.9/1105)<14,3>2/1256)<25,3>2/

 2266)<36,3>.5/2266)<35,3>.5/1250)<21,3>.6/22)<29,1>.6/125)<23,3>.6/120)<18,2>.6/2216)<33,3>.6/1155)<16,3>.6/2200)<27,3>.6/1155)<16,3>.6/1200)<4,3>.7/1206)<19,3>.7/2206)<31,3>.7/2216)<30,3>.7/1250)<22,3>.7/1105)<14,3>.7/2200)<7,3>.7/2200)<8,3>.7/1100)<1,3>.8/1100)<2,3>.8/1256)<25,3>.8/1206)<20,3>.8/120)<17,3>.9/220)<26,3>1/2216)<34,3>1.1/125)<24,3>1.1/1200)<3,3>1.2/2206)<32,3>1.2/1105)<13,3>1.2/1256)<26,3>1.3////120)<18,3>0/1250)<21,1>.1/2266)<36,2>.1/1206)<19,3>.2/220)<27,3>.2/2216)<29,1>.3/2216)<30,3>.3/2216)<33,3>.3/1155)<15,1>.4/1100)<1,1>.4/1100)<2,1>.4/2200)<7,1>.4/2200)<8,1>.4/1155)<16,3>.4/125)<23,3>.4/2266)<35,3>.5/1250)<22,3>.6/1200)<4,3>.6/1206)<20,3>.6/2206)<31,3>.7/120)<17,3>.7/1105)<14,3>.7/1256)<25,3>.7/2220)<20,3>.8/2216)<34,3>.9/125)<24,3>.9/1200)<3,3>1/2206)<32,3>1/1105)<13,3>1.1/1256)<26,3>1.1/

 1100)<1,2>.7/1100)<2,2>.7/1206)<20,2>.9/120)<17,3>1/1206)<19,3>1.1/2216)<34,3>1.2/120)<18,3>1.3/2216)<29,3>1.3/2216)<30,2>1.4/2206)<32,3>1.4/1256)<26,3>1.5/1200)<3,3>1.5/2216)<33,3>1.6/1105)<13,3>1.6/2220)<28,3>1.7/2266)<35,3>1.8/1256)<25,3>1.8/125)<24,3>1.9/2266)<36,3>2/2206)<31,3>2/1200)<4,3>2.1////1206)<19,3>0/1250)<21,2>0/2266)<36,2>.1/2216)<29,1>.2/2216)<30,3>.3/1155)<15,1>.3/120)<18,3>.4/1100)<1,1>.4/1100)<2,1>.4/2200)<7,1>.4/2200)<8,1>.4/1155)<16,3>.4/2266)<35,3>.6/1250)<22,3>.6/1206)<20,3>.8/220)<27,3>.8/120)<17,3>1/2216)<33,3>1.1/2220)<28,3>1.3/125)<23,3>1.3/2216)<34,3>1.5/1200)<4,3>1.6/125)<24,3>1.6/1200)<3,3>1.7/2206)<32,3>1.8/2206)<31,3>1.8/1105)<13,3>1.8/1256)<26,3>1.8/1.95)<14,3>1.9/1256)<25,3>2/

 120)<18,1>.5/2206)<31,2>.5/2216)<33,2>.5/1256)<25,2>.7/1200)<4,2>.8/1105)<14,2>.9/2266)<36,2>1/1206)<19,2>1/125)<23,3>1.3/2266)<35,3>1.3/2220)<27,3>1.3/2211)<30,3>1.4/2211)<29,1>1.4/1100)<1,1>1.4/1100)<2,1>1.4/1250)<21,3>1.5/1206)<20,3>1.5/2200)<7,3>1.6/2200)<8,3>1.6/1155)<15,3>1.6/1155)<16,3>1.6/1250)<22,3>1.6/120)<17,3>1.7/2216)<34,3>1.9/2220)<26,3>1.9/125)<24,3>1.9/1200)<3,3>2/2206)<32,3>2/1105)<13,3>2/1256)<26,3>2.1////1105)<14,2>0/1200)<4,2>.3/2206)<33,2>.4/120)<18,1>.5/2206)<31,2>.5/125)<23,1>.7/1256)<25,2>.7/2220)<27,1>.1/1206)<19,2>1.3/1250)<21,1>1.6/2266)<36,2>1.6/2211)<29,1>1.8/2211)<30,3>1.8/1155)<15,1>1.8/1100)<1,1>1.9/1100)<2,1>1.9/2200)<7,1>1.9/2200)<8,1>1.9/1155)<16,3>1.9/2266)<35,3>2/1250)<22,3>2/1206)<20,3>2/120)<17,3>2.2/220)<28,3>2.3/2216)<34,3>2.3/125)<24,3>2.4/1200)<3,3>2.4/2206)<32,3>2.5/1105)<13,3>2.5/1256)<26,3>2.5/

 1105)<14,1>.3/1200)<4,1>.5/2206)<31,2>.9/1256)<25,2>.9/120)<18,1>1.3/2216)<33,2>1.3/125)<23,2>1.3/2220)<27,2>1.6/1250)<21,1>1.7/2266)<36,3>1.7/1155)<15,3>1.8/2211)<29,1>1.8/1155)<16,3>1.8/2266)<35,3>1.8/1206)<19,2>1.8/2200)<7,1>1.8/2200)<8,1>1.8/1250)<22,3>1.8/2211)<30,3>1.8/1100)<1,3>1.9/1100)<2,3>1.9/1206)<20,3>2/120)<17,3>2.1/2220)<28,3>2.2/2216)<34,3>2.2/125)<24,3>2.3/1200)<3,3>2.3/2206)<32,3>2.4/1105)<13,3>2.4/1256)<26,3>2.4////1105)<14,1>.2/1200)<4,1>.7/1256)<25,2>.8/2206)<31,2>.9/2216)<33,2>1.6/120)<18,1>1.6/125)<23,1>1.8/2220)<27,1>2/1206)<19,2>2.2/1250)<21,1>2.4/2266)<36,2>2.4/2211)<29,1>2.5/2211)<30,3>2.6/1155)<15,1>2.6/1100)<1,1>2.6/1100)<2,1>2.6/2200)<7,1>2.6/2200)<8,1>2.6/1155)<16,3>2.6/2266)<35,3>2.8/1250)<22,3>2.6/1206)<20,3>2.7/120)<17,3>2.8/2220)<26,3>2.8/2216)<34,3>2.9/125)<24,3>2.9/1200)<3,3>/

 220)<26,3>.6/120)<17,3>.7/2216)<34,3>.8/1200)<3,3>.8/125)<24,3>.6/2206)<32,3>.8/1105)<13,3>.9/2216)<29,2>.9/2211)<30,1>.9/1256)<26,3>1/1206)<20,3>1.1/2200)<7,3>1.1/2200)<8,3>1.1/1100)<1,3>1.2/1100)<2,3>1.2/120)<18,3>1.2/1250)<22,3>1.3/2220)<27,3>1.3/1250)<21,3>1.5/1206)<19,3>1.6/1155)<16,3>1.5/2216)<33,3>1.6/1155)<15,3>1.6/120)<24,3>1.6/1256)<25,3>1.6/125)<23,3>1.7/2206)<31,3>1.8/1105)<14,3>1.8/2266)<35,3>2/////1155)<15,3>0/1100)<1,3>0/1100)<2,3>0/2200)<7,3>0/2200)<8,3>0/1155)<16,3>1.1/2211)<30,2>.1/2211)<29,2>.1/2266)<36,3>.1/1250)<21,3>.2/2266)<35,3>.2/1250)<22,3>.2/1206)<19,3>.4/1206)<20,3>.4/120)<17,3>.7/120)<18,3>.7/2220)<28,3>.9/2216)<34,3>1.1/2220)<27,3>1.2/125)<24,3>1.2/1200)<3,3>1.3/2206)<32,3>1.4/1105)<13,3>1.4/2216)<33,3>1.4/1256)<26,3>1.5/125)<23,3>1.7/120)<4,3>1.9/2206)<31,3>2.2/1105)<14,3>2.3/1256)<25,3>2.3/

```
51 763.4 970.6  2206(31,2).7/1200(4,1).7/1105(14,1).7/1256(25,2).7/120(18,1).8/
2216(33,2).8/2266(36,2).8/125(23,2).8/1206(19,2).9/2201(27,2).9/1250(21,1).9/22
06(35,3)1/1155(15,3)1/2211(29,1)1/1155(16,3)1/2200(7,1)1/2200(8,1)1/2211(30,3)1/
1250(22,3)1/1100(1,1)1/1100(2,1)1/1206(20,3)1.1/1201(17,3)1.1/2201(26,3)1.2/2216
(34,3)1.2/125(24,3)1.2/1200(3,3)1.2/2206(32,3)1.2/1105(13,3)1.3/1256(26,3)1.3/
//2206(31,2)8/1256(25,2)1/1105(14,2)1.2/1200(4,1).2/2216(33,2).4/120(18,1).4/12
5(23,1).5/2201(27,1).7/1206(19,2).7/1250(21,1).9/2266(36,2).9/2211(29,1).9/2211
(30,3)1/1155(15,1)1/1100(1,1)1/1100(2,1)1/2200(7,1)1/2200(8,1)1/1155(16,3)1/2266
(35,3)1/1250(22,3)1/1206(20,3)1.1/1201(17,3)1.1/2201(28,3)1.2/2216(34,3)1.2/125i
(24,3)1.2/1200(3,3)1.2/2206(32,3)1.2/1105(13,3)1.2/1256(26,3)1.3/

52 763.4 1015  1105(14,1).3/1200(4,1).4/2206(31,2).4/1256(25,2).4/120(18,1).4/2
216(33,2).4/125(23,1).5/2266(36,2).5/1206(19,2).5/2201(27,1).5/1250(21,1).5/226
6(35,3).5/1155(15,1).5/1155(16,3).5/2200(7,1).5/2200(8,1).5/2211(28,1).5/2211(30
,3).5/1250(22,3).5/1100(1,1).6/1100(2,1).6/1206(20,3).6/1201(17,3).6/2201(28,3).
6/2216(34,3).6/125(24,3).6/1200(3,3).6/2206(32,3).6/1105(13,3).7/1256(26,3).7//
//1200(4,1)0/1256(25,2).1/1105(14,1).1/2206(31,2).1/2216(33,2).3/120(18,1).3/12
5(23,1).3/2201(27,1).4/1206(19,2).4/1250(21,1).5/2266(36,2).5/2211(29,1).5/2211
(30,3).5/1155(15,1).5/1100(1,1).5/1100(2,1).5/2200(7,1).5/2200(8,1).5/1155(16,3/
.5/2266(35,3).6/1250(22.3).6/1206(20,3).6/1201(17,3).5/2201(28,3/.6/2216(34,3).6
/125i(24,3).6/1200(3,3).6/2206(32,3).7/1105(13,3).7/1256(26,3).7/

53 763.4 1065.4  1201(18,2).9/2216(33,3).9/2206(31,3)1/1200(4,3)1.1/1105(14.3)1.
2/2266(36,3)1.2/1256(25,3)1.4/125i(23,3)1.5/2201(27,3)1.5/2266(35,3)1.6/1206(19.
3)1.5/2211(29,1).6/2211(30,3)1.7/1100(1,3)1.9/1100(2,3)1.9/1250(21,3)2/2200(7,3
)2.1/2200(8,3)2.1/1155(15,3)2.1/1155(16,3)2.2/1250(22,3)2.2/1206(20,3)2.2/1201(1
7,3)2.6///2201(27,2)0/125i(23,3).1/1201(16,2).2/2216(33,3).2/1200(4,3).4/1206(1
9,2).5/2206(31,3).7/1105(14,3).8/1256(25,3).9/1250(21,1).3/2266(36,2).5/2211(2
9,1).9/2211(30,3)2/1155(15,1)2.1/1100(1,1)2.2/1100(2,1)2.2/2200(7,1)2.2/2200(8,
1)2.2/1155(16,3)2.2/2266(35,3)2.4/1250(22,3)2.4/1206(20,3)2.7/1201(17,3)3/

54 763.4 1061.3  1206(19,2).7/1201(16,2).1/2216(33,3).4/1100(1,2).6/1100(2,2/
1,6/1256(25,3).7/2206(31,3).8/2266(36,2).9/2266(35,2).9/2211(30,3/2/1206(20,
3/2/2211(29,2/2.1/1200(4,3/2.2/1105(14,3)2.4/1201(17,3)2.5/2201(27,3)2.8////1200
(4,3)0/2201(27,1).2/125i(23,3).3/2206(31,3).3/1105(14,3).5/1256(25,3).5/1201(18,
2).6/2216(33,3).6/1206(19,2).9/1250(21,1).6/2266(36,1).0/2211(29,1)2.2/2211(30
,3)2.3/1155(15,1)2.4/1100(1,1)2.5/1100(2,1)2.5/2200(7,1)2.5/2200(8,1)2.6/1155(16
,3)2.5/2266(35,3)2.7/1250(22,3)2.7/1206(20,3)3/

55 763.4 1170.6  1100(1,3).4/1100(2,3).4/1206(19,3).5/1206(20,3).7/2211(25.3)1/2
211(30,3)1/1201(16,3)1.1/1201(17,3)1.3/2266(35,3)1.4/2266(36,3)1.7/2216(33,3)1.9
/2216(34,3)1.9/2201(26,3)2.3/1200(3,3)2.5/2206(32,3)2.5////1155(15,1)0/2211(30.2
).1/1100(1,1).1/1100(2,1).1/2200(7,1).1/2200(8,1).1/1155(16,3).2/2266(36,3).2/12
5^(21,3).3/2211(29,1).3/2266(35,3).4/1250(22,3).5/1206(19,3).7/1206(20,3).9/1201
(17,3).3/1201(18,3)1.4/2201(26,3)1.8/2216(34,3)2.1/2201(27,3)2.2/125i(24,3)2.4/
120w(3,3)2.6/2216(33,3)2.7/2206(32,3)2.8/1105(13,3)2.8/1256(26,3)2.9/

56 763.4 1932.3  1201(18,2).1/2216(33.3).2/2206(31,3).3/1206(19,3).3/1256(25,3/.
3/1200(4,3).3/2266(36,3).3/1105(14,3).4/2266(35,3).4/2211(30,3).4/1100(1,3).4/11
00(2,3).4/2211(29,1).6/2201(27,3).5/125i(23,3).5/1206(20,3).5/2200(7,3).6/2200(8
,3).6/1250(21,3).6/1201(17,3).6/1250(22,3).7/1155(15,3.7/1155(16,3).7/2216(34,3
).8/2201(28,3).8/125i(24,3).9/1200(3,3).9/2206(32,3).9/1105(13,3).9/1256(26,3)1/
///125i(23,3/0/2201(27,1)0/1200(4,3).1/1201(18,2).1/2216(33,3).1/2206(31,3).2/12
06(19,2).2/1105(14,3).2/1256(25,3).2/1250(21,1).4/2266(36,2).4/2211(29,1).5/2211
(30,3).6/1155(15,1).6/1100(1,1).6/1100(2,1).6/2200(7,1).6/2200(8,1).6/1155(16,3/
.6/2266(35,3).7/1250(22,3).7/1206(20,3 9/1201(17,3).8/2201(28,3).8/2216(34,3)1/

v 1300(8,3).6/ ; vv 1300(8,3).5/

125i(24,3)1/1200(3,3)1.1/2206(32,3)1.1/1105(13,3)1.1/1256(26,3)1.1/
```

57 1051.1 114.2 1256(26,3)1.5/1200(3,3)1.6/1105(13,3)1.6/2206(32,3)1.6 2201 29,3
1.7/1251(24,3)1.7/2216(34,3)1.8/1201(17,3)1.9/2211(29,2)2.3/2211(30,1)2.4/1256(
25,3)2.4/1200(4,3)2.7////1201(19,3)2.2/2201(27,3)2.2/1250(21,1)3.3/1205(19,2)2/226
6(36,2)3.5/2216(33,3)3.5/1251(23,3)3.8/2211(29,1)3.8/2211(30,3)3.9/1155(15,1)3.9/1200(
1,1)1/1100(2,1)1/2200(7,1)1/2200(8,1)1/1200(4,3)1/1155(16,3)1/2266(35,2)1.2/1250
(22,3)1.2/2206(31,3)1.3/1105(14,3)1.4/1205(20,3)1.4/1256(25,3)1.4/1201(17,3)1.7/
2201(25,3)1.9/2216(34,3)2.1/1251(24,3)2.2/1200(3,3)2.3/2206(32,3)2.4/1105(13,3)2
.5/1256(26,3)2.5/

56 1051.1 279 1201(17,2)1.8/1206(20,2)1/2216(34,3)1.2/2206(32,3)1.6/1256(26,3)1.
8/1200(3,3)1.9/1105(13,3)2////1200(3,3)1.1/2206(32,3)1.2/1105(13,3)1.3/1256(26,3)1.4
/2201(20,1)1.4/1251(24,3)1.6/1201(17,2)1.8/2216(34,3)1.8/1206(20,2)1.2/1250(22,1)2.3
/2266(35,2)2.6/

55 1051.1 327.2 1201(17,1)1.3/2216(34,2)1.3/2206(32,2)1.4/1200(3,1)1.5/1105(13,
2)1.5/1256(26,2)1.6/1206(20,1)1.9/1251(24,2)1.8/2201(26,2)2.2////1105(13,1)2.2/2
00(9,1)2.6/1256(26,2)2.7/2216(34,1)2.7/2206(32,2)2.8/1206(20,1)1.4/2266(35,1)1.6/120
1(17,1)1.7/1251(24,1)2/2201(20,1)2.7/

54 1051.1 333 2211(30,3)1.4/2211(29,2)1.5/1201(18,3)1.6/1100(1,3)1.6/1100(2,3)1.6/12
06(19,3)1.8/1206(20,3)1/1201(17,3)1.3/2216(33,3)1.4/2266(35,3)1.7/2216(34,3)1.9/2
266(36,3)2/2201(27,3)2/2201(26,3)2/1200(4,3)2.1/2200(7,3)2.1/2200(6,3)2.1/2206(3
1,3)2.2/1251(24,3)2.4/1200(3,3)2.4/2206(32,3)2.5/1105(14,3)2.5/1105(13,3)2.6/125
5(25,3)2.8////1250(21,2)0/1206(19,3)1.1/2211(29,1)3.3/2266(36,2)3.3/2211(30,3)1.4/11
55(15,1)1.5/1100(1,1)1.6/1100(2,1)1.6/2200(7,1)1.6/2200(8,1)1.6/1155(16,3)1.7/1201(18,
3)1.8/2266(35,3)1.5/1250(22,3)1/1206(20,3)1.3/2201(27,3)1.5/1201(17,3)1.8/2216(33,
3)2/2201(28,3)2.2/1251(23,3)2.4/2216(34,3)2.5/1251(24,3)2.7/1200(4,3)2.8/1200(3,
3)2.9/

51 1051.1 392.6 2266(35,2)1.4/1100(1,1)1.9/1100(2,1)1.9/1206(20,3)1.2/1206(19,3)1.
3/2266(36,3)1.5/2211(29,3)1.6/2211(30,3)1.6/1201(17,3)1.7/1201(18,3)1.9/2216(34,
3)2/2200(7,3)2.6/2200(6,3)2.6////1206(20,3)0/2266(35,2)1.1/1250(22,2)1.1/2211(30,1
)1.4/1201(17,3)1.4/2211(29,3)1.5/1155(16,1)1.6/1100(1,1)1.8/1100(2,1)1.6/2200(7,1)1.6/2
200(6,1)1.8/1155(15,3)1.8/2201(28,3)1.8/2266(36,3)1.1/1250(21,3)1.1/2216(34,3)1.2/1
251(24,3)1.4/1206(19,3)1.6/1200(3,3)1.6/2206(32,3)1.8/1105(13,3)1.9/1256(26,3)1.
9/1201(16,3)2.2/2201(27,3)3/

52 1051.1 398 2211(30,1)1.3/2211(29,1)1.5/2200(7,3)1.8/2200(6,3)1.8/1250(22,3)1.9/12
01(17,3)1/1201(18,3)1/1100(1,3)1/1100(2,3)1/1250(21,3)1.1/2201(27,3)1.1/1206(20,
3)1.2/2201(28,3)1.2/1155(16,3)1.2/1155(15,3)1.3/2216(34,3)1.4/1206(19,3)1.4/1251
(24,3)1.4/2216(33,3)1.5/1200(3,3)1.6/1200(4,3)1.7/1251(23,3)1.7/2206(32,3)1.7/22
06(35,3)1.8/1105(13,3)1.8/2206(31,3)1.9/1256(25,3)2/1105(14,3)2/2266(36,3)2/1256
(26,3)2////2211(30,2)0/1155(15,1)0/1100(1,1)1.1/1100(2,1)1.1/2200(7,1)1.1/2200(6,1)
.1/2266(36,3)1.1/1250(21,3)1.2/1155(16,3)1.2/2211(29,1)1.2/2266(35,3)1.4/1250(22,3)1.4
/1206(19,3)1.5/1206(20,3)1.7/1201(18,3)1/1201(17,3)1.1/2201(26,3)1.4/2201(27,3)1.6
/2216(34,3)1.7/1251(24,3)1.8/1200(3,3)2/2216(33,3)2/2206(32,3)2.1/1105(13,3)2.2/
1256(26,3)2.2/1251(23,3)2.4/1200(4,3)2.0/

53 1051.1 407.2 1155(15,3)1.6/1155(16,3)1.6/1250(21,3)1.6/2200(7,1)1.6/2200(6,1)1.6/
1250(22,3)1.6/2211(29,1)1.6/2266(36,3)1.7/2266(35,3)1.7/2211(30,1)1.7/2201(27,3)1.8/2
06(19,3)1.8/1201(18,3)1.8/1100(1,3)1.8/1100(2,3)1.8/1251(23,3)1.9/1206(20,3)1.9/2216(3
3,3)1.8/1201(17,3)1/1200(4,3)1/2201(28,3)1/2206(31,3)1.1/1105(14,3)1.1/2216(34,3)
1.1/1251(24,3)1.1/1200(3,3)1.2/1256(25,3)1.2/2206(32,3)1.2/1105(13,3)1.2/1256(26
,3)1.3////2266(35,3)0/1250(22,3)0/2211(29,3)0/2211(30,1)0/1155(16,1)1.1/1100(1,1)
.1/1100(2,1)1.1/2200(7,1)1.1/2200(8,1)1.1/1155(15,3)1.1/1206(20,3)1.1/2266(36,3)1.2/12
50(21,3)1.2/1201(17,3)1.3/1206(19,3)1.4/2201(28,3)1.6/2216(34,3)1.6/1201(18,3)1.6/1251
(24,3)1.6/1200(3,3)1.7/2206(32,3)1.8/1105(13,3)1.8/1256(26,3)1.8/2201(27,3)1.6/2216(33
,3)1/1251(23,3)1.2/1200(4,3)1.3/2206(31,3)1.5/1105(14,3)1.5/1256(25,3)1.6/

54 1051.1 416.0 **

65 106.1 462.6 22(1(29,2).2/22(1(30,2).3/1100(1,3).6/1100(2,3).6/1206(20,3).9/120(1(16,3)1/120(1(17,3)1/1206(19,3)1.1/2216(34,3)1.7/2266(35,3)1.7/2216(33,3)1.6/220(1(28,3)1.8/2200(7,3)1.9/2200(8,3)1.9/2266(36,3)2.1/2220(1(27,3)2.1/1250(22,3)2.1/125(1(24,3)2.2/1200(3,3)2.2/2206(32,3)2.3/1105(13,3)2.4/1256(26,3)2.7////1100(1,1)0/1100(2,1)0/2200(7,1)0/2200(8,1)0/1155(15,3)0/1155(16,3).1/2221(1(30,2).2/2211(29,2).2/2266(36,3).3/1250(21,3).4/2266(35,3).4/1250(22,3).4/1205(20,3).8/1206(19,3).8/1201(17,3)1.3/1201(16,3)1.5/2201(28,3)1.8/2216(34,3)2.1/1251(24,3)2.3/2201(27,3)2.3/1200(3,3)2.5/2206(32,3)2.7/1105(13,3)2.8/1256(26,3)2.8/2216(33,3)2.9/

66 106.1 477.4 120(1(18,1).6/2216(33,2).7/1206(19,2).9/2206(31,3)1/1256(25,3)1.2/2266(36,3)1.2/1200(4,3)1.3/1105(14,3)1.3/2266(35,3)1.4/2221(1(30,3)1.5/1100(1,2)1.6/1100(2,2)1.6/2221(1(27,3)1.7/2221(1(29,1)1.7/1251(23,3)1.8/1206(20,3)1.8/2200(7,3)2.2/2200(8,3)2.2/1201(1(17,3)2.2/1250(21,3)2.2/1250(22,3)2.3/1155(15,3)2.3/1155(16,3)2.4/2216(34,3)2.5/2201(20,3)2.6/1251(24,3)2.7/1200(3,3)2.8/2206(32,3)2.8/////1105(14,3)0/1256(25,3).1/2206(31,3).1/1251(23,2).2/1200(4,3).3/2201(27,1).5/1201(18,2).8/2216(33,3).8/1206(19,2)1/1250(21,1).5/2266(36,2)1.7/2211(29,1)2/2211(30,3)2.1/1155(15,1)2.1/1100(1,1)2.2/1100(2,1)2.2/2200(7,1)2.2/2200(8,1)2.2/1155(16,3)2.2/2266(35,3)2.3/1250(22,3)2.3/1206(20,3)2.5/1201(17,3)2.6/

67 106.1 496 22(1(29,3).3/2211(30,2).5/1100(1,3).8/1100(2,3).8/1206(20,3).9/2(1(17,3)1.1/1206(19,3)1.3/1201(16,3)1.3/2266(35,3)1.5/2216(34,3)1.7/2200(7,3)1.7/2200(8,3)1.7/2201(28,3)1.7/1250(22,3)1.9/2266(36,3)1.9/1251(24,3)2.1/1250(21,3)2.1/1200(3,3)2.2/2201(27,3)2.3/2206(32,3)2.3/1105(13,3)2.4/1256(26,3)2.7////1250(22,2).1/2211(30,1)2/2266(35,3).2/1206(20,3).2/2211(29,3).3/1155(16,1).4/1100(1,1).6/1100(2,1).6/2200(7,1).6/2200(8,1).6/1155(15,3).6/1201(17,3).8/2266(36,3)1/1250(21,3)1/2201(28,3)1.3/1206(19,3)1.5/2216(34,3)1.6/1251(24,3)1.9/1200(3,3)2.1/1201(16,3)2.2/2206(32,3)2.3/1105(13,3)2.4/1256(26,3)2.4/

68 106.1 535.1 22(1(29,1).5/2211(30,3).6/1201(16,3).7/1206(19,3)1/1100(1,3)1.1/1100(2,3)1.1/2216(33,3)1.1/2201(27,3)1.2/2266(35,3)1.2/2200(7,3)1.2/2200(8,3)1.2/1250(21,3)1.3/2266(36,3)1.3/1250(22,3)1.3/1206(20,3)1.3/1155(15,3)1.5/1155(16,3)1.5/1200(4,3)1.5/1201(17,3)1.6/1251(23,3)1.6/2206(31,3)1.7/1105(14,3)1.8/1256(25,3)1.9/2201(28,3)2/2216(34,3)2.1/1251(24,3)2.3/1200(3,3)2.5/2206(32,3)2.6/1105(13,3)2.7/1256(26,3)2.9////1250(21,2).1/1206(19,3).1/2266(36,2).2/2211(29,1).3/2211(30,3).4/1155(15,1).5/1201(16,3).6/1100(1,1).6/1100(2,1).6/2200(7,1).6/2200(8,1).6/1155(16,3).7/2266(35,3).7/1250(22,3).9/1206(20,3)1.3/2201(27,3)1.3/2201(17,3).7/2216(33,3)1.6/2201(28,3)2.1/1251(23,3)2.1/2216(34,3)2.3/1251(24,3)2.5/1200(4,3)2.5/1200(3,3)2.7/2206(32,3)2.9/1105(13,3)2.9/2206(31,3)2.9/1256(26,3)2.9/

69 106.1 567.8 1100(1,1).4/1100(2,1).4/1206(19,2).6/1206(20,2).7/2266(35,2).9/120(1(17,3)1.1/120(1(18,3)1.1/2266(36,2)1.1/2216(34,3)1.2/2211(29,3)1.2/2211(30,3)1.2/2216(33,3)1.3/2206(32,3).4/1256(26,3)1.4/1200(3,3)1.4/1256(25,3)1.5/1105(13,3)1.5/2201(20,3)1.6/2206(31,3)1.6/1251(24,3)1.6/1200(4,3)1.7/1105(14,3)1.6/2201(27,3)1.8/2200(7,3)2/2200(8,3)2/1250(22,3)2.1/1251(23,3)2.1/1250(21,3)2.2////1250(21,1)0/2266(36,2).1/1201(18,3).1/1206(19,3).1/2211(29,1).3/2211(30,3).3/2201(27,3).4/1155(15,3).4/1100(1,1).4/1100(2,1).4/2200(7,1).4/2200(8,1).4/1155(16,3).4/2266(35,3).6/1250(22,3).6/2216(33,3).6/1206(20,3).7/1251(23,3).7/1201(17,3).8/1200(4,3).9/2201(28,3)1/2206(31,3)1/1105(14,3)1.1/2216(34,3)1.1/1256(25,3)1.1/1251(24,3)1.2/1200(3,3)1.3/2206(32,3)1.3/1105(13,3)1.4/1256(26,3)1.4/

70 106.1.1 586.5 1206(19,2).2/1100(1,1).3/1100(2,1).3/120(18,2).3/2216(33,3).4/1206(20,3).5/2266(36,2).5/2211(30,3).5/2266(36,3).5/2211(29,3).5/1255(26,3).6/2200(31,3).5/1201(17,3).5/1200(4,3).5/2216(34,3).7/1105(14,3).7/2201(27,3).0/2201(28,3).0/2206(32,3).0/1201(3,3).0/2200(7,3).0/2200(8,3).0/1251(23,3).0/1105(13,3).0/1251(24,3).0/1256(26,3).0/1250(22,3).0/1250(21,3).0/1155(16,3)//1155(15,3)//2201(27,3)0/1206(19,2).1/2216(33,3).1/120(18,3).1/1250(21,1).2/1251(23,3).2/2266(36,2).2/1200(4,3).3/2211(29,1).4/2211(30,3).4/1155(15,1).4/2206(31,3).4/1100(1,1).5/1100(2,1).5/2200(7,1).5/2200(8,1).5/1155(16,3).5/1105(14,3).5/1256(25,3).6/2266(35,3).6/1250(22,3).5/1206(20,3).6/1201(17,3).7/2201(20,3).8/2216(34,3).9/1251(24,3).9/1200(3,3)1/2206(32,3)1/1105(13,3)1/1256(26,3)1/

71 106.1.1 637.5 1250(21,2).7/1251(23,3).7/2201(27,2).7/1155(15,3).7/1155(16,3).8/2200(7,1).8/2200(8,1).8/2211(29,1).8/1250(22,3).8/1200(4,3)1/1105(14,3)1/2211(30,1).1/2206(31,3).1/2216(33,3)1.1/120(18,3).2/1256(25,3).3/1206(19,3).4/2266(36,3)1.4/1100(1,3).4/1100(2,3).4/2266(35,3).4/1206(20,3).6/1201(17,3).6/2201(28,3).7/1251(24,3).8/2216(34,3).9/1200(3,3)2/2206(32,3)2.1/1105(13,3)2.1/1256(26,3)2.2////120(18,3).2/2201(27,3).2/1250(21,1).3/1206(19,2).3/2266(36,2).4/2216(33,3).5/2211(29,1).7/1251(23,3).7/2211(30,3).8/1155(15,1).8/1100(1,1).9/1100(2,1).8/2200(7,1).9/2200(8,1).9/1155(16,3).9/1200(4,3).9/2266(35,3)1/1250(22,3)1/2206(31,3)1.1/1105(14,3)1.2/1206(20,3).2/1256(25,3).3/1201(17,3).5/2201(28,3).7/2216(34,3).8/1251(24,3).9/1200(3,3)2/2206(32,3)2.1/1105(13,3)2.2/1256(26,3)2.2/

72 106.1.1 720.0 1201(17,1).6/2216(34,2).7/1206(20,2).8/2206(32,2).9/1200(3,2).9/1105(13,2)2/1256(26,3)2.1/1251(24,2)2.3/2201(28,2)2.4////1256(26,2)0/1200(3,1).1/2206(32,2).1/1105(13,1).5/2216(34,2)1.1/1201(17,1).1/1251(24,1).4/2201(28,1)2.2/1206(20,1)2.4/2266(35,1)2.5/

73 106.1.1 750.4 1200(4,2).3/1251(23,2).3/1105(14,2).4/2201(27,2).5/2206(31,3).5/1256(25,3).5/2216(33,3).7/1250(21,3).8/2211(29,1).8/1201(18,2).8/1155(15,3).6/1155(16,3).8/2200(7,3).8/2200(8,3).8/1250(22,3).9/2211(30,1).9/1206(19,3)1/1100(1,3)1.1/1100(2,3)1.1/2266(36,3)1.1/2266(35,3)1.2/1206(20,3)1.2/1201(17,3)1.2/2201(28,3)1.2/1251(24,3)1.3/2216(34,3)1.3/1200(3,3)1.4/2206(32,3)1.4/1105(13,3)1.4/1256(26,3)1.5////2216(33,2)0/1201(18,1).1/1200(4,2).1/1251(23,1).3/1105(14,2).4/1256(25,3).4/2206(31,3).5/2201(27,1).7/1206(19,2).9/1250(21,1)1.1/2266(36,2)1.2/2211(29,1)1.3/2211(30,3)1.4/1155(15,1)1.4/1100(1,1)1.4/1100(2,1)1.4/2200(7,1)1.4/2200(8,1)1.4/1155(16,3)1.4/2266(35,3)1.5/1250(22,3)1.5/1206(20,3)1.6/1201(17,3)1.7/2201(28,3)1.8/2216(34,3)1.8/1251(24,3)1.9/1200(3,3)1.9/2206(32,3)2/1105(13,3)2/1256(26,3)2/

74 106.1.1 757.6 1201(17,3).3/2216(34,3).4/2206(32,3).5/1206(20,3).5/1200(3,3).8/2211(29,3).9/1105(13,3).9/2201(28,3).9/1256(25,3).9/1100(1,3)1/1100(2,3)1/1251(24,3)1.1/2211(30,2)1.1/1206(19,3)1.4/1201(18,3)1.4/2200(7,3)1.8/2200(8,3)1.8/2266(35,3)1.9/1250(22,3)1.9/2216(33,3)2/2201(27,3)2.1/2266(36,3)2.2/1200(4,3)2.4/2266(23,3)2.6////1250(22,1)0/1201(17,3).1/2266(35,2).1/1206(20,3).2/2201(26,3).4/2211(30,1).5/2211(29,3).6/1155(16,1).6/2216(34,3).6/1100(1,1).7/1100(2,1).7/2200(7,1).7/2200(8,1).7/1155(15,3).8/1251(24,3).8/1200(3,3).9/2266(36,3)1/1250(21,3)1/2206(32,3)1.1/1105(13,3)1.1/1256(26,3)1.1/1206(19,3)1.3/1201(18,3)1.7/2201(27,3)2.3/2216(33,3)2.7/1251(23,3)3/

75 106.1.1 763.5 1201(17,2).7/1206(20,2)1/2216(34,3)1/2206(32,3)1.6/1200(3,3)1.6/1100(1,3)1.8/1100(2,3)1.8/1250(26,3)2/1105(13,3)2/2211(29,3)2.2/2201(26,3)2.4/1251(24,3)2.5/2211(30,2)2.6////2216(34,3)0/1201(17,2)0/2201(26,2).2/1251(24,3).3/1206(19,2).3/1200(3,3).6/2206(32,3).8/1105(13,3)1/1256(26,3)1/1250(22,1).3/1.66(3K,2)1.6/2211(30,1)2.4/2211(29,3)2.6/1155(16,1)2.7/1100(1,1)2.8/1100(2,1)2.9/2200(7,1)2.9/2200(8,1)2.0/1155(15,3)3/

76 1061.1 821.5 1105(14,2).8/1200(4,1).8/125(23,2)/2206(31,2)/.2/1256(25,2)/.2/220(27,2)/.4/2216(33,2)/.4/120(18,1)/.4/1250(21,1)/.4/1155(15,3)/.7/1155(15,3)/.7/2200(7,1)/.7/2200(8,1)/.7/2211(29,1)/.7/1250(22,3)/.8/2266(36,3)/.8/22(1(30,3)/.8/1206(19,3)/.8/2266(35,3)/.8/1100(1,3)2/1100(2,3)2/1206(20,3)2./120(17,3)2.2/220(28,3)2.3/2216(34,3)2.4/125(24,3)2.4/1200(3,3)2.5/2206(32,3)2.5/1105(13,3)2.5/1256(25,3)2.6////1105(14,2)8/1200(4,2).3/2216(33,2).5/120(18,1).5/2206(31,2).5/125(23,1).8/1256(25,2).8/2200(27,1)1.3/1206(19,2)1./1250(21,1)1.8/2266(36,2)2/2211(29,1)2.1/2211(30,3)2.2/1155(15,1)2.2/1100(1,1)2.2/1100(2,1)2.2/2200(7,1)2.2/2200(8,1)2.2/1155(16,3)2.3/2266(35,3)2.3/1250(22,3)2.3/1206(20,3)2.4/120(17,3)2.6/220(28,3)2.7/2216(34,3)2.8/125(24,3)2.9/1200(3,3)2.9/2206(32,3)3/1105(13,3)3/1256(25,3)3/

77 1061.1 882.5 120(18,1).7/1200(4,2).7/1105(14,2).7/2216(33,2).7/2206(31,2).7/1256(25,2)1./125(23,2)1/2266(36,3)1.2/220(27,2)1.2/1206(19,2)1.2/2266(36,3)1.3/2211(29,1)1.4/1250(21,3)1.4/1155(15,3)1.4/2211(30,3)1.4/1155(16,3)1.4/2200(7,3)1.5/2200(8,3)1.6/1250(22,3)1.6/1100(1,3)1.6/1100(2,3)1.6/1206(20,3)1.7/120(17,3)1.8/220(28,3)1.9/2216(34,3)2/125(24,3)2/1200(3,3)2.3/2206(32,3)2.2/1105(13,3)2.2/1256(25,3)2.3////2216(33,2)8/120(18,1).1/1200(4,2).1/125(23,1).3/1105(14,2).5/1256(25,3).5/2206(31,3).5/220(27,1).8/1206(19,2)1./1250(21,1)1.4/2266(36,2)1.5/2211(29,1)1.6/2211(30,3)1.7/1155(15,1)1.7/1100(1,1)1.8/1100(2,1)1.8/2200(7,1)1.8/2200(8,1)1.8/1155(16,3)1.8/2266(35,3)1.8/1250(22,3)1.8/1206(20,3)2/120(17,3)2.1/220(28,3)2.2/2216(34,3)2.3/125(24,3)2.4/1200(3,3)2.4/2206(32,3)2.5/1105(13,3)2.5/1256(25,3)2.6/

78 1061.1 933.2 2216(31,2).8/1200(4,1).8/1105(14,2).8/120(18,1).8/2216(33,2).8/1256(25,2).9/2266(36,2).9/125(23,1).9/1206(19,2).9/1250(21,1)1/220(27,1)1/2266(35,3)1/1155(15,1)1/1155(16,3)1/2211(29,1)1/2200(7,1)1/2200(8,1)1/2211(30,3)1.1/1100(1,1)1.1/1100(2,1)1.1/1250(22,3)1.1/1206(20,3)1.1/120(17,3)1.2/220(28,3)1.2/2216(34,3)1.2/125(24,3)1.2/1200(3,3)1.3/2206(32,3)1.3/1105(13,3)1.3/1256(25,3)1.3////1200(4,2).1/1105(14,2).1/2216(33,2).1/120(18,1).1/125(23,1).3/2206(31,2).3/1256(25,3).3/220(27,1).5/1206(19,2).6/1250(21,1).7/2266(36,2).7/2211(29,1).8/2211(30,3).8/1155(15,1).8/1100(1,1).8/1100(2,1).8/2200(7,1).8/2200(8,1).8/1155(16,3).8/2266(35,3).8/1250(22,3).8/1206(20,3).8/120(17,3)1/220(28,3)1/2216(34,3)1/125(24,3)1.1/1200(3,3)1.1/2206(32,3)1.1/1105(13,3)1.1/1256(25,3)1.1/

79 1061.1 970.5 1155(16,3).8/1155(16,3).8/1250(21,1).9/2200(7,1).9/2200(8,1).9/1250(22,3).9/2211(29,1)1/2266(35,3)1/2211(30,1)1/2266(36,3)1/220(27,3)1.2/1206(19,3)1.2/1100(1,3)1.2/1100(2,3)1.2/120(18,3)1.2/1206(20,3)1.2/125(23,3)1.2/120(17,3)1.3/2216(33,3)1.3/220(28,3)1.3/1200(4,3)1.4/2216(34,3)1.4/125(24,3)1.4/2206(31,3)1.5/1105(14,3)1.5/1200(3,3)1.5/2206(32,3)1.5/1105(13,3)1.6/1256(25,3)1.6/1256(26,3)1.6////1250(22,2)8/2211(30,1)1/1206(20,3)1/2266(35,3)1/2211(29,3)1/1155(16,1).2/1100(1,1).2/1100(2,1).2/2200(7,1).2/2200(8,1).2/1155(15,3).2/120(17,3).3/2266(36,3).4/1250(21,3).4/220(28,3).5/1206(19,3).6/2216(34,3).6/125(24,3).7/1200(3,3).8/120(18,3).8/2206(32,3).8/1105(13,3).9/1256(26,3).9/220(27,3)1.2/2216(33,3)1.4/125(23,3)1.5/1200(4,3)1.6/2206(31,3)1.8/1105(14,3)2/1256(25,3)2.1/

80 1061.1 1015 220(27,2).4/125(23,3).5/1105(14,3).6/1200(4,3).6/1256(25,3).6/2200(7,3).6/2200(8,3).6/1250(21,3).6/1250(22,3).7/1155(16,3).7/1155(15,3).7/2206(31,3).7/2211(29,1).7/2211(30,1).7/2200(20,3).7/125(24,3).8/120(18,3).8/2216(33,3).8/1200(3,3).9/120(17,3).8/1105(13,3).9/2216(34,3).9/2206(32,3).9/1100(1,3)1/1100(2,3)1/1256(26,3)1/1206(20,3)1/1206(19,3)1/2266(36,3)1.3/2266(35,3)1.3////2206(31,3)8/1105(14,3)8/1256(25,3)8/125(23,2).1/1200(4,3).1/220(27,1).2/120(18,2).3/2216(33,3).3/1206(19,2).6/1250(21,3).6/2266(36,2).7/2211(29,1).8/2211(30,3).8/1155(16,1).8/1100(1,1).8/1100(2,1).8/2200(7,1).8/2200(8,1).8/1155(15,3).8/2266(35,3).8/1250(22,3).8/1206(20,3)1/120(17,3)1.1/2201(28,3)1.2/2216(34,3)1.3/125(24,3)1.3/1200(3,3)1.3/2206(32,3)1.4/1105(13,3)1.4/1256(26,3)1.4/

91 1061.1 1021.5 **

82 106.1 1045.5 22 11(29,2)1.4/22 11(30,2)1.4/1201(18,3)1.4/1201(17,3)1.5/1100(1
,3)1.6/1100(2,3)1.6/1256(25,3)1.7/1206(20,3)1.8/2216(34,3)1.8/2216(33,3)1.9/2201
(28,3)2/1206(19,3)2/1200(4,3)2.1/2206(31,3)2.2/1200(3,3)2.2/1251(24,3)2.3/1105(1
4,3)2.5////1201(18,3).2/1250(21,1).4/2201(27,3).4/1206(19,2).5/2266(36,2).6/2216
(33,3).8/2211(29,1)1.1/1251(23,3)1.2/2211(30,3)1.3/1155(15,1)1.3/1100(1,1)1.5/11
00(2,1)1.5/2200(7,1)1.5/2200(8,1)1.5/1155(16,3)1.5/1200(4,3)1.5/2266(35,3)1.7/12
50(22,3)1.7/2206(31,3)2/1206(20,3)2.1/1105(14,3)2.1/1256(25,3)2.2/1201(17,3)2.4/
2201(28,3)2.8/

83 106.1 1174 2266(35,3).5/2266(36,3).7/1206(19,3).8/1100(1,3)1.1/1100(2,3)1.1
/2211(30,3)1.1/1201(18,3)1.2/2211(29,2)1.2/1206(20,3)1.3/2216(33,3)1.7/1201(17,3
)1.8/2200(7,3)2.3/2200(8,3)2.3/2201(27,3)2.4/2216(34,3)2.4/1250(22,3)2.5/1250(21
,3)2.6/1251(23,3)3////2211(30,2)0/1155(15,1).1/2266(36,3).2/1250(21,3).2/1100(1,
1).2/1100(2,1).2/2200(7,1).2/2200(8,1).2/2211(29,1).2/1155(16,3).2/2266(35,3).5/
1250(22,3).5/1206(19,3).6/1206(20,3).9/1201(18,3)1.3/1201(17,3)1.4/2201(28,3)1.8
/2201(27,3)2.1/2216(34,3)2.2/1251(24,3)2.4/1200(3,3)2.6/2216(33,3)2.6/2206(32,3)
2.8/1105(13,3)2.9/1256(26,3)2.9/

84 106.1 1241.5 **

* Refers to the cases displayed in (a), plus all the other transitions in prompt coincidence with the thee gates, not shown in (a).

** Due to the impossibility of placing the 416.0, 1021.5 and 1241.5 keV transitions on the level scheme(see section 4.1), it was not deemed necessary to obtain any multipolarity values for them.

†† Absence of underlinings indicates deviations in excess of 3.5 experimental errors for multipolarities implied by the other two gates. In these cases, see (c) starting on the next page, where the multipolarities chosen are listed for all the three gates with their corresponding(even if in excess of 3.5 experimental errors) relative deviations.

(All angles) refers to (0°, 90°), (0°, 0°) and (90°,90°) formats.
(0°& 90°) refers to (0°,90°) and (90°, 0°) .
In each of the cases above(i.e. for a given gate and transition), the comparisons to theory from the (all angles) formats are separated from the (0° 90°) batch by //// .("all angles" coming first) Absence of entries before or after //// indicates deviations from theory were larger than 3.5 experimental errors for all possible multipolarity combinations in the respective angular correlation formats, or no data were available.

(c)Summary table of the transition multipolarities chosen in (b). Each entry contains the multipolarities and their degree of stretchedness(see Table 5.1.5 for the meaning of "stretchedness" codes) of the corresponding gate and transition(in this particular order), as well as the F.O.M.'s obtained for each of the four HWHM's(in parantheses) used in calculations(HWHM = 0, 4, 6 and infinite, respectively). In each entry, the first row corresponds to all three cells, while the second to the first cell only(i.e. 0° - 90°). See captions of Table 5.1.4(a) and (b) and of Table 5.1.5 .

Gate(keV)	1061.1	763.4	333.1
E_γ(keV)			
114.2	1100(9.8,9.8,9.8,2.3)	1100(9.8,2.0,1.9,9.8)	1100(0.6,0.3,0.4,0.9)
	1100(1.0,1.0,1.0,1.0)	1100(1.2,1.2,1.2,1.2)	1100(0.5,0.5,0.5,0.5)
279.0	1100(9.8,9.8,9.8,9.8)	1100(1.2,1.3,1.7,9.8)	1100(2.1,2.5,9.8,9.8)
	1100(4.0,4.0,4.0,4.0)	1100(2.0,2.0,2.0,2.0)	1100(2.8,2.8,2.8,2.8)
***	1105(9.8,9.8,9.8,9.8)	1105(9.8,9.8,9.8,2.4)	1105(9.8,9.8,9.8,9.8)
***	1105(9.8,9.8,9.8,4.0)	1105(9.8,9.8,7.8,2.0)	1105(9.8,9.8,9.1,2.8)
327.2	1206(1.9,1.9,9.8,9.8)	*	*
	1206(1.4,3.2,4.3,5.1)	*	*
333.1	1100(2.2,1.3,0.6,6.8)	1100(1.9,1.1,1.0,1.9)	**
	1100(0.6,0.6,0.6,0.6)	1100(1.5,1.5,1.5,1.5)	**

352.5'	1100(0.9,1.0,1.3,1.9)	1100(9.8,9.8,9.8,9.8)	1100(0.5,1.1,1.6,2.4)
	1100(0.8,0.8,0.8,0.8)	1100(3.9,3.9,3.9,3.9)	1100(0.3,0.3,0.3,0.3)
361.6	**	1100(0.9,0.9,0.9,1.1)	1100(1.7,1.7,1.9,9.8)
	**	1100(0.8,0.8,0.8,0.8)	1100(1.1,1.1,1.1,1.1)
***	**	1200(2.3,1.4,1.0,1.2)	1200(9.8,9.8,9.8,2.0)
***	**	1200(3.5,1.7,0.5,0.8)	1200(8.3,5.3,3.4,1.1)
398.0	1201(9.8,1,7,1.0,0.2)	1201(1.9,1.5,1.4,1.3)	1201(1.4,0.5,0.4,0.9)
	1201(4.7,2.1,1.0,0.1)	1201(0.6,0.6,1.1,1.6)	1201(1.7,0.0,0.6,1.3)
407.3	1200(9.8,1.4,1.0,0.9)	1200(9.8,9.8,9.8,2.0)	1200(1.8,1.0,0.6,0.6)
	1200(4.0,2.4,1.3,1.0)	1200(7.4,4.9,3.2,1.2)	1200(3.0,1.6,0.7,0.3)
462.7	1200(9.8,9.8,9.8,0.8)	1200(9.8,2.3,0.9,1.8)	1200(2.0,0.8,1.3,2.6)
	1200(9.9,7.1,3.8,0.0)	1200(7.0,3.4,1.0,1.9)	1200(3.0,0.5,1.1,3.0)
***	1201(9.8,2.0,1.0,0.5)	1201(2.0,0.5,0.7,1.5)	1201(0.6,1.3,1.8,2.3)
***	1201(6.4,[illegible] 1.5,0.0)	1201(2.9,0.3,0.8,1.9)	1201(0.2,1.6,2.3,3.0)
477.3	1200(9.8,1.6,1.3,2.0)	1200(9.8,9.8,9.8,9.8)	1200(1.0,0.7,0.8,1.2)
	1200(3.7,1.3,0.3,2.2)	1200(5.4,2.9,1.3,0.7)	1200(0.0,0.4,0.3,1.2)
491.0	**	1200(0.9,0.6,0.9,1.5)	1200(1.2,0.4,0.7,1.6)
	**	1200(1.5,0.3,0.6,1.5)	1200(2.0,0.5,0.6,1.8)

,0.8,0.6) 1100(1.5,0.9,0.6,1.2) 1100(1.0,1.0,1.2,2.1)
,0.6,0.6) 1100(0.1,0.1,0.1,0.1) 1100(0.9,0.9,0.9,0.9)

,9.8,1.1) 1105(9.8,9.8,9.8,1.6) 1105(9.8,9.8,9.8,2.1)
,5.5,0.6) 1105(9.8,8.3,4.3,0.1) 1105(9.8,6.5,3.0,0.9)

,0.7,0.9) 1201(0.8,1.7,2.0,2.5) 1201(1.4,0.7,0.8,1.1)
,0.6,0.6) 1201(0.9,2.2,2.7,3.2) 1201(2.3,0.5,0.2,0.9)

1201(1.0,1.2,1.3,1.4) 1201(0.6,0.6,0.7,0.9)
1201(1.2,1.5,1.6,1.8) 1201(0.9,0.1,0.2,0.6)

1200(0.8,1.0,1.2,1.5) 1200(1.4,0.8,0.7,1.0)
1200(0.7,1.1,1.4,1.8) 1200(2.3,1.1,0.3,0.6)

,1.1,1.3) 1201(9.8,9.8,2.0,1.5) 1201(1.6,1.1,1.0,1.1)
,0.1,0.4) 1201(6.5,4.1,3.2,2.2) 1201(2.1,1.1,0.7,0.2)

,0.3,0.6) 1201(1.1,0.8,0.8,0.9) **
,0.1,0.5) 1201(0.2,0.5,0.7,1.0) **

,1.2,1.2) 1201(0.2,0.7,1.0,1.4) 1201(2.0,1.9,1.9,2.0)
,0.2,0.9) 1201(0.2,0.9,1.2,1.8) 1201(0.8,2.1,2.6,3.1)

,9.8,9.8) 1100(0.6,0.2,0.2,0.7) 1100(0.9,0.6,0.3,0.2)
,4.8,4.8) 1100(0.2,012,0.2,0.2) 1100(0.2,0.2,0.2,0.2)

750.5	1200(0.8,0.3,0.5,1.0)	1200(1.5,0.9,0.7,0.9)	1200(1.2,0.6,0.5,0.6)
	1200(1.1,0.1,0.6,1.4)	1200(2.6,1.4,0.6,0.4)	1200(2.0,1.0,0.4,0.3)
757.7	1200(9.8,9.8,2.4,0.7)	1200(9.8,9.8,2.1,1.2)	1200(9.8,9.8,9.8,9.8)
	1200(8.8,5.5,3.3,0.7)	1200(5.8,3.3,1.6,0.4)	1200(8.5,5.1,2.9,0.3)
763.4	1100(2.3,1.8,1.9,9.8)	**	1100(1.6,1.4,1.4,0.7)
	1100(2.9,2.9,2.9,2.9)	**	1100(1.1,1.1,1.1,1.1)
820.5+	1200(0.9,1.0,1.4,2.1)	1200(1.0,0.8,1.1,1.6)	1200(0.9,0.4,0.4,1.0)
822.3	1200(1.0,0.3,1.2,2.2)	1200(0.8,0.3,1.0,1.9)	1200(1.0,0.0,1.7,1.5)
882.5	1200(1.0,0.7,1.1,1.7)	1200(0.6,1.1,1.5,2.0)	1200(0.9,0.4,0.5,1.1)
	1200(1.5,0.1,0.7,1.8)	1200(0.7,1.5,2.0,2.6)	1200(1.8,0.2,0.9,1.7)
933.1	1200(0.8,0.9,1.0,1.1)	1200(9.8,9.8,1.6,0.4)	1200(0.4,0.3,0.5,0.8)
	1200(0.5,0.1,0.4,0.8)	1200(6.2,3.6,1.9,0.0)	1200(0.4,0.2,0.5,0.9)
970.7	1200(9.8,1.9,1.4,1.3)	1200(0.7,0.8,0.9,1.1)	1200(1.8,1.3,1.0,0.6)
	1200(5.0,3.1,1.8,0.2)	1200(0.2,0.3,0.6,1.0)	1200(2.2,1.4,0.8,0.2)
1014.9	1200(1.4,0.9,0.6,0.6)	1200(0.4,0.4,0.5,0.6)	no values due to
	1200(1.5,0.5,0.1,0.9)	1200(0.0,0.2,0.4,0.5)	poor statistics
1045.5	1200(9.8,9.8,2.1,0.9)	1200(9.8,1.7,1.1,2.3)	1200(9.8,1.5,0.7,1.9)
	1200(8.2,4.2,1.6,1.5)	1200(5.9,2.6,0.4,2.2)	1200(5.4,2.4,0.4,1.9)

***	1201(9.8,2.2,1.4,1.2)	1201(1.4,0.9,1.4,2.0)	1201(1.4,0.6,1.0,1.6)
***	1201(3.7,0.9,0.2,1.5)	1201(2.1,0.2,1.2,2.2)	1201(1.9,0.2,1.0,1.9)
1061.1	**	1100(1.7,1.6,1.8,2.3)	1100(2.8,2.0,1.6,1.4)
	**	1100(2.5,2.5,2.5,2.5)	1100(2.4,2.4,2.4,2.4)
***	**	1105(9.8,9.8,9.8,2.4)	1105(9.8,9.8,9.8,1.6)
***	**	1105(7.5,3.1,0.5,2.5)	1105(9.8,9.8,8.1,2.4)
1170.5*	1100(1.5,1.2,1.1,1.4)	1100(1.3,0.6,0.4,1.4)	1100(2.0,1.7,1.6,1.9)
1172.7	1100(0.2,0.2,0.2,0.2)	1100(0.1,0.1,0.1,0.1)	1100(2.4,2.4,2.4,2.4)
1932.1	**	1300(2.2,1.2,0.6,0.6)	1300(0.4,0.4,0.5,0.6)
	**	1300(3.1,1.6,0.5,0.6)	1300(0.1,0.2,0.4,0.6)
***	**	1200(1.1,0.6,0.3,0.6)	1200(0.4,0.5,0.6,0.6)
***	**	1200(1.6,0.7,0.1,0.6)	1200(0.2,0.4,0.5,0.6)

* Not in coincidence with the respective gate(see Fig. 4.1.1). Since only the information from one gate was available, which in turn has rather high F.O.M.'s, it was decided not to assign any multipolarity to the 327.2 keV transition, hence no spin to the level from which it de-excites(see fig. 4.1.1).

** Not in coincidence with the respective gate(see Fig. 4.1.1).

*** Other possible choices for the 1061.1,495.8, 1045.5, 462.7, 279.0, 361.6, 559.4 and 1932.1 keV transitions with closest F.O.M.'s to the ones corresponding to the actual choices. See text for discussion.

' Represents both 352.5 keV transitions(see Fig. 4.1.1).

Table 5.1.5

(a) Angular correlation calculations(Draper, 1984, private communication;see text) for the (90°, 0°), (0°, 90°), (0°, 0°), (90°, 90°, 90°) and (90°, 90°, 0°) formats(the last two formats refering to the (90°, 90°) format for ϕ = 90° and 0°, respectively). The actual angular correlations(the W's) are equal to the entries below. The first two digits in the first column(λ_1 and λ_2) refer to the multipolarities carried by the first and second γ-rays involved(see text), respectively. The last two digits in the first column(λ_1^n and λ^n refer to the non-stretchedness of λ_1 and λ_2, respectively, as follows: values of 0, 1, or 2 refer to $\lambda - \Delta I$ (thus 0 indicates stretched) while values of 5 and 6 refer to $\Delta I = 0$ for $\lambda = 1$ (dipoles) and $\lambda = 2$(quadrupoles), respectively. Values of 3 and 4 are not used, while calculations for $\Delta I = 0$ for $\lambda = 3$(octupoles) were not performed due to unlikeliness of this occurence. Calculations described above were performed for the m-states distributions HWHM = 0, 4, 6 and infinity.

	HWHM = 0						HWHM = 4			
$\lambda_1\lambda_2\lambda_1^n\lambda^n$	(90°,0°)	(0°,90°)	(0°,0°)	(90°,90°,90°)	(90°,90°,0°)	(90°,0°)	(0°,90°)	(0°,0°)	(90°,90°,90°)	(90°,90°,0°)
1100	.812	.812	.509	1.233	1.390	.877	.877	.646	1.150	1.274
1200	1.416	.522	.802	.969	.691	1.356	.675	.978	1.015	.818
2100	.522	1.416	.802	.969	.691	.675	1.356	.978	1.015	.818
1300	1.955	.499	1.210	.972	.633	1.677	.617	1.196	.985	.687
3100	.499	1.955	1.210	.972	.633	.617	1.677	1.196	.985	.687
2200	.905	.905	1.536	.303	.803	1.024	1.024	1.519	.557	.872
2300	1.238	.067	2.114	.199	.794	1.252	.932	1.079	.403	.875

3200	.867	1.230	2.114	.199	.794	.932	1.252	1.079	.403	.875
3300	1.193	1.193	2.424	.127	.893	1.139	1.139	2.345	.235	.953
1105	1.711	.539	1.054	.995	.720	1.480	.689	1.061	1.016	.905
1150	.539	1.711	1.070	1.018	.693	.670	1.485	1.059	1.036	.767
1155	1.115	1.135	2.230	.285	.849	1.084	1.090	1.041	.467	.930
1201	1.682	.071	1.003	1.310	1.527	1.227	.068	.878	1.156	1.251
2110	.910	1.653	1.036	1.260	1.580	.871	1.213	.890	1.112	1.309
1206	.053	.679	.073	1.078	1.076	.620	.037	.480	1.111	1.188
2160	.694	.020	.012	1.050	1.054	.861	.579	.513	1.091	1.179
1250	.932	1.109	1.066	.267	.842	1.007	1.108	1.669	.494	.923
2105	1.069	.942	1.032	.324	.789	1.105	1.020	1.649	.537	.866
1251	1.050	1.046	2.101	1.145	.701	.880	1.493	1.521	1.005	.774
2115	1.020	1.097	2.147	1.233	.690	1.402	.929	1.466	1.072	.730
1256	.083	1.420	.127	.711	.717	.529	1.400	.606	.948	.795
2165	1.352	.013	.025	.724	.730	1.359	.619	.632	.963	.810
2201	1.013	1.589	1.763	1.013	.651	.921	1.337	1.375	.945	.801
2210	1.561	1.064	1.757	1.156	.587	1.353	.937	1.353	1.028	.697
2211	1.677	1.774	2.043	1.495	1.921	1.235	1.200	1.214	1.246	1.453
2206	.125	1.189	.159	.752	.760	.516	1.289	.717	.968	.849
2260	1.174	.013	.021	.030	.845	1.276	.530	.654	1.045	.930
2216	.252	1.383	.149	.985	.978	.601	1.160	.672	.950	1.008
2261	1.186	.021	.024	.735	.730	1.072	.523	.434	.847	.841
2266	.259	.016	.001	1.365	1.365	.723	.631	.631	1.349	1.496
1301	1.733	.532	1.028	.952	.697	1.275	.723	.918	1.045	.927
3110	.554	1.704	1.061	.862	.760	.732	1.229	.967	.971	1.009
1350	1.274	1.053	2.548	.170	.083	1.211	1.000	2.087	.328	.969
3105	1.030	1.303	2.514	.260	.812	1.009	1.256	2.038	.403	.887
1351	1.062	1.139	2.125	.320	.019	.923	1.203	1.555	.639	.886
3115	1.010	1.133	2.203	.505	.662	1.150	.996	1.434	.793	.728
2301	1.041	.912	1.033	.337	.024	.974	1.094	1.447	.659	.862
3210	.922	1.009	1.840	.556	.714	1.108	1.011	1.377	.823	.753
2310	2.111	1.015	2.464	1.282	.591	1.681	.050	1.651	1.087	.632
3201	1.004	2.063	2.449	1.064	.701	.944	1.644	1.721	.923	.741
2311	1.676	1.083	2.094	1.116	.596	1.277	1.004	1.267	1.039	.816
3211	.843	1.816	2.120	.705	.614	.902	1.179	1.143	.078	.931
2360	1.561	.012	.025	.564	.572	1.516	.489	.670	.886	.652
3206	.118	1.649	.280	.666	.613	.450	1.589	.897	.888	.699
2361	1.145	.013	.024	1.017	1.023	1.140	.577	.527	1.089	1.069
3216	.357	1.430	.191	.941	.910	.577	1.224	.894	1.026	1.021
3301	1.070	1.236	2.508	.221	.732	.904	1.328	1.032	.514	.834
3310	1.201	1.043	2.543	.370	.587	1.348	.924	1.593	.734	.633
3311	.793	1.097	2.205	.650	.871	1.042	1.073	1.257	.042	.847

Repeat of above for

	HWHM = 6					HWHM = infinity				
1100	.917	.917	.788	1.084	1.188	.975	.975	1.050	.875	1.050
1200	1.250	.009	.987	1.029	.871	1.036	1.036	.929	1.036	.929
2100	.009	1.250	.987	1.029	.871	1.036	1.036	.929	1.036	.929
1300	1.438	.788	1.093	1.012	.757	1.062	1.062	.875	1.062	.875
3100	.788	1.438	1.093	1.012	.757	1.063	1.063	.875	1.063	.875
2200	1.020	1.020	1.388	.717	.962	.952	.952	1.111	.952	1.111
2300	1.143	.948	1.609	.550	.975	.909	.909	1.174	.909	1.174
3200	.948	1.143	1.609	.550	.975	.909	.909	1.174	.909	1.174
3300	1.044	1.044	1.815	.438	1.067	.944	.944	1.316	.944	1.316
1105	1.312	.000	1.022	1.027	.850	1.042	1.042	.815	1.042	.815
1150	.015	1.525	1.005	1.045	.815	1.057	1.057	.885	1.057	.885
1155	1.026	1.034	1.586	.625	1.022	.901	.901	1.199	.901	1.199
1201	1.090	.097	.078	1.081	1.139	.893	.893	1.014	.893	1.014
2110	.608	1.071	.905	1.046	1.192	.970	.970	1.060	.970	1.060
1206	.013	.912	.740	1.075	1.165	.971	.971	1.059	.971	1.059
2160	.925	.702	.700	1.050	1.169	.960	.960	1.080	.960	1.080
1250	.918	1.061	1.481	.657	1.010	.918	.918	1.164	.918	1.164
2105	1.060	1.016	1.454	.592	.955	.940	.940	1.119	.940	1.119
1251	.880	1.300	1.275	.903	.035	1.019	1.019	.963	1.019	.963
2115	1.304	.822	1.204	1.036	.706	1.051	1.051	.899	1.051	.899

1250	.700	1.290	.014	1.027	.036	1.069	1.069	.002	1.069	.002	
2105	1.260	.700	.706	1.030	.047	1.089	1.069	.062	1.069	.062	
2201	.900	1.200	1.191	.949	.057	.999	.999	.957	.999	.957	
2210	1.228	.926	1.141	1.005	.755	1.025	1.025	.069	1.025	.069	
2211	1.193	1.068	1.002	1.130	1.299	1.044	1.044	1.156	1.044	1.156	
2206	.705	1.233	.086	1.031	.900	1.052	1.052	.047	1.052	.947	
2260	1.236	.805	.849	1.095	.000	1.089	1.089	.972	1.089	.972	
2216	.737	1.030	.774	.937	.974	.905	.905	.911	.905	.911	
2261	.907	.706	.679	.885	.024	.887	.887	.760	.887	.760	
2266	.915	.071	1.016	1.250	1.503	1.069	1.069	1.400	1.069	1.400	
1301	1.167	.030	.935	1.044	.957	1.019	1.019	.963	1.019	.963	
3110	.827	1.119	1.003	.901	1.042	.977	.977	1.047	.977	1.047	
1350	1.000	.961	1.785	.513	1.075	.056	.056	1.287	.056	1.287	
3105	.973	1.138	1.697	.575	.990	.895	.899	1.203	.890	1.203	
1351	.940	1.129	1.354	.773	.964	.961	.961	1.070	.961	1.070	
3115	1.156	1.010	1.210	.890	.796	1.039	1.039	.922	1.039	.922	
2301	.970	1.002	1.301	.793	.941	.972	.972	1.065	.972	1.065	
3210	1.111	1.030	1.204	.917	.825	1.039	1.039	.949	1.039	.949	
2310	1.440	.885	1.302	1.049	.706	1.083	1.083	.073	1.083	.073	
3201	.856	1.300	1.399	.924	.022	1.016	1.016	.909	1.016	.909	
2311	1.165	.960	1.099	1.014	.050	1.011	1.011	.928	1.011	.926	
3211	.967	1.076	1.025	.923	.953	.978	.978	.966	.978	.966	
2360	1.368	.762	.771	1.003	.705	1.004	1.004	.759	1.004	.759	
3206	.734	1.403	.946	.977	.757	1.064	1.064	.050	1.064	.050	
2361	1.120	.019	.759	1.094	1.068	1.049	1.049	1.004	1.049	1.004	
3216	.759	1.140	1.033	1.024	1.077	.992	.992	1.103	.992	1.103	
3301	.917	1.203	1.530	.679	.920	.942	.942	1.112	.942	1.112	
3310	1.267	.901	1.268	.070	.706	1.059	1.059	.067	1.059	.067	
3311	1.042	1.051	1.152	.916	.914	1.013	1.013	1.001	1.013	1.001	

(b) Ratios of the numbers in (a) to the (90°, 0°) and (0°, 90°) formats, as explained below, for each row of the following table. The four digits in the first column have the same meaning as in (a) .

```
THEORY RATIOS A9(1:3),A10(1:3),B9(1:3),B10(1:3) PRINTED NEXT.  A9-D9 ARE NORM'D
TO (90,0); A10-D10 TO (0,90).  (1:3)=(90LB),(0,0),(90,90,(.0+90L.Z+0)↑
A,B,C,D ARE MMMM=0,4,8,INFINITY.
```

1100	1.00	.63	1.67	1.00	.63	1.67	1.00	.74	1.42	1.00	.74	1.42
1200	.37	.62	.63	2.71	1.69	1.43	.59	.72	.63	2.01	1.45	1.27
2100	2.71	1.69	1.43	.37	.62	.53	2.01	1.45	1.27	.50	.72	.63
1300	.25	.82	.36	3.93	2.43	1.41	.37	.71	.45	2.72	1.94	1.21
3100	3.93	2.43	1.41	.25	.62	.36	2.72	1.94	1.21	.37	.71	.45
2200	1.00	1.70	.70	1.00	1.70	.70	1.00	1.40	.79	1.00	1.40	.79
2300	.70	1.71	.55	1.43	2.44	.78	.74	1.50	.62	1.34	2.02	.84
3200	1.43	2.44	.78	.70	1.71	.55	1.34	2.02	.84	.74	1.50	.62
3300	1.00	2.45	.61	1.00	2.45	.61	1.00	2.06	.71	1.00	2.06	.71
1105	.32	.82	.46	3.17	1.96	1.45	.45	.72	.57	2.21	1.59	1.27
1150	3.17	2.00	1.41	.32	.63	.44	2.20	1.56	1.21	.46	.71	.55
1155	1.02	2.00	.66	.00	1.00	.65	1.01	1.70	.77	.99	1.60	.76
1201	.62	.00	.09	1.91	1.15	1.71	.71	.72	1.00	1.41	1.01	1.42
2110	1.02	1.14	1.67	.65	.63	.92	1.39	1.03	1.40	.72	.74	1.05
1205	12.01	1.30	20.31	.00	.11	1.59	1.35	.77	1.09	.74	.57	1.40
2150	.03	.02	1.52	34.70	.60	52.74	.67	.60	1.35	1.49	.09	2.01
1250	1.19	2.00	.78	.04	1.50	.65	1.10	1.65	.03	.91	1.51	.76
2105	.00	1.71	.55	1.13	1.94	.74	.92	1.49	.72	1.00	1.62	.70
1251	1.76	2.00	.76	.57	1.14	.43	1.70	1.73	.93	.59	1.02	.55
2115	.66	1.17	.44	1.87	1.96	.73	.63	.99	.64	1.60	1.50	.07
1256	22.07	2.02	11.36	.04	.09	.60	2.86	1.30	1.66	.30	.49	.59

2185	.01	.02	.54	.	1.92	56.06	.30	.47	.62	2.62	1.22	1.62
2201	1.49	1.74	.71	.67	1.17	.40	1.45	1.49	.90	.69	1.03	.62
2310	.89	1.16	.45	1.47	1.69	.66	.69	1.00	.56	1.44	1.44	.01
2211	1.06	1.22	1.09	.95	1.15	1.03	.97	.98	1.14	1.03	1.01	1.10
2206	9.61	1.27	8.07	.11	.13	.84	2.50	1.39	1.69	.40	.56	.60
2260	.01	.02	.72	90.31	1.62	64.09	.42	.61	.75	2.37	1.22	1.77
2218	5.49	.69	3.89	.10	.11	.71	1.93	1.12	1.66	.52	.58	.86
2261	.02	.02	.62	56.40	1.14	34.01	.49	.40	.79	2.05	.03	1.61
2268	.06	.00	5.27	18.19	.06	05.31	.87	.87	2.03	1.15	1.00	2.32
1301	.31	.59	.43	3.26	1.93	1.41	.67	.72	.75	1.76	1.27	1.31
3110	3.08	1.92	1.42	.33	.62	.48	1.60	1.32	1.37	.60	.79	.01
1320	.83	2.00	.50	1.21	2.42	.70	.83	1.72	.69	1.20	2.07	.83
3105	1.27	2.44	.80	.79	1.93	.54	1.26	2.04	.79	.80	1.62	.63
1351	1.07	2.00	.60	.93	1.07	.63	1.30	1.68	.91	.77	1.29	.70
3115	1.11	2.16	.62	.90	1.94	.56	.84	1.21	.62	1.19	1.44	.74
2301	.80	1.78	.70	1.14	2.01	.00	1.12	1.49	.84	.89	1.32	.75
3210	1.10	2.00	.74	.05	1.70	.63	.91	1.24	.69	1.10	1.36	.76
2310	.49	1.17	.35	2.00	2.43	.72	.61	.98	.43	1.96	1.92	.84
3201	2.[illegible]	2.44	.77	.49	1.19	.37	3.95	2.04	.92	.51	1.05	.47
2311	.65	1.25	.42	1.55	1.93	.85	.79	.99	.67	1.27	1.26	.86
3211	2.15	2.51	.75	.46	1.17	.35	1.20	1.16	.94	.03	.97	.78
3360	.01	.02	.37	.	2.42	47.53	.32	.44	.40	3.10	1.37	1.43
3295	13.97	2.37	5.28	.07	.17	.38	3.24	1.01	1.48	.31	.56	.46
2261	.01	.02	.89	88.08	1.85	78.80	.51	.46	.94	1.90	.91	1.86
3218	4.01	.54	2.57	.25	.13	.84	2.12	1.55	1.77	.47	.73	.03
3301	1.15	2.40	.58	.87	2.09	.51	1.47	2.03	.85	.68	1.38	.58
3310	.07	2.12	.44	1.15	2.44	.51	.69	1.10	.40	1.46	1.72	.71
3311	1.38	2.78	1.04	.72	2.01	.76	1.03	1.21	.81	.97	1.17	.79

THEORY RATIOS C9(1:3),C10(1:3),D9(1:3),D10(1:3) PRINTED NEXT. A9-D9 ARE NORM'D TO (90,9): A10-D10 TO (0,90). (1:3)=(90,9),(0,0),(90,90,(.0+90)1.2+0:)†
A,B,C,D ARE HWHM=0,4,6,INFINITY.

1100	1.00	.88	1.27	1.00	.86	1.27	1.00	1.00	1.00	1.00	1.00	1.00
1200	.65	.79	.72	1.55	1.22	1.12	1.00	.90	.92	1.00	.90	.92
2100	1.55	1.22	1.12	.65	.79	.72	1.00	.90	.92	1.00	.90	.92
1200	.52	.78	.56	1.87	1.42	1.05	1.00	.82	.86	1.00	.82	.86
3100	1.87	1.42	1.05	.53	.78	.56	1.00	.82	.88	1.00	.82	.86
2200	1.00	1.35	.89	1.00	1.35	.85	1.00	1.17	1.13	1.00	1.17	1.13
2300	.83	1.41	.79	1.21	1.70	.95	1.00	1.29	1.23	1.00	1.29	1.23
3200	1.21	1.70	.95	.83	1.41	.79	1.00	1.29	1.23	1.00	1.29	1.23
3300	1.00	1.83	.90	1.00	1.83	.90	1.00	1.56	1.45	1.00	1.56	1.45
1105	.61	.78	.67	1.64	1.28	1.11	1.00	.89	.90	1.00	.88	.90
1150	1.62	1.24	1.06	.61	.76	.65	1.00	.84	.87	1.00	.84	.87
1155	1.01	1.55	.92	.99	1.53	.91	1.00	1.33	1.26	1.00	1.33	1.26
1201	.82	.81	1.03	1.22	.98	1.26	1.00	1.02	1.02	1.00	1.02	1.02
2110	1.21	1.02	1.31	.83	.85	1.09	1.00	1.09	1.07	1.00	1.09	1.07
1206	1.12	.91	1.41	.89	.81	1.26	1.00	1.09	1.07	1.00	1.09	1.07
2160	.85	.84	1.24	1.10	1.20	1.47	1.00	1.13	1.10	1.00	1.13	1.10
1250	1.05	1.48	.94	.95	1.41	.89	1.00	1.27	1.21	1.00	1.27	1.21
2105	.96	1.37	.85	1.04	1.43	.89	1.00	1.19	1.15	1.00	1.19	1.15
1261	1.48	1.45	.98	.68	.98	.87	1.00	.95	.96	1.00	.95	.96
2115	.71	.92	.84	1.41	1.31	.91	1.00	.88	.88	1.00	.86	.88
1258	1.05	1.04	1.12	.88	.83	.80	1.00	.81	.85	1.00	.81	.85
2195	.62	.82	.78	1.83	1.01	1.13	1.00	.81	.85	1.00	.81	.85
2261	1.33	1.31	.98	.75	.99	.72	1.00	.96	.97	1.00	.96	.97
2310	.75	.93	.88	1.33	1.23	.87	1.00	.85	.88	1.00	.85	.88
2211	.97	.88	1.15	1.06	1.01	1.19	1.00	1.11	1.09	1.00	1.11	1.09
2208	1.01	1.16	1.22	.82	.72	.78	1.00	.90	.92	1.00	.90	.92
2260	.89	.89	.80	1.53	1.05	1.23	1.00	.89	.91	1.00	.89	.91
2218	1.41	1.05	1.31	.71	.74	.93	1.00	1.01	1.01	1.00	1.01	1.01
2201	.71	.60	.84	1.41	.82	1.10	1.00	.86	.89	1.00	.86	.89
2288	.96	1.11	1.58	1.05	1.17	1.67	1.00	1.32	1.25	1.00	1.32	1.25
1301	.72	.00	.03	1.39	1.12	1.16	1.00	.95	.96	1.00	.95	.96
3110	1.35	1.21	1.25	.74	.90	.92	1.00	1.07	1.06	1.00	1.07	1.06
1350	.88	1.02	.88	1.13	1.04	1.00	1.00	1.50	1.40	1.00	1.50	1.40

3105	1.17	1.74	.93	.88	1.[illegible]	.89	1.00	1.34	1.27	1.00	1.34	1.27
1351	1.20	1.44	.98	.93	1.20	.81	1.00	1.12	1.10	1.00	1.12	1.10
3115	.88	1.06	.71	1.24	1.19	.80	1.00	.89	.91	1.00	.89	.91
2301	1.11	1.33	.93	.90	1.20	.84	1.00	1.10	1.00	1.00	1.10	1.00
3210	.93	1.08	.78	1.00	1.17	.82	1.00	.91	.93	1.00	.91	.93
2210	.81	.90	.54	1.03	1.47	.80	1.00	.81	.84	1.00	.81	.84
3201	1.02	1.03	.90	.82	1.01	.61	1.00	.97	.98	1.00	.97	.98
2311	.93	.96	.77	1.20	1.14	.93	1.00	.92	.93	1.00	.92	.93
3211	1.11	1.06	.98	.93	.96	.80	1.00	.99	.99	1.00	.99	.99
2350	.68	.85	.58	1.00	1.01	1.00	1.00	.70	.76	1.00	.70	.76
3200	1.01	1.29	1.09	.82	.87	.57	1.00	.00	.84	1.00	.00	.84
2301	.73	.00	.98	1.37	.93	1.31	1.00	.96	.97	1.00	.96	.97
3210	1.58	1.36	1.41	.87	.91	.86	1.00	1.11	1.09	1.00	1.11	1.09
3201	1.31	1.07	.96	.78	1.27	.73	1.00	1.10	1.14	1.00	1.10	1.14
3310	.77	1.00	.58	1.29	1.29	.75	1.00	.82	.85	1.00	.82	.85
3311	1.01	1.11	.88	.99	1.10	.87	1.00	.98	.99	1.00	.99	.99

† Weighted average of $\Phi = 90^{\circ}$ and 0°, in the (90°, 90°) format(see text).

be a stretched E2; making it a stretched E3 would be impossible(it would give it a lifetime of the order of 10^{-3} sec!; see Fig. 5.2.15) in the light of the results found in section 5.2 .

Thus, it appears one cannot but marginally make the 1932.1 keV transition a stretched E3(considering the F.O.M.'s in Table 5.1.4(c)). One can decrease the multipolarity of any of the five transitions at the bottom of the main cascade by one unit, or increase the multipolarity of either the 361.6 or 559.4 keV transitions by one unit, thus, making the 1932.1 keV transition a stretched E2(see Fig. 4.1.1), with almost as good(in some case equally good)F.O.M.'s as for the case actually chosen.

Table 4.1.2 shows tentative assignments(indicated by parantheses) of all transition multipolarities(and parities based on the lifetime information given in section 5.2) above the isomer.

5.2 Life-Time Information from the RF - Ge and Ge - Ge TAC's

The data was also sorted such that points of coordinates(E_γ, RF - Ge TAC(γ)) were incremented in a two dimensional spectrum, where E_γ refers to the energy of coincident γ-rays, and RF - Ge TAC(γ) refers to the time distribution of the γ-ray in question, with respect to the arrival of the cyclotron RF pulse. The beam tuning(at the 88-inch cylcotron at L.B.L.)is usually such that the time difference between the RF and the beam pulse is stable within a few nsec, i.e.

the RF comes ~ 3 nsec before or after the arrival of the beam pulse. (see section 3.2). The arrival time of the RF pulse is thus about ± 3 nsec within the time of the formation of the compound nucleus, which is also(within about 10^{-15} sec)the time when γ-ray de-excitation process starts). This RF - beam time spread will introduce uncertainties in the transition lifetimes, as discussed below.

Fig. 5.2.1 shows a "bird's-eye view" of such the two-dimensional spectrum RF - Ge TAC(γ) X E_γ, while Fig. 5.2.2 shows the collapse of this two-dimensional spectrum on the RF - Ge TAC axis. The gates 1,2 and 3 were used in the sorting of coincident data in establishing the sequence of the transitions in the level scheme(all detectors being used) as well as for the angular correlation measurements (selected detectors being used; see section 5.1). Gate 1 is the prompt gate, where all transitions which are prompt with respect to each other are distributed within a FWHM of about 9 nsec. This is the gate used in all analysis of coincidences above the 480 nsec isomer. Gate 3(which starts about 13 nsec away from where gate 1 terminates; time increases from right to left in all TAC spectra), was used in sorting coincidences below the 480 nsec isomer. One can see the symmetry of gate 1, with respect to the axis passing through its middle(not drawn) from the very close similarity of the regions marked L and R.

Fig. 5.2.3 shows the RF - Ge TAC spectrum(background-subtracted) for the 1061.1 keV transition(see Fig. 4.1.1). It shows a quite narrow time distribution(FWHM ≈ 7.5 nsec) with respect to the start of the γ-ray cascade, very little tail, and thus, just about the most

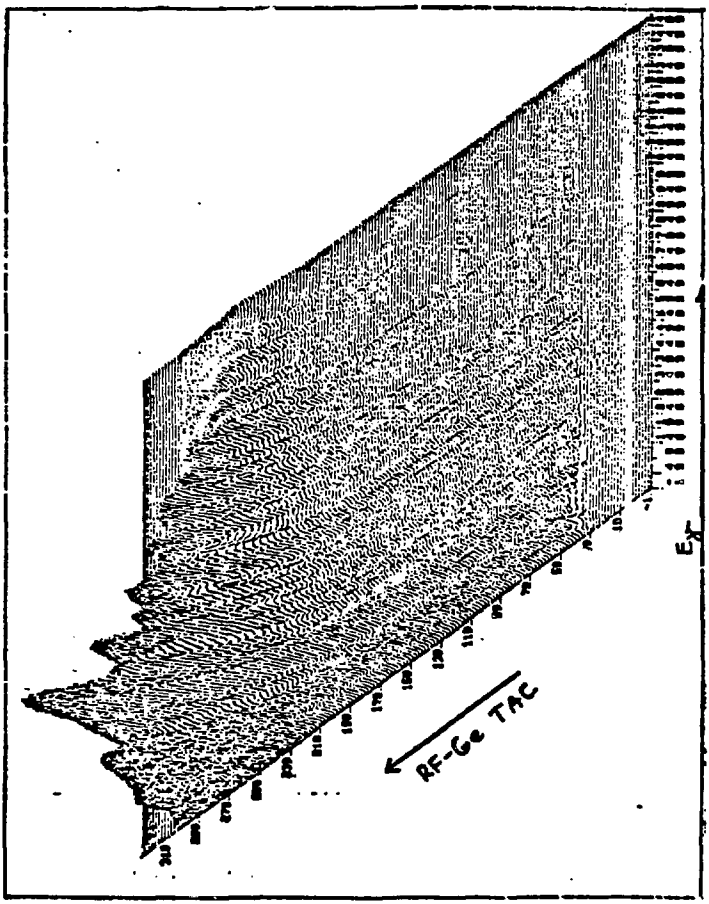

Fig. 5.2.1

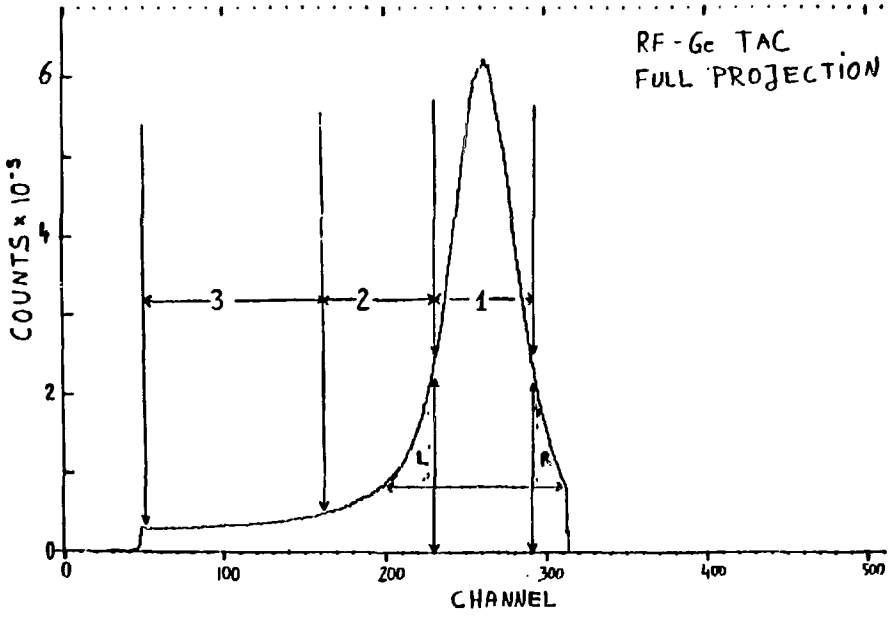
RF-Ge TAC
FULL PROJECTION
COUNTS x 10^-3
6
4
2
0
3
2
1
L
R
0
100
200
300
400
500
CHANNEL

Fig. 5.2.2

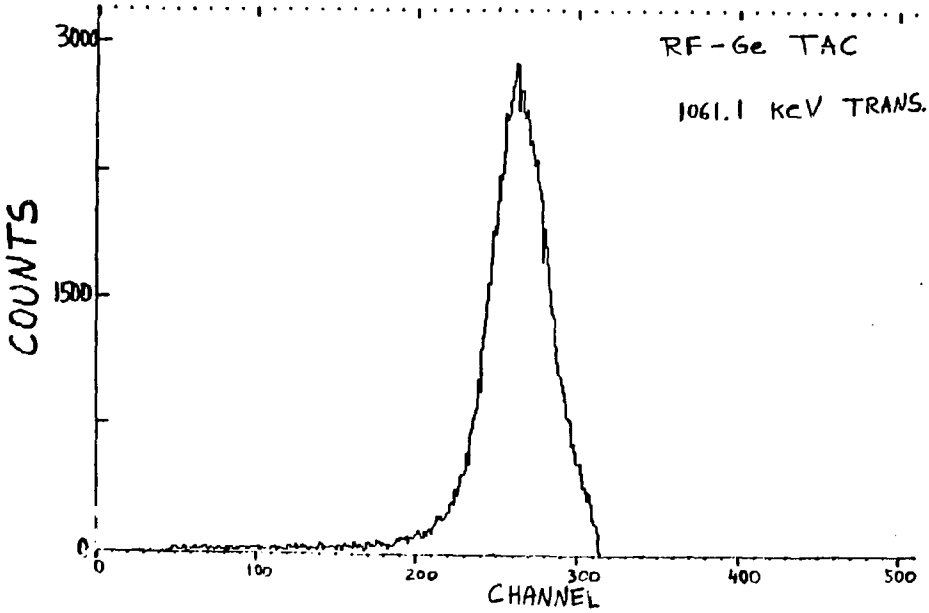
RF-Ge TAC
1061.1 KeV TRANS.
COUNTS
3000
1500
0
0
100
200
300
400
500
CHANNEL

Fig. 5.2.3

"prompt" RF - Ge TAC spectrum of all transitions above the isomer, and all the RF Ge TAC spectra for all transitions above the isomer were compared to the one for the 1061.1 keV γ-ray. Figs. 5.2.4-6 show the RF - Ge TAC spectra for the 763.4, 477.3 and 882.5 keV(thus spanning most of the level scheme) transitions plotted on the same $\log_{10}$ plot with the RF -Ge TAC spectrum for the 1061.1 keV transition. Very little difference starts to develop as the transition energy to which the 1061.1 keV is compared, decreases. However, Fig. 5.2.7, shows quite a perfect meanlife tail for the 327.2 keV transition, from which one can infer a value of about 10 nsec for its meanlife. Since the 327.2 keV transition feeds into the $I = 17^-$ level(see Fig. 4.1.1), the RF - Ge TAC spectra of all transitions de-exciting from that level and the ones below it should show a delayed component. However, according to Table 4.1.2, since the 763.4 keV transition is about 5 times more intense than the 327.2 keV transition, it is about 5 times more likely that ^{148}Dy would de-excite down the prompt main band(i.e. through the $I = 18^+$, 19^-, etc, levels) than via the 327.2 keV transition. Thus, the RF - Ge TAC spectra for all the transitions below the 763.4 keV transition should show a delayed component, with about 20 percent the number of counts under the prompt peak. This was indeed found for all those spectra(of which only the one for the 1061.1 keV transition is shown, in Fig. 5. 2.3)

A problem is the jitter of the crossing of the discriminator threshold level by low energy transitions, but the 327.2 keV transition RF - Ge TAC seems to have a real exponentially falling

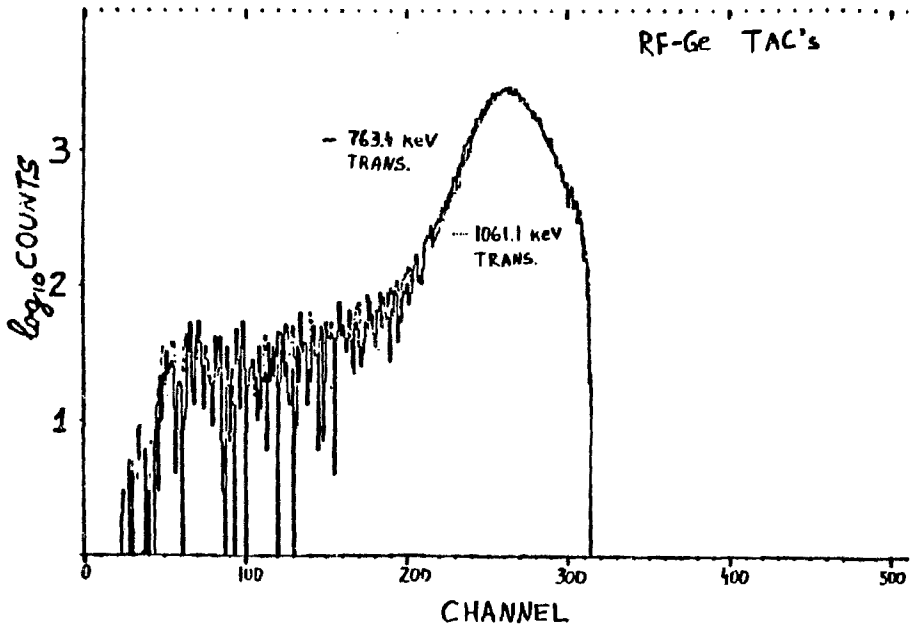
RF-Ge TAC's
763.4 keV TRANS.
1061.1 keV TRANS.
$\log_{10}$ COUNTS
3
2
1
0
100
200
300
400
500
CHANNEL

Fig. 5.2.4

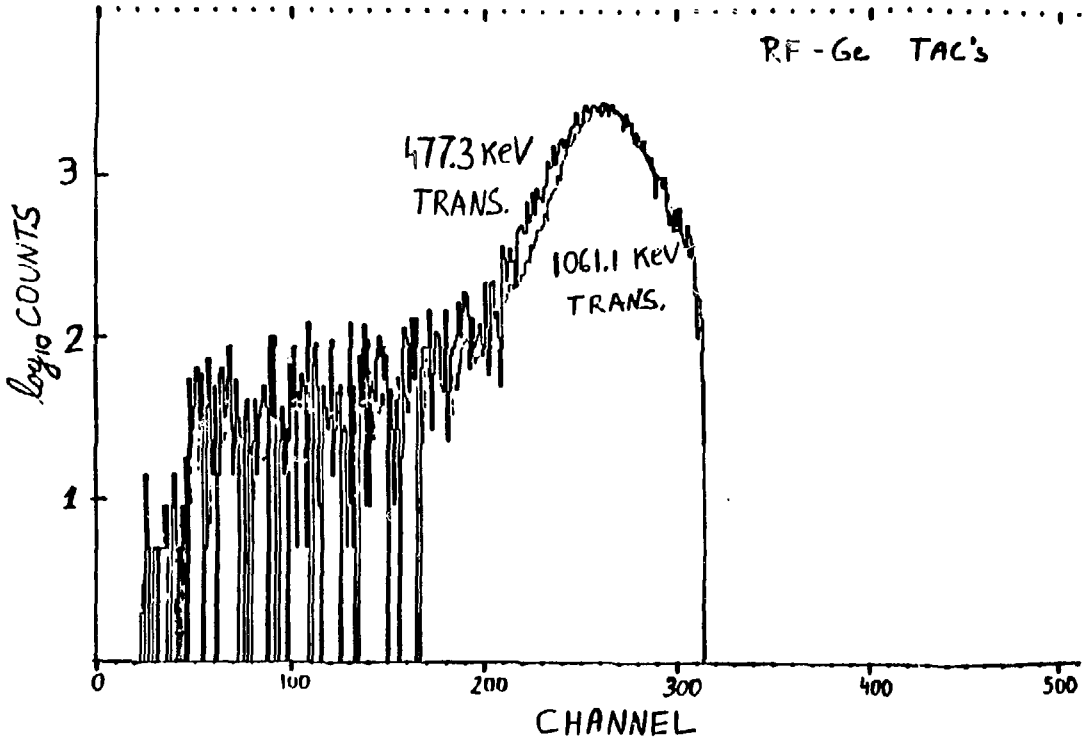
RF - Ge TAC's
477.3 KeV
TRANS.
1061.1 KeV
TRANS.
$\log_{10}$ COUNTS
3
2
1
0
100
200
300
400
500
CHANNEL

Fig. 5.2.5

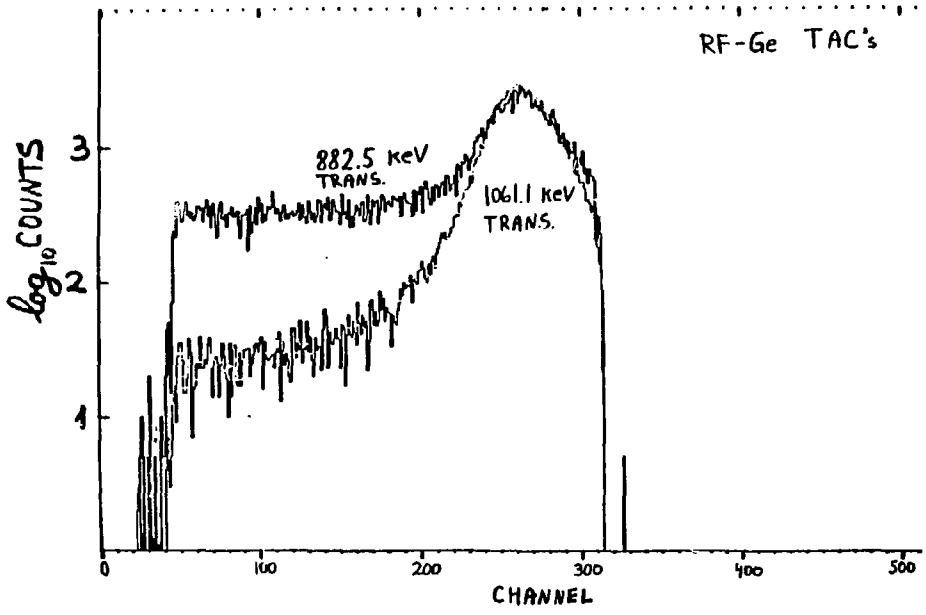
RF-Ge TAC's
882.5 keV
TRANS.
1061.1 keV
TRANS.
log10 COUNTS
3
2
1
0
100
200
300
400
500
CHANNEL

Fig. 5.2.6

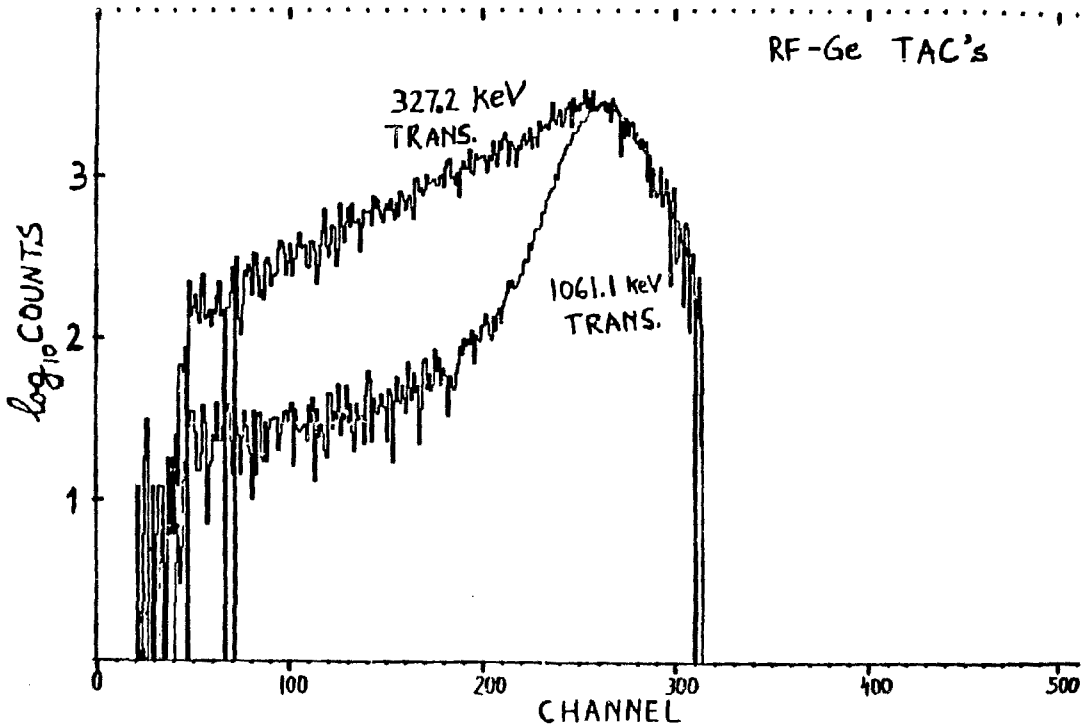
RF-Ge TAC's
327.2 keV
TRANS.
1061.1 keV
TRANS.
log10 COUNTS
3
2
1
0
100
200
300
400
500
CHANNEL

Fig. 5.2.7

tail, indicative of a meanlife. If timing electronics and triggering conditions are nearly identical in both branches of the TAC, then all time jitter and walk would be symmetric, as is the prompt coincidence peak of the TAC. Its FWHM is indicative of the contributions of all sources of time uncertainty. Uncertainty in the zero-crossing for electronics pulses associated with low-energy transitions(because of noise riding on the pulse) produces broadening of the prompt peak of the corresponding RF - GE TAC . In order to investigate this in the case of our transitions, if one plots the ratio of the FWHM of the prompt part of the RF - Ge TAC to the same FWHM for the 1061.1 keV transition(R_2^{PR}) vs the transition energy for all the experimentally observed transitions above the 480 nsec isomer, one obtains the plot in Fig. 5.2.8. A similar plot was done for the "prompt half"(i.e. the right hand half), $R_{1/2}^{PR}$, of the prompt peak of the RF - Ge TAC in question. This is perhaps a more accurate measure of the promptness of the transitions with respect to the 1061.1 keV γ-ray. Fig. 5.2.9 shows such a plot. In both Fig. 5.2.8 and Fig. 5.2.9 there plotted four similar points for four known prompt transitions($E_\gamma \approx$ 151, 424, 670 and 1074 keV; Deleplanque 1984, private communication) in ^{150}Dy(for which the data was taken with exactly the same equipment and under exactly the same experimental conditions the ^{148}Dy run was done). As one can see, those four points fall right in the middle of the pattern for ^{148}Dy points, covering a sizeable transition energy range. From the analysis of those two plots, it was deduced that the "tail" effect shown by the RF - Ge TAC of most low energy transitions (with the

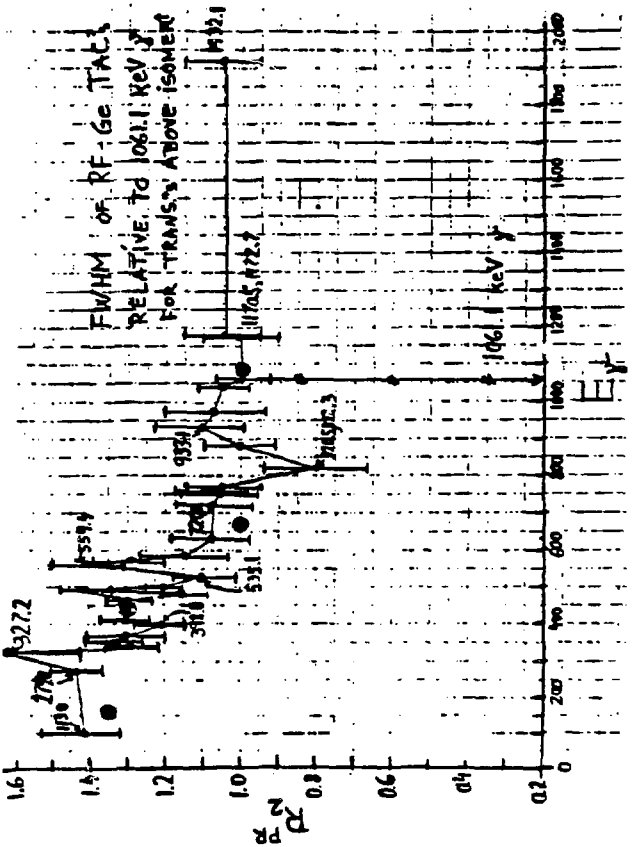
FWHM OF RF-Ge TACs
RELATIVE TO 1061.1 KeV γ
FOR TRANS'S ABOVE ISOMER
1061.1 KeV γ
1.6
1.4
1.2
1.0
0.8
0.6
0.4
0.2
0
200
400
600
800
1000
1200
1400
1600
1800
2000

Fig. 5.2.8

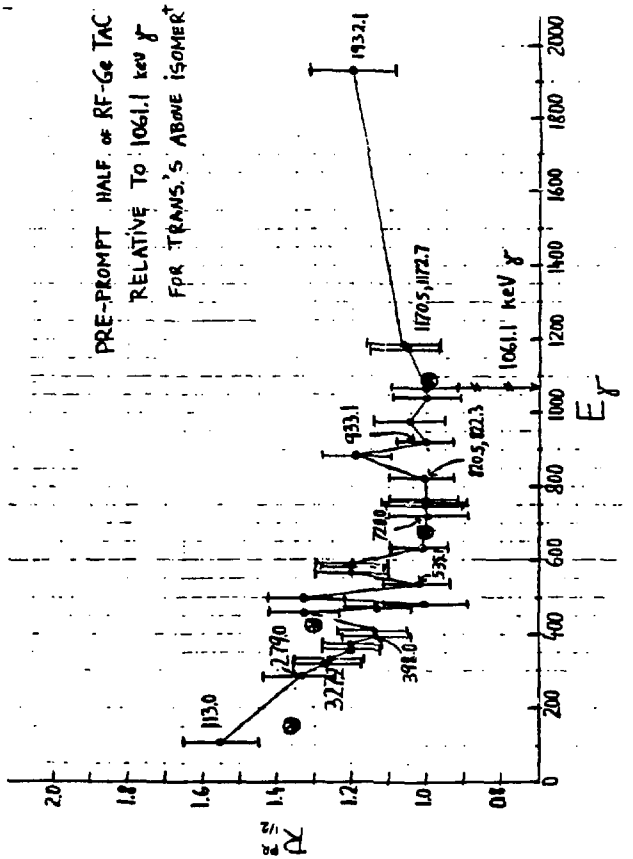
PRE-PROMPT HALF OF RF-Ge TAC
RELATIVE TO 1061.1 keV γ
FOR TRANS.'S ABOVE ISOMER+
1932.1
1170.5, 1172.7
1061.1 keV γ
933.1
820.5, 822.3
710
595.1
398.0
279.0
327
113.0
E_γ
$T_{1/2}$ PR
2.0
1.8
1.6
1.4
1.2
1.0
0.8
0
200
400
600
800
1000
1200
1400
1600
1800
2000

Fig. 5.2.9

possible exception of the 327.2 keV transition)is most likely due to electronics and not to any nuclear lifetime effect. This was also confirmed by similar plots involving the FW(1/5)M(full-width at-1/5-maximum)(not shown here) which show the 327.2 keV point well above the other points, thus strengthening the belief of a true nuclear lifetime associated with the 327.2 keV transition. Fig. 5.2.6 shows that the 882.5 keV transition has quite a tail, thus seemingly giving it a lifetime of more than 10 nsec. However, there is a 883.5 keV transition in ^{148}Gd de-exciting from a level with a half-life of about 17.5 nsec, and thus, since the two transitions are close enough in energy such that gating on one will include a sizeable chunk of the other, it is interpreted that the 882.5 keV transition in ^{148}Dy(Fig. 4.1.1)does not have any delay. Indeed, gating on the 882.5 keV transition for the RF - Ge TAC gate 3, one only sees the three transitions in ^{148}Gd(and the 511 keV annihilation peak) which together with the 883.5 keV γ-ray, come from the 17.5 nsec level(see Fig. 5.2.10). It is possible that using gate 2 might have shown some transitions in ^{148}Dy.

Table 5.2.1 shows the difference between the centroid of the background-subtracted RF - Ge TAC of all transitions above the isomer and the centroid of the background-subtracted RF - Ge TAC of the 1061.1 keV transition. The background subtraction was done by running a horizontal line through the average background fluctuations(in the tail part)of the RF - Ge TAC spectrum for each transition. The centroid difference thus obtained represents the meanlife of the exponential decay of the level in question.

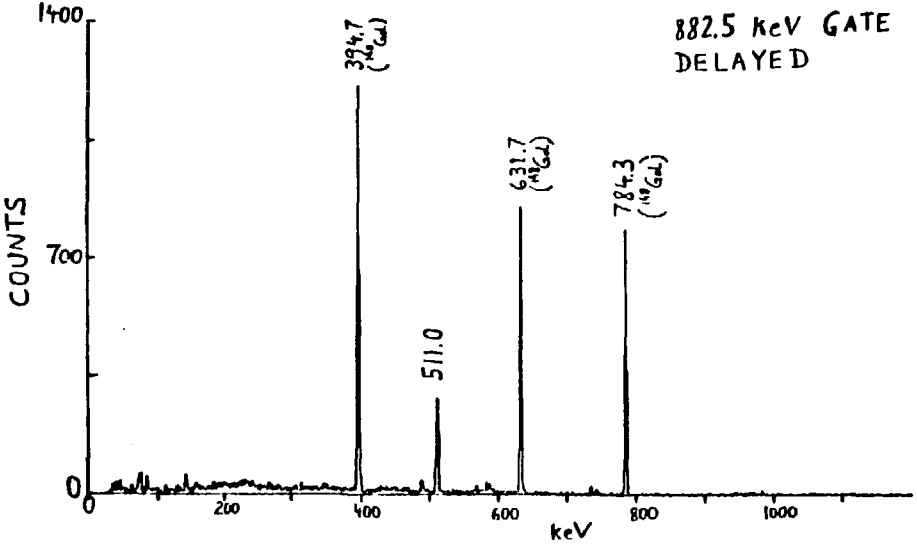
882.5 keV GATE
DELAYED
COUNTS
1400
700
0
394.7
511.0
631.7
784.3
0
200
400
600
800
1000
keV

Fig. 5.2.10

TABLE 5.2.1

LIFE-TIME INFORMATION FROM RF-Ge TAC for Transitions Above the 480 nsec Isomer

I_i^π	→	I_f^π	E_{level} (keV)	E_γ (keV)	Prompt γ[a] CENTROID (BKGD SUB) (CHAN.NO.)	CENTROID (BKGD SUB) (CHAN.NO.)	b Δ(nsec)
11^-	→	10^+	3980.2	1061.1	263.0±2.	263.0±2	0.0
12^-	→	11^-	4476.0	495.8	263.0±2.	259.4±2	0.64±.5
14^-	→	12^-	5521.5	1045.5	263.0±2.	262.1±2	0.16±.5
16^-	→	14^-	5984.2	462.7	263.0±2.	258.5±2	0.80±.5
17^-	→	16^-	6263.2	279.0	263.0±2.	259.6±3	0.60±.7
(18^+)	→	17^-	7026.6	763.4	263.0±2.	262.0±2	0.18±.5
(19^-)	→	(18^+)	8197.1	1170.5	263.0±2.	265.2±3	0.39±.5
(20^-)	→	(19^-)	8530.2	333.1	263.0±2.	261.0±2	0.35±.5
(21^-)	→	(20^-)	9167.8	637.6	263.0±2.	262.0±2	0.18±.5
(21^-)	→	(19^-)	9167.8	970.7	263.0±2.	264.6±4	0.28±.7
(22^-)	→	(21^-)	9702.9	535.1	263.0±2.	261.0±3	0.35±.6
(22^-)	→	(20^-)	9702.9	1172.7	263.0±2.	266.0±4	0.53±.7
(23^-)	→	(22^-)	10055.4	352.5	263.0±2.	260.9±2	0.37±.5
(23^-)	→	(21^-)	10100.9	933.1	263.0±2.	261.7±4	0.23±.8
(24^-)	→	(23^-)	10453.4	352.5'	263.0±2.	260.9±2	0.37±.8[c]
(24^-)	→	(23^-)	10453.4	398.0	263.0±2.	261.2±3	0.32±.6
(26^-)	→	(24^-)	10930.7	477.3	263.0±2.	260.5±3	0.44±.6
(28^-)	→	(26^-)	11813.2	882.5	263.0±2.	263.4±3	0.07±.6[d]
(29^+)	→	(27^+)	12533.2	720.0	263.0±2.	263.3±3	0.05±.6
(30^+)	→	(29^+)	13100.9	567.7	263.0±2.	260.2±3	0.50±.6
(31^-)	→	(30^+)	13215.1	114.2	263.0±2.	258.6±4	0.78±.7
$(22^-)^{us}$	→	(20^-)	9287.9	757.7	263.0±2.	263.0±3	0.0 ±.6
$(24^-)^{us}$	→	$(22^-)^{us}$	10110.2	822.3	263.0±2.	263.0±4	0.0 ±.8[e]
$(24^-)^{us}$	→	(22^-)	10110.2	407.3	263.0±2.	254.8±3	1.45±.6
(26^-)	→	$(24^-)^{us}$	10930.7	820.5	263.0±2.	263.0±3	0.0 ±.6[e]
$(13^-)_{11s}$	→	10^+_{11s}	4857.2	1932.1	263.0±2.	270.5±3	1.33±.6
$(14^-)_{11s}$	→	$(13^-)_{11s}$	5410.6	559.4	263.0±2.	256.7±3	1.11±.6
(15^-)	→	$(14^-)_{11s}$	5772.2	361.6	263.0±2.	258.5±3	0.80±.6
17^-	→	(15^-)	6263.2	491.0	263.0±2.	260.6±3	0.43±.6

TABLE 5.2.1 (Continued)

LIFE-TIME INFORMATION FROM RF-Ge TAC for Transitions Above the 480 nsec Isomer

I_i^{π}	→	I_f^{π}	E_{level}(keV)	E_{γ}(keV)	Prompt γ^d CENTROID (BKGD SUB) (CHAN.NO.)	CENTROID (BKGD SUB) (CHAN.NO.)	b Δ(nsec)
				INDIVIDUAL SIDE TRANSITIONS			
(*)	→	17^-	6590.4	327.2	263.0±2.	256. ±4	1.24±.7
(20^-)	→	19^-	8783.9	586.8	263.0±2.	259.5±4	0.62±.7
(25^-)	→	(23^-)	11070.3	1014.9	263.0±2.	260.6±4	0.42±.7

a The 1061.1 keV γ-ray was chosen as the most "prompt" transition (see section 3.2), and so, its RF - Ge TAC as the reference to which mean-lives were measured (see below).

b Δ = CENTROID (TAC of 1061.1 keV γ) - CENTROID (TAC of γ) (also the mean-like, see text) (in nsec).

c Error based on statistics relative to first 352.5 keV transition

d Contains the ^{148}Gd transitions 882.2 keV and 883.5 keV (below the 17.5 nec isomer; see Lundardi et.al.).

e The have same RF - Ge TAC spectrum.
Poor statistics prvented obtaining a value for Δ for the 750 keV transition.

* A multipolarity value could not be obtained from angular correlation measurements(see section 5.1).

^{us} and ^{lls} refer to levels belonging to the upper side-band and left lower side-band, respectively(see Fig. 4.1.1).

In addition to the RF - Ge TAC, the data were also sorted in the (E_γ, Ge - Ge TAC(γ)) format, where Ge - Ge TAC(γ) represents the time distribution of the transition in question with respect to the coincident transition, in coincidence with which the above two-dimensional spectrum was obtained. The Ge - Ge TAC gave information about the time elapsed between the detection of any two given coincident γ-rays. Fig. 5.2.11 shows the collapse of such a two-dimensional spectrum on the Ge - Ge TAC axis(the nature of the left shoulder in the main peak is not understood). Figs. 5.2.12-14 show the linear plots of the Ge - Ge TAC's for the 763.4, 477.3 and 882.5 keV γ-rays, obtained from the two-dimensional spectrum E_γ- Ge - Ge TAC in coincidence with the 1061.1 keV γ-ray, on the same plot with the Ge - Ge TAC spectrum of the 462.7 keV γ-ray. In other words, the three figures compare the time distributions of the 763.4, 477.3 and 882.5 keV γ-rays relative to the 1061.1 keV γ-ray to the similar time distribution of the 462.7 keV, which is immediately above the 1061.1 keV transition. No differences in the Ge - Ge TAC centroids or shapes are observed. Table 5.2.2 depicts centroid shifts and meanlives for transitions above and below the 480 nsec isomer. For the transitions above the isomer, as it can be seen from Table 5.2.1, meanlives of 0.0-2.0 nsec, with about as large experimental errors, are obtained. The treatment above, however, does not account all possible sources of experimental uncertainty(such as the RF - beam time spread, for example). Considering all such possible error sources, it was deemed necessary to relax the above values for the meanlives to values $\lesssim$ 5 nsec . Thus, no precise lifetime information could be derived

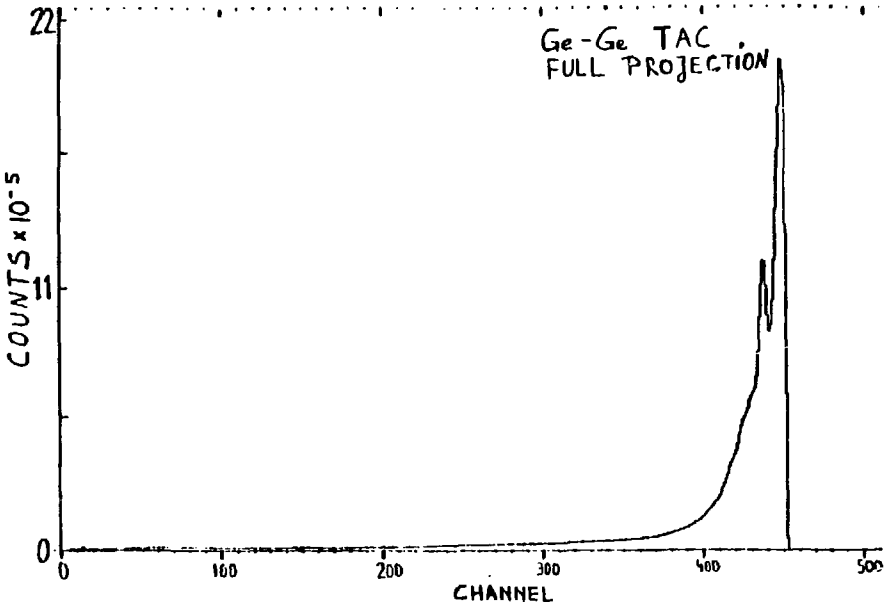
Ge-Ge TAC
FULL PROJECTION
COUNTS x 10^-5
22
11
0
0
100
200
300
400
500
CHANNEL

Fig. 5.2.11

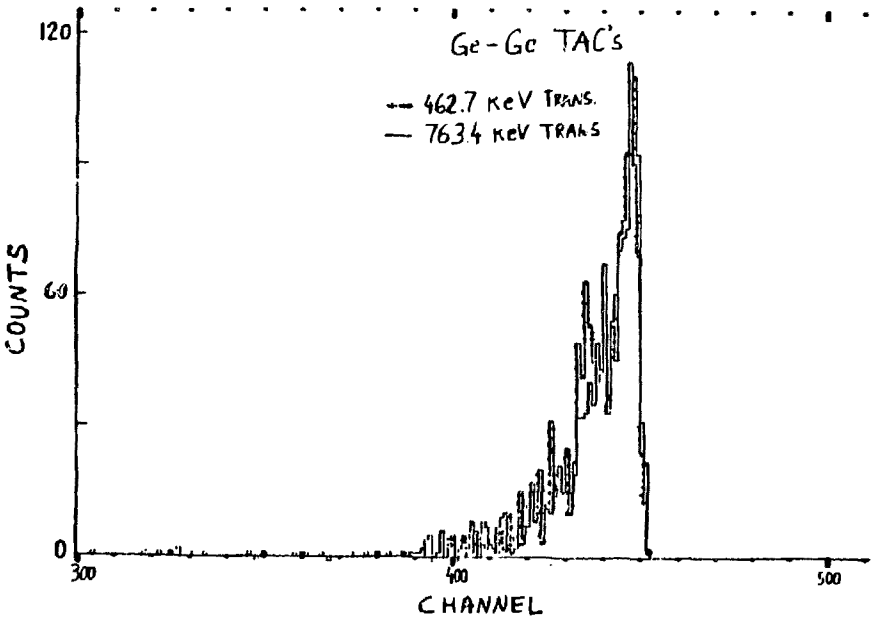
Ge-Ge TAC's
462.7 keV TRANS.
763.4 keV TRANS
120
60
0
COUNTS
300
400
500
CHANNEL

Fig. 5.2.12

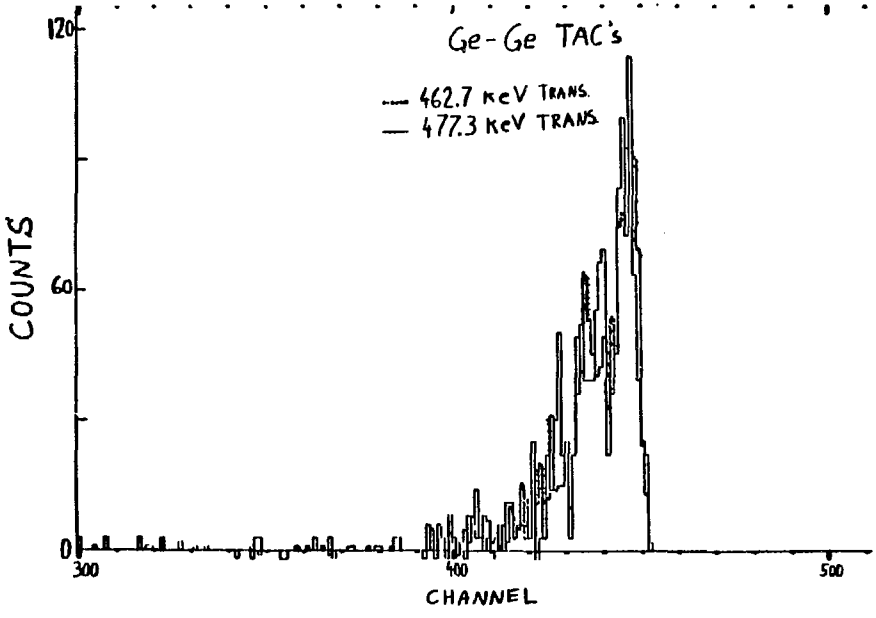
Ge-Ge TAC's
462.7 keV TRANS.
477.3 keV TRANS.
COUNTS
120
60
0
300
400
500
CHANNEL

Fig. 5.2.13

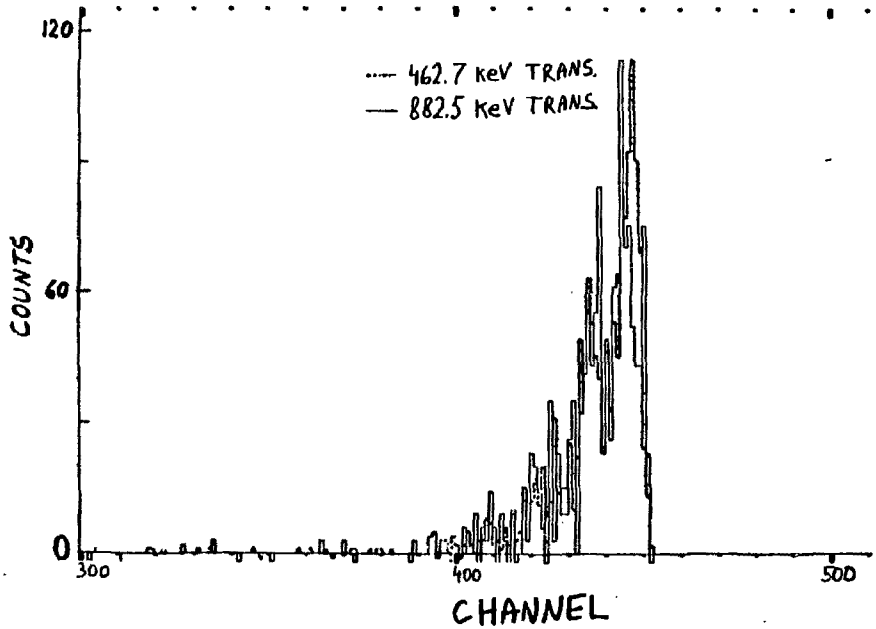
120
60
0
COUNTS
462.7 keV TRANS.
882.5 keV TRANS.
300
400
500
CHANNEL

Fig. 5.2.14

Table 5.2.2

Shifts of Ge - Ge TAC spectra centroids of transitions above the 480 nsec isomer, Δ(nsec), from the centroid of the Ge - Ge TAC spectrum of the 462.7 keV transition for prompt(RF - Ge TAC gate 1) coincidences with the 1061.1 and 1170.5 keV transitions. Similar centroid shifts with respect to the 1687.5 keV transition, measured for the transitions below the 480 nsec isomer for delayed(RF - Ge TAC gate 3) coincidences with the 660.8 keV transition. The mean-life time measurements are explained in the text.

Prompt coincidences with the 1061.1 keV transition

Transition		Δ	Mean-Life[a]
$I_i^\pi \rightarrow I_f^\pi$	E_γ(keV)	(nsec)	(nsec)
$12^- \rightarrow 11^-$	95.8	0.13 ± 0.66	1.52 ± 0.60
$14^- \rightarrow 12^-$	1045.5	0.35 ± 0.66	1.23 ± 0.60
$16^- \rightarrow 14^-$	462.7	0.0	1.54 ± 0.60
$17^- \rightarrow 16^-$	279.0	0.09 ± 0.66	1.56 ± 0.60
$(18^+) \rightarrow 17^-$	763.4	0.42 ± 0.66	1.23 ± 0.60
$(19^-) \rightarrow (18^+)$	1170.5	-0.09 ± 0.66	1.74 ± 0.60
$(20^-) \rightarrow (19^-)$	333.1	0.35 ± 0.66	1.23 ± 0.60
$(21^-) \rightarrow (20^-)$	637.6	0.46 ± 0.66	1.19 ± 0.60
$(21^-) \rightarrow (19^-)$	970.7	0.33 ± 0.66	1.32 ± 0.60

$(22^-)\to(21^-)$	535.1	0.66 ± 0.66	0.99 ± 0.60
$(22^-)\to(20^-)$	1172.7	-0.11 ± 0.88	1.76 ± 0.70
$(23^-)\to(22^-)$	352.5	0.51 ± 0.66	1.15 ± 0.60
$(24^-)\to(23^-)'$	352.5'	0.55 ± 0.88	1.10 ± 0.70
$(23^-)\to(21^-)$	933.1	0.44 ± 0.88	1.21 ± 0.70
$(24^-)\to(23^-)$	398.0	0.35 ± 0.66	1.23 ± 0.60
$(26^-)\to(24^-)$	477.3	0.24 ± 0.66	1.41 ± 0.60
$(28^-)\to(26^-)$	882.5	0.70 ± 0.66	0.95 ± 0.70
$(29^+)\to(28^-)$	720.0	0.48 ± 0.66	1.17 ± 0.60
$(30^+)\to(29^+)$	567.7	0.55 ± 0.66	1.10 ± 0.60
$(31^-)\to(30^+)$	114.2	3.85 ± 0.88	5.50 ± 0.71
$(22^-)^{us}\to(20^-)^{us}$	757.7	0.88 ± 0.66	0.77 ± 0.60
$(24^-)^{us}\to(22^-)^{us}$	822.3	0.77 ± 0.66	0.88 ± 0.60
$(24^-)^{us}\to(22^-)$	407.3	0.66 ± 0.66	0.99 ± 0.60
$(26^-)\to(24^-)^{us}$	820.5	1.10 ± 0.88	0.55 ± 0.70
		Individual Side Transitions	
$(**)\to 17^-$	327.2	0.68 ± 0.66	0.97 ± 0.60
$(20^-)\to(19^-)$	586.8	-0.11 ± 0.66	1.76 ± 0.60
$(25^-)\to(23^-)$	1014.9	0.33 ± 0.66	1.32 ± 0.60
		Prompt coincidences with the 1170.5 keV transition	
$11^- \to 10^+$	1061.1	0.44 ± 0.66	1.21 ± 0.60

2.7	0.24 ± 0.66	1.41 ± 0.60
2.1	-0.51 ± 0.66	2.16 ± 0.60
9.4	0.24 ± 0.66	1.41 ± 0.60
1.6	0.26 ± 0.66	1.39 ± 0.60
2.0	0.49 ± 0.88	2.11 ± 0.75
1.0	0.26 ± 0.66	1.39 ± 0.60

e - Ge TAC spectrum from the "prompt" peak for ansition(average values from prompt coincidences he 1061.1 and 1170.5 keV transitions)

2.7	7.0 ± 2.5	1.53 ± 0.50

Coincidences with the delayed 660.8 keV transition[b] (below the 480 nsec isomer)

7.5	0.0	12.0 ± 1.3
2.7	3.0 ± 1.6	9.2 ± 1.3
9.8	2.3 ± 1.4	9.7 ± 1.3
7.3	0.2 ± 1.6	12.3 ± 1.4
9.2	*	*
9.4	*	*
4.3	*	*
1.2	*	15.9 ± 1.8
4.1	9.5 ± 1.6	21.5 ± 1.3

$10^+ \rightarrow 8^+$	86.9	*	*

[a] The difference(in nsec) between the centroid of the 462.7 keV Ge - Ge TAC "prompt" peak and the centroid of the whole Ge - Ge TAC spectrum of the respective transition.

[b] Same as ([a]) above, only the 462.7 keV transition is replaced by the 1687.5 keV transition, below the 480 nsec isomer.

* Poor statistics prevented obtaining a value.

** A multipolarity value could not be obtained from angular correlation measurements(see section 5.1).

us and lls refer to upper side-band and left lower side-band, respectively(see Fig. 4.1.1).

from the present work, which indicates that there probably are no delays associated with any of the transitions above the 480 nsec isomer.

With this in mind, when using the single-particle half-life (proportional to the meanlife) vs. E_γ curves displayed in Figs. 5.2.15-16(see Blatt, 1979), one should pick half-lives $\lesssim$ 5nsec. This criterion was followed in trying to choose parities for all the transitions above the isomer(with the exception of the 327.2 keV transition, for which, since no multipolarity assignment was made in section 5.1, it was not deemed necessary to be assigned a parity). This was the manner in which the tentative parity assignments of the experimental levels in Table 4.1.2(and also see Fig. 4.1.1) were made.

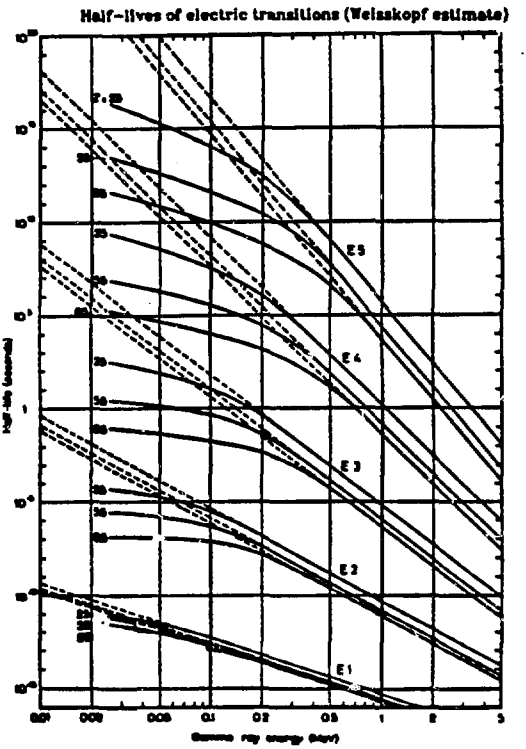
Half-lives of electric transitions (Weisskopf estimate)
E5
E4
E3
E2
E1

Fig. 5.2.15

Half-lives of magnetic transitions (Weisskopf estimate)

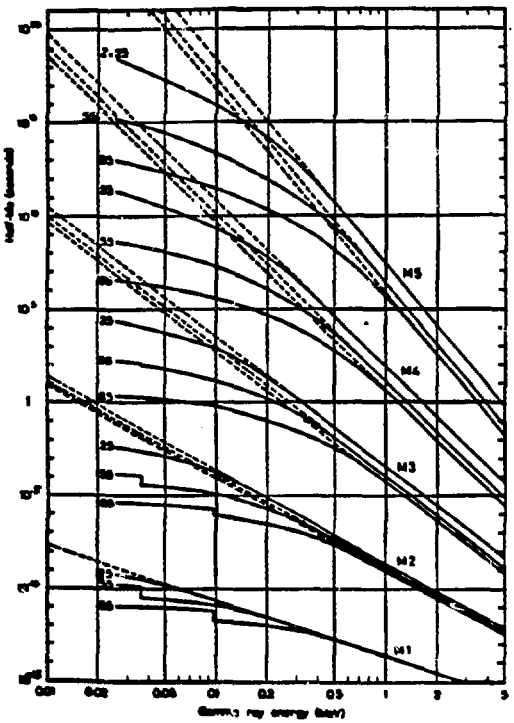

Fig. 5.2.16

Chapter 6

Two-Particle-Octupole Exchange Coupling and the Deformed Independent Particle Model as Applied to the Discrete Levels of ^{148}Dy

High-spin particle-hole excitations studied in ^{146}Gd(N = 82)(Kleinheinz et al, 1979) have indicated the presence of a large gap in the single-particle spectrum, at Z = 64, and an even larger gap at N = 82(Fig. 6.0.0). Several investigations(Broda et al, 1979 and Kleinheinz(Argonne), 1979) have shown that the yrast spectra of some few-valence-particle nuclei in the vicinity of ^{146}Gd can be well described by the spherical shell model with empirical one- and two-nucleon interaction energies. High-spin states in nuclei close to the doubly magic ^{208}Pb have been studied successfully with similar techniques(Bergström, Bormio Meeting, 1978), which seems to indicate that the fully(or nearly fully) aligned few-nucleon yrast configurations are rather similar in the ^{146}Gd and ^{208}Pb regions.

The one-particle nuclei ^{147}Gd and ^{147}Tb have been found(Kleinheinz et al, 1979, Broda et al, 1979) to have yrast states up to about 4 MeV excitation energy which result from coupling the valence nucleons to the ^{146}Gd core states. Earlier studies of the three-valence nucleus ^{149}Dy(Stefanini et al, 1976) identified a $27^-/2$ isomeric state of configuration $\pi h^2_{11/2}\nu f_{7/2}$, and gave partial

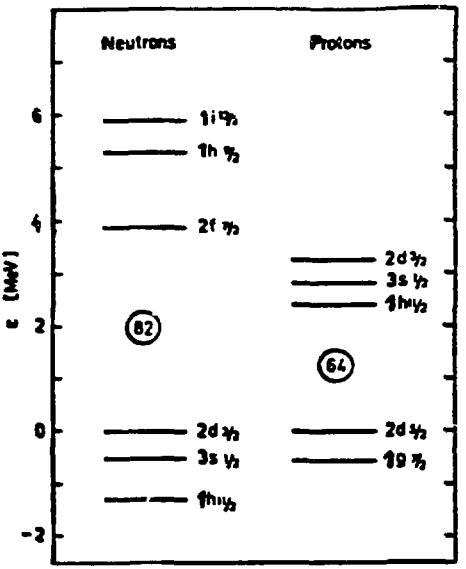
Neutrons
Protons
6
4
2
0
-2
ε [MeV]
1i 13/2
1h 9/2
2f 7/2
82
2d 3/2
3s 1/2
1h11/2
2d 3/2
3s 1/2
1h11/2
64
2d 5/2
1g 7/2

Fig. 6.0.0

configurations of the states populated in the decay to the $\nu f_{7/2}$ ground state.

From Fig. 6.0.0 one can predict that the yrast states in ^{148}Dy would involve $h_{11/2}$ protons, since the $h_{11/2}$ proton orbitals are the immediate ones after the Z = 64 gap. Similar promotion of neutrons would involve elevating them across the N = 82 gap, at a considerably higher energy expense. One would thus hope to observe a complete $\pi h^2_{11/2}$ spectrum, which, in fact, was identified by Daly et al (1978 and 1980). The coupling of the two $h_{11/2}$ protons to 10^+, thus generating ten units of angular momentum at low excitation energy cost (see Fig. 6.0.0) plays an important role in the yrast spectroscopy of ^{148}Dy.

At I = 10, ^{148}Dy exhausts that valence spin and, above the $(\pi h^2_{11/2})10^+$ state, the present work indicates the presence of two states of the type $\pi h^2_{11/2} \times 3^-$, obtained by exciting the low-lying 3^- octupole state of the ^{146}Gd core. The rest of the states above the isomeric 10^+ state are interpreted as components of "maximal weight" configurations as obtained within the Deformed Independent Particle Model (DIPM). For this model, use is made of empirically based spherical single particle energies, a pairing force in the BCS approximation with gap parameters varying with the particle number projection, as well as the Strutinsky renormalization (Døssing et al, 1980 and Neergard, 1982).

6.1 The $\pi h^2_{11/2}$ Spectrum and the Negative Parity States Below the 480 nsec Isomer

The 10^+ isomeric state at 2919.1 keV in ^{148}Dy is the fully aligned $\pi h^2_{11/2}$ state, while the 8^+(a 65 nsec isomer; see Daly et al, 1980, and Haas et al, 1981, Julin et al, 1982 and Ward et al, 1983), 6^+, 4^+, 2^+ and the ground state 0^+ are the rest of the members of the $\pi h^2_{11/2}$ multiplet. The members of such a multiplet have even-valued spins because of the following: in the m-scheme, the wave function for the two nucleons in the same level(i.e. "equivalent" to each other), is:

$$\phi(j^2;\, mm') = \phi(nljm,nljm') = -\,\phi(nljm',nljm) = -\,\phi(j^2;\, m'm) \qquad (6.1.1)$$

where $m,m' = -j,-j+1,\ldots,1,\ldots,j$.

In the J-scheme, the wave function of the configuration of total spin J and z-component M, constructed from two nucleons with equal spins j, and different z-components, m and m', is:

$$\phi(j^2;\, JM) = \sum_{m,m'} C^{j\ j\ J}_{m\ m'\ M}\, \phi(j^2;\, mm'), \qquad (6.1.2)$$

where the Clebsch-Gordon coefficient above has the property $C^{j\ j\ J}_{m\ m'\ M} = (-1)^{2j-J} C^{j\ j\ J}_{m'\ m\ M}$(see deShalit and Feshbach, 1974), which together with (6.1.1) makes the right-hand side of (6.1.2) zero

if j is half-integer, unless J is even.(Essentially, this is the Pauli principle.)

The $\pi h^2_{11/2}$ multiplet levels with I > 6, particularly the 8^+ and 10^+ states, probably have very pure $\pi h^2_{11/2}$ configurations because the only other available proton orbitals are the $s_{1/2}$ and the $d_{3/2}$ above the Z = 64 gap, and the $d_{5/2}$ and the $g_{7/2}$ below it, and one cannot obtain spins of 8 or higher from such configurations. In general, energy spectra of two-valence-particle nuclei give information about two-nucleon residual interactions(e.g. Schiffer and True, 1976). Daly et al(1980) provided first information about two-$h_{11/2}$-proton residual interactions.

In ^{146}Gd, the lowest 5^- and 7^- states have a predominant $\pi d^{-1}_{5/2}h_{11/2}$ configuration(Kleinheinz et al, 1979). The 5^- and 7^- states in ^{148}Dy lie(see chapter 4 for their level energies) about 300 keV lower than the 5^- and 7^- states in ^{146}Gd. A plausible explanation is their being components of a "maximal weight" state of the fully aligned configuration $(\pi d^{-1}_{5/2}h_{11/2})8^-$(with the valence $\pi h^2_{11/2}$ coupled to spin zero and so, unexcited), as predicted by DIPM(section 6.3). Due to their lying about 300 keV lower in ^{148}Dy than in ^{146}Gd(particle-hole excitations are expected at higher energies in ^{148}Dy than in ^{146}Gd), one might interpret the 2348.3 and 2738.1 keV levels in ^{148}Dy as being the two lowest lying members of the two multiplets $(\pi h_{11/2}s_{1/2})5^-$ and $(\pi h_{11/2}d_{3/2})7^-$, respectively. The above configurations are of the two-particle type, and should occur at low excitation energies in ^{148}Dy, therefore being predominantly responsible for the configura-

tions of the two levels in question.

The 3^- level in ^{148}Dy has been found most likely to be the result of the $(\pi h^2_{11/2})_0 \times 3^-$ coupling(see next section).

6.2 Two-Particle-Octupole Excitations

At I = 10, the two-particle valence spin is exhausted and higher-spin two-particle states must involve the excitation of the ^{146}Gd core. The lowest excited state of the core is most likely the collective 3^-, because the $h_{11/2}$ and the $d_{5/2}$ proton orbitals are the closest to the Z = 64 gap(see Fig. 6.0.0) and the 3^- state is the lowest odd-parity one can get. Therefore, it is most likely that some of the states above I = 10 are of the type $(\pi h^2_{11/2})_{10} \times 3^-$.

The experimental work indicates the presence of a strong 1061.1 keV stretched E1 transition de-exciting from the 3980.2 keV 11^- level to the 10^+ isomer. Its interpretation is(as given before by Daly et al(1980) and Kleinheinz(1980))as the lowest member of the octupole multiplet built on the $(\pi h^2_{11/2})10^+$ state. In addition, the previously reported 1932.1 keV stretched E2 transition (Haas et al, 1981 and Julin et al, 1982(p.78)) could perhaps be changed into a stretched E3 according to the present experimental work(see section 5.1). This 1932.1 keV E3 transition also populates the isomeric 10^+ state, and could be interpreted as the highest member of the octupole

multiplet built on the $(\pi h^2_{11/2})10^+$ state.

In order to understand the $\pi h^2_{11/2} \times 3^-$ coupling in ^{148}Dy, it is better to consider first the case(Broda et al, 1979) of one $h_{11/2}$ proton coupled to the 3^- excitation of ^{146}Gd, as in ^{147}Tb. In this case, one has one $h_{11/2}$ proton in the ground state of ^{147}Tb, and the lowest octupole coupling state, the state with $I^\pi = 15^+/2$, decays to the ground state via $\Delta I = 2$ transitions. When the $h_{11/2}$ valence proton is added to the 3^- state of the ^{146}Gd core, the large $\pi d^{-1}_{5/2} h_{11/2}$ component of the octupole state wave function will be blocked by the Pauli principle, changing the energies of some coupled states with respect to the unperturbed ^{146}Gd 3^- energy.(In contrast to ^{208}Pb, where many proton and neutron particle-hole excitations contribute to the 2.6 MeV 3^- state(Hamamoto, 1974), preliminary RPA(random phase approximation) calculations(Dehesa, Speth and Kleinheinz, 1980, unpublished) seem to give a value of ≈ 0.75 for the amplitude of the $\pi d^{-1}_{5/2} h_{11/2}$ component of the 1.6 MeV 3^- state in ^{146}Gd. From here on, it will be approximated that the configuration $\pi d^{-1}_{5/2} h_{11/2}$ is the only component of the 3^- state wave function for ^{146}Gd.)

For the octupole excitations built on the $\pi h_{11/2}$ ground state of ^{147}Tb, one considers the Hamiltonian:

$$H = H_{coll} + H_p + H' \qquad (6.2.1)$$

where H' is the leading order particle-vibrational coupling term, which for small vibrational amplitudes α can be written as $H' = k\alpha F(x)$(Bohr

and Mottelson, 1975). The one-particle operator F(x) describes the dependence of the potential on the particle variables(position, spin, isospin) and k is a coupling constant. The collective Hamiltonian (the Hamiltonian of the ^{146}Gd core), H_{coll}, has eigenstates $|I_{coll}\rangle$, such that $H_{coll}|I_{coll}\rangle = E_{coll}|I_{coll}\rangle$, where the one-phonon states have $I^{\pi}_{coll} = 2^{+}, 3^{-}, \ldots$ and $E_{coll} = \hbar\omega_L = \hbar\sqrt{C_L/B_L}$. The single-particle Hamiltonian(the Hamiltonian, e.g., for the $h_{11/2}$ proton orbiting the ^{146}Gd core), H_p, can be written in the usual form $H_p = KE + V(r)$, where KE is the kinetic energy of the orbiting $h_{11/2}$ proton and V(r) can be chosen as a sum of Coulomb, Woods-Saxon and spin-orbit terms(Hamamoto, 1974).

Following Bohr and Mottelson's treatment(or Hamamoto's, 1974), one can take the perturbing Hamiltonian as $H' = -k_{\lambda}(r)\sum_{\mu} \alpha_{\lambda\mu} Y^{*}_{\lambda\mu}(\theta,\phi)$, where, in our case $\lambda = 3$ and (r,θ,ϕ) represent the position of the $h_{11/2}$ proton outside the ^{146}Gd core. The first two terms in (6.2.1) represent the unperturbed Hamiltonian, H_0, and, in the limit when $H' = 0$, the wave functions of eigenstates of the multiplet $(j_1\lambda)I$(i.e. states of total spin I, which is the result of coupling the single-particle angular momentum j_1 to the λ of the core vibration) are of the form $|\Psi_0\rangle_I = (|j_1\rangle|\lambda\rangle)_I$. In the case of ^{147}Tb(the ^{146}Gd core vibration $\lambda=3$), I can take all half-integer values from 5/2 through 17/2($|j_1 - \lambda| < I < j_1 + \lambda$, where $j_1 = 11/2$ and $\lambda = 3$). The unperturbed excitation energies of all members of the septuplet $(11/2, 3)I$ will be given by:

$$E^{I}_{0} = \langle \Psi_0 | H_0 | \Psi_0 \rangle_I = E_{3^-} + E(\pi h_{11/2}) \qquad (6.2.2)$$

where E_{3^-} is the octupole vibrational energy of the ^{146}Gd core and $E(\pi h_{11/2})$ is the excitation energy of the $h_{11/2}$ proton outside the core. The octupole vibrational energy E_3 above, is collective in nature, and its main component could be obtained by promoting a proton from the $d_{5/2}$ orbital (thereby creating a hole there) across the Z = 64 gap into the $h_{11/2}$ orbital. Fig. 6.0.0 shows this $E(h_{11/2}) - E(d_{5/2})$ to be the lowest possible core excitation able to give 3^-. In principle, one could also obtain 3^- by promoting a proton from the $g_{7/2}$ orbital into the the $h_{11/2}$ orbital. However, $E(h_{11/2}) - E(g_{7/2})$ is somewhat larger than the similar term above and more importantly, it does not have $\Delta l = 3$.

Turning H' on, the shifts δE_I^* in the excited states of ^{147}Tb will not vanish and the lowest-order non-zero contributions to these shifts will come from the second-order in H'. There are four terms represented by four Feynman diagrams (see Hamamoto(1974), p.75) which all exhibit a one-particle line with angular momentum j, which is interpreted as an intermediate state (of spin j) of the single-particle potential. The first pair of diagrams involve vertices where j_1 and λ go to j (j representing a particle and a hole, respectively). The second pair of diagrams involve vertices where j_1 goes to λ and j (j representing a particle and a hole, respectively). The second-order contribution to the energy shifts of the septuplet (11/2, 3)I in ^{147}Tb, derived from the first pair of Feynman diagrams, is

$$\delta E_I^* = -\sum_j \frac{|\langle (j,\lambda)I|H'|j\rangle|^2}{E_j - E_{j_1} - \hbar\omega}\,\delta(j,I) \qquad (6.2.3)$$

where the sum above is over all single-particle orbits(particles and holes) with angular momentum j, as long as j = I(due to the presence of the Kroenecker delta). In the case of ^{147}Tb, experiments to date have only given I = 15/2 and 17/2 members(Broda et al, 1979). The contribution of the second pair of Feynman diagrams to the shifts above can be written

$$\delta E_I^* = -\sum_j \frac{|\langle (j\lambda)j_1|H'|j_1\rangle|^2}{E_j + \hbar\omega - E_{j_1}}(2j_1+1)\,W(\lambda j_1 j_1 \lambda; jI) \qquad (6.2.4)$$

where the sum is over all single-particle orbits j(including particles and holes) and W is the Racah coefficient. The final expression for δE_I^* should be the combination of (6.2.3) and (6.2.4). However, the presence of terms involving j = 15/2 and 17/2 in (6.2.3) makes the denominators of those terms much larger than the similar denominators in (6.2.4), where j encompasses levels near the Z = 64 gap(see Fig. 6.0.0). The denominators in (6.2.3) involve terms such as $E_{17/2} - E_{11/2} - \hbar\omega$, which can be several times larger than terms such as $E_{5/2} + \hbar\omega - E_{11/2}$, due to high-energy lying orbitals like $k_{17/2}$, or $j_{15/2}$, for example(see Lederer et al(1978)). In the light of the above considerations, the dominant contribution to the shift δE_I^* is the term in (6.2.4) with j = 5/2 .

The matrix element in (6.2.4) can be transformed according to

the following(see Hamamoto(1974), p.72):

$$|\langle (j_1\lambda) j_2 | H' | j_2 \rangle|^2 = \frac{2j_1+1}{2j_2+1} |\langle (j_2\lambda) j_1 | H' | j_1 \rangle|^2 = \tag{6.2.5}$$
$$= \frac{2\lambda+1}{2j_2+1} |\langle (j_1^{-1} j_2)\lambda | H' | \lambda \rangle|^2$$

The shift δE_I^*, thus becomes the following:

$$\delta E_I^* = (2*3+1) W(3\ 11/2\ 11/2\ 3; 5/2\ I) \frac{|\langle (d_{5/2}^{-1} h_{11/2}) 3 | H' | 3^- \rangle|^2}{E(h_{11/2}) - E(d_{5/2}) - E_{3^-}} \tag{6.2.6}$$

The treatment above thus gives the following expression for E_I^*, the energy of a level of total spin I, for the case of an odd nucleon orbiting a nearly spherical core(^{146}Gd here), when the perturbation above, H', is turned on:

$$E_I^* = E(h_{11/2}) + E_{3^-} + 7W(3\ 11/2\ 11/2\ 3; 5/2\ I)* \tag{6.2.7}$$
$$* \langle (d_{5/2}^{-1} h_{11/2}) 3 | H' | 3^- \rangle / [E(h_{11/2}) - E(d_{5/2}) - E_{3^-}]$$

The left part of Fig. 6.2.1 illustrates the comparison of experiment vs. the predictions from (6.2.7), which can give the excitations of the lowest members of the coupling of the $h_{11/2}$ proton to the 3^- phonon : I = 13/2, 15/2, 17/2(obtained from coupling 11/2 to $|I_z^3| = 1,2,3$). Experimentally(Broda et al, 1979), two states, $15^+/2$ and $17^+/2$, with energies 1265.7 and 2037.7 keV, respectively, have been identified. A 772.0 keV M1 transition was observed to de-excite the

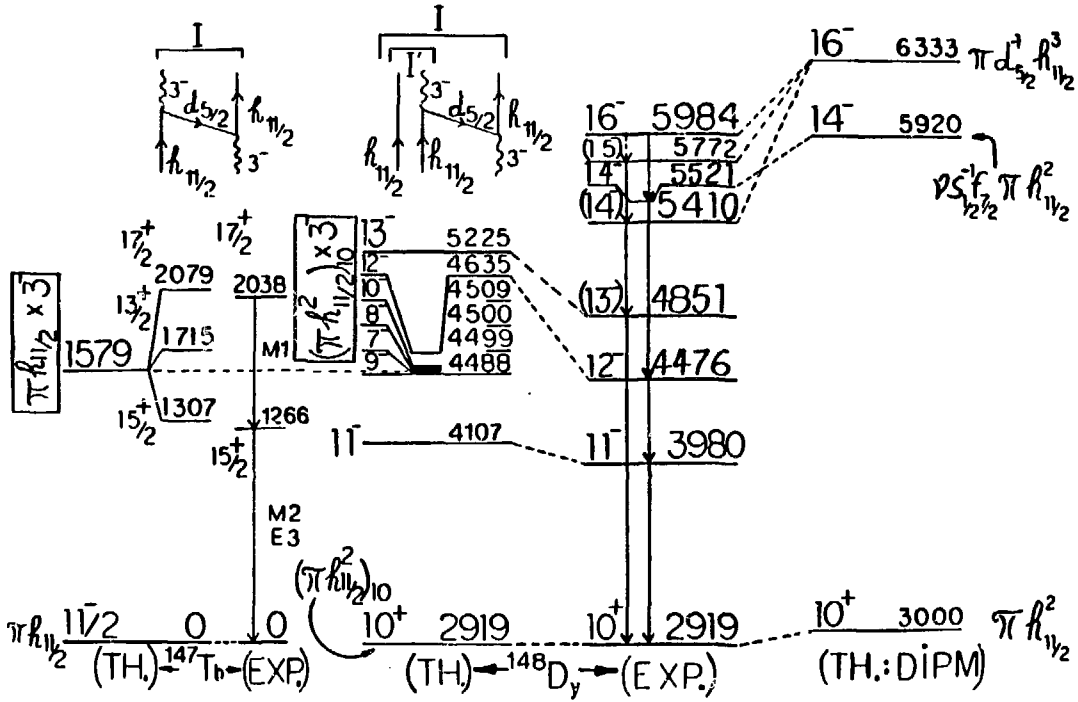
I
I'
3⁻
d5/2
h11/2
3⁻
h11/2
h11/2
3⁻
d5/2
h11/2
3⁻
π h11/2 x 3
1579
17/2+
2079
13/2+
1715
15/2+
1307
17/2+
2038
M1
1266
15/2+
M2
E3
(π h11/2²)10 x 3
13⁻
5225
12⁻
4635
10
4509
8
4500
7
4499
9⁻
4488
11⁻
4107
16⁻
5984
(15)
5772
14⁻
5521
(14)
5410
(13)
4851
12⁻
4476
11⁻
3980
16⁻
6333
π d5/2⁻¹ h11/2³
14⁻
5920
ν s1/2⁻¹ f7/2 π h11/2²
π h11/2
11/2⁻
0
0
(TH.) ←147Tb→ (EXP.)
10⁺
2919
10⁺
2919
(TH.) ←148Dy→ (EXP.)
10⁺
3000
π h11/2²
(TH.: DIPM)

Fig. 6.2.1

$17^+/2$ state to the $15^+/2$ state, which, in turn, populates the $11^-/2$ ground state via an $\Delta I = 2$, 1265.7 keV transition.

Calculating W(3 11/2 11/2 3;5/2 I) for I = 15/2 and 17/2(see Edmonds, 1974), gives -1/22 and +1/12, respectively, which says that for I = 15/2, the Pauli principle enhances(rather than reduces, as it does for I = 17/2) the $\pi d^{-1}_{5/2} h_{1/2}$ component in ^{146}Gd 3^- phonon, because the two $h_{11/2}$ protons are in a more anti-symmetric than symmetric arrangement. Thus, the state with I = 17/2 is pushed up in energy because of more Pauli blocking(than for I = 15/2). The coefficient 7W can be taken as a measure of Pauli blocking in this case(7W = 1 meaning complete Pauli blocking).

From the one-particle-phonon coupling, in the case of ^{147}Tb, one can use the experimental 772.0 keV splitting between the $17^+/2$ and $15^+/2$ states in taking the difference of equations (6.2.7), to calculate the second order matrix element in (6.2.6):

$$\left(\frac{|\langle(d^{-1}_{5/2}h_{11/2})3|H'|3^-\rangle|^2}{E(h_{11/2})-E(d_{5/2})-E_{3^-}}\right)_{exp} = \tag{6.2.8}$$

$$= (E^*_{17/2^-} - E^*_{15/2})/[7W(17/2) - 7W(15/2)] =$$

$$= 856.3 \text{ keV} .$$

From Fig. 6.0.0, $E(h_{11/2}) - E(d_{5/2}) = 2.5$ MeV, which then gives(after obtaining $E(H_{11/2}) - E(d_{5/2}) - E_{3^-} = 0.92$ MeV)

$$|\langle(d_{5/2}^{-1}h_{11/2})3|H'|3^-\rangle| \approx 0.86 \text{ MeV}. \qquad (6.2.9)$$

The Feynman diagram in Fig. 6.2.1, for ^{147}Tb, illustrates the particle-octupole vibration coupling(to second order): the incoming 3^- vibration disintegrates into a particle-hole pair, the hole of which recombines with the incoming particle making the outgoing vibration.

In the case of ^{148}Dy, one has two $h_{11/2}$ protons coupled to spin I', which couples to $\lambda = 3$ for a total spin I . The unperturbed wave function is now $|\Psi_0\rangle_I = (|(h^2_{11/2})_{I'}\rangle|\lambda\rangle)_I$. Similarly to the ^{147}Tb case, the unperturbed excitation energies of the members of the multiplet (I' 3)I are given by $E_0^I = E_{3^-} + E[(h^2_{11/2})_{I'}]$.

In a way similar to the ^{147}Tb case discussed above, one can obtain the second order correction to the energy E^* :

$$\delta E_I^* = \sum_{I'} \left[\frac{|{}_I\langle(d_{5/2}^{-1}h_{11/2})3|\langle(h^2_{11/2})_{I'}|H'|(h^2_{11/2})_{I'}\rangle|3^-\rangle_I|^2}{[(E(h_{11/2})-E(d_{5/2})+2E(h_{11/2}))-(E_{3^-}+2E(h_{11/2}))]} \right] B_F \qquad (6.2.10)$$

where B_F is the geometrical factor for the case of three-angular-momentum coupling($\vec{5}/2 + \vec{11}/2 = \vec{3}$; $\vec{11}/2 + \vec{11}/2 = \vec{I'}$ and $\vec{3} + \vec{I'} = \vec{I}$):

$$B_F = \begin{Bmatrix} 11/2 & 11/2 & I' \\ 11/2 & 5/2 & 3 \\ I' & 3 & I \end{Bmatrix} (\sqrt{2I'+1})^2 (\sqrt{2*3+1})^2 (\sqrt{2})^2 = \qquad (6.2.11)$$

$$= 14(2I' + 1)\begin{Bmatrix} 11/2 & 11/2 & I' \\ 11/2 & 5/2 & 3 \\ I' & 3 & I \end{Bmatrix}$$

The factor of $\sqrt{2}$ comes from the normalization of the wave function for the two $h_{11/2}$ outside protons; $\{\quad\}$ denote 9-j coefficients.

Using (6.2.12), one can simplify (6.2.11) to get(Kleinheinz, 1980):

$$\delta E^{*} = 14(2I' + 1)\begin{Bmatrix} 11/2 & 11/2 & I' \\ 11/2 & 5/2 & 3 \\ I' & 3 & I \end{Bmatrix}\frac{\left|\langle(d_{5/2}^{-1}h_{11/2})3|H'|3^{-}\rangle\right|^{2}}{\left[E(h_{11/2})-E(d_{5/2})-E_{3^-}\right]} \qquad (6.2.12)$$

One can see that the expression above involves the same interaction matrix element as in the ^{147}Tb case. The factor in front of it, B_F(here also referred to as the "blocking factor", just like in the ^{147}Tb case) requires computation of the 9-j coefficients for the appropriate I'. Table 6.2.1(a) lists the 9-j coefficients(C), B_F's and the corresponding second order energy shifts δE(keV), for the I'= = 0,2,4,6,8 and 10 cases.

Fig. 6.2.1 illustrates the comparison between the two-particle-octupole vibration coupling predictions and present experiment for the octupole vibrations built on the maximally aligned $(\pi h_{11/2}^{2})_{10}$ state. The energy of the 13^{-} member of such coupling would be, according to the treatment above,

Table 6.2.1

(a)Values of the 9-j coefficients C(11/2,11/2,I';11/2,5/2,3;I',3,I) for coupling the $h^2_{11/2}$ protons with I', to the octupole vibration 3^- of the ^{146}Gd core, for a resulting spin I. Also, values of the blocking factor, B_F(14(2I' + 1) X C) and the resulting level energy shift, δE(keV).(See text for discussion.)

	C	B_F	δE(keV)
I' = 10			
I = 7	-5.119×10^{-7}	-1.51×10^{-4}	+0.13
I = 8	$+6.562\times10^{-6}$	$+1.93\times10^{-3}$	+1.65
I = 9	-4.244×10^{-5}	-1.25×10^{-2}	-10.68
I = 10	$+1.772\times10^{-4}$	$+5.21\times10^{-2}$	+44.60
I = 11	-4.842×10^{-4}	-1.42×10^{-1}	-121.90
I = 12	$+5.411\times10^{-4}$	$+1.59\times10^{-1}$	+136.20
I = 13	$+2.886\times10^{-3}$	$+8.48\times10^{-1}$	+726.30
I' = 8			
I = 5	$+1.892\times10^{-6}$	$+0.45\times10^{-3}$	+0.39
I = 6	-2.163×10^{-5}	-5.14×10^{-3}	-4.40
I = 7	$+1.023\times10^{-4}$	$+24.40\times10^{-3}$	+20.80
I = 8	-2.030×10^{-4}	-48.30×10^{-3}	-41.40
I = 9	-2.600×10^{-4}	-61.80×10^{-3}	-52.90
I = 10	$+2.269\times10^{-3}$	$+54.00\times10^{-2}$	+462.20
I = 11	$+1.861\times10^{-3}$	$+44.29\times10^{-2}$	+379.10

	C	B_F	δE(keV)
I' = 6			
I = 3	-1.261×10^{-5}	-2.29×10^{-3}	-1.96
I = 4	$+3.784\times10^{-5}$	$+6.88\times10^{-3}$	+5.89
I = 5	$+8.577\times10^{-5}$	$+15.61\times10^{-3}$	+13.36
I = 6	-7.114×10^{-4}	-12.94×10^{-2}	-110.76
I = 7	$+1.072\times10^{-3}$	$+19.51\times10^{-2}$	+167.00
I = 8	$+2.988\times10^{-3}$	$+54.38\times10^{-2}$	+465.49
I = 9	$+1.290\times10^{-3}$	$+23.48\times10^{-2}$	+200.99
I' = 4			
I = 1	-1.603×10^{-4}	-2.01×10^{-2}	-17.21
I = 2	$+4.810\times10^{-4}$	$+6.06\times10^{-2}$	+51.87
I = 3	-5.029×10^{-4}	-6.34×10^{-2}	+54.27
I = 4	-8.964×10^{-4}	-11.29×10^{-2}	-96.64
I = 5	$+2.787\times10^{-3}$	$+35.12\times10^{-2}$	+300.62
I = 6	$+3.544\times10^{-3}$	$+44.65\times10^{-2}$	+382.20
I = 7	$+1.085\times10^{-3}$	$+13.67\times10^{-2}$	+117.01
I' = 2			
I = 1	$+1.299\times10^{-3}$	$+9.09\times10^{-2}$	+77.81
I = 2	-3.896×10^{-3}	-27.27×10^{-2}	-233.43
I = 3	$+4.636\times10^{-3}$	$+32.45\times10^{-2}$	+277.77
I = 4	$+5.574\times10^{-3}$	$+39.02\times10^{-2}$	+334.01
I = 5	$+1.482\times10^{-3}$	$+10.37\times10^{-2}$	+88.77
I' = 0			
I = 3	$+1.190\times10^{-2}$	$+1.67\times10^{-1}$	+142.60

(b)Values of the 9-j coefficients C(11/2,11/2,I';11/2,5/2,3;I",3,I) used in the diagonalization of the total Hamiltonian for the $(\pi h^2_{11/2})_{I',I''} \times 3^-$ system in the two-dimensional basis of states with I',I"= 8 and 10, for the cases of total spin I = = 10 and 11. Also, values of the corresponding blocking factor, $B_F(=14\sqrt{(2I'+1)(2I''+1)} * C)$ and resulting level energy shift, δE(keV).(See text for discussion.)

	C	B_F	δE(keV)
I'= 10 ; I"= 8			
I = 10	-4.333×10^{-4}	-1.146×10^{-1}	-0.098
I = 11	$+1.897\times10^{-3}$	$+5.018\times10^{-1}$	+0.429
I'= 8 ; I"= 10			
I = 10	-4.333×10^{-4}	-1.146×10^{-1}	-0.098
I = 11	$+1.897\times10^{-3}$	$+5.018\times10^{-1}$	+0.429

$$E^{*}_{13^-}(\text{oct.}) = E[(h^2_{11/2})_{10^+}] + E_{3^-} + \tag{6.2.13}$$

$$+ 14(2\times10 + 1)\begin{Bmatrix} 11/2 & 11/2 & 10 \\ 11/2 & 5/2 & 3 \\ 10 & 3 & 13 \end{Bmatrix} * 856.3 \text{ keV}$$

where the value of 856.3 keV from the ^{147}Tb case was used for the term $|\langle(d^{-1}_{5/2}h_{11/2})3|H'|3^-\rangle|^2/[E(h_{11/2})-E(d_{5/2})-E_{3^-}]$, and $E[(h^2_{11/2})_{10^+}]$ is the energy of the 10^+ level (see Fig. 6.2.1).

As far as the 12^- and 13^- members of the octupole coupling are concerned, they can only come from the 3^- vibration built on the 10^+ state. However, the 11^- member can also be obtained from building the 3^- vibration on the configuration $(\pi h^2_{11/2})8^+$, so, one must diagonalize the total Hamiltonian in the two-dimensional basis formed by the perturbed wave functions $|\Psi(I')\rangle_I$ and $|\Psi(I'')\rangle_I$, where I' and I" represent the possible spin couplings of the $\pi h^2_{11/2}$ pair such that a total spin of I (in this case I = 11) is reached.

If H is the total Hamiltonian (including the perturbation H') then one has:

$$H \sum_{I'} |\Psi(I')\rangle_I = E_I \sum_{I'} |\Psi(I')\rangle_I \tag{6.2.14}$$

and similarly for I", where E_I is the excitation energy of the perturbed system in the state of total spin I. Multiplying both sides of (6.2.15) by ${}_I\langle\Psi(I'')|$ and using the hermiticity of H, one finds E_I

by solving the following equation for the lowest E_I:

$$\det\begin{vmatrix} {}_I\langle\Psi(I')|H|\Psi(I')\rangle_I - E_I & {}_I\langle\Psi(I')|H|\Psi(I'')\rangle_I \\ {}_I\langle\Psi(I'')|H|\Psi(I')\rangle_I & {}_I\langle\Psi(I'')|H|\Psi(I'')\rangle_I - E_I \end{vmatrix} = 0 \qquad (6.2.15)$$

The matrix elements on the diagonal represent the perturbed energies of the state of I = 11, when the two $h_{11/2}$ protons are coupled to I'= 10 and I"= 8, respectively. Their actual expressions are $E_{10^+} + E_{3^-} + \delta E_{10,10}$ and $E_{8^+} + E_{3^-} + \delta E_{8,8}$, respectively, where E_{3^-} is the unperturbed 3^- excitation and the two δE's refer to the second order perturbation energy shifts when I'= 10 and 8, respectively(see Table 6.2.1(a)). The off-diagonal elements reduce to only $\delta E_{10,8}$ and $\delta E_{8,10}$, respectively, because the matrix element of H between unperturbed states of different spin couplings of $\pi h^2_{11/2}$ configuration vanishes, so the zeroth and first order approximations to the off-diagonal elements vanish, leaving only the second order approximation. These "off-diagonal" shifts have the same expression as (6.2.12), except for the blocking factor, B_F, which has the form

$$B_F = 14\sqrt{(2I'+1)(2I''+1)}\begin{Bmatrix} 11/2 & 11/2 & I' \\ 11/2 & 5/2 & 3 \\ I'' & 3 & I \end{Bmatrix} \qquad (6.2.16)$$

This can be obtained in the same manner as (6.2.11), to which the expression above reduces for I'= I". Table 6.2.1(b) shows the numerical values for B_F's and the corresponding δE's, for the cases I'= 10 and

I"= 8(and when I' and I" are switched) for I = 11 and 10. Since the 9-j coefficients calculated in Table 6.2.1(b) are the same upon switching I' and I"(Edmonds, 1974), the off-diagonal elements in (6.2.16) are the same.

Using Table 6.2.1(a) and (b), one can actually insert the proper numbers(in keV) in (6.2.16), and thus one must solve the following:

$$\det \begin{vmatrix} 4377 - E_I & 429.5 \\ 429.5 & 4790 - E_I \end{vmatrix} \qquad (6.2.17)$$

which gives as the lowest E_I, the value of about 4107 keV for the "diagonalized" 11^- state in the two-dimensional basis discussed above. The same treatment for the member with I = 10, gives a lowest "diagonalized" excitation energy of about 4509 keV.

Since there were not any experimental counterparts observed for the members with I = 7,8 and 9, and since their "diagonalization" would involve solving determinant equation of third degree(for I = 8 and 9, since they can be formed from I'= 10, I"= 8 and I'"= 6) and fourth degree(for I = 7, since it can be formed from I'= 10, I"= 8, I'"= 6 and I' = 4), it was deemed unnecessary to get involved in such complicated algebra. Therefore, Fig. 6.2.1 depicts the "diagonalized" members with I = 10 and 11, as well as the I = 12 and 13 members, which needed no diagonalization since they can only come from I'= 10. As an example, for I = 9, one would have to diagonalize the following matrix:

$$\begin{pmatrix} E_{10} + E_3 + \delta E_{10,10} & \delta E_{10,8} & \delta E_{10,6} \\ \delta E_{8,10} & E_8 + E_3 + \delta E_{8,8} & \delta E_{8,6} \\ \delta E_{6,10} & \delta E_{6,8} & E_6 + E_3 + \delta E_{6,6} \end{pmatrix}$$

where, as we saw in the cases before, the off-diagonal elements which are symmetrical with respect to the diagonal are equal. In an analogous way, the 4 X 4 matrix corresponding to the I = 7 case can easily be found. It can be seen that all products involving off-diagonal elements from a matrix such as the one above, are considerably smaller than the product of the diagonal elements. For example, for the cases I = 8 and 9, the smallest value for E_I is, without making a large error, $E_6 + E_3 + \delta E_{6,6}$, where $\delta E_{6,6}$ can be calculated from Table 6.2.1(a), giving E_I's of ≈ 4782 and 4518 keV, respectively. In the same manner, one gets E_I ≈ 4123 keV for the 7^- member.

In the present experiment, it was found(in agreement with Haas et al, 1981 and Julin et al, 1982(p.78)) that there exist a 1061.1 keV stretched E1 transition de-exciting from the 3980.2 keV 11^- level to the 2919.1 keV 10^+ level and a 495.8 keV stretched M1 transition de-exciting from the 4476.0 keV 12^- level to the 3980.2 keV 11^- level. In addition, it was tentatively found that a 1932.1 keV stretched E3 transition(E2 is equally plausible; see section 5.1) de-excites from the 4851.2 keV 13^- level, also to the same 10^+ level. It seems that these three transitions may be members(so far, the only ones) of such a $(\pi h^2_{11/2})_{10}$ X 3^- coupling. The arguments in their favor are their all de-exciting to the 2919.1 keV

10^+ level (on which the considered $\lambda = 3$ vibrations are built) and the marginal agreement for their energy splitting between theory and experiment: 590 and 528 vs. 375 and 496 keV, respectively.

The different shifting of the $(\pi h^2_{11/2})_{I'} \times 3^-$ multiplet states in energy, is entirely an angular momentum recoupling problem in the present case, where the Pauli interference between the $h_{11/2}$ nature of the collective 3^- vibration and the $h_{11/2}$ proton outside the core, is strongly manifested. All energy shifts involve the same matrix element (6.2.10), differing only in the 9-j coefficients, i.e. in the way $\vec{I}'(= \vec{11}/2 + \vec{11}/2)$, $\vec{3}$ and $\vec{I}''$ couple for a total $\vec{I}$. The 13^- component is pushed up rather high above the unperturbed 3^- state built on the 10^+ level, because of the Pauli blocking, which is stronger in ^{148}Dy, with two $h_{11/2}$ protons (maximally aligned) outside the ^{146}Gd core, than in the case of ^{147}Tb, which only has one such $h_{11/2}$ proton. This is shown by the blocking factor, $B_F = 0.85$ (see Table 6.2.1 for $I' = 10$ and $I = 13$), considerably higher than the corresponding highest $B_F = 0.58$ for ^{147}Tb (for $I = 17/2$).

In conclusion, it is possible that we have observed the three highest-spin members of the $(\pi h^2_{11/2})_{10} \times 3^-$ coupling in ^{148}Dy. All three observed members above are yrast levels, and comparison with theory is not unreasonable. The calculated energies for the other members of this coupling (the $I = 7$, 8 and 9 not being the diagonalized values, as discussed above) are also displayed in Fig. 6.2.1, which also shows the corresponding Feynman diagram in the case of ^{148}Dy. The 3^- state below the 480 nsec 10^+ isomer (see

Fig. 4.1.1) could be interpreted as the 3^- vibration built on the $(\pi h^2_{11/2})_{0^+}$. The excitation energy of 1687.5 keV of the 3^- level in ^{148}Dy is higher than the 1579.3 keV value for the 3^- octupole excitation in ^{146}Gd, fact which could be interpreted as due to the Pauli blocking. The B_F factor for this case(see Table 6.2.1) is 2/12, (considerably smaller than for the I' = 10 case, since the two $h_{11/2}$ protons have their spins anti-parallel here), which states that two of the twelve $h_{11/2}$ protons are present in the 0^+ ground state of ^{148}Dy. The calculated shift, δE = +142.6 keV compares with the experimental $E_{3^-}(^{148}Dy) - E_{3^-}(^{146}Gd)$ = 108.2 keV value. The experimental value above is smaller than the one predicted, possibly because the valence proton pair in ^{148}Dy partially occupies the $s_{1/2}$ and the $d_{3/2}$ orbitals too. This means less involvement of the proton pair in the $h_{11/2}$ orbital, resulting in a less strong Pauli blocking, which means a smaller shift from the unperturbed $E_{3^-}(^{146}Gd)$ value.

Fig. 6.2.1 also shows, on the right side, the 10^+, 14^- and 16^- states of "maximal weight" given by the deformed independent particle model(DIPM)(Døssing, private communication, 1984), of which the experimental levels connected might be components. The single-particle configurations are given on the right of the DIPM levels, and one can see that the 16^- level has the same configuration as the members of the $(\pi h^2_{11/2})_{I'} \times 3^-$ coupling. However, the latter(ranging in spin from 7 through 13) have a more collective nature than the former, which is pure single-particle. This is so, because the ^{148}Dy calculations use the experimental matrix element

from ^{147}Tb, which fairly probably involves an octupole vibration of the ^{146}Gd core. However, the existence of a predominant component of the 3^- state might seem to make this state not highly collective. In contrast, in ^{208}Pb, the 3^- state can be expressed by a combination of many particle-hole configurations, none of which is predominant, which is to be expected for a highly collective state. However, the 3^- collectivities in ^{146}Gd and ^{208}Pb are very similar, the experimental B(E3)'s being about 37 and 32 W.u., respectively(Lunardi et al, 1984 and Hamamoto, 1974, respectively). According to the results in section 5.2, the 1932.1 keV E3 transition has an upper limit on its meanlife(like the other transitions above the 10^+ level) of about 5 nsec, which translates into a half-life of 3.5 nsec. Fig. 5.2.15 gives a half-life of 9 nsec for a 1932 keV E3 single-particle transition. Thus, not much collectivity is needed to make the experimental information about the lifetime of the 1932.1 keV transition match with the possibility that this transition can be an E3 .

Next section deals with the DIPM. The comparison to experiment is extended beyond the 16^- level.

6.3 The Use of the Deformed Independent Particle Model (DIPM) for the Levels Not Explained in Previous Section

This model attempts to describe "non-rotating" stationary states (in the vicinity of ^{146}Gd)of "maximal weight" in terms of some mean static field. The corresponding single-particle density, as well as an appropriate static mean field are symmetric with respect to that quantization axis. Description in terms of a mean static field are sometimes common for aligned shell model states. However, any realistic description(Neergard, 1983) of a non-rotating nucleus(such as ^{148}Dy) must always consider strong two-body correlations induced by nucleon interactions in mutually reversed time orbits.

The version of the DIPM used here replaces the self-consistent determination of the mean field by a phenomenological single-particle potential and a Strutinsky renormalization procedure(Døssing et al, 1980 and Neergard, 1983). The theoretical formulation of the DIPM version used here has been done in detail in literature(see references above) and only the very basic ideas will be presented here.

The DIPM states are defined to have maximal magnetic quantum number along the symmetry axis, i.e.

$$I \equiv M \equiv \langle \sum_i m_i a_i^\dagger a_i \rangle_\gamma = \sum_{i \in S} m_i \qquad (6.3.1)$$

where m_i is the projection of the single-particle spin j_i on the

symmetry axis, $a_i^\dagger$ and a_i are the single-particle creation and annihilation operators, respectively, and S is the set of all single-particle labels. Such states are called states of "maximal weight". While I increases, more and more pairs must be broken in order to satisfy (6.3.1) with the available orbitals. This increases the number of possibilities for the respective quasi-particles to combine their spins into stretched configurations. Thus, in the high spin regions of non-rotating nuclei especially, it is expected that aligned(or nearly so) configurations will dominate the yrast lines, because of the high angular momenta involved in these configurations.

Configurations responsible for such maximal weight states are obtained by successively promoting particles from the core(thereby creating holes) such that the least amount of energy is expended for the corresponding spin achieved. This is so since these states must primarily explain yrast levels. For example, after the $(\pi h_{11/2}^2)$ excitations exhaust the available spin(0,2,4,6,8 and 10), the least excitation able to increase the spin over 10ħ is the one obtained by elevating a $d_{5/2}$ proton into the $h_{11/2}$ orbital across the Z = 64 gap. This configuration, $\pi d_{5/2}^{-1} h_{11/2}$, has a pure single-particle nature, with a maximum total spin of 8 and a minimum of 3. It is also(as we saw in section 6.2)the most predominant component of the collective 3^- octupole vibration of the ^{146}Gd core.

The experimental levels 3^-,5^- and 7^- could be interpreted as component states of the maximally aligned $(\pi d_{5/2}^{-1} h_{11/2})8^-$

configuration. However, the previous section presented an interpretation for the 3^- level, while the 5^- and 7^- levels might have the single-particle configurations $(\pi h_{11/2} s_{1/2})5^-$ and $(\pi h_{11/2} d_{3/2})7^-$, respectively, since, as discussed in the previous section, the valence proton pair partially occupies the $s_{1/2}$ and $d_{3/2}$ orbitals.

The maximum spin that each such DIPM single-particle configuration has can be determined by the usual rule governing the angular momentum addition for configurations j^N, with $N > 2$: The number of permissible states of M(where $M = \sum_i m_i$) in the m-scheme is the number of all possible sets of N half-integers, m_1, $m_2, \ldots, m_N$, such that no two m_i's are the same and provided two sets obtainable from each other by permutations are identical. For example, Fig.6.2.1 shows the configuration for the 16^- maximal weight state to be $\pi d_{5/2}^{-1} h_{11/2}^3$. The maximum M one can get from $(11/2)^3$ is $11/2 + 9/2 + 7/2 = 27/2$, which added onto the maximum 5/2 gives a maximum spin of 16 for that state. The configuration $h_{11/2}^3$ cannot have all half-integer spins allowed(see de-Shalit(1974), chapter IV). However, inclusion of $d_{5/2}^{-1}$ can easily be seen to make all integer-spin(0 through 16)states as possible components of the 16^- maximal weight state with the single-particle configuration above.

The energy of such a maximal weight configuration was taken to be:

$$E = \langle H \rangle_{\mathcal{N}} - E_{Str.} + E_{LD} , \qquad (6.3.2)$$

which was minimized with respect to the matrix elements between time-reversed states of the neutron and proton single-particle Hamiltonian, and also with respect to β, the shape parameter of the single-particle potential. Thus, the DIPM states obtained in this way have the lowest energy for the respective single-particle configuration. This must be true, since the largest overlap among nucleon wave functions occurs when the respective m's are parallel or anti-parallel. The anti-parallel m-alignment, however, gives states of considerably higher energy and lower spin, and, hence, not of interest here. H represents the single-particle plus pairing Hamiltonian, while Ψ is the wave function of the stationary state of independent quasi-particles in some single-particle and pair field. The other two terms in (6.3.2) are the Strutinsky smooth sum of the energies of the lowest N(this case 82) neutron and Z(this case 66) proton states and the sum of the surface and Coulomb energies of a liquid drop with the shape of the single-particle potential, respectively.

Fig. 6.3.1 shows the single-particle energies vs. β(for neutrons only), and from such a plot one can find the energies of the single-particle orbitals for the corresponding β, responsible for the various configurations. This energy term would be the first one in (6.3.3) below, which gives the exact expression for the single-particle Hamiltonian, including pairing(for detailed treatment see Døssing et al, (1980) and Neergard(1983)):

$$h = \epsilon_{sph.}(N_{sh.}, j^2, m_t) + \sum_{k=x,y,z}(\omega_k - \delta_{m_t})(b_k^{+} b_k + 1/2) \qquad (6.3.3)$$

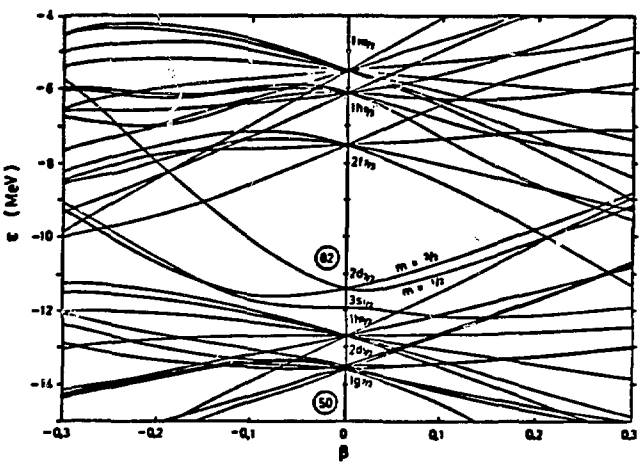
-4
-6
-8
-10
-12
-14
ε (MeV)
-0,3
-0,2
-0,1
0
0,1
0,2
0,3
β
82
50
1h11/2
1h9/2
2f7/2
2d3/2
3s1/2
1h11/2
2d5/2
1g7/2
m = 3/2
m = 1/2

Fig. 6.3.1

where $N_{sh.} = \sum_{k=x,y,z} b_k^{\dagger} b_k$, $\omega_x = \omega_y = q^{1/3}\mathring{\omega}_{m_t}$, $\omega_z = q^{-2/3}\mathring{\omega}_{m_t}$ and $\mathring{\omega}_{m_t} = (41\text{MeV}/A^{1/3})[1 - (2m_t/3)(N - Z)/A]$, where q is the ratio of the distance between poles to the equator diameter which enters in $\beta(\beta = (16\pi/5)^{1/2}(q - 1)/(q + 2))$ and the isospin z-component $m_t = 1/2$ for neutrons and $-1/2$ for protons. A particular choice for $\varepsilon_{sph.}$ would be the Nilsson Hamiltonian. The important orbitals taken into the DIPM calculations are $1g_{7/2}$, $2d_{5/2}$, $1h_{11/2}$, $3s_{1/2}$ and $2d_{3/2}$ for the protons and $1h_{11/2}$, $3s_{1/2}$, $2d_{3/2}$, $2f_{7/2}$, $1h_{9/2}$ and $1i_{13/2}$ for the neutrons(see Fig. 6.0.0). I refer to the appropriate literature(Dørssing et al, 1980) as to how the detailed calculations of the enrgies of such orbitals were made, since this goes beyond the scope of the present work.

Fig. 6.3.2 depicts a plot of the experimental energies vs. $I(I + 1)$ for ^{148}Dy(from the present work), from which an average of the $\left(\frac{2\mathcal{J}_{eff}^{(1)}}{\hbar^2}\right)_{yr} = 95.7$ MeV^{-1} was obtained as the inverse of the average of the three slopes indicated on the plot. Each one of these slopes was obtained from a linear regression done for a group of level energies vs. $I(I + 1)$, lying as close as possible to a straight line. For each of the slopes obtained, only yrast levels were considered. The average value of $\left(\frac{2\mathcal{J}_{eff}^{(1)}}{\hbar^2}\right)_{yr}$ over the whole range of experimental spins does reach the spherical rigid-body value $(2\mathcal{J}_0/\hbar^2) = 107.5$ MeV^{-1}(obtained from the relations in chapter 1, p.9), but not the liquid drop value of 122-140 MeV^{-1}(see Dørssing et al(1980). Using the expression for the moment of inertia for an oblate shape spinning with respect to its symmetry axis(see (1.0.6), with $\mathcal{J}_0$ given above, one gets $\beta = -0.18$.

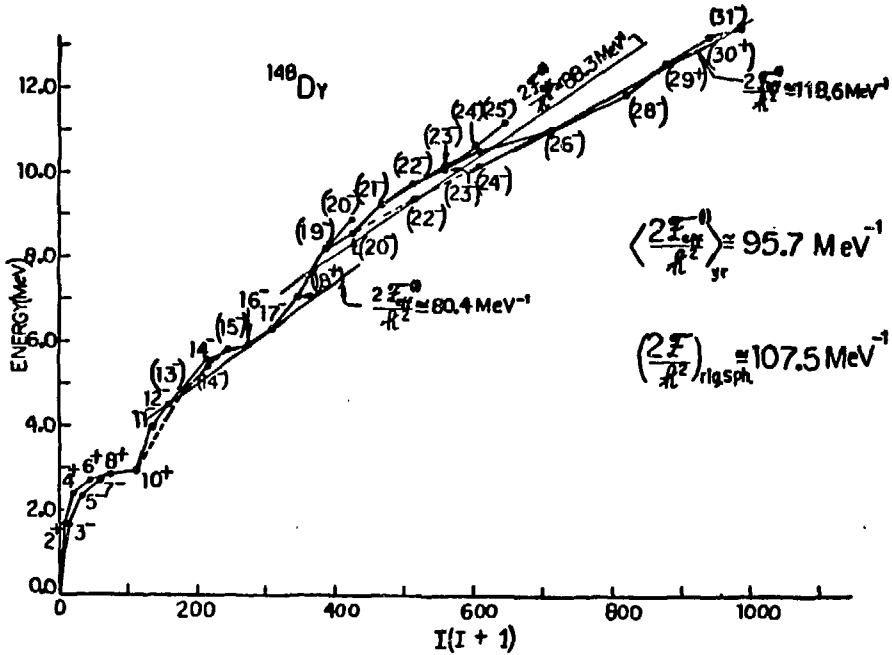
148Dy
ENERGY(MeV)
I(I + 1)
0.0
2.0
4.0
6.0
8.0
10.0
12.0
0
200
400
600
800
1000
2+
3−
4+
5−
6+
7−
8+
10+
11−
12−
(13−)
14−
(14−)
(15−)
16−
17−
(18+)
(19−)
(20+)
(20−)
(21−)
(22−)
(22−)
(23−)
(23−)
(24−)
(24−)
(25−)
(26−)
(28−)
(29+)
(30+)
(31−)
2ℱ*/ħ² ≃ 80.4 MeV⁻¹
2ℱ*/ħ² ≃ 88.3 MeV⁻¹
2ℱ*/ħ² ≃ 118.6 MeV⁻¹
⟨2ℱ*eff/ħ²⟩yr ≃ 95.7 MeV⁻¹
(2ℱ/ħ²)rig.sph ≃ 107.5 MeV⁻¹

Fig. 5.3.2

Fig. 6.2.1 shows the 10^+, 14^- and 16^- levels given from *DIPM plotted on the same diagram with the two-particle-octupole* coupling levels. This was done because the experimental levels 14^-(both), 15^- and 16^- are involved in the two-particle-octupole coupling picture: the 5521 keV 14^- populates the octupole coupling component 12^-, while the 5410 keV 14^-, 5772 keV 15^- and 5984 keV 16^- levels have been found to populate the highest member(13^-) of the presumed octupole coupling(see Fig. 6.2.1), while themselves being possible components of the DIPM 6333 keV 16^- level. The 6263 keV 17^- experimental level is probably a component of the DIPM 17^- state, and they are both shown in Fig. 6.3.3 This figure also shows DIPM calculations through the 26^+ maximal weight state(Døssing, 1984, private communication). Connections are made to various experimental levels, as close in energy as possible to theoretical values, deemed as possible components of the indicated DIPM configurations.

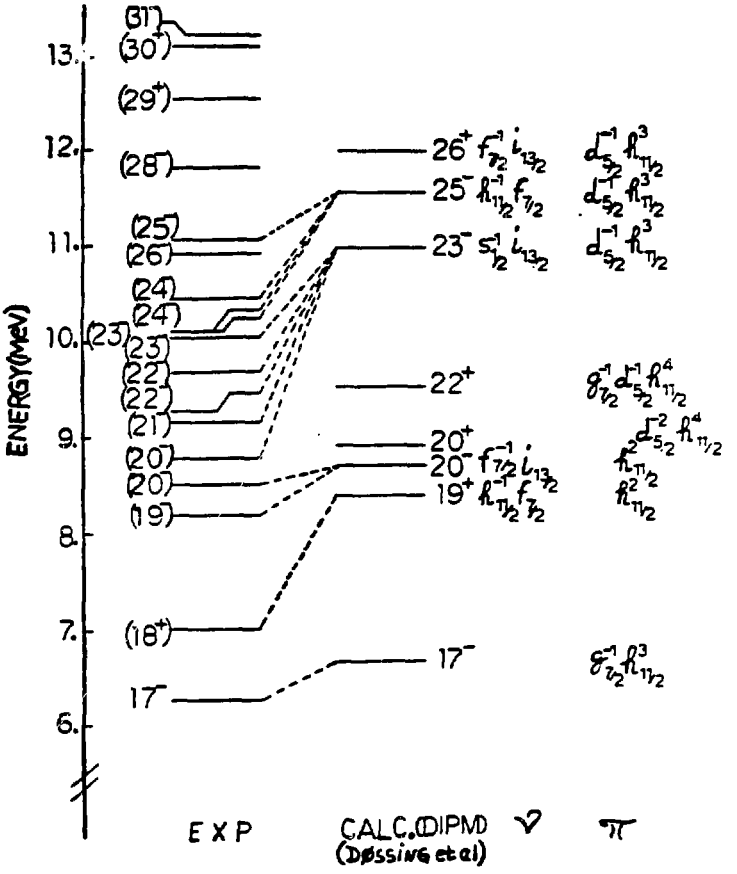
ENERGY(MeV)
13.
12.
11.
10.
9.
8.
7.
6.
(31)
(30+)
(29+)
(28-)
(25)
(26)
(24)
(24)
(23)
(23)
(22)
(22)
(21)
(20)
(20)
(19)
(18+)
17-
26+ f7/2-1 i13/2
25- h11/2-1 f7/2
23- s1/2-1 i13/2
22+
20+
20- f7/2-1 i13/2
19+ h11/2-1 f7/2
17-
d5/2-1 h11/2 3
d5/2-1 h11/2 3
d5/2-1 h11/2 3
g7/2-1 d5/2-1 h11/2 4
d5/2-2 h11/2 4
h11/2 2
h11/2 2
g7/2-1 h11/2 3
EXP
CALC.(DIPM)
(Døssing et al)
ν
π

Fig. 6.3.3

Appendix

A schematic diagram of the electronics set-up used in the data acquisition is shown in Fig. A.1 . The fast outputs from all 12 Ge's were timed within about 1 nsec(with the help of a multichannel analyzer) in their arrival at the inputs of the constant-fraction discriminators(C.F.D.)(after being properly differentiated and integrated by the time-to-filter amplifiers(T.F.A.)). The signals from the six phototubes of a BGO element were "mixed" at the pre-amplifier(see Fig. A.1) and run through C.F.D. before being sent to the anti-coincidence units, where the overlapping of their pulse(about 150 nsec long) with the fast Ge pulse prevented the anti-coincidence unit from providing an output. Thus, only Ge pulses not arriving at the same time (within about 150 nsec) with BGO-element pulses went on through the anti-coincidence unit(see Fig. A.1) to the "OR" and the "Multiplicity Logic" units. The time-to-amplitude converters(T.A.C.) (ORTEC-made) had their ranges set at 100 nsecs. The output of the "OR" box(a FAN-IN/FAN-OUT, ORTEC-made) provided the stop of the Ge - Ge TAC. Had the "OR" started the GE - Ge TAC, it would have introduced considerable error in the start of the TAC, since it fired all the time. The "Multiplicity Logic Unit", to which all the 12 non-coincident with-the-BGO-element Ge's had their fast outputs inputted, was set on > 1(i.e. it fired if at least two inputs were present) and started both the Ge - Ge and the RF - Ge TAC's(the latter being stopped by the arrival of the RF).

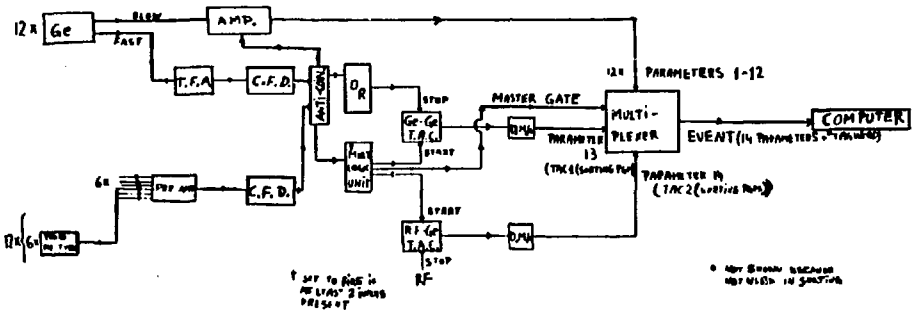
12 x
Ge
SLOW
FAST
AMP.
T.F.A
C.F.D.
ANTI-SUM
OR
STOP
Ge-Ge
T.A.C.
START
ANTI SUM UNIT
MASTER GATE
D/M
PARAMETER 13
(TAC 1 (LOSING PUL
12 x
PARAMETERS 1-12
MULTI-PLEXER
EVENT (14 PARAMETERS
COMPUTER
PARAMETER 14
(TAC 2 (LOSING PUL
Ge
PRE AMP
C.F.D.
12 x Ge
START
RF-Ge
T.A.C.
STOP
RF
D/M

Fig. A.1

The output of the "Multiplicity Logic Unit" was essentially the Master Gate(MG), since no event was written on tape unless at least at least two Ge's fired. Using a fast oscilloscope(capable of triggering on signals at least as fast as 5 nsec) it was arranged that the MG overlap the slow outputs of all the 12 Ge's as well as the outputs out of the delay-mixer-gates (D.M.G.), out of which the two TAC's were directed to the multiplexer, where all the parameters making up a typical event were collected in order to be sent to the ModComp computer to be written on tape.

The sorting of the data acquired as described above, was made with the help of the "EVA5" programs(see Belshe, 1984), of which two examples are shown on the last pages of the appendix. The first was used to sort "all the Ge's"(in order to construct the level scheme) while the second was used in the "angular correlation" sorting, where only the Ge's in the backward direction and those at 90° with respect to the beam axis were used. The variables "TAC1" and "TAC2" refer to the Ge - Ge and RF - Ge TAC's, respectively, while the gates "SM1", "SM2" and "SM3" refer to the gates 1, 2 and 3, respectively placed on the RF - Ge TAC(see chapters 3 and 5).

The sorting language is simple enough that one can follow the sorting algorithms without further explanation. The sorting programs shown corrected the Ge calibration for the "zero-offset" by adding or subtracting from the channel number written on tape(which was a number from zero to 4095) for each Ge, the ratio of the zero-offset to the gain of the respective Ge(represented by the "DATA OFFSET"'s in the sorting programs(see the last pages of the Appendix). This

point can be easily seen from Fig. A.2(a), which graphically shows the relation between the energy of the γ-ray detected by the detector in question and the channel number where that pulse height was stored. In the example in Fig. A.2(a), one can easily see that the ratio of the magnitude of the zero-offset to the gain needs to be subtracted from each channel value in order to make the E_γ vs. channel line pass through the origin.

The average gain of all 12 Ge's was found to be E_γ= 1.199*Channel + 0.0(for 2048-channel Ge spectra), from ^{152}Eu calibration performed at the end of the run. Fig. A2(b) illustrates the accuracy of the calibration: The ordinate represents E_γ(run) - E_γ^L(keV), while the abscissa represents E_γ(keV); E_γ(run) represents the centroids(in keV) of the ^{152}Eu points, obtained with the above calibration, while E_γ^L represents the ^{152}Eu γ-ray energies according to Lederer et al(1978).(The ^{152}Eu γ-ray energies used are: 121.8, 244.7, 344.3, 411.1, 444.0, 488.5, 778.9, 867.4, 963.4, 1085.8, 1112.1, 1212.9, 1299.2 and 1408.0 keV.) The deviations of all E_γ's > 121.8 keV from the accepted values are displayed.

In Fig. A.3 is shown an example of the use of the peak-curve-fitting routine which can be used to find the net area(i.e. above the background) under the γ-ray peaks. This is achieved with the help of the spectrum analysis "SUSIE"(Belshe, 1984). The command "FIT" fits a curve of the shape A + Bx + Cexp[-(x - D)^2/E] + up to two more such gaussians(A, B, C, D, E, etc. are constants) to the region which the user marks with the help of screen cursors: two marks on the left and right of the peak(s) to be fitted(for the linear background, A +

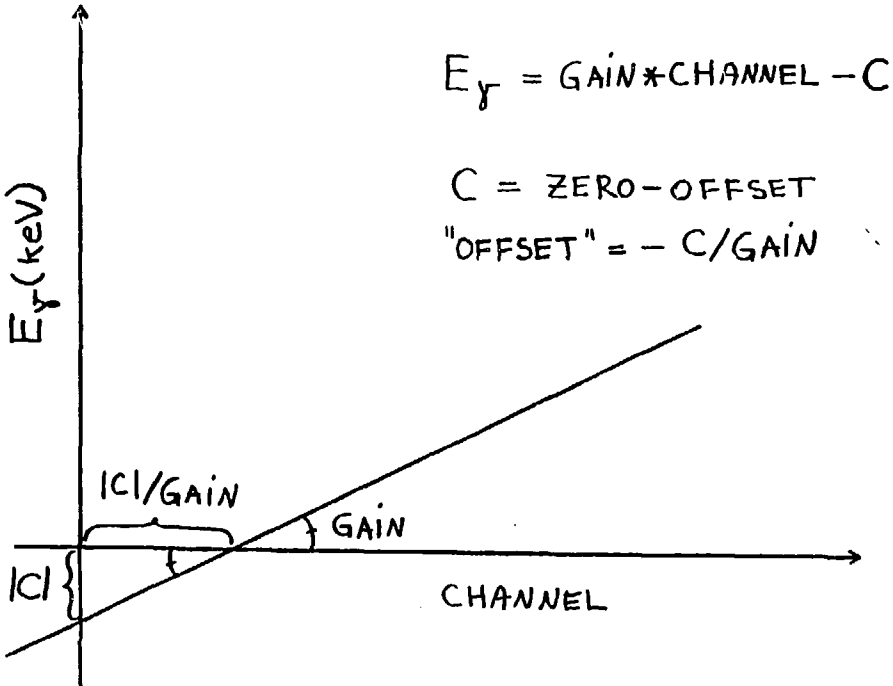
$E_\gamma = GAIN * CHANNEL - C$
$C = ZERO-OFFSET$
"OFFSET" $= -C/GAIN$
E_γ (keV)
$|C|/GAIN$
GAIN
$|C|$
CHANNEL

Fig. A.2(a)

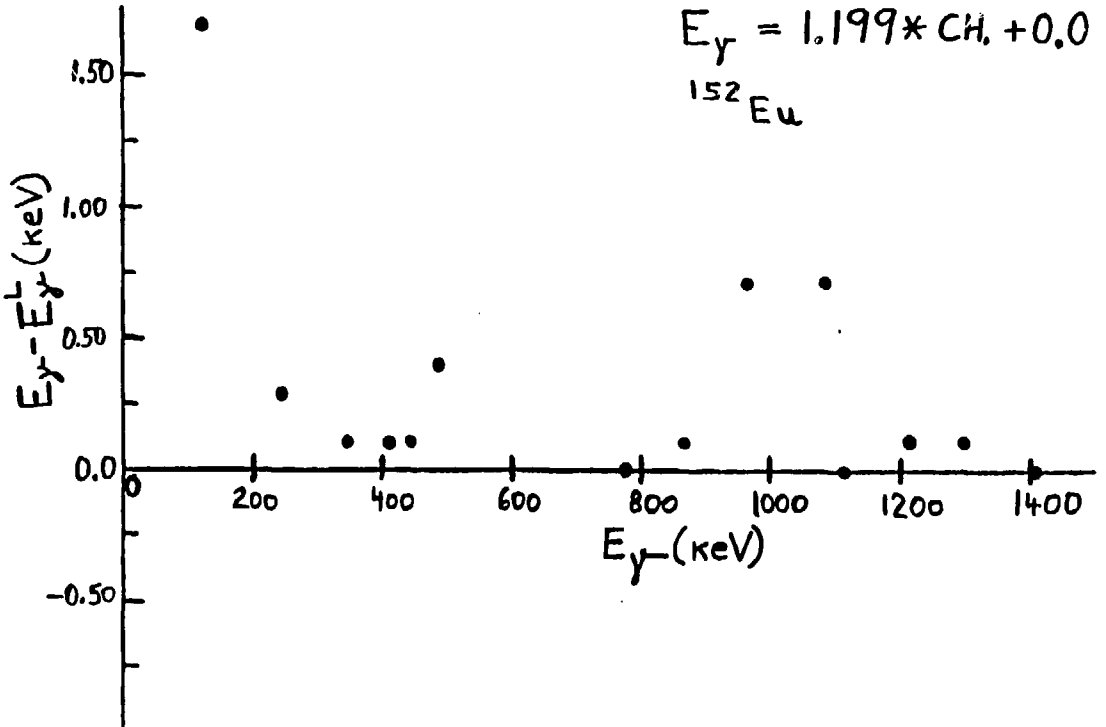
$E_\gamma = 1.199 * CH. + 0.0$
^{152}Eu
1.50
1.00
0.50
0.0
−0.50
$E_\gamma - E_\gamma^L$ (keV)
0
200
400
600
800
1000
1200
1400
E_γ (keV)

Fig. A.2(b)

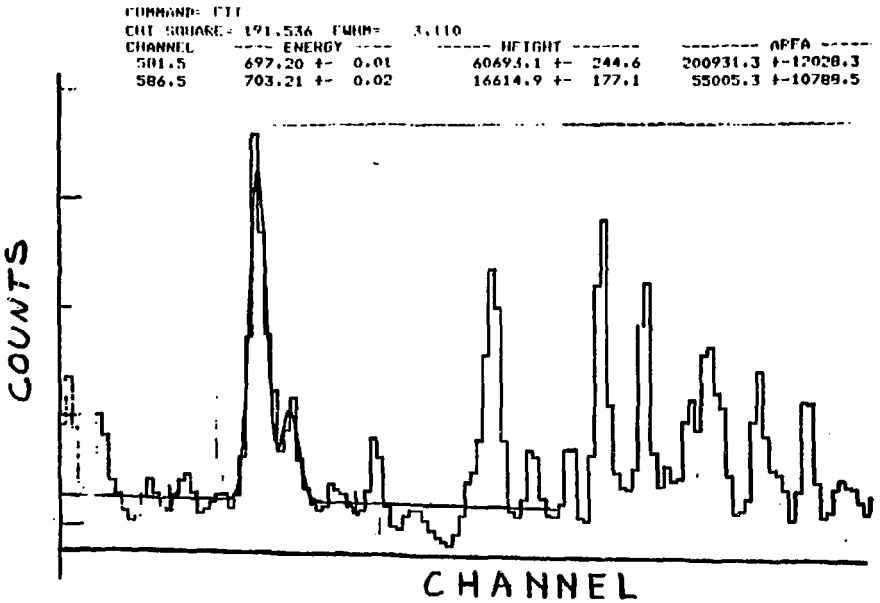
COMMAND: FIT
CHI SQUARE= 191.536 FWHM= 3.110
CHANNEL ---- ENERGY ---- ------ HEIGHT ------- -------- AREA -----
501.5 697.20 +- 0.01 60693.1 +- 244.6 200931.3 +-12028.3
586.5 703.21 +- 0.02 16614.9 +- 177.1 55005.3 +-10789.5
COUNTS
CHANNEL

Fig. A.3

+ Bx), plus one(or two, or three) mark(s) denoting the approximate region where the centroid(s) of the peaks are located.

EVA5 Sorting Program for All Detectors Coincidences

```
EVA 5E:  COMPILATION OF HI9DB3      14:55:59   7/07/84
  1   [
  2   | ***** HI9DY8   *********
  3   | *** TWO DIMENSIONAL X=GE  Y=GE PROGRAM FOR CORRELATIONS ***
  4   | * 09 JUL84 SORT FOR 3 TAC SLICES TAPE 3
  5   | ***  GD     *******
  6   | FORMAT TAG 1 0 3
  7   | FORMAT ADC 1 4 12
  8   | FORMAT GADC 1 4 14
  9   | SPEC SNG1(12) 2048 2
 10   | SPEC STACG 512 2
 11   | SPEC STACR 512 2
 12   | DSPEC GEM1 2048 2048 1
 13   | DSPEC GEM2 2048 2048 1
 14   | DSPEC GEM3 2048 2048 1
 15   | DATA OFFSET1 -4
 16   | DATA OFFSET2 +3
 17   | DATA OFFSET3 -24
 18   | DATA OFFSET4 -31
 19   | DATA OFFSET5 -11
 20   | DATA OFFSET6 -15
 21   | DATA OFFSET7 -16
 22   | DATA OFFSET8 -8
 23   | DATA OFFSET9 -16
 24   | DATA OFFSET10 -45
 25   | DATA OFFSET11 -8
 26   | DATA OFFSET12 +79
 27   | GATE SM1 166 300
 28   | GATE SM2 50 120
 29   | GATE SM3 398 450
 30   | GATE WG 0 2047
 31   | RVAR RAN
 32   | RVAR REA
 33   | IVAR I
 34   | IVAR N
 35   | IVAR C
 36   | IVAR NGEL
 37   | IVAR GEL1(12)
 38   | IVAR TAC1
 39   | IVAR TAC2
 40   | IVAR JGEL
 41   | IVAR LGEL
 42   | IVAR KGEL
 43   | IVAR EVSIZE
 44   | SET NGEL=0
 45   | SET N=1
 46   | GET C TAG(N)
 47   | ADD 1
 48   | STA C
 49   | [
 50   | | IF LE 12
 51   | |   * READ GE'S
 52   | |   [
```

```
 53   ! !    ! [
 54   ! !    ! ! LDA NGEL
 55   ! !    ! ! IF CE 12
 56   ! !    ! !   GOTO FINI
 57   ! !    ! ]
 58   ! !    ! FETCH GADC(N)
 59   ! !    ! ADD OFFSET1(C)
 60   ! !    ! [
 61   ! !    ! ! IF NOT LG
 62   ! !    ! !   GOTO SKIP
 63   ! !    ! ]
 64   ! !    ! STEP NGEL.1
 65   ! !    ! STA GEL1(NGEL)
 66   ! !    ! INC SNG1(C)
 67   :SKIP
 68   ! !    ! STEP N.1
 69   ! !    ! GET C TAG(N)
 70   ! !    ! ADD 1
 71   ! !    ! STA C
 72   ! !    ! IF LE 12
 73   ! !    !   REPEAT
 74   ! !    ]
 75   ! !    *READ TACS
 76   ! !    [
 77   ! !    ! IF EQ 13
 78   ! !    !   FETCH TAC1 ADC(N)
 79   ! !    !   INC STACG
 80   ! !    !   STEP N.1
 81   ! !    !   GET C TAG(N)
 82   ! !    !   ADD 1
 83   ! !    !   STA C
 84   ! !    ]
 85   ! !    [
 86   ! !    ! IF EQ 14
 87   ! !    !   FETCH TAC2 ADC(N)
 88   ! !    !   INC STACR
 89   ! !    !   STEP N.1
 90   ! !    ]
 91   ! !    * CREATE 2D SPECTRA
 92   ! !    [
 93   ! !    ! FOR JGEL 1 NGEL
 94   ! !    !   [
 95   ! !    !   ! LDA GEL1(JGEL)
 96   ! !    !   ! CAX
 97   ! !    !   ! LDA JGEL
 98   ! !    !   ! ADD 1
 99   ! !    !   ! STA LGEL
100   ! !    !   ! [
101   ! !    !   ! ! IF LGEL GT NGEL
102   ! !    !   ! !   GOTO FINI
103   ! !    !   ! ]
104   ! !    !   ! FOR KGEL LGEL NGEL
105   ! !    !   !   [
106   ! !    !   !   ! LDA GEL1(KGEL)
```

```
107   | |   |   |   | CAY
108   | |   |   |   | [
109   | |   |   |   | | IF TAC2 SM1
110   | |   |   |   | |   INC GEM1
111   | |   |   |   | |   IXY
112   | |   |   |   | |   INC GEM1
113   | |   |   |   | ]
114   | |   |   |   | [
115   | |   |   |   | | IF TAC2 SM2
116   | |   |   |   | |   INC GEM2
117   | |   |   |   | |   IXY
118   | |   |   |   | |   INC GEM2
119   | |   |   |   | ]
120   | |   |   |   | [
121   | |   |   |   | | IF TAC2 SM3
122   | |   |   |   | |   INC GEM3
123   | |   |   |   | |   IXY
124   | |   |   |   | |   INC GEM3
125   | |   |   |   | ]
126   | |   |   |   | IXY
127   | |   |   |   NEXT KGEL
128   | |   |   ]
129   | |   |   NEXT JGEL
130   | |   | ]
131   | |   ]
132   :FINI
133   | |   [
134   | |   | IF TAG(N) EQ 15
135   | |   |   SET EVSIZE=N
136   | |   |   GOTO END
137   | |   | ELSE
138   | |   | STEP N.1
139   | |   | REPEAT
140   | |   ]
141   :END
142   | ]
143   ]

COMPILATION COMPLETED 14:56:12
PROGRAM SIZE          322 OF  10000
SYMBOLS USED           60 OF    500
SPEC DESCRIPTORS       17 OF    200
EXTENDED MEMORY    247936 OF 253952
2-D SPECTRA      12583040 WORDS 3074 TRACKS
2-D GATES                0 OF     20
```

EVA5 Sorting Program for Angular Correlations

```
EVA 5E:  COMPILATION OF H9DY822L    23:09:45   9/28/84
  1   [
  2   | **** H19DY822AA********
  3   | *** TWO DIMENSIONAL X-GE  Y-GE PROGRAM FOR CORRELATIONS ***
  4   | * 09 JUL84 SORT FOR 3 TAC SLICES TAPE 22A ANG CORREL
  5   | ***    GD     *******
  6   | FORMAT TAG 1 0 3
  7   | FORMAT ADC 1 4 12
  8   | FORMAT GADC 1 4 14
  9   | SPEC SNG1(12) 2048 2
 10   | SPEC STACG 512 2
 11   | SPEC STACR 512 2
 12   | DSPEC GEAC1 2048 2048 1
 13   | DSPEC GEA0 2048 2048 1
 14   | DSPEC GEA90 2048 2048 1
 15   | DATA OFFSET1 -4
 16   | DATA OFFSET2 +3
 17   | DATA OFFSET3 -24
 18   | DATA OFFSET4 -30
 19   | DATA OFFSET5 -10
 20   | DATA OFFSET6 -14
 21   | DATA OFFSET7 -15
 22   | DATA OFFSET8 -7
 23   | DATA OFFSET9 +1
 24   | DATA OFFSET10 -45
 25   | DATA OFFSET11 -8
 26   | DATA OFFSET12 +31
 27   | GATE SM1 229 292
 28   | GATE KX1 1 7
 29   | GATE KY1 6 12
 30   | GATE KY2 7 9
 31   | GATE WG 0 2047
 32   | RVAR RAN
 33   | RVAR REA
 34   | IVAR I
 35   | IVAR N
 36   | IVAR C
 37   | IVAR NGEL
 38   | IVAR GEL1(12)
 39   | IVAR JET1(12)
 40   | IVAR TAC1
 41   | IVAR TAC2
 42   | IVAR JGEL
 43   | IVAR LGEL
 44   | IVAR KGEL
 45   | IVAR EVSIZE
 46   | SET NGEL=0
 47   | SET N=1
 48   | GET C TAG(N)
 49   | ADD 1
 50   | STA C
 51   | [
 52   | | IF LE 12
```

```
53   ! !   * READ GE'S
54   ! !   [
55   ! !   ! [
56   ! !   ! ! LDA NGEL
57   ! !   ! ! IF GE 12
58   ! !   ! !   GOTO FINI
59   ! !   ! ]
60   ! !   ! FETCH GADC(N)
61   ! !   ! ADD OFFSETI(C)
62   ! !   ! [
63   ! !   ! ! IF NOT WG
64   ! !   ! !   GOTO SKIP
65   ! !   ! ]
66   ! !   ! STEP NGEL.1
67   ! !   ! STA GEL1(NGEL)
68   ! !   ! INC SNG1(C)
69   ! !   ! LDA C
70   ! !   ! STA JET1(NGEL)
71   :SKIP
72   ! !   ! STEP N.1
73   ! !   ! GET C TAG(N)
74   ! !   ! ADD 1
75   ! !   ! STA C
76   ! !   ! IF LE 12
77   ! !   !   REPEAT
78   ! !   ]
79   ! !   *READ TACS
80   ! !   [
81   ! !   ! IF EQ 13
82   ! !   !   FETCH TAC1 ADC(N)
83   ! !   !   INC STACG
84   ! !   !   STEP N.1
85   ! !   !   GET C TAG(N)
86   ! !   !   ADD 1
87   ! !   !   STA C
88   ! !   ]
89   ! !   [
90   ! !   ! IF EQ 14
91   ! !   !   FETCH TAC2 ADC(N)
92   ! !   !   ADD 1
93   ! !   !   STA TAC2
94   ! !   !   INC STACR
95   ! !   !   STEP N.1
96   ! !   ]
97   ! !   * CREATE 2D SPECTRA
98   ! !   [
99   ! !   ! IF TAC2 SM1
100  ! !   !   FOR JGEL 1 NGEL
101  ! !   !     [
102  ! !   !     ! IF JET1(JGEL) KX1
103  ! !   !     !   IF JET1(JGEL) NE 2
104  ! !   !     !     IF JET1(JGEL) NE 5
105  ! !   !     !       IF JET1(JGEL) NE 6
106  ! !   !     !         LDA GEL1(JGEL)
```

```
107   | |   |     |        CAX
108   | |   |     |        LDA JGEL
109   | |   |     |        ADD 1
110   | |   |     |        STA LGEL
111   | |   |     |        [
112   | |   |     |        | IF LGEL GT NGEL
113   | |   |     |        |   GOTO FINI
114   | |   |     |        ]
115   | |   |     |        FOR KGEL LGEL NGEL
116   | |   |     |          [
117   | |   |     |          | [
118   | |   |     |          | | IF JET1(KGEL) KX1
119   | |   |     |          | |   IF JET1(KGEL) NE 2
120   | |   |     |          | |     IF JET1(KGEL) NE 5
121   | |   |     |          | |       IF JET1(KGEL) NE 6
122   | |   |     |          | |         LDA GEL1(KGEL)
123   | |   |     |          | |         CAY
124   | |   |     |          | |         [
125   | |   |     |          | |         | INC GEA0
126   | |   |     |          | |         | IXY
127   | |   |     |          | |         | INC GEA0
128   | |   |     |          | |         | IXY
129   | |   |     |          | |         ]
130   | |   |     |          | ]
131   | |   |     |          | IF JET1(KGEL) KY1
132   | |   |     |          |   IF JET1(KGEL) NOT KY2
133   | |   |     |          |     LDA GEL1(KGEL)
134   | |   |     |          |     CAY
135   | |   |     |          |     [
136   | |   |     |          |     | IF TAC2 SM1
137   | |   |     |          |     |   INC GEAC1
138   | |   |     |          |     ]
139   | |   |     |          ]
140   | |   |     |        NEXT KGEL
141   | |   |     ]
142   | |   |     [
143   | |   |     | IF JET1(JGEL) KY1
144   | |   |     |   IF JET1(JGEL) NOT KY2
145   | |   |     |     LDA GEL1(JGEL)
146   | |   |     |     CAX
147   | |   |     |     LDA JGEL
148   | |   |     |     ADD 1
149   | |   |     |     STA LGEL
150   | |   |     |     [
151   | |   |     |     | IF LGEL GT NGEL
152   | |   |     |     |   GOTO FINI
153   | |   |     |     ]
154   | |   |     |     FOR KGEL LGEL NGEL
155   | |   |     |       [
156   | |   |     |       | IF JET1(KGEL) KY1
157   | |   |     |       |   IF JET1(KGEL) NOT KY2
158   | |   |     |       |     LDA GEL1(KGEL)
159   | |   |     |       |     CAY
160   | |   |     |       |     INC GEA90
```

```
161   ! !   !     !       !     IXY
162   ! !   !     !       !     INC GEA90
163   ! !   !     !       !     IXY
164   ! !   !     !      ]
165   ! !   !     !    NEXT KGEL
166   ! !   !    ]
167   ! !   !  NEXT JGEL
168   ! !   ]
169   ! ]
170   :FIN1
171   ! [
172   ! ! IF TAG(N) EQ 15
173   ! !   SET EVSIZE=N
174   ! !   GOTO END
175   ! ! ELSE
176   ! ! STEP N.!
177   ! ! REPEAT
178   ! ]
179   :END
180   ]
```

```
COMPILATION COMPLETED 23:09:53
PROGRAM SIZE            522 OF   10000
SYMBOLS USED             73 OF     500
SPEC DESCRIPTORS         17 OF     200
EXTENDED MEMORY     247936 OF  253952
2-D SPECTRA       12585088 WORDS 1537 TRACKS
2-D GATES                 0 OF      20
```

References

Belshe, R.A. 1984. "EVA Reference Manual" and "SUSIE Reference Manual", *LBL Internal Documents(unpublished).*

Bergström, I. 1978. "Proc. XVI Int. Winter Meeting on Nuclear Physics, Bormio", I. Iori ed. vol.II : 636.

Blatt, J.M., Weisskopf, V.F. 1979. "Theoretical Nuclear Physics", Springer-Verlag.

Bohr, A., Mottelson, B.R. 1974. Phys. Scr. 10A : 13.

Bohr, A., Mottelson, B.R. 1969 and 1975. "Nuclear Structure", vol.1 and vol.2, respectively, W.A. Benjamin, Reading, Mass.

Broda, R., Ogawa, M., Lunardi, S., Maier, M.R., Daly, P.J., Kleinheinz, P. 1979. Z. Phys. A285 : 423.

Broda, R., Behar, M., Kleinheinz, P., Daly, P.J., Blomqvist, J. 1979. Z. Phys. A293 : 135.

Broda, R., Kleinheinz, P., Lunardi, S., Blomqvist, J. 1982. O.R.N.L. Conf. Proc. : 389.

Broda, R., Kleinheinz, P., Daly, P.J., Behar, M., Blomqvist, J. *1982. O.R.N.L. Conf. Proc. : 397.*

Burde, J., Dines, E.L., Shih, S., Diamond, R.M., Draper, J.E., Lindenberger, K.H., Schuck, C., Stephens, F.S. 1982. Phys. Rev. Lett. 48 : 530.

Cerkaski, M., Dudek, J., Szymanski, Z., Anderson, C.G., Leander, G., Åberg, S., Nilsson, S.G., Ragnarsson, I. 1977. Phys. Lett. B70 : 9

Cohen, S., Plasil, F., Swiatecki, W.J. 1974. Ann. Phys. 82 : 557.

Daly, P.J., Kleinheinz, P., Broda, R., Lunardi, S., Backe, H., Blomqvist, J. 1980. Z. Phys. A298 : 173.

Daly, P.J. 1984. "5th. Nordic Meeting on Nuclear Physics(March 12-16, 1984, Jyvaskyla, Finland): Proceedings" : 5 .

Dehesa, J.S., Speth, J., Kleinheinz, P. 1980.(unpublished).

de Shalit, A., Feshbach, H. 1974. "Theoretical Nuclear Physics, vo.1: Nuclear Structure", J. Wiley and Sons, Inc.

Diamond, R.M., Stephens, F.S. 1980. Ann. Rev. Nucl. Part. Sci. 30 : 85.

Diamond, R.M., Stephens, F.S. 1981. "The High-Resolution Ball" (proposal)(unpublished).

Diamond, R.M. 1984. Conf. on Instrumentation for Heavy-Ion Nucl. Research, O.R.N.L., LBL-18642.

Døssing, T., Neergaard, K., Matsuyanagi, K., Chang, H.C. 1977. Phys. Rev. Lett. 39 : 1395.

Døssing, T., Neergaard, K., Sagawa, H. 1980. J. de Physique 41 : : 10.

Døssing, T., Neergaard, K., Sagawa, H. 1980. Phys. Scr. 24 : 258.

Edmonds, A.R. 1974. "Angular Momentum in Quantum Mechanics", Princeton Univ. Press.

Frauenfelder, H., Steffen, M.R., deGroot, S.R., Tolhoek, H.A., Huiskamp, W.J. 1965. "Angular Distribution of Nuclear Radiation", K. Siegbahn, editor of "Alpha-, Beta- and Gamma-Ray Spectroscopy", North Holland Publ. Co. .

Haas, B., Ward, D., Andrews, H.R., Hausser, O.,Ferguson, A.J., Sharphey-Schaffer, J.F., Alexander, T.K., Trautmann, W., Horn, D., Taras, P., Skensved, P., Khoo, T.L., Smither, R.K., Ahmad, I., Davids,

C.N., Kutschera, W., Levenson, S., Dors, C.L. 1981. Nucl. Phys. A362 : : 254.

Hager, R.S., Seltzer, E.C. 1968. Nucl. Data A4 : 1.

Hammamoto, I. 1974. Phys. Reports 10 : 64.

Holm, A. 1979. I.E.E.E. NS-26 : 4569.

Horn, D., Hausser, O., Faestermann, T., McDonald, A.B., Alexander, T.K., Beene, J.R., Herrlander, C.J. 1977. Phys. Rev. Lett. 39 : 389.

Johnson, A., Ryde, H., Szlarkier, J. 1971. Phys. Lett. B34 : 605.

Julin, R., Yates, S.W., Lunardi, S., Soramel-Stanco, F., Kleinheinz, P., Chevallier, A., Chevallier, J., Haas, B., Khazrouni, S., Schultz, N., Blomqvist, J. 1982. O.RN.L. Conf. Proc. : 76.

Julin, A., Yates, S.W., Soramel-Stanco, F., Lunardi, S., Kleinheinz, P., Blomqvist, J. 1982. O.R.N.L. Conf. Proc. : 78.

Kleinheinz, P., Broda, R., Daly, P.J., Lunardi, S., Ogawa, M., Blomqvist, J. 1979. Z. Phys. A290 : 279.

Kleinheinz, P. 1980. J. de Physique 41 : 10.

Knoll, G.F. 1979. "Radiation Detection and Measurement", J. Wiley and Sons, Inc. .

Kownacki, J., Ludziejewski, J., Sujkowski, Z., Arnold, H., Ryde, H. 1974. Nucl. Phys. A236 : 125.

Lederer, C.M., Shirley, V.S., Browne, E., Dairiki, J.M., Doebler R.E., Shibab-Eldin, A.A., Jardine, L.J., Tuli, J.K., Buyrn, A.B. 1978. "Table of Isotopes", seventh edition, J. Wiley and Sons, Inc. .

Lunardi, S., Kleinheinz, P., Piiparinen, M., Ogawa, M., Lach, M., Blomqvist, J. 1984. Phys. Rev. Lett. 53 : 1531.

Neergaard, K. 1983. Phys. Scr. T5 : 51.

Newton, J.O., Lee, I.Y., Simon, R.S., Aleonard, M.M., El Masri, Y., Stephens, F.S., Diamond, R.M. 1979. Phys. Rev. Lett. 34 : 99.

Nolte, E., Gui, S.Z., Colombo, G., Korschinek, G., Eskola, K. 1982. Z. Phys. A306 : 223.

Northcliffe, L.C., Schilling, R.F., 1970. Nucl. Data Tables 7 : : 233.

Schiffer, J.P., True, W.W. 1976. Rev. Mod. Phys. 48 : 191.

Stefanini, A.M., Daly, P.J., Kleinheinz, P., Maier, M.R., Wagner, R. 1976. Nucl. Phys. A258 : 34.

Stefanini, J.P., Kleinheinz, P., Maier, M.R. 1976. Phys. Lett. 62b : 405.

Stephens, F.S. 1984. "High-Spin Physics" LBL-18721(unpublished).

Ward, D., Andrews, H.R., Haas, B., Taras, P., Rud, N. 1983. Nucl. Phys. A397 : 161.

Figure Captions

Chapter 1:

Fig. 1.1(p.2): Angular momenta as a function of the mass number A, where the fission barrier vanishes(according to the liquid-drop model) and where it is about 8 MeV, are shown by the solid and the dashed lines, respectively. The dotted line represents an estimate of the boundary between particle evaporation and γ-ray emission(above and below, repsectively). See text for explanation.

Fig. 1.2(p.5): The decay modes of excitation for the reaction indicated. Neutron emissions are indicated by the long arrows, while the short arrows represent the emitted γ-rays.

Fig. 1.3(p.5): Typical γ-ray de-excitation paths the nucleus undertakes to the ground state. See text for explanation.

Fig. 1.4(p.5): The left side of the figure shows the lowest order approximations to the rigid-body moments of inertia for prolate(P) and oblate(O) shapes rotating parallel(||) or perpendicular($\perp$) to the symmetry axis. The right side displays the corresponding energy trajectories for $\beta \approx 0.3$ and $A \approx 160$.

Fig. 1.5(p.11): Plots of twice the moment of inertia(top), total spin(middle) and the aligned spin(bottom) vs. the rotational frequency $\hbar\omega = E_\gamma/2$, for the yrast states in ^{158}Er(see Burde et al (1982)for details). The left side of the figure shows the change in

how ^{158}Er generates its angular momentum, from the collectively rotating prolate shape spinning with respect to an axis perpendicular to its symmetry axis(for states 2^+ through 8^+) to the situation where pairs of high-j nucleons break up and align their angular momenta along the rotational axis. In the latter case, if the x-axis is the axis of rotation, then $I_x = R + j_x$, not just R, as in the former case.

Fig. 1.6(p.14): It illustrates the other extreme way(from the collective rotation) for the nucleus to generate angular momentum, namely by single-particle angular momentum alignment.

Chapter 2:

Fig. 2.2.1(a)(p.19): A photograph of the 12 Compton-suppressed Ge modules surrounding the target in the small chamber. One can see the three rings(with 4 Ge's each), below, above and in the same horizontal plane with the beam-line leading to the target chamber. The beam-line can be seen passing through the two middle modules in the horizontal plane. The Ge detectors themselves cannot be seen because they are inside the BGO shields, but one can see the liquid-nitrogen dewars and BGO pre-amps.

Fig. 2.2.1(b)(p.19): Diagram of a BGO Compton-suppression shield, showing a 5 X 5 cm Ge detector inside(illustrating the Compton-scattering of an incident γ-ray) and two of the six photo-multiplier tubes(which are meant to register the Compton-scattered γ'-ray which will be used in the anti-coincidence)

on the back surface. Also shown, is a NaI "cap" on the front taper.(See Diamond(1984)for details about the BGO shield design.)

Fig. 2.2.1(c)(p.20): The Ge detector angular positions: θ is the angle subtended by the Ge in the x-z plane and ranges between 0° and 360°; ϕ is the angle subtended by the vector connecting the origin(i.e. the target) to the Ge and the x-z plane(just like indicated in the figure) and ranges between 0° and 360° ; θ_p and ϕ_p are the usual polar angles(measured as indicated in the figure) and ranging from 0° to 180° and from 0° to 360°, respectively. The angles θ and ϕ were measured from the experimental set-up(see Fig. 2.2.1(a)). The angles θ_p and ϕ_p were calculated to the following easily deriveable expressions: $\theta_p = \arccos(\cos\theta \cos\phi)$, for all θ's between 0° and 360° and $\phi_p = \left\{ 2\pi \text{ and } \pi \right\} \pm \arcsin[\sin\phi/\cos(\theta_p - 90°)]$, for θ ranging between 0° and 180°, and for θ ranging between 180° and 360°, respectively. One can derive the above expressions easily with the help of the cube (drawn in dashed lines) in the figure.

Fig. 2.3.1(p.26): In order to illustrate the considerable improvement that Compton suppression brings to the peak-to-total ratio(P/T), two ^{60}Co spectra are shown: both taken by a 20 percent Ge detector, only one with the bare Ge, while the other with the Compton-suppresses Ge (normalized to the same full-energy peak heights). In the former spectrum, one can see the Compton edges quite pronouncedly, appearing just in the region where one wants to have a low background. (See Diamond(1984)for details which go beyond the scope of the present work.)

Chapter 3:

Fig. 3.1.1(p.36): A "bird's eye" view of a parcel of a two-dimensional coincidence matrix(the axes being in channels) as a typical example of the data sorting. The coincidence matrix was obtained in coincidence with the RF - Ge TAC gate 1(see Fig. 5.2.2). The tall peaks in the lower left corner are due to the Pb X-rays(see Fig. 3.3.2).

Fig. 3.3.1(p.44): A window in the full projection(a one-dimensional spectrum) of the prompt two-dimensional coincidence matrix. It is shown as an example as to how gates were on the foreground plus background and on the background in the right(R) and left(L) regions of the peak of interest.

Fig. 3.3.2(p.45): Full projection(i.e. the collapse of all the rows on the x-axis, or equivalently, since the matrix has been symmetrized, the collapse of all the columns on the y-axis) of the two-dimensional coincidence matrix for the "prompt" RF - Ge TAC gate(gate 1 in Fig. 5.2.2). Due to the matrix symmetrization, number of counts in this spectrum is twice the number of counts taken during the run(this is true for all gated spectra obtained from such two-dimensional matrices, except for the spectra derived from the (0°, 90°) matrix, where no symmetrization was made, naturally(see chapter 5)). The γ-ray transition energies above the peaks refer to ^{148}Dy which represents the 4n channel of the reaction ^{40}Ar + $^{112}Cd \rightarrow {}^{152}Dy^{*}$. The three γ-ray transition energies marked

with * refer to three more intense transitions below the 480 nsec isomer in ^{148}Dy. All the other energies refer to transitions above that isomer. The peaks marked "X-rays" refer to the ≈ 75 keV $K\alpha_1$ X-ray and the ≈ 85 and 87 keV X-rays($K\beta'_1$ and $K\beta'_2$, respectively) in ^{208}Pb(backing the ^{112}Cd target)(see Lederer et al, 1978). The lower case letters indicate various impurities present, as follows(the reaction channel is indicated in parantheses): a : ^{149}Dy(3n); b : ^{145}Gd(α3n); c : ^{146}Gd(α2n); d : ^{148}Gd(α); e : ^{147}Tb(p4n) and f : ^{148}Tb(p3n). Level schemes for the impurities present can be found in the literature, as follows: ^{149}Dy(Julin et al, 1982), ^{145}Gd(Kownacki et al, 1974), ^{146}Gd(Broda et al, 1982(p.389)), ^{148}Gd(Lunardi et al, 1984) and ^{147,148}Tb(Broda et al, 1982(p.397)) It appears that none of the known transitions in ^{147}Dy(5n) were strongly enough populated to be observed. See Nolte et al(1982) and Daly(1984) for the ^{147}Dy level scheme and how it was constructed.

Fig. 3.3.3(p.47): Same full projection as in Fig. 3.3.2, only for the "delayed" RF - Ge TAC gate(gate 3 in Fig. 5.2.2). The first four more intense transitions above the 480 nsec isomer are indicated with *. The other indicated energies refer to the transitions below that isomer. The small-case letters have the same meaning as in Fig. 3.3.2.

Fig. 3.4.1(p.50): Plots of the efficiency(for the four Ge's indicated) vs. E_γ as obtained from a ^{152}Eu source(filled circles). The point at 121.8 keV was not used in obtaining the efficiency above 160 keV. The triangles were obtained with a ^{133}Ba source, to get the efficiency below 160 keV.

† The $\log_{10}$ of the number of counts in those plots is the same as $\log_{10}\epsilon$, because the number of counts were corrected for γ-ray branching(for ^{152}Eu they were normalized to the 121.8 keV transition; for ^{133}Ba, see text). See Lederer et al(1978) for the γ-ray energies and their branching ratios for ^{152}Eu and ^{133}Ba.

Fig. 3.4.1(a)(p.52): The ^{152}Eu points, obtained under identical experimental conditions as the ^{133}Ba points, but different than for Fig. 3.4.1, are shown. The symbol ✝ has the same meaning as in Fig. 3.4.1 .;#1,#5, etc refer to the Ge's involved.

Fig. 3.4.2(p.53): Plot of the Ge relative efficiency vs E_γ used in obtaining relative transition intensities. The curve turns downward below about 160 keV, because the Sn and Ag absorbers backed by Cu in front of the Ge's absorbed most of the low-energy γ-rays.(Sn or Ag can absorbe most of of the γ-rays below about 100 keV and Cu can absorb the low-energy X-rays given off by Sn or Ag.(The X-rays given off by Cu are too low in energy to worry about(see Lederer et al, 1978).)

Fig. 3.5.1(p.56): A window of the spectrum in coincidence with the 1061.1 keV transition(above the 480 nsec isomer), uncorrected for efficiency or electron conversion, showing the 495.8 keV peak, as an example of how the errors in the transition intensities were calculated(see text).

Fig. 3.5.2(p.62): Plot of the total conversion coefficient, α_T(being the sum of α_K, α_L and α_M, obtained from Hager and Seltzer(1968)) vs. the transition energy, ΔE_{if}, for Z = 66, for the multipolarities and electromagnetic character indicated.

Chapter 4:

Fig. 4.1.1(p.64): The level scheme of ^{148}Dy from the present work.

Fig. 4.1.2(p.66): The spectrum in coincidence with the 1061.1 keV transition, after proper subtraction of spectra in coincidence with appropriate backgrounds(see chapter 3), for the "prompt" RF - Ge TAC gate(gate 1 in Fig. 5.2.2). The spectrum shown has not been manipulated in any way(except for the background subtraction). The absence of the 1061.1 keV transition(on which the gating is made) is indicated.

Fig. 4.1.3(p.75): The spectrum in coincidence with the 1170.5 keV transition, obtained in the same way as Fig. 4.1.2 .

Fig. 4.1.4(p.76): The spectrum in coincidence with the 1172.7 keV transition, obtained in the same way as Fig. 4.1.2 . One can see that the 535.1 and 637.6 keV transitions are considerably reduced in intensity, compared to Fig. 4.1.3, thus supporting the claim that they are both crossed by the 1172.7 keV transition.

Fig. 4.1.5(p.77): The spectrum in coincidence with the 720.0 keV transition, obtained in the same way as Fig. 4.1.2 .

Fig. 4.1.6(p.79): The spectrum in coincidence with the 491.0 keV transition, obtained in the same way as Fig. 4.1.2 . The lower-case letters refer to the same impurities as in Fig. 3.3.2 .

Figs. 4.1.7-4.1.8(p.83-84): Bar plots which illustrate the variation of transition intensities as one proceeds upwards in spin

(indicated at the bottom of the corresponding transition intensity bar)for the gates indicated. The heights of the bars represent the appropriate transition intensities, normalized such that the height of the bar corresponding for the 495.8 keV transition is equal to the number of counts under the peak of that transition in the corresponding un-manipulated gated spectrum. The errors in the transition intensities are indicated to the right of the corresponding bar. In both figures, one can see the smooth decrease of the bar heights above the gate, and the approximate equality of the bar heights below the gate.

Fig. 4.3.1(p.105): The spectrum in coincidence with the 660.8 keV transition, obtained in the same way as Fig. 4.1.2, except that the "delayed" RF - Ge TAC gate(gate 3 in Fig. 5.2.2) was used here. The γ-ray energies marked with * represent transitions above the 480 nsec isomer(see text).

Chapter 5:

Fig. 5.0.0(p.108): Diagram of the simplest angular correlation experiment.

Fig. 5.1.1(p.109): A cascade involving two γ-rays in rapid sequence. Coupling of the three level spins involved in the cascade shown. Distributions of m-states for a given level of spin I_i, from which a given γ-ray transition de-excites, and for the level of spin I, populated by such a transition.

Fig. 5.2.1(p.152): A "bird's eye" view of a parcel of the

two-dimensional spectrum RF - Ge TAC vs. E_γ(of coincident γ-rays).

Fig. 5.2.2(p.153): Full projection of the two-dimensional matrix RF - Ge TAC X E_γ on the TAC axis. It indicates the gates used in the sorting of the data. The widths of the gates 1, 2, and 3 are(approx.): 11, 13 and 20 nsec, respectively. The calibration is about 0.18 nsec per channel(as is for all the other RF - Ge TAC spectra).

Fig. 5.2.3(p.154): The RF - Ge TAC spectrum for the 1061.1 keV transition.

Figs. 5.2.4-5.2.7(p.156-159): The RF - Ge TAC spectra for the 763.4, 477.3, 882.5 and 327.2 keV transitions(all above the 480 nsec isomer) plotted on the same plot with the RF - Ge TAC sectrum for the 1061.1 keV transition, respectively. The TAC spectra for each of the four transitions above was normalized to the peak of the 1061.1 keV TAC curve.

Fig. 5.2.8(p.161): The ratios of the FWHM's of the RF - Ge TAC's of the transitions above the 480 nsec isomer to the FWHM of the 1061.1 keV RF - Ge TAC, plotted vs. E_γ.

Fig. 5.2.9(p.162): Plot of the same nature as in Fig. 5.2.8, only for the pre-prompt half of the corresponding RF - Ge TAC's(see text).

Fig. 5.2.10(p.164): The spectrum in coincidence with the 882.5 keV transition, obtained for RF - Ge TAC gate 3(delayed)(see text for discussion).

Fig. 5.2.11(p.168): Full projection of the two-dimensional matrix Ge - Ge TAC X E_γ(of coincident γ-rays) on the TAC axis.(Calibration is about 0.20 nsec per channel. as is for all the Ge - Ge

TAC spectra.)

Figs. 5.2.12-5.2.14(p.169-171): Plots of the Ge - Ge TAC's for the 763.4, 477.3 and 882.5 keV transitions on the same plot with the Ge - Ge TAC spectrum for the 462.7 keV transition(all in coincidence with the 1061.1 keV transition), respectively.(See text for their construction).

Figs. 5.2.15-5.2.16(p.177-178): Plots of the half-lives of single-particle electric and magnetic transitions vs. E_γ, respectively. (See Blatt and Weisskopf, 1979.)

Chapter 6:

Fig. 6.0.0(p.180): Central part of the spherical single-particle spectrum(ϵ being the relative single-particle energy) used in the DIPM calculations(see Døssing et al, 1980).

Fig. 6.2.1(p.190): Comparison of theoretical calculations involving the two-particle-octupole coupling, vs. experimental values, for levels above the 480 nsec isomer. Also shown are comparisons to the DIPM calculations for other experimental levels through 16^-.

Fig. 6.3.1(p.208): Plot of neutron single-particle enegies vs. the deformation parameter β(see Døssing et al(1980)).

Fig. 6.3.2(p.210): Plot of level energies vs. I(I + 1), derived from experiment.

Fig. 6.3.3(p.212): Comparison of experimental level energies(on the left) to calculated level energies according to the DIPM(on the

right) for the rest of the levels not covered in Fig. 6.2.1 .

Appendix :

Fig. A.1(p.214): Diagram of the electronics set-up used in the data acquisition.

Fig. A.2(a)(p.217): Typical energy calibration plot of E_γ vs. channel for a Ge detector, illustrating the zero-offset correction that must be made in the sorting of the data.

Fig. A.2(b)(p.218): Accuracy of the E_γ calibration in terms of deviations of experimental ^{152}Eu γ-ray centroids(obtained according to the calibration displayed on the figure)from the accepted values (see Lederer et al(1978)), plotted vs. the ^{152}Eu γ-ray energies.

Fig. A.3(p.219): Example of a Gaussian fitting of a peak with the help of the program "SUSIE"(see Belshe, 1984).

Acknowledgements

I would like to thank my advisor, Prof. James E. Draper, for his patience and invaluable help, without which the present work would not have been possible. Training as an experimental nuclear physicist is a long and difficult process, and one could not do much better than have Jim as coach. It has been a rare privilege to be his student !

I have been very fortunate to work with the Diamond/Stephens group in the Nuclear Science Division at L.B.L. . My sincere thanks and appreciation go to Drs. Richard M. Diamond, Marie-Agnes Deleplanque and Frank S. Stephens for their more than generous help during my stay at L.B.L. . It has been a real treat to work with them !

I wish to thank Drs. Thomas Døssing, Bent Herskind, Augusto O. Macchiavelli, Henry Muehry, Martin Redlich, Peer Tjøm and Claire Schuck for the insightful discussions we had during my almost five years at L.B.L. .

I am greateful to Prof.Dr. Peter Kleinheinz for his telephone comments on ^{148}Dy .

I thank Bob Belshe for his tremendous help with the computer analysis, and Mon Lee for his valuable help with the hardware.

I am greateful to Ann Fitzgerald and Lisa Sheffield from the Nuclear Science Division for their big help with the word-processing of this dissertation.